WILEY-VCH

Arvydas Survila

Electrochemistry of Metal Complexes

Applications from Electroplating to Oxide Layer Formation

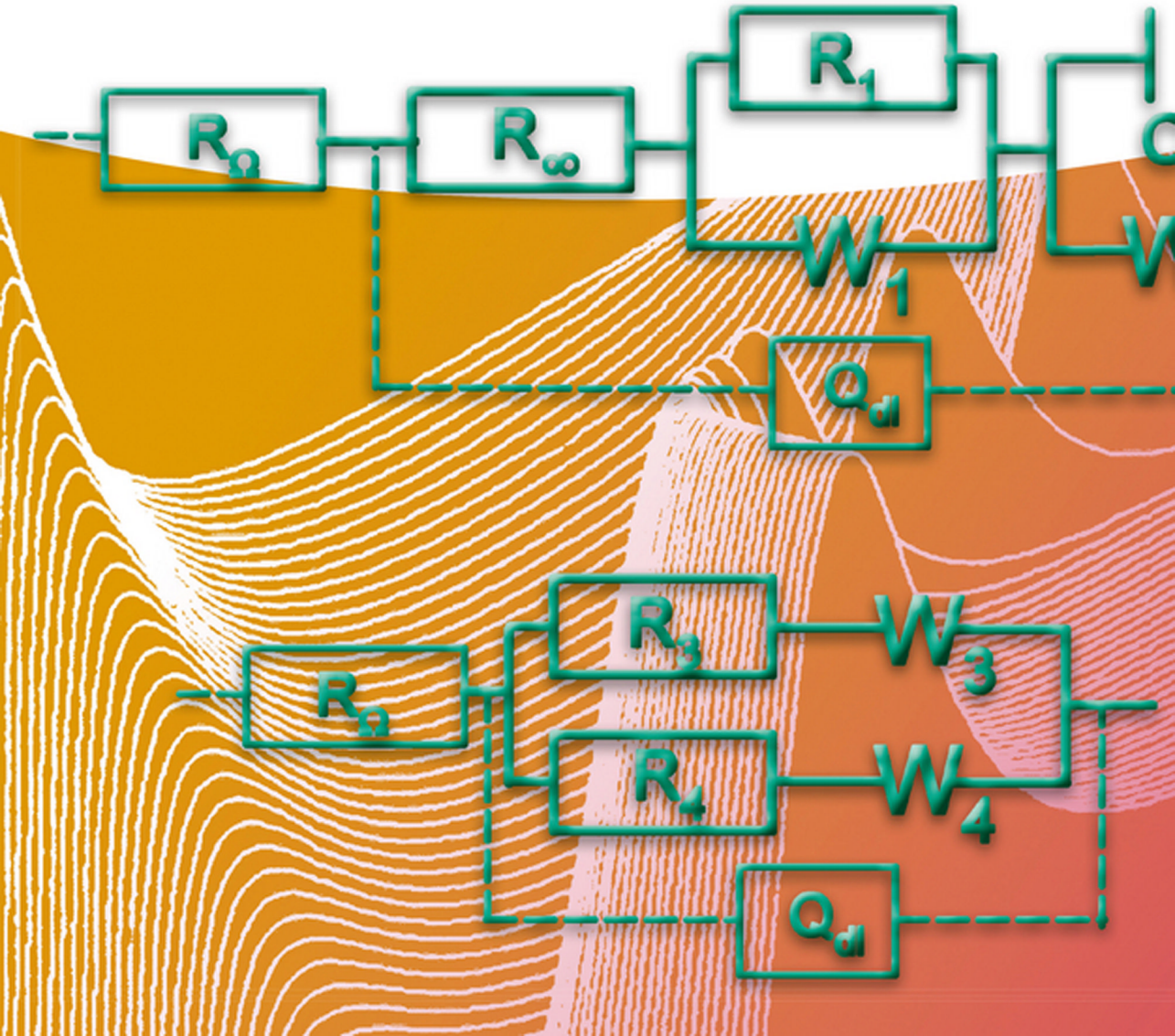

Arvydas Survila

Electrochemistry of Metal Complexes

Related Titles

Gileadi, E.

Physical Electrochemistry
Fundamentals, Techniques and Applications

2011
Print ISBN: 978-3-527-31970-1; also available in electronic formats

Schlesinger, M., Paunovic, M. (eds.)

Modern Electroplating

5th Edition
2010
Print ISBN: 978-0-470-16778-6; also available in electronic formats

Endres, F., MacFarlane, D., Abbott, A. (eds.)

Electrodeposition from Ionic Liquids

2008
Print ISBN: 978-3-527-31565-9; also available in electronic formats

Arvydas Survila

Electrochemistry of Metal Complexes

Applications from Electroplating to Oxide Layer Formation

WILEY-VCH
Verlag GmbH & Co. KGaA

The Author

Prof. Dr. Arvydas Survila
Center for Physical Sciences & Technology
Goštauto str. 9
01108 Vilnius
Lithuania

Library of Congress Card No.: applied for

British Library Cataloguing-in-Publication Data
A catalogue record for this book is available from the British Library.

Bibliographic information published by the Deutsche Nationalbibliothek
The Deutsche Nationalbibliothek lists this publication in the Deutsche Nationalbibliografie; detailed bibliographic data are available on the Internet at <http://dnb.d-nb.de>.

Print ISBN: 978-3-527-33877-1
ePDF ISBN: 978-3-527-69126-5
ePub ISBN: 978-3-527-69125-8
Mobi ISBN: 978-3-527-69127-2
oBook ISBN: 978-3-527-69124-1

Typesetting Laserwords Private Limited, Chennai, India
Printing and Binding Markono Print Media Pte Ltd, Singapore

Printed on acid-free paper

Contents

Preface

Chemical processes involving metal complexes can be found at every step, from the transformations observed in nature and ending with the various chemical industries, purposefully carried out by man. Among the latter are prominent processes occurring at the interface metal/solution, the end result of which is a production of electric energy or production of various products of electrolysis, including metallic coatings having a different purpose.

Qualitative anticorrosive, decorative, abrasion-resistant, and heat-resistant coatings are usually obtained by the electrolysis of solutions containing coordination compounds (complexes) of metals. Electrochemical processes involving these compounds are rather complicated because they proceed through several different stages, such as the mass transfer of chemically interacting particles, adsorption, charge transfer, formation of new phases, and so on.

Various problems of the electrochemistry of these systems have frequently been discussed in the literature including my book: A. Survila, *Electrode Processes in Systems of Labile Complexes of Metals* (Mokslas, Vilnius 1989), published sometime ago. Since then, a long time has passed and there has been progress in the field of theory and practice, in the field that deserves comprehension and generalization. In this regard, there was an interest to write a book in which all the major stages of electrochemical processes (mass transport, adsorption, charge transfer) are sequentially covered, putting special emphasis on their deep interrelation. I decided on this difficult task, using data published at different times in the literature, as well as theoretical and experimental material accumulated in the last half-century. In addition, it seemed appropriate to present in this book not only basic questions of electrochemistry of metal complexes including the actual plating problems, but also some other phenomena that would be possible to be classified as "related". I hope that spontaneous formation of semiconducting oxide layers, appearance of current oscillations, specifics of hydrogen evolution could also be of interest to the reader.

The material presented in this book is divided into 11 chapters. A systematic analysis of electrochemical processes involving metal complexes starts with general considerations on equilibria in solutions (Chapter 1). Their main equilibrium properties are considered and general principles of quantitative description of their composition are presented. Acquaintance with the equilibrium properties of

complex systems continues in Chapter 2, which analyzes the processes occurring at the interface metal/solution and discusses the electrodes of the first and second kinds. The principles of their quantitative descriptions are presented together with selected experimental data. Along with the known points, the reader will also find a description of other, less known self-extinguishing characteristics of these systems. This part of book is intended to provide background information, sufficient for an intelligible understanding of the material that is developed in next chapters.

Next chapters acquaint readers with the theory and common experimental practice for studying electrochemical reactions of metal complexes. Regularities of mass transport of chemically interacting particles considered in Chapter 3 serve for determining the surface concentrations of complexes and ligands. Furthermore, these data make it possible to reveal the peculiarities of electrochemical processes (Chapter 4) and form the basis for quantitative modeling of electrochemical processes (Chapter 5) and determining their mechanism (Chapter 6).

Theoretical developments are widely used in experimental investigation of real electrochemical systems (Chapters 8 and 9). The core part of the book deals with all important aspects of electroplating, including a systematic discussion of codeposition of metals and formation of alloys. It also discusses such related subjects as oxide layer formation (Chapter 10) and hydrogen evolution as a side reaction (Chapter 11).

The material presented in this book are designed for a wide range of readers. A major part of the material included in this book was presented at Vilnius University for senior students who have completed introductory courses in chemistry of coordination compounds and electrochemistry, though the first two chapters are easy comprehensible even for younger students. Problems regarding the quantitative description of electrochemical processes and the determination of their mechanism differ in complexity. Some of them are aimed at senior graduate or postgraduate students; others suggest a higher level of competence and, it is hoped will also be of interest to professional electrochemists.

Materials relating to the processes occurring in real systems may be useful for people working in engineering or manufacturing. The same can be said about Chapter 10. Electrochemical mechanisms and the role of ligand in formation of light-sensitive oxide layers may be of interest to researchers who have less contact with the electrochemistry.

In the book, much space is allotted to theoretical and experimental research performed by the author at the Institute of Chemistry (at present, Center of Physical Sciences and Technology, Vilnius, Lithuania) in collaboration with a capital research team. I wish to acknowledge a valuable contribution of my coauthors, whose names appear in the literature references. Two persons I would like to mention particularly. One of them is a nice experimenter Stasė Kanapeckaitė, with whom I had a pleasure to work with successfully for several decades. Another is

my wife Audronė Survilienė, who not only carried out a number of important experiments but also created the conditions for the successful work on this book.

Vilnius, 2015 *Arvydas Survila*

Symbols and Abbreviations

Subscripts

a	anodic
b	bulk
c	cathodic
ct	charge transfer
d	diffusion
dl	double layer
eq	equilibrium
fb	flat band
F	Faradaic
H	proton donors and acceptors
inv	inversion
lim	limiting
L	ligand
M	metal
N	Nernstian
O	oxidant
oc	open circuit
p	peak
pol	polarization
r	reaction
R	reductant
s	surface
Ω	ohmic
1/2	half-wave

Roman Symbols

a	activity
{X}	activity of species X
A	area
B	adsorption constant
c	concentration
$[X]$	concentration of species X
C	differential capacitance
D	diffusion coefficient
E	electrode potential
E^0	standard potential
$E^{o/}$	formal potential
ΔE_a	activation energy
f	frequency
F	Faraday constant
G	Gibbs free energy
H	enthalpy
i	current density
i_0	exchange current density
I	ionic strength
j	imaginary unit $\sqrt{-1}$
J	flux
k	rate constant of homogeneous reaction
K	stepwise stability constant
m	mass
M	molar mass
n	stoichiometric number of electrons involved in electrochemical reaction
$\overline{n}$	average coordination number
N_A	Avogadro constant
Q	charge; constant phase element
r	radius
R	gas constant
R	resistance
s	complex variable
S	entropy
t	time
T	absolute temperature
u	auxiliary variable
v	potential scan rate
V	volume
w	rate of chemical reaction
W	Warburg impedance
x	coordinate (distance)
Y	admittance

z_i	charge number of ion i
Z	impedance
$Z^{/}$	real part of impedance
$Z^{//}$	imaginary part of impedance

Greek Symbols

α	charge transfer coefficient
α_j	formation degree of species j
β	cumulative stability constant of complex species
β^{H}	cumulative stability constant of protonated ligand
γ	activity coefficient
Γ	adsorption (surface excess)
δ	diffusion layer thickness
ϵ	surface charge density
η	overvoltage
μ	electrochemical potential
ν	kinematic viscosity; stoichiometric coefficient
σ	surface tension (energy)
θ	surface coverage
τ	transition time; exposure duration
ψ	shift of electrical phase
ν	angular frequency
Ω	angular rotation velocity

Abbreviations

AES	Auger electron spectroscopy
AME	antimony microelectrode
CPE	constant phase element
DEL	double electric layer
EAC	electrically active complex
EC	equivalent circuit
EDTA	ethylenediamine tetraacetic acid
EDS	energy-dispersive X-ray spectroscopy
EIS	electrochemical impedance spectroscopy
EMF	electromotive force
EQCM	electrochemical quartz crystal microbalance
fcc	face-centered cubic
hcp	hexagonal close packed
IL	ideal lability
IPS	isopotential solutions
LL	limited lability

LPS	linear potential sweep
NTP	normalized Tafel plot
PEG	polyethylene glycol
RDE	rotating disk electrode
SAS	surface-active substance
scc	simple cubic cell
SEM	scanning electron microscopy
SERS	surface-enhanced Raman spectroscopy
UPD	underpotential deposition
VA	voltammetry
XP	X-ray photoelectron
XPS	X-ray photoelectron spectroscopy
XRD	X-ray diffraction

1
Introduction

At present, coordination compounds are widely applied in various fields of science and technology. One hundred and fifty years have passed since the time when Cato Maximilian Guldberg and Peter Waage formulated the Law of Mass Action. They suggested that the driving force (chemical affinity) for both forward and backward reactions is equal when the mixture is at equilibrium (today, the expression for the equilibrium constant is derived by setting the chemical potential of forward and backward reactions to be equal). The elaboration of successful theory became one of the cornerstones of coordination chemistry. This branch of science started to develop rapidly only in the middle of the past century after Jannik Bjerrum announced his thesis [1] in 1941, which was later translated into many languages. The key to Bjerrum's method was the use of the then recently developed glass electrode and pH meter to determine the concentration of hydrogen ions in solution. Bjerrum recognized that the formation of a metal complex with a ligand was a kind of acid–base equilibrium: there is competition for the ligand, L, between the metal ion, M^{n+}, and the hydrogen ion, H^+.

Main conceptions of this work, which have not lost their value and importance up to date, provided a strong stimulus for further investigations. The number of publications devoted to the problems of coordination compounds started to grow at a fast rate. The first calculations were done by hand using the so-called graphical methods. The next key development was the use of computer programs. This permitted the examination of more complicated systems. One can judge the intensity of the development of this sphere having compared a small number of works published before 1941, containing abundance of data on the characteristics of various systems collected in several volumes of "Stability Constants" [2–7]. Later, these data were critically assessed when publishing a reference book [8] containing the most reliable values of constants. Currently, a lot of critical reviews were published (most of them in the *Pure and Applied Chemistry*), and thousands of stability constants can be found in different databases.

Coordination compounds found their application in various areas including plating, which did not lose its importance until now. Much interest in the recent investigations was shown in the problems of an applied nature, underlining the effect of plating parameters such as current density, deposition time, temperature, and pH in relation to the phase composition, structure, and quality of deposit.

Electrochemistry of Metal Complexes: Applications from Electroplating to Oxide Layer Formation, First Edition.
Arvydas Survila.

To gain a better insight into the nature of electrochemical processes involving metal complexes, the kinetic regularities of the processes should be revealed and considered invoking adequate theoretical models. These problems take a considerable place in this book.

We start with the consideration of equilibrium processes taking place in the solutions containing metal complexes. As the relevant theoretical aspects are widely elucidated in the literature, we present only the most general knowledge that is closely related to the problems to be considered.

1.1 Equilibrium Properties of Complex Systems

1.1.1 General Definitions

A molecular entity formed by the reversible association of two or more chemical species (molecules, atoms, or ions) is referred to as *complex*. Very different kinds of bonds can be involved in this formation, but in the following, the charge transfer complexes will be considered for the most part. These compounds contain the central ion (most commonly a metal ion) that is bound with several groups of electron donors called *ligands*. They can be both neutral particles and ions.

The number of bonds that the central ion forms with electron-donor species is designated as its *coordination number* (π-bonds are not considered in determining the coordination number). In turn, depending on the number of bonds that a single ligand particle forms, they are classified as *uni-* or *monodentate, bidentate*, and so on, ligands. Ligands, bound with the central particle by coordination bonds, constitute an inner coordination sphere.

The so-called *chelates* belong to the category of inner-sphere complexes. The chelating ligands have several unshared electron pairs giving rise to two or more coordination bonds. The term *chelate* is derived from the Greek word for the claw of a crawfish, as the ligand grasps the metal ion like a crawfish grasps its catch with its claws. Such complexes are much more stable than the compounds made of monodentate ligands because of the liberation of a larger number of solvent molecules. This leads to an increase in the number of species present in the system and, therefore, an increase in entropy. An increase in entropy makes the formation of the chelated complex more favorable.

Depending on the number of central particles in a single molecule of a complex compound, complexes are categorized into *mononuclear* and *polynuclear* ones. In the latter, metal ions can be bound directly or through a ligand particle ("ligand bridge").

A certain part of ligands can have no direct contact with the central particle with which they are linked by weaker (electrostatic or van der Waals) interactions or a hydrogen bond. The position of such ligands in space around the central ion is not strictly defined. They constitute a second coordination sphere, and compounds of

this type are called *outer-sphere complexes*. Main attention in this book is concentrated on the processes involving mononuclear inner-sphere complexes.

1.1.2 Equilibrium in the Solutions of Complex Compounds

Solvated ions, which form when dissolving substances in some solvent W, in essence are coordination compounds with a saturated inner coordination sphere. If the solvent is water, the so-called aqua complexes form. In this case, the number of immediately bound monodentate ligands (H_2O molecules) is equal to the coordination number, N, of the metal ion.

Upon addition of ligands X and Y to the solution containing solvate complexes MW^{n+}, the former can displace part of W molecules in the inner coordination sphere forming extra complexes. Usually, this process takes place until equilibrium is established:

$$MW_N^{n+} + pXW_x + qYW_y \rightleftharpoons MX_pY_qW_r^{n+} + sW. \tag{1.1}$$

[1)]The constant of this equilibrium is called *the overall* or *cumulative stability constant* of the $MX_pY_qW_r^{n+}$ complex. The quantitative expression for cumulative stability constant, β_{pq}, can be greatly simplified by removing those terms that are constant. The number of water molecules attached to each metal ion is constant. In dilute solutions, the concentration of water is effectively constant. Then, the equation written without indicating molecules of the solvent becomes:

$$\beta_{pq} = \frac{\{MX_pY_q^{n+}\}}{\{M^{n+}\}\{X\}^p\{Y\}^q}. \tag{1.2}$$

Here, {X} should be read as "the activity of X" and likewise for the other terms in curly brackets. The reciprocal quantity is called *instability constant*. As activity is the product of concentration and activity coefficient (γ), this definition could also be written as

$$\beta_{pq} = \frac{[MX_pY_q^{n+}]}{[M^{n+}][X]^p[Y]^q} \times \frac{\gamma_{pq}}{\gamma_M\gamma_X\gamma_Y} \tag{1.3}$$

where [X] represents the concentration of species given in square brackets.

To avoid the complications involved in using activities, stability constants are determined, where possible, in a medium consisting of a solution of a background electrolyte at high ionic strength, that is, under conditions in which γ can be assumed to be always constant. Any chemical interactions between the species in equilibrium and the background electrolyte are unwanted, but such interactions

1) For the sake of simplicity, here and hereinafter, we shall treat ligands as having no charge. This simplification is of no importance when equilibrium properties of complex systems or when regularities of diffusive mass transfer are considered. However, the charge of ligands and complexes is necessary to be taken into account, considering the structure of the double electric layer, migration mass transfer, the mechanism of the electrode reaction, and so on.

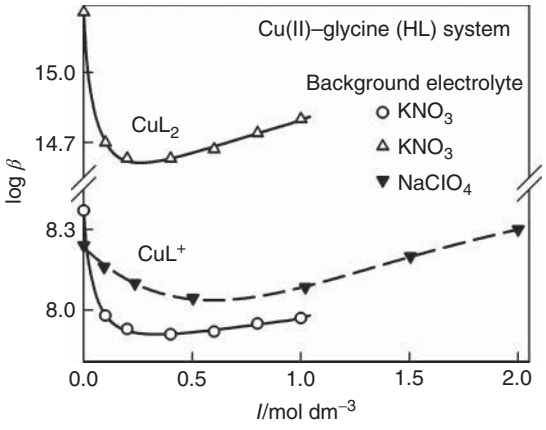

Figure 1.1 Stability constants of Cu(II)–glycine complexes obtained at different ionic strength with nitrate [9] and perchlorate [10] as background electrolytes.

might occur in particular cases. Stability constants are reported for a given ionic strength I (or extrapolated to $I = 0$). They refer to the specific ionic medium used in their determination and different values are obtained under different conditions. Furthermore, stability constant values depend on the specific electrolyte used, even at the same ionic strength. The effect of these factors can be seen from the example given in Figure 1.1.

Often, stability constants are determined for experimental conditions that deviate from the standard conditions used by convention in thermodynamics and refer to concentrations, but not to activities. Such *conditional (apparent) stability constants* are used whenever the activity coefficients and concentrations of the species are not known or not accessible, or when these simplifications are sufficient to treat certain equilibrium. As outlined next, β values expressed in concentration terms, that is,

$$\beta_{pq} = \frac{[\mathrm{MX}_p\mathrm{Y}_q^{n+}]}{[\mathrm{M}^{n+}][\mathrm{X}]^p[\mathrm{Y}]^q}, \tag{1.4}$$

are preferable in material balance equations. Sometimes, the so-called *mixed stability constants* are found in the expressions in which both concentrations and activities are used. The latter characteristic is most often applied to H^+ ions whose activity is very easily obtained from the pH values.

The more the equilibrium Eq. (1.1) is shifted to the right, the more stable are the complexes. This concept of *stability* of complexes should not be confused with *lability* of complexes, which depends on the rate of direct and reverse reactions: the larger the rate constants of these reactions are, the sooner the state of equilibrium is reached and the more labile the complex formed is. As β values depend on the ratio of the rate constants only, complexes with the same β may be both labile and inert.

It should be noted that cumulative stability constants characterize complete dissociation of the complex compound. It is clear that the equilibria, representing the

splitting out of a single ligand particle, are depicted by a relevant *partial (stepwise) stability constant.* A cumulative constant can always be expressed as the product of stepwise constants. Conversely, any stepwise constant can be expressed as a quotient of two or more overall constants. There is no agreed notation for stepwise constants, though a symbol such as K_j is also found in the literature. It is best always to define each stability constant by reference to an equilibrium expression.

The β values depend on standard changes of enthalpy ΔH^0 and entropy ΔS^0 according to the following equation:

$$\ln \beta = -\frac{\Delta H^0}{RT} + \frac{\Delta S^0}{R}. \tag{1.5}$$

If the temperature interval ΔT does not exceed ~30 K, dependence of thermodynamic functions on temperature may be ignored and the following isobar equation may be obtained:

$$\frac{\mathrm{d} \ln \beta}{\mathrm{d}T} = \frac{\Delta H^0}{RT^2}, \tag{1.6}$$

according to which the average ΔH^0 can be calculated. For that purpose, linear $\log \beta$ dependence on $1/T$ is depicted, the slope of which, according to Eq. (1.5), is equal to $-\Delta H^0/2.303R$.

In qualitatively describing equilibrium properties of complex system, certain functions are often used.

Function of formation (average coordination number) $\overline{n}$*:* Let us imagine that with gradual dissociation of complexes ML_N^{n+}, a certain number of species ML_j^{n+} involving less number of ligands forms until equilibrium is established. Then, the material balance equations relating total (analytic) concentrations of metal and ligand (c_M and c_L, respectively) to concentrations of specific particles acquire the following expressions:

$$[\mathrm{M}^{n+}] + [\mathrm{ML}^{n+}] + [\mathrm{ML}_2^{n+}] + \ \ldots \ + [\mathrm{ML}_N^{n+}] = c_\mathrm{M}, \tag{1.7}$$

$$[\mathrm{L}] + [\mathrm{ML}^{n+}] + 2[ML_2^{n+}] + \ \ldots \ + N[\mathrm{ML}_\mathrm{N}^{n+}] = c_\mathrm{L}, \tag{1.8}$$

According to the definition, the function $\overline{n}$ represents the average number of ligand particles involving M^{n+} ions:

$$\overline{n} \equiv (c_\mathrm{L} - [\mathrm{L}])/c_\mathrm{M}. \tag{1.9}$$

Having expressed concentration $[\mathrm{ML}_j^{n+}]$ of each complex through the corresponding β_j, we obtain from Eqs. (1.7) to (1.9) the following:

$$\overline{n} = \frac{\sum_{j=0}^{N} j\beta_j [\mathrm{L}]^j}{\sum_{j=0}^{N} \beta_j [\mathrm{L}]^j}, \tag{1.10}$$

where $\beta_0 = 1$, N is the maximum number of ligand particles in the complex. If L is a monodentate ligand, which completely displaced molecules of the solvent in the inner coordination sphere of the solvate complex, N equals the coordination number of the complexing agent M^{n+}.

The degree of formation α_j is defined as a partial molar fraction of the complex ML_j^{n+}:

$$\alpha_j \equiv \frac{[ML_j^{n+}]}{c_M} = \frac{\beta_j[L]^j}{\sum_{j=0}^{N} \beta_j[L]^j}. \tag{1.11}$$

The complexation degree Φ shows to what extent the solvate complex concentration decreases in the complex system:

$$\Phi \equiv c_M/[M^{n+}] = \sum_{j=0}^{N} \beta_j[L]^j. \tag{1.12}$$

All the three functions depend solely on the concentration of free ligand [L]. The function α_j is used to characterize the distribution of complex species, whereas the remaining two are applied in different methods for determining the constants β_j. The following equation represents interrelation between these functions:

$$\alpha_j = \beta_j[L]^j/\Phi, \tag{1.13}$$

$$\overline{n} = \partial \ln \Phi/\partial \ln [L], \tag{1.14}$$

$$\overline{n} = j - \partial \ln \alpha_j/\partial \ln [L]. \tag{1.15}$$

At a certain [L] value, $\overline{n}$ becomes an integer, which is equal to *j*. Then, according to Eq. (1.15), $\partial \ln \alpha_j/\partial \ln [L] = 0$ and molar fraction of ML_j^{n+} acquires the maximum value.

1.1.3 Distribution of Complexes and Ligands in the Solution

Seeking to successfully investigate the electrochemical processes taking place in the metal|solution interphase, it is necessary to know the composition of the phases; therefore, first and foremost, it is necessary to establish the distribution of complexes and ligands in the solution volume. It follows from the above-presented equations that values of the stability constant β and the concentration of free ligand [L] determine the molar fractions α_j of the components of the complex system unambiguously. Hence, α_j dependencies on [L] are the simplest characteristics, which provide information about the composition of complex solutions. It is in this form that the largest part of data in literature is presented. Even a special atlas of diagrams was drawn to characterize the composition of some complex systems [11].

Despite the fact that it is quite simple to form α_j dependencies on [L], such manner of provision of information has one major drawback: the concentration of free ligand in an actual solution is not known in advance, and therefore, it is to be evaluated. If the solution contains a sufficiently large excess of ligand, the inner coordination sphere of complexes becomes saturated and ML_N^{n+} prevails in the solution. Then, an approximate equation $[L] \approx c_L - Nc_M$ applies to the concentration of free ligand. However, some prevailing complexes are often impossible to distinguish. Moreover, free ligand L can react not only with M^{n+} but also with other ions, for example, with H^+:

$$L + mH^+ \rightleftharpoons LH_m^{m+}. \tag{1.16}$$

Then, it is also necessary to evaluate [L] dependence on the solution pH by making use of the equilibrium constants of this type, β_m^H:

$$\beta_m^H = \frac{[LH_m^{m+}]}{[L][H^+]^m}. \tag{1.17}$$

Thus, in a general case to calculate the composition of the complex system, the material balance equations are necessary. If we assume that complexes of ML_j^{n+} type form in the monoligand system, and protonated ligand LH_m^{m+} is unable to form coordination bonds with M^{n+} ions, it follows from Eqs. (1.4), (1.7), (1.8), and (1.17) that

$$\sum_{j=0}^{N} \beta_j [M^{n+}][L]^j = c_M, \tag{1.18}$$

$$\sum_{j=0}^{N} j\beta_j [M^{n+}][L]^j + \sum_{m=0}^{M} \beta_m^H [L][H^+]^m = c_L, \tag{1.19}$$

where all β values are expressed in concentration terms. As H^+ ion concentration can be calculated by means of the known pH value of the solution and the activity coefficient of these ions, two unknown quantities $[M^{n+}]$ and [L] remain in Eqs. (1.16) and (1.19). Having determined these two quantities, the equilibrium concentrations of complexes and ligands are calculated by means of relevant expressions of the known stability constants β. When the system under investigation is made up of several ligands, or more complicated (mixed) complexes may be formed in it, it is necessary to change or supplement material balance equations accordingly. They are not difficult to solve using digital methods or personal computers.

We present several examples of distribution of complexes in the solution. In calculating their concentrations, β values taken from the reference book [4] were used. Figure 1.2 represents the composition of cyanide Ag(I) solutions depending on free (part a) and total (part b) ligand concentrations. In the first case the amount of complexes is unambiguously determined by free cyanide concentration $[CN^-]$; therefore, the data of this part are valid for different solutions irrespective of what total Ag(I) and cyanide concentrations and pH values of solutions are. Despite this advantage, such representation of the composition of the complex system has

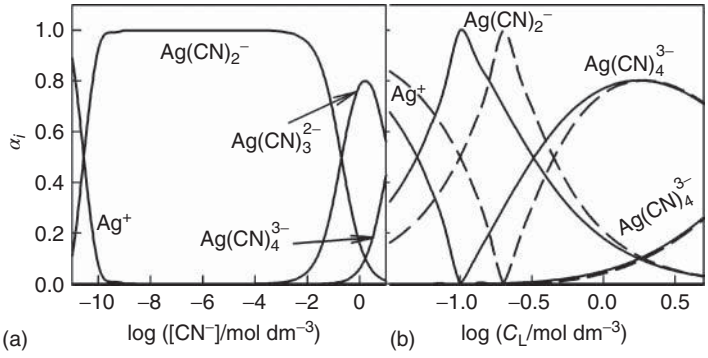

Figure 1.2 Distribution of Ag(I) cyanide complexes versus concentration of free (a) and total (b) cyanide. The total Ag(I) concentration in the part b is equal to 0.05 M (solid lines) and 0.1 M (dotted lines).

one serious drawback: free ligand concentration is not known in advance, and therefore, it is necessary to determine it somehow.

To control the composition of plating baths, several decades ago, attempts were made to titrate free cyanide by using $AgNO_3$ solution using KI as an indicator. This approach was often applied in analyzing Cu(I)–cyanide solutions, which were analogous by their complex composition and which were made from insufficiently pure reactants. According to [12], during titration, the following chemical reactions take place:

$$AgNO_3 + 2NaCN \rightarrow NaAg(CN)_2 + NaNO_3, \tag{1.20}$$

$$AgNO_3 + KI \rightarrow AgI \downarrow + KNO_3, \tag{1.21}$$

that is, after all CN^- ions are bound into the soluble Ag(I) complex, AgI precipitate forms, which shows that the equivalent point has been reached. It was Bek *et al.* [13] who drew attention to the fact that identification of concentrations (c_{titr}) of "free" cyanide determined in this way with true [CN^-] was incorrect. Our analysis showed that, during titration, due to the shift of equilibrium Eq. (1.20), part of cyanide, displaced from complexes $Cu(CN)_3^{2-}$ and $Cu(CN)_4^{3-}$, reacts and complexes $Cu(CN)_2^-$ remain in the solution at the equivalent point. When the ratio $r < 3$, the value c_{titr} exceeds the true concentration of free cyanide by 2–3 orders of magnitude.

Those diagrams have a more real practical value in which such well-controlled values as total concentration of metal and ligand are used. It is seen from Figure 1.2 that when increasing ligand concentration, the complexation degree of the system increases. Complex ions $Ag(CN)_2^-$ prevail in the region of lower ligand concentrations; however, in the region of higher concentrations, the number of cyanide ions in the inner coordination sphere of complexes grows up to 4. Abscises of the maxima of concentration profiles in the graphs a and b differ significantly. Moreover, distribution of complexes, as can be seen, depends to a certain extent on the total

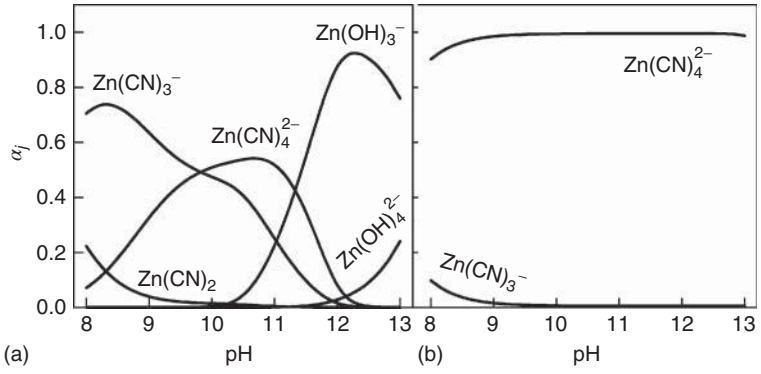

Figure 1.3 Distribution of Zn(II) cyanide and hydroxide complexes versus pH. Total Zn(II) and cyanide concentrations are equal, respectively, to 0.4 and 1.8 mM (a) and to 0.01 and 0.1 M (b).

concentration of metal. The data presented in part b apply to alkaline solutions in which the formation of HCN forms of protonated ligand may be ignored. Besides, the possibility of formation of insoluble AgCN, which can be checked by means of the product of solubility of this compound, is not taken into account here.

In case of more complicated systems, it is risky to forecast their composition even roughly. For example, from literature [3, 4] it is known that Zn^{2+} can form coordination compounds both with CN^- and with OH^- ions. Having used stability constants of such complexes and the material balance equations, it is possible to calculate the composition of the system whose example is presented in Figure 1.3. The amount of zinc cyanide and hydroxide complexes depends on Zn(II) concentration. If it is low (such solutions are usually used in polarographic investigations) within a certain pH interval, both complexes can exist (Figure 1.3a). If Zn(II) concentration is higher (such solutions are used in a voltammetric analysis and plating industry), cyanide complexes prevail in the system and formation of hydroxide complexes is very poor (Figure 1.3b).

It should be noted that data about formation of mixed complexes in this system could also be found. For example, in interpreting the data of potentiometric titration, the opinion was expressed [14] that with the aforementioned compounds such complex ions as $Zn(CN)_3(OH)^{2-}$ or $Zn(CN)_3(OH)_2^{3-}$ can be formed. However, the existence of the latter complexes has not been supported by other independent methods thus far; therefore, there is no final answer to this question. Mixed complexes can form in other systems as well, for example, in alkaline Cu(II) solutions containing various ethanolamines.

Figure 1.4 shows distribution of Ag(I)–thiocyanide complexes in solutions in which both mono- and polynuclear complexes can be found. Here, molar fractions α_j of the species containing two or three Ag^+ ions are not in line with the definition (1.10) and are enlarged two or three times, respectively. In this way, it is more convenient to represent the degree of di- or trimerization of Ag^+ ions. Furthermore, as in case of mononuclear complexes, the sum of all α_j remains equal to unity.

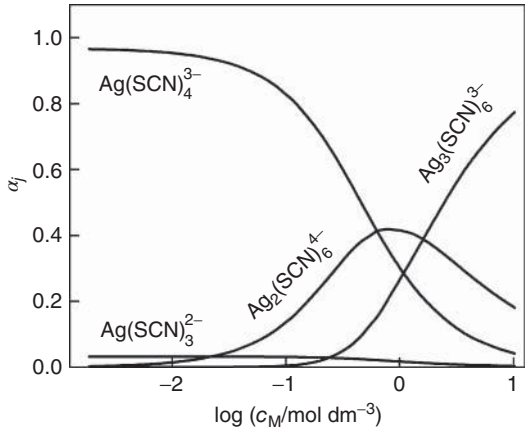

Figure 1.4 Distribution of Ag(I)–thiocyanide complexes versus total Ag(I) concentration. $c_L = 3$ M, $T = 293$ K.

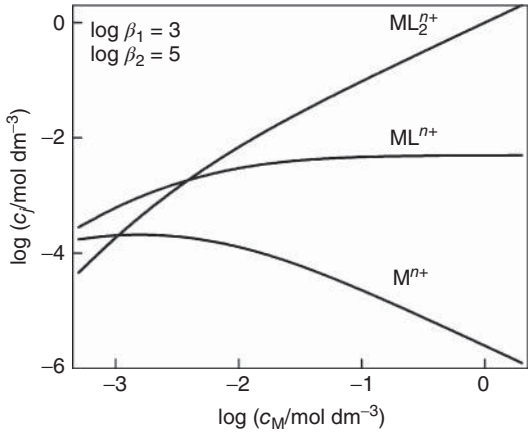

Figure 1.5 Distribution of complexes in the model system with dilution of the solution. The ratio r is constant and equal to 4.

We would like to draw the readers' attention to one peculiarity of complex systems related to changes in their composition when diluting solutions. In this case, c_L and c_M change accordingly; however, the ratio $r = c_L/c_M$ remains unchanged. It can be expected that in diluting solutions of the coordination compounds, concentrations of various species decrease proportionally. However, from the example presented (Figure 1.5), it can be seen that this supposition is absolutely incorrect. In this relation, it should be noted that in diluting solutions, the concentration of free metal ions (aqua complexes) $[M^{n+}]$, as a rule, increases.

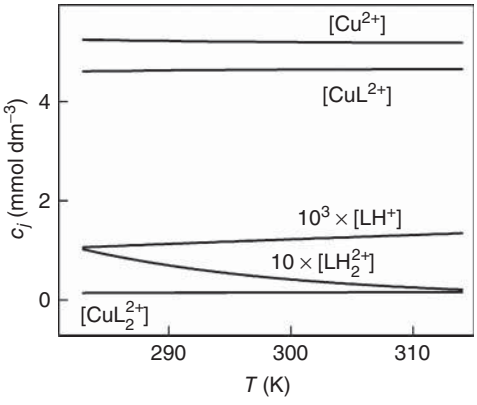

Figure 1.6 Temperature effect on the distribution of Cu(II)–ethylenediamine complexes. Total metal and ligand concentrations are equal to 0.01 and 0.005 M, respectively, at a pH of 5.3.

This is determined by relevant changes in chemical equilibria. This phenomenon is impossible in the solutions of simple salts.

The effect of temperature on the distribution of complexes is not definitive either. It is especially difficult to forecast when the solution contains forms of protonated ligand, which are unable to form coordination compounds with metal ions. The Cu(II)–ethylenediamine system in which such particles as Cu^{2+}, CuL^{2+}, CuL_2^{2+}, L, LH^+, and LH_2^{2+} form (here, ethylenediamine is symbolized as L) may serve as an example of such an object. Entropy of formation of both Cu(II) complexes is negative; therefore, with the increase in temperature, their stability decreases. However, protonated forms of ethylenediamine, which, with an increase in temperature, decompose and increase the concentration of the active form of ligand L, have the same property. These competing interactions give the results shown in Figure 1.6: the concentration of the particles containing Cu(II) practically does not depend on temperature. A rather low concentration of L (it is not represented in the figure) and that of LH_2^{2+} change more significantly. This effect can be treated as the peculiarity of this ligand-deficient system.

In summing up, the conclusion may be drawn that the variety of the composition of complex systems is really wide. Distribution of the components depends on various factors, such as total concentration of metal and ligand, pH and temperature of solutions, and so on. Sometimes, it is possible to establish the concentrations of some components by means of experimental methods too using spectrophotometry or indicator (ion-selective) electrodes. Though, as mentioned earlier, some methods of the analysis may greatly distort the reality. Therefore, it is worth calculating the composition of the system in each specific case using reliable values of stability constants.

References

1. Bjerrum, J. (1941) *Metal-Ammine Formation in Aqueous Solution*, Haase, Copenhagen.
2. Bjerrum, J., Schwarzenbach, G., and Sillen, L.G. (1967) *Stability Constants. Part I. Organic Ligands*, Chemical Society, London.
3. Bjerrum, J., Schwarzenbach, G., and Sillen, L.G. (1958) *Stability Constants. Part II. Inorganic Ligands*, Chemical Society, London.
4. Sillen, L.G. and Martel, A.E. (1964) *Stability Constants of Metal-Ion Complexes*. Special Publication No. 17, Chemical Society, London.
5. Sillen, L.G. and Martel, A.E. (1971) *Stability Constants of Metal-Ion Complexes*. Special Publication No. 25, Chemical Society, London.
6. Högfeldt, E. (1982) *Stability Constants of Metal-Ion Complexes. Part A. Inorganic Ligands*, Pergamon Press, New York.
7. Perrin, D.D. (1979) *Stability Constants of Metal-Ion Complexes. Part B. Organic Ligands*, Pergamon Press, New York.
8. Smith, R.M. and Martel, A.E. (1974–1977) *Critical Stability Constants*, vol. 1–4, Plenum Press, New York.
9. Daniele, P.G., Rigano, C., and Sammartano, S. (1982) Ionic strength dependence of formation constants. Part II: potentiometric study of the copper (II)-malonate-glycinate system In the range $0.01 \leq I \leq 1.0$. *Transition Met. Chem.*, **7** (2), 109–112.
10. Gergely, A., Nagypal, I., and Farkas, E. (1974) NMR study of the proton exchange process in aqueous solutions of copper(II)-amino acid parent complexes. *Magy. Kem. Foly.*, **80**, 545–549.
11. Kragten, J. (1978) *Atlas of Metal-Ligand Equilibria in Aqueous Solution*, John Wiley & Sons, Inc., New York.
12. Langford, K. and Parker, J.E. (1971) *Analysis of Electroplating and Related Solutions*, R. Draper LTD, Teddington.
13. Zhukov, B.D., Borodikhina, L.I., Shchekochikhin, V.M., Poddubny, N.P., and Bek, R.Y. (1973) Study of electrodeposition of copper from cyanide electrolytes. The composition of the cyanide copper plating electrolyte. *Izv. SO AN SSSR. Ser. Kchim.*, **9** (4), 57–59.
14. Marsicano, F., Monberg, C., Martincigh, B.S., Murray, K., May, P.M., and Williams, D.R. (1988) The existence and stability of mixed-ligand complexes in aqueous solutions containing zinc and cyanide ions at elevated pH values. *J. Coord. Chem.*, **16** (4), 321–339.

2
Equilibrium Electrode Potentials

When the metal M comes into contact with the equilibrated solution containing complexes of the same metal, a new nonequilibrium heterogeneous system forms at the initial moment. For the new equilibrium to be achieved, electrochemical potentials of the components, for example, those of metal ions M^{n+}, in both phases (those of metal and the solution), must become equal. During this process, a certain charge is transferred through the interface and a double electric layer (DEL) of a certain structure forms at the boundary metal|solution. As a result, concentrations of oxidized and reduced forms change; however, these changes are usually very small. They can be detected by traditional methods of analysis by using electrodes with a highly developed surface and small volumes of the contact solution.

It is impossible to experimentally determine potential jumps that formed in the interface because differences of electric potential between the points in different phases are impossible to measure. During the experiment, it is possible to determine only the electromotive force (EMF) of a certain circuit consisting of working and reference electrodes. The primary standard of reference electrode is the standard hydrogen electrode (SHE) whose potential is considered to be equal to zero. Therefore, the EMF of this circuit is considered to be the potential E of the working electrode referred to the hydrogen scale. The EMF consists of various potential jumps occurring in different boundaries: metal|solution, metal|metal (contact potential difference), and solution|solution (diffusion potential). When the system contains the excess of properly selected supporting electrolyte, the latter potential difference may be ignored. As the contact difference of the potentials is a constant value, changes in the EMF of this circuit will depend on how the potential jump changes in the ionic part of the DEL.

Different electrodes can be classified by the peculiarities of the equilibration. *Electrodes of the first kind* contain electronic conductors as the reduced forms and ions, particularly complex ions, as the oxidized forms. Metal M (phase I) in contact with the solution of M^{n+} ions (phase II) is a typical example. The equilibrium can be established with respect to cations and anions; in the absence of ligands, the cations are more typical. *Electrodes of the second kind* contain a metal, a poorly soluble compound of this metal (which is usually a salt, but it may be oxide or hydroxide as well), and an electrolyte which can establish a solubility equilibrium with the precipitate. As an example, we refer to Ag(s)|AgCl(s)|KCl(aq) electrode,

Electrochemistry of Metal Complexes: Applications from Electroplating to Oxide Layer Formation, First Edition. Arvydas Survila.

which is also used as a reference. There can also be *electrodes of the third kind,* which have two phases of insoluble compounds [1].

The principles of thermodynamics state that the parameter defining the equilibrium should not depend on the mechanism of equilibration; therefore, the potential of the equilibrium potential E_{eq} depends only on the initial and final states, which are represented by a relevant record of the electrochemical change (electrode reactions). Hence, in describing the electrode potential, any convenient form of the Nernst equation can be used.

2.1 Electrodes of the First Kind

Let us assume that the equilibrium between various complexes ML_j^{n+}, free metal ions M^{n+}, and free ligand L is established in the solution phase of the system under investigation. During the electrochemical change, particles containing M^{n+} reduce forming a crystal lattice of metal M. If, for example, free metal ions M^{n+} are assumed to be electrochemically active, the charge transfer reaction will be as follows:

$$M^{n+} + ne \rightleftarrows M, \tag{2.1}$$

and the Nernst equation will acquire the following form:

$$E_{eq} = E^0 + \frac{RT}{nF} \ln\{M^{n+}\}, \tag{2.2}$$

where activity of metal ions $\{M^{n+}\} = \gamma[M^{n+}]$, and γ is the activity coefficient of these ions. When the solution contains an excess of the supporting electrolyte, its ionic strength changes insignificantly and γ can be regarded as a constant value. Then,

$$E_{eq} = E^{0/} + \frac{RT}{nF} \ln[M^{n+}], \tag{2.3}$$

and the new constant

$$E^{0/} = E^0 + \frac{RT}{nF} \ln \gamma \tag{2.4}$$

is called the formal electrode potential. Unlike the standard E^0, this value depends on the solution concentration and the nature of supporting ions.

Now let us consider another variant assuming that the complex particle ML_p^{n+} takes part in the charge transfer reaction:

$$ML_p^{n+} + ne \rightleftarrows M + pL. \tag{2.5}$$

The following modification of the Nernst equation corresponds to it:

$$E_{eq} = E_p^{0/} + \frac{RT}{nF} \ln \frac{[ML_p^{n+}]}{[L]^p}. \tag{2.6}$$

As both, Eqs. (2.3) and (2.6), expressions apply to one and the same equilibrium state, they give the same E_{eq} value. Having written the expression of the stability

constant β_p of the complex ML_p^{n+} and having compared the said equations, we obtain the relation between the formal potentials:

$$E_p^{0/} = E^{0/} - \frac{RT}{nF} \ln \beta_p. \tag{2.7}$$

Having used the expression of the complexation degree Φ, it follows from Eqs. (1.12) and (2.3) that

$$E_{eq} = E_p^{0/} - \frac{RT}{nF} \ln \Phi + \frac{RT}{nF} \ln c_M. \tag{2.8}$$

In systems involving aqua complexes, when ligand is absent, $c_M = [M^{n+}]$ and $\Phi = 1$. It is easy to see that addition of ligand cause a certain decrease in the equilibrium potential. When $c_M = \text{const}$, its shift ΔE_{eq} is described by the following equation:

$$\Delta E_{eq} = -\frac{RT}{nF} \ln \Phi. \tag{2.9}$$

It should be noted that this equation also applies to the shift of the half-wave potential, $\Delta E_{1/2}$, in polarography if the diffusion coefficients of particles are the same.

In analyzing the slopes of E_{eq} dependence on ln[L], the average coordination number $\overline{n}$ can be established. It follows from Eq. (2.8) that

$$\frac{\partial \ln E_{eq}}{\partial \ln[L]} = -\frac{RT}{nF} \frac{\partial \ln \Phi}{\partial \ln[L]}. \tag{2.10}$$

The relationship between E_{eq} and $\overline{n}$ is obtained from this equation and from Eq. (1.14):

$$\frac{\partial \ln E_{eq}}{\partial \ln[L]} = -\overline{n}\frac{RT}{nF}. \tag{2.11}$$

If $\overline{n}$ acquires the value of the integer, for example, p, this shows that particles ML_p^{n+} prevail in the solution. Equations (1.18), (1.19), and (2.3) were used to calculate E_{eq} dependencies on various parameters of the complex system.

We shall begin looking at how the equilibrium potential varies during the potentiometric titration when a certain volume (V) of the solution containing ligand L is added to the solution containing simple M^+ ions (aqua complexes) and a certain quantity of monoligand complex ML^+ is formed. The reversible $M|M^+$ electrode of the first kind can be taken as the indicator, whose equilibrium potential can serve as a measure of M^+ concentration, according to the Nernst equation. Some examples of simulated titration curves are presented in Figure 2.1, where the shift of the equilibrium potential (ΔE_{eq}) versus V is plotted. A sharp decrease in E_{eq} is observed at the equivalent point, whose depth depends on the stability constant (K) of ML^+ complex. The potential drop displays the demarcation between two different states of the system. On the left, there is a lack of ligand and "free" M^+ ions predominate in the analyte. In contrast, the system contains an excess of ligand in the right-side area, where ML^+ species prevail. Hence, a transition from

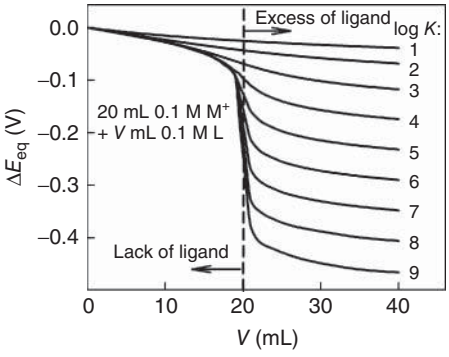

Figure 2.1 Potentiometric titration curves obtained at different stability of ML^+ complexes (log K values are given at the respective curves). 0.1 M solutions of M^+ (20 ml) and ligand (volume V) are used. Dilution effects are accounted for.

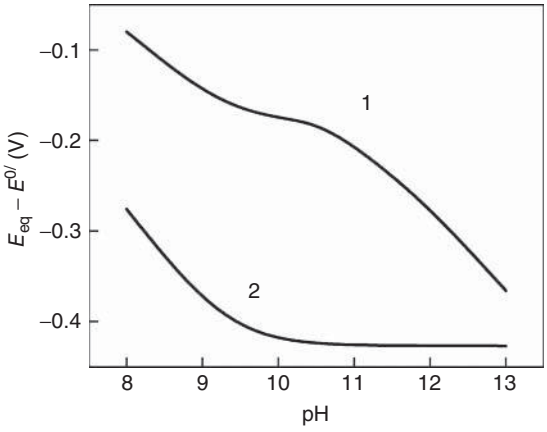

Figure 2.2 Variations of Zn equilibrium potential with pH of Zn(II) cyanide solutions at c_M and c_L, which are equal, respectively, to 0.4 and 1.8 mM, (curve 1); 0.01 and 0.1 M (curve 2).

one state (a lack of ligand) to another (an excess of ligand) is accompanied by a rather sharp potential drop.

It should be noted that even in the case of the same complex system, E_{eq} changes may be of a different nature, depending on the ratio of metal and ligand concentrations. The data presented in Figure 2.2 represent the peculiarities of distribution of complexes in cyanide Zn(II) solutions (see Figure 1.3). Polarographic investigations of this system showed [2] that the first curve in Figure 2.2, when properly transformed (see Eq. (2.9) and its comment), coincides well with the experimental dependence of the half-wave potential on pH.

Figure 2.3 shows E_{eq} dependence on the dilution of solutions in the system Cu|Cu(II), ethylenediamine. As this ligand has protonated forms, which do not form stronger complexes with Cu(II), the complexation degree Φ can be regulated

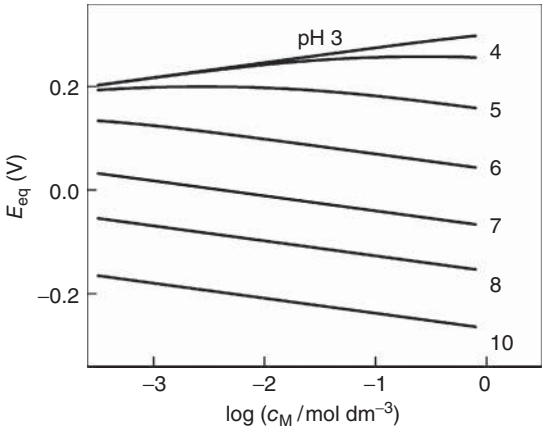

Figure 2.3 Variations of the equilibrium potential of Cu electrode with dilution of Cu(II)–ethylenediamine solutions. The ratio $r = c_L/c_M$ is kept constant and equal to 4.

by changing pH of the solutions. Φ is low at pH < 3, and the system has properties typical of aqua complexes: when diluting such solutions, E_{eq} decreases. It is natural that E_{eq} also decreases with pH (with increasing in Φ). However, along with this, the character of E_{eq} dependence on c_M changes radically: now the equilibrium potential increases with decreasing in total Cu(II) concentration. As the ratio r is kept constant, this means that E_{eq} increases with dilution of solution. This phenomenon is one of the peculiarities of complex systems. It was observed in Cu(II) solutions containing glycine [3] but was interpreted in another way.

As E_{eq} values in metal complex solutions depend on many factors, various possibilities occur to change them in a desirable way. Let us remember that such a change in the total metal and ligand concentrations brings about shifts in the equilibrium potential in different directions: when increasing c_M, E_{eq} increases, but when increasing c_L, it decreases. Therefore, there always exist a number of *isopotential solutions* in which c_M and c_L are different but E_{eq} remains constant. A series of such solutions can be chosen experimentally or their composition can be calculated. For this purpose, it is necessary to fix some constant M^{n+} ion concentration, which, according to Eq. (2.3), determines the electrode potential unambiguously. Then, taking different [L] values, in accordance with Eqs. (1.18) and (1.19), analytical (total) concentrations of reactants necessary to make solutions are calculated. If protonated ligands exist in the system, the pH value of the solution is also specified.

The following regularity applies to isopotential solutions

$$\frac{\partial \log[ML_j^{n+}]}{\partial \log[L]} = j, \tag{2.12}$$

which follows from the definition of the stability constant β_j when $[M^{n+}] = \text{const}$ (see Eq. (1.4)). Distribution of Ag(I) cyanide complexes within the series of isopotential solutions is shown in Figure 2.4. The stability constant of AgCN species

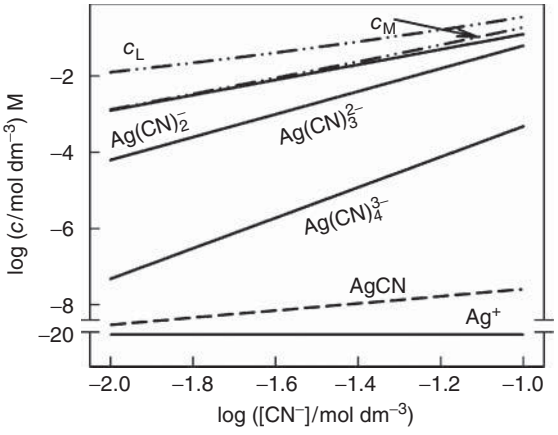

Figure 2.4 Variations of concentrations of Ag(I) cyanide complexes in a series of isopotential solutions. Total concentrations of Ag(I)and cyanide are shown by dotted lines.

has not been known thus far; therefore, their supposed concentration is marked by dotted line. It is seen from the figure that $\log[Ag(CN)_j^{1-j}]$ dependencies on log $[CN^-]$ are lines with a slope equal to the number j of ligand particles in a relevant complex. Due to the aforementioned properties, isopotential solutions are convenient in determining the mechanism of electrode reactions. The theory of this method shall be presented next.

2.2
Equilibria Involving Ions of the Intermediate Oxidation State

According to [4], reactions involving complexes and related to changes in the oxidation number of the central metal can be divided into two groups:

1) reactions, during which complexes are reduced to atoms afterward forming a crystal metal lattice;
2) charge–exchange reactions when the central atom also changes its oxidation number but remains in the solution phase in the form of a soluble compound.

If in boundary metal|solution, a consecutive charge transfer takes place in several steps, there is probability that complexes formed of partly reduced metal ions will accumulate in the solution till a certain equilibrium concentration is reached. Then, the above-specified two groups of reactions become related, and the process of the equilibration acquires peculiarities. Some of them were established in studying the system $Cu|Cu^{2+}, Cu^+$ [5]; however, as far as we know, analogous complex systems have not been investigated thus far. In this relation, the analysis of the systems formed of metal ions of different oxidation number becomes important.

To be more specific, let us assume that there exist stable enough M^{2+} and M^+ ions forming relevant complexes with ligand L. The solution of these complexes

may be produced in several ways. One of them is to simply dissolve M(I) and M(II) salts and ligand L. Then, M(I) and M(II) complexes are formed, whose stability is determined by the constants β_i and β_j, respectively. Besides, homogeneous redox reactions related to electron transfer between metal ions with different oxidation state may take place in the solution formed [4]. However, it follows from the conservation law of the charge that total M(I) and M(II) complex concentrations (c_{1M} and c_{2M}) remain unchanged, that is, due to recharge of central metal ions, they remain the same. It is possible to determine the complex composition of this solution on the basis of the same above-specified principles. For this purpose, it is necessary to formulate relevant equation of material balance:

$$[M^+]\sum_{i=0}^{N_1}\beta^i[L]^i = c_{1M}, \tag{2.13}$$

$$[M^{2+}]\sum_{j=0}^{N_2}\beta_j[L]^j = c_{2M}, \tag{2.14}$$

$$[M^+]\sum_{i=0}^{N_1} i\beta_i[L]^i + [M^{2+}]\sum_{j=0}^{N_2} j\beta_j[L]^j + [L] = c_L. \tag{2.15}$$

If now we place metal M in the solution under study, which is in the first state defined earlier, a new (second) state is to be set, which is characterized not only by equilibria between the components in the solution phase but also by electrochemical equilibrium at the boundary metal|solution. Then, an electrode should be reversible with respect to both ions (M^{2+} and M^+). Applying the Nernst equation to this case, we obtain

$$E_{eq} = E_1^{0/} + \frac{RT}{F}\ln[M^+] = E_2^{0/} + \frac{RT}{2F}\ln[M^{2+}]. \tag{2.16}$$

It follows that the relation between M^{2+} and M^+ equilibrium concentrations is determined by the difference in formal potentials $\Delta E^{0/} = E_1^{0/} - E_2^{0/}$ of the $M|M^+$ and $M|M^{2+}$ electrodes:

$$[M^{2+}] = [M^+]^2 \exp\left(\frac{2F\Delta E^{0/}}{RT}\right). \tag{2.17}$$

In a general case, $[M^{2+}]$ and $[M^+]$ values that follow from Eqs. (2.13)–(2.15) and from condition (2.17) do not coincide; therefore, transfer from the first state into the second one is related to corresponding changes, which are caused by chemical reactions. First and foremost, interaction between the electrode metal phase and one of the solution components should be attributed to them:

$$M + M^{2+} \rightleftarrows 2M^+, \tag{2.18}$$

which is accompanied by a corresponding shift of chemical equilibria between M^{2+}, M^+, and L. Having labeled concentrations in the said states by superscripts (1) and (2), respectively, and having applied the mass and charge conservation law, we obtain

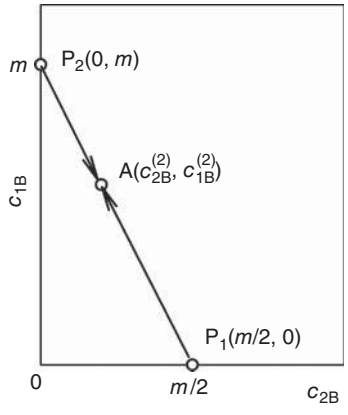

Figure 2.5 Diagram explaining the transition of complex system to equilibrium state A, when the condition $c_{1B}^{(1)} + 2c_{2B}^{(1)} = \text{const}$ holds. The P1 → A transition involves the direct reaction (2.18) with dissolution of metal; and the P2 → A transition involves the reverse reaction.

$$c_{1B}^{(1)} + 2c_{2B}^{(1)} = c_{1B}^{(2)} + 2c_{2B}^{(2)} = \text{const} \equiv m. \tag{2.19}$$

Hence, initial solutions of various compositions, to which the condition $c_{1B}^{(1)} + 2c_{2B}^{(1)} = \text{const}$ applies, when in contact with metal M, will reach one and the same equilibrium state, represented by the point A in Figure 2.5. Two limiting cases of the first state are possible. In the event M(I) complexes are absent from the initial solution, this state corresponds to the point $P_1(m/2, 0)$, which is on the abscissa axis. Another case deals with the opposite supposition, when M(II) is absent from the solution. The point $P_2(0, m)$, which is on the ordinate, represents the initial state. The remaining cases fall under the segment P_1P_2. The final state is the same for all these cases, and it is represented by the point A, the coordinates of which are obtained after solving Eqs. (2.13)–(2.15) using conditions (2.17) and (2.19).

It follows from this analysis that transfer to the equilibrium state A may be accompanied by both electrodeposition of the metal phase and its anodic dissolution. In their turn, both processes may bring about profound changes in the composition of the solution. Seeking to assess it quantitatively, let us assume that M^{2+} does not form coordination compounds with ligand L and M^+ forms the complex ML^+ whose stability constant is β_1. We shall also assume that there are no M(I) particles in the initial solution. Having immersed a sufficiently large amount of metal M into this solution, it will start reacting according to reaction (2.18), reducing the M^{2+} concentration to a certain equilibrium value. On the basis of the above-presented equations, it is possible to evaluate what part α of M^{2+} ions will react with M until complete electrochemical equilibration of the system. The results depend on $\Delta E^{0/}$ and β_1 (Figure 2.6).

If $E_1^{0/} < E_2^{0/}$, almost all M^{2+} ions should be reduced to M^+ (curve 1). In the opposite case, α depends on β_1 and increases with an increase in the stability of M(I) complexes. Curve 4 corresponds approximately to the system, which contains Cu^{2+} and Cu^+ ions.

Upon equilibration, the open-circuit potential also changes in a certain way. When studying this effect, the assumption is to be made that at the initial moment, when the intermediate M^+ ions are absent, it is close to the equilibrium potential

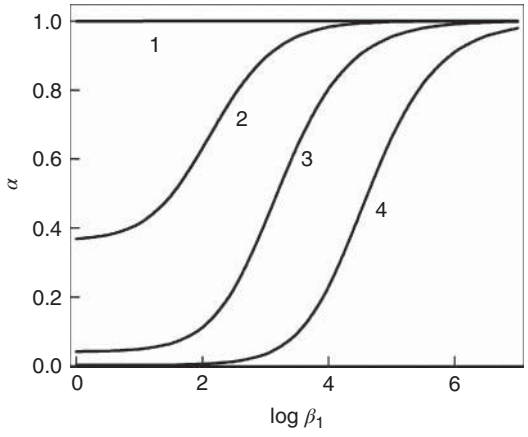

Figure 2.6 Molar fraction of M(II) converted into M(I) during equilibration versus stability constant of ML^+ species. Differences in formal potentials, $\Delta E^{0/}$, are as follows: −0.06 (1), 0.06 (2), 0.12 (3), and 0.2 V (4). Initial concentrations of M(II) and ligand are 0.01 and 0.02 M, respectively.

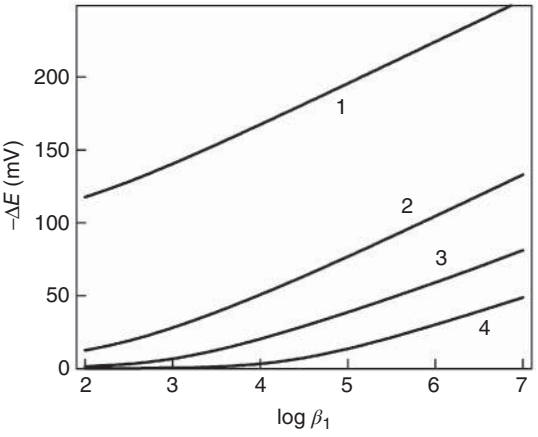

Figure 2.7 Changes in electrode potential in the equilibration process versus stability constant of ML^+ species. Differences in formal potentials, $\Delta E^{0/}$, are as follows: −0.06 (1), 0.06 (2), 0.12 (3), and 0.2 V (4). Initial concentrations of M(II) and ligand are 0.01 and 0.02 M, respectively.

$M|M^{2+}$, which, according to the Nernst equation, is determined by the initial concentration M^{2+}. It is clear that the final state is described by the Nernst equation (2.16). The calculated changes of the electrode potential, that is, differences in their final and initial values ΔE are represented in Figure 2.7. Depending on the values of $E_1^{0/}$ and β_1, ΔE may be quite high.

The data of the two latter figures may be also used in characterizing the systems, in which complexes of both metal oxidation states exist. In this case, β_1 should

be treated as the ratio of the stability constants of corresponding M(I) and M(II) complexes.

The transfers discussed depend on the rate of the charge exchange between metal and solution phases. In turn, exchange current density is determined not only by the rate constants of these processes but also by concentration of corresponding ions. When the amount of M(I) complexes is small, the electrode potential, as already mentioned, will in essence depend on $[M^{2+}]$. Hence, transfer into the total electrochemical equilibrium may be kinetically restricted, and due to that, the system may stay in the initial state for a long time, which, strictly speaking, is not an equilibrium one. These transfers may be initiated by adding a small amount of M(I) salt to the solutions, or by processing them with finely dispersed particles of corresponding metal. Such procedures may be useful in investigating experimentally the systems with a stepwise charge transfer mechanism.

2.3 Electrodes of the Second Kind

As mentioned earlier, electrodes of the second kind contain the phase boundary M|MX|KX, where MX is a less soluble metal M compound, and KX is a highly soluble substance, which has a common anion with MX.[1)] Mechanism of forming systems of this type is simple and well investigated, and the quantitative expression of the equilibrium potential (corresponding modifications of the Nernst equation) is well known. Concentration of ions M^{n+}, which are in the solution phase and participate in the electrode reaction $M^{n+} + ne \rightleftarrows M$, is rather low because it is determined by the product of solubility of compound MX. By adding ligand, it is possible to significantly increase the total concentration of metal in the solution; however, the M(n) complexation degree Φ must not be too high because then the phase of insoluble MX will become unstable and will decompose. On the contrary, in case of too low Φ, the electrode of the second kind will remain together with its own quantitative characteristics. The equilibrium potential, as in the ligand-free system, will depend on the concentration of anions X according to the same modification of the Nernst equation.

The case where an insoluble intermediate compound forms is more complicated, though, in our opinion, more interesting. In this relation, let us continue with the analysis of the system that was considered in Section 2.2. Let us make an additional assumption that insoluble hydroxide MOH (or the product of its decomposition – M_2O) may form within it. In this case, the maximum M^+ ion concentration in the solution $[M^+]_{max}$ is defined by the solubility product of the said compound or the expression equivalent to it:

$$\log [M^+]_{max} = a - pH, \tag{2.20}$$

where a is a certain constant.

1) For the sake of simplicity stoichiometric coefficients of the compounds are not given.

Let us imagine that equilibrium $[M^+]$, which formed in the second state (see Section 2.2), is larger than its critical value corresponding to expression (2.20). Then, a certain part of M(I) is to change into an insoluble compound. The decrease in the amount of this component in the solution phase will upset the equilibria that were reached before causing its relevant shifts. All the macroprocesses of the system will come to a stop after a complete (total) equilibrium has been reached, which includes in the case under consideration the following:

- Equilibria between M^+ ions, ligand L particles, and M(I) complexes, as well as analogous equilibria between M^{2+}, L, and M(II) complexes in the solution phase. Material balance Eqs. (2.13)–(2.15) with corresponding stability constants are used for their quantitative description.
- The equilibrium between M(I) and M (II), which is realized through the metal phase of the electrode. Quantitatively, it can be characterized by recording the expression of the equilibrium constant K of process (Eq. (2.18)), or by using an equivalent Eq. (2.17).
- Equilibrium between insoluble compound and soluble phases, which is controlled by condition Eq. (2.20).

In case of the equilibrium under study, the composition of the complex system may differ in essence from the earlier described one when the electrode of the first kind is formed. Now, by means of Eq. (2.20), concentration of ions M^+ of the intermediate oxidation number is described and, having inserted the value $[M^+]_{max}$ in Eq. (2.17), $[M^{2+}]$ is found. As from the electrochemical point of view, ligand is considered to be inert, its total concentration remains unchanged during the processes. Then, the equilibrium concentration of free ligand [L] can be found from Eq. (2.15). Then, with known $[M^+]$, $[M^{2+}]$, and [L] values and the stability constants β of the complexes, using material balance equations (see expressions (2.13) and (2.14)) total concentrations of M(I) and M(II) can be calculated. Subsequently, these quantities shall be labeled with the symbols c_{1M} and c_{2M}, respectively, emphasizing the fact that they are different from the values c_{1B} and c_{2B}, which existed prior to the formation of the insoluble compound.

It is not difficult to evaluate the amount of the insoluble product in m_{MX} (moles), which forms in the V volume solution. Let us assume that the initial solution does not contain M(I) compounds at all: $c_{1B}^{(1)} = 0$. Now, it is necessary to have in mind the fact that the term $c_{1B}^{(2)}$ in Eq. (2.19) consists of two parts: c_{1M} and amount of M(I) from which the insoluble solution was formed. Then,

$$m_{MX}/V = c_{2B}^{(1)} - c_{2M} - c_{1M}/2. \tag{2.21}$$

To show to what extent the said processes can take place in a specific case, we shall present several calculation results obtained for the system Cu|Cu(II), ethylenediamine [6]. The amount of Cu_2O, which has been formed in $1\,dm^3$ solutions of different composition, is shown in Figure 2.8. It goes without saying that only positive m_{Cu_2O} values have a physical sense. They indicate the area in which Cu_2O is thermodynamically stable. Moreover, the larger the m_{Cu_2O} value, the greater is the thermodynamic probability of the Cu_2O formation. In those

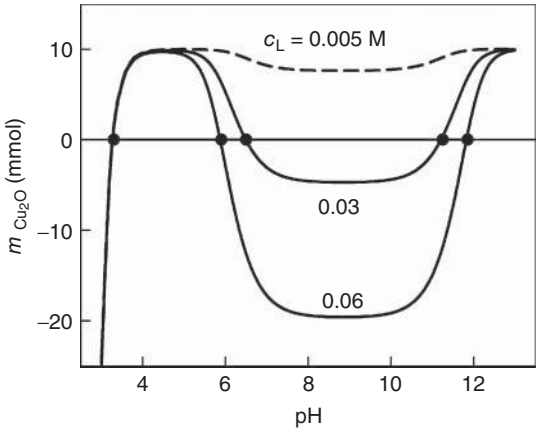

Figure 2.8 pH dependencies of Cu_2O amount formed in the Cu|Cu(II), ethylenediamine system. Initial concentration of Cu(II) is equal to 0.01 M; the total ligand concentration is indicated.

pH regions where this value is negative, the Cu_2O phase should not form. The depth of the curve minimum reflects the stability of the system, which increases with the increase in ligand concentration. Dependence calculated for ligand concentration that is equal to 0.005 M is represented by a dotted line, underlying the circumstance that it cannot be verified experimentally due to the formation of insoluble $Cu(OH)_2$ in the solution. This possibility can always be assessed by comparing corresponding calculation results with the solubility product of Cu(II) hydroxide.

The points where the curves intersect the abscissa axis can be used in drawing phase diagrams of complex systems (Figure 2.9). They show the areas where

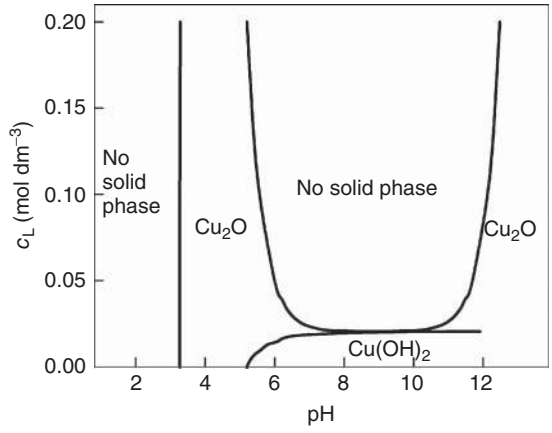

Figure 2.9 Phase diagram of the Cu|Cu(II), ethylenediamine system simulated at $c_{Cu(II)} = 0.01$ M.

Cu_2O (phase layer) and $Cu(OH)_2$ precipitates can form. It is interesting that in the case of the systems under investigation, there exist two Cu_2O stability zones – in slightly acid and alkaline media. This effect is determined by two competing processes. When increasing pH, the OH^- ion concentration increases; however, at the same time, the degree of complexation of the system increases too because the amount of protonated ligands decreases. The analysis shows that diagrams of this type can be obtained only with a certain ratio between the stability constants of complexes and protonated ligands. In the opposite case, the intermediate zone, in which Cu_2O is unstable, disappears.

2.4 Open-Circuit Potentials: Examples of Experimental Investigations

The open-circuit electrode potential E_{oc} can be of various nature. If several conjugated electrochemical processes can take place at the boundary, usually the mixed (steady-state) potential is set, and the electrode is not in equilibrium with solution. A typical example of this case can be the degradation of metals in solutions when the electrode acquires a certain corrosion potential.

The equilibrium state has several properties characteristic of it. Some of them deserve mention:

- No macrochemical changes take place at the boundary;
- E_{oc} value does not depend on the solution stirring intensity;
- E_{oc} value does not depend on the electrode surface state (the degree of the surface roughness, existence of adsorption layers, which do not participate in the charge transfer reaction, etc.);
- After switching off cathodic or anodic polarization, E_{oc} returns to the same initial value;
- E_{oc} value coincides with E_{eq}, which is calculated according to the Nernst equation.

As a fundamental parameter of electrochemical kinetics, overvoltage, is reckoned from E_{eq}, it is very important to establish the equilibrium nature of E_{oc}. Experimental verification of the specified criteria most often allows drawing an unambiguous conclusion on this subject. However, in studying complex systems, we encounter certain problems whose nature and ways of solving them will become clear from the examples presented next.

2.4.1 System Cu/Cu(I),CN^-

Due to its wide application in the plating industry, this subject of investigation has a 100-year-old history. Without dwelling on these problems related to kinetics and mechanism of electrochemical processes in this system, we are going to devote main attention to the copper electrode potentials E_{Cu}, which were measured under

the open-circuit conditions, and to their theoretical interpretation. One of the major features of the equilibrium potential E_{eq} is the fact that the Nernst equation applies to it. In performing these calculations, a convenient form of the Nernst equation can be chosen, which depends on the assumption about the charge transfer mechanism. However, it is necessary to underline that the results of correct calculation must not depend on the mechanism adopted.

Having made the assumption that Cu^+ aqua complexes participate in the charge transfer stage, that is, the process $Cu^+ + e \rightleftarrows Cu$ is occurring at the boundary, the Nernst equation will have a simple expression:

$$E_{eq} = E^{0/} + \frac{RT}{F} \ln[Cu^+]. \tag{2.22}$$

Assuming that one of Cu(I) cyanide complexes is electrochemically active, which participates in the process $Cu(CN)_j^{1-j} + e \rightleftarrows Cu + jCN^-$, the Nernst equation will become more complicated:

$$E_{eq} = E_j^{0/} + \frac{RT}{F} \ln \frac{[Cu(CN)]_j^{1-j}}{[CN^-]^j}. \tag{2.23}$$

When a more convenient variant of the equation is chosen, the first thing that draws attention is simplicity of Eq. (2.22), as well as the circumstance that the value of the standard potential of the electrode $Cu|Cu^+$ ($E^0 = 0.521$ V) is reliable and can be found in any reference book. However, concentration of "free" Cu^+ ions is not an obvious value, and having made no necessary calculations, the $[Cu^+]$ changes are difficult to image. Despite their more complicated form, equations of type Eq. (2.23) have the advantage that when using them, sometimes it is possible to make certain simplifications. For example, with a sufficient excess of ligand, complexes with saturated inner coordination sphere most often prevail in the solution. Let us assume that this assumption is valid for the system under investigation too and the prevailing complex is $Cu(CN)_4^{3-}$. Then, $[Cu(CN)_4^{3-}] = c_M$, and $[CN^-] = c_L - 4c_M$. What remains to do is to verify this assumption, which turns out to be incorrect. This prevailing complex [7] (Figure 2.10) is absent even from the solutions containing a seemingly large excess of ligand.

Hence, having chosen Eq. (2.22), all we have to do is to find the concentration of free Cu^+ ions by means of material balance Eqs. (1.17) and (1.18), which contain the stability constants β. In this connection, the problem of reliability of these values arises. It was a long time ago that attention was drawn to the fact [8] that according to various sources of literature, values of the stability constants of $Cu(CN)_2^-$ differed by 8 orders of magnitude. It is thought [8] that the value $\log \beta_2 = 24$, which was established at temperature 20 °C by means of solubility and potentiometric methods studying CuCN solutions in cyanic acid [9], should be regarded as the most reliable. Values of other constants – β_3 and β_4 – established by means of infrared spectroscopy [8], calorimetry [10], and potentiometry [11–13] methods coincide much better. It should be noted here that on the whole, in this specific case too, the use of potentiometric methods to establish stability constants is well-grounded provided that there is evidence

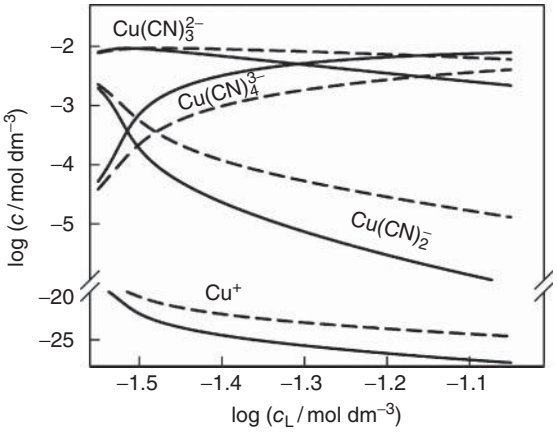

Figure 2.10 Distribution of Cu(I) cyanide complexes versus the total ligand concentration at 293 (solid lines) and 323 K (dotted lines). $c_{Cu(I)} = 0.01$ M, pH 10.2.

about the equilibrium nature of the open-circuit potential. However, there are contradictions concerning this issue too. It was stated [14] that due to electrode passivation, the difference between E_{Cu} and E_{eq} can exceed 0.3 V. However, in works [9, 11–13], the assumption was made that the Nernst equation could be applied to the E_{Cu} description and it could be used to establish the β values. This seems to be acceptable when temperatures are not comparatively high (20–25 °C). However, in establishing enthalpies of the formation of Cu(I) cyanide complexes, experimental data obtained within a wider range of temperatures are used. In this case, the ΔH values cited in works [8, 10] differ from those calculated from the experimental data [11, 13].

It was noticed [12] that deaeration of Cu(I) and Au(I) cyanide solutions gives rise to the E_{oc} variations and the potentials of relevant electrodes change going through the maximum. This process takes several hours until the steady state is reached. Phenomena of metal corrosion in the presence of cyanides and dissolved oxygen are well known. At some point of time, cyanides were even used to extract gold from the gold-deficient ores. Investigations [7] carried out with solutions of different temperatures showed that CN^- ions were not completely inert in deaerated Cu(I) solutions. It was discovered that at the time of the cyclic change of temperature lasting several hours, E_{Cu} failed to acquire the initial value and had a tendency to increase. It was also established that these effects did not depend on the state of the electrode surface but were related to changes in the solution phase, which occurred due to its interaction with the metal Cu electrode. During a longer contact, a diffusion layer with the certain concentration gradient forms at the electrode surface. Then, the E_{Cu} value depends on the solution stirring intensity. Irrespective of these phenomena, by means of properly chosen methodology, it is possible to obtain stable and well-repeating results. Solutions were deaerated by purified nitrogen for 1 h at room temperature. Then, the Cu

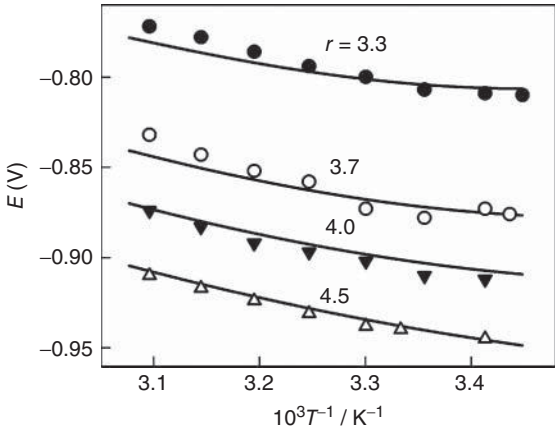

Figure 2.11 Variations of experimental open-circuit potentials (symbols) and simulated equilibrium potentials (lines) with temperature; pH is 10.2, $c_M = 0.01$ M. The ratio $r = c_L/c_M$ is indicated at the respective curves.

electrode was placed in the solutions that were constantly stirred and the temperature was changed rather slowly (~1 K min^{-1}). Errors of such experiments did not exceed 5%.

When E_{eq} was calculated according to Eqs. (1.17), (1.18), and (2.22), the average activity coefficient of Cu^+ ions γ was assumed to be equal to 0.6 [15], and in accordance with [8–13], the following values of the constants were adopted for 293 K temperature: $\log \beta_2 = 24.3$, $\log \beta_3 = 29.0$, $\log \beta_4 = 30.9$, $\log \beta^H = 9.31$. Eq. (1.6) and the ΔH values from [10] were used for a quantitative evaluation of β_j temperature dependence. Enthalpy $\Delta H = 37$ kJ mol^{-1} of the process $HCN \rightleftarrows H^+ + CN^-$ was calculated from [16] data. Besides, the temperature coefficient of $Cu|Cu^+$ electrode, $dE^0/dT = 0.813$ mV K^{-1}, was evaluated. The example of the results obtained is shown in Figure 2.11.

Despite the fact that different macroprocesses whose nature is discussed in our work [7] are possible in the system under study in the open-circuit conditions, the experimental E_{Cu} and theoretical E_{eq} values coincide very well. More significant differences between them have been observed only at higher temperatures when cyanide excess in the solution is not large. Hence, the conclusion can be drawn that within a rather wide range of solution compositions and temperatures, potentials of nonpolarized Cu electrodes are close to the equilibrium ones, which were calculated according to the Nernst equation. Due to a sufficiently large exchange current density within this system ($i_0 = 2–10$ mA cm^{-2} [17]), corrosion processes are unable to effect the E_{eq} value to a greater extent.

Experiments showed that an average corrosion current density $i = 0.15$ mA cm^{-2}. Having used a well-known kinetic equation

$$\Delta E = \frac{RT}{nF}\frac{i}{i_0}, \tag{2.24}$$

describing a voltammogram at low overvoltages, where the system can be regarded as linear, we obtain that deviations from the equilibrium potential ΔE are ~0.5–2 mV, that is, they do not exceed experimental errors. The above-presented statements about especially great differences between E_{Cu} and E_{eq} have to be admitted as being at variance with reality. Incorrectly evaluated concentration of free cyanide, which was established by means of titration (see above), should be considered to be its main reason.

2.4.2
System Cu/Cu(II), β-Alanine

The simplest amino acids such as glycine and α- or β-alanine are well-known ligands. If they are assigned the general formula LH, the equilibria in which proton donors and acceptors participate can be written as follows:

$$LH_{2+} \underset{H^+}{\overset{OH^-}{\rightleftharpoons}} LH \underset{H^+}{\overset{OH^-}{\rightleftharpoons}} L^-. \tag{2.25}$$

Anion L^- is the active form of ligand, which together with Cu(II) forms complexes CuL^+ and CuL_2. Ligand species LH and LH_2^+ do not form stronger coordination bonds because a free pair of electrons at the nitrogen atom is used to connect the proton. The complexation degree of Cu(II) solutions falls in the sequence glycine > α-alanine > β-alanine; therefore, the most favorable conditions for the Cu_2O layers to form are in the solutions containing the latter ligand. Critical pH, at which the Cu_2O layers become thermodynamically stable, is about 3.3.

The reliability of the β values presented in literature raises no doubts. To characterize the Cu|Cu(II) β-alanine system, we selected from [16] such data, which best matched the ionic strength of the solutions: $\log \beta_1 = 7.34$, $\log \beta_2 = 12.8$, $\log \beta_1^H = 10.2$, $\log \beta_2^H = 13.84$. When calculating equilibrium potentials, apart from these values, the values of standard potentials and the activity coefficients of Cu^+ and Cu^{2+} ions equal to 0.6 and 0.07 [18], respectively, were used. The latter value is rather low in the sulfate medium (solutions containing 0.3 M K_2SO_4) because Cu^{2+} ions tend to form associates with SO_4^{2-}.

Using traditional experimental methodologies, it is impossible to achieve the above-described total equilibrium. Therefore, it is necessary to take into consideration the circumstance that certain processes are not in the equilibrium state. In this connection, the choice of specific modification of the Nernst equation is no longer a matter of convenience but requires an additional theoretical substantiation. It is necessary to resolve the problem which of the charge transfer stages determines the electrode potential. The analysis showed that in the case of the Cu|Cu(II), β-alanine system, this process is transfer of the first electron to Cu^{2+} ion

$$Cu^{2+} + e \rightleftarrows Cu^+ \tag{2.26}$$

Then

$$E_{eq} = E_{21}^{0/} + \frac{RT}{F} \ln \frac{[Cu^{2+}]}{[Cu^{+}]}. \tag{2.27}$$

This equation was used when calculating potentials of the first and second kind of electrodes (Figure 2.12). In the first case, $[Cu^+]$ was obtained from the constant $K = 6 \times 10^{-7}$ M at the equilibrium

$$Cu + Cu^{2+} \rightleftarrows 2Cu^{+}. \tag{2.28}$$

This procedure is equivalent to the use of Eq. (2.17). When evaluating the possibility of Cu_2O formation, that is, in the case of second kind of electrodes, the following was performed. Cu^+ concentrations, which were calculated in two ways, were compared: in the above-specified way and using condition (2.20) under which M^+ is Cu^+ ions and $a = -0.84$ [19]. The lower $[Cu^+]$ value was inserted in Eq. (2.27).

E_{eq} dependencies on pH obtained for the electrodes of the first kind are shown in Figure 2.12 by dotted lines. Experimental E_{Cu} values coincide well with theoretical ones in the sufficiently acid medium only where pH < 3.3. In less acid solutions (3.3 < pH < 6), their deviations from the E_{eq} values calculated for the first kind of electrode are observed. In this transitional sphere, the Nernst equations no longer apply for E_{Cu} quantitative description and kinetic data are necessary for that. Finally, in alkaline media, the experimental E_{Cu} values correspond with the equilibrium characteristics of the electrode of the second kind.

It should be noted that oxide layers formed on Cu at pH > 5 are easily established visually. Their color depends on pH of solutions and the duration of exposition. Experiments carried out by means of electrochemical quartz crystal microgravimetry (EQCM) showed [20] that at first, the Cu electrode

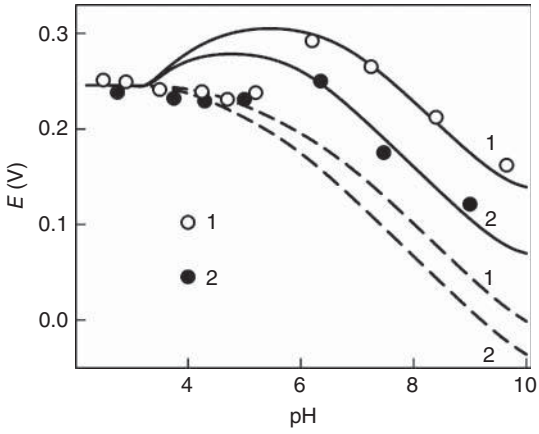

Figure 2.12 Comparison of experimental E_{Cu} (symbols) and E_{eq} values simulated for the electrode of the first (dotted lines) and second (solid lines) kind. Cu|Cu(II), β-alanine system; $c_M = 0.01$ M; the ratio $r = c_L/c_M$ is equal to 4 (1) and 10 (2).

mass decreased irrespective of pH of the solutions with which it was in contact. However, within a certain time during which the solution layer adjacent to the electrode becomes saturated with Cu^+ ions, the electrode mass either stabilizes ($pH < 3.3$) or begins to increase due to the formation of oxides in less acid media. The composition of these layers, their properties, and impact on the electroreduction processes of metals will be discussed in the next Chapter 10.

References

1. Damaskin, B.B., Petrii, O.A., and Tsirlina, G.A. (2001) *Electrochemistry*, Khimiya, Moscow (in Russian).
2. Survila, A., Juozėnienė, B., and Višomirskis, R. (1982) Kinetics of Zn reduction on dropping Hg electrode in cyanide solutions. *Proc. Lithuanian Acad. Sci. Ser. B*, **4** (131), 35–42.
3. Skonecki, E. and Bialozor, S.G. (1980) On the mechanism of copper cathodic deposition from aminoacetic acid electrolyte. *Elektrokhimiya*, **16** (7), 1025–1028.
4. Kravtsov, V.I. (1985) *Equilibrium and Kinetics of Electrode Reactions Involving Metal Complexes*, Leningrad State University, Leningrad.
5. Molodov, A.I., Markos'yan, G.N., Lyumkis, I.R., and Losev, V.V. (1973) The study of the influence of the concentration of univalent copper on copper open-circuit potential. *Elektrokhimiya*, **9** (10), 1460–1467.
6. Survila, A., Kanapeckaitė, S., and Survilienė, A. (2001) Cathodic processes in ligand-deficient Cu|Cu(II), ethylenediamine system. *J. Electroanal. Chem.*, **501** (1-2), 151–159.
7. Sabonienė, E., Mikučionis, G., and Survila, A. (1987) Unpolarized Cu electrode potentials in Cu(I) cyanide solutions. *Proc. Lithuanian Acad. Sci. Ser. B*, **6** (163), 26–33.
8. Penneman, R.A. and Jones, L.H. (1956) Infrared absorption studies of aqueous complex ions. II. Cyanide complexes of Cu (I) in aqueous solution. *J. Chem. Phys.*, **24** (2), 293–296.
9. Vladimirova, M.G. and Kakovskii, I.A. (1950) Physico-chemical constants of the formation and the composition of the lower copper cyanide complex. *Zh. Prikl. Khim.*, **23** (6), 580–598.
10. Izzat, R.M., Johnston, H.D., Watt, G.D., and Christensen, J.J. (1967) Thermodynamics of metal cyanide coordination. VI. Copper (I) and silver (I)-cyanide systems. *Inorg. Chem.*, **6** (1), 132–135.
11. Bek, R.Y., Zhukov, B.D., Borodikhina, A.I., and Poddubnii, N.P. (1973) Study of electrodeposition of copper from cyanide electrolytes. II. Constants of copper cyanide complex formation. *Izv. SO AN SSSR. Ser. Khim.*, **9** (4), 52–56.
12. Hancock, P.D., Finkelstein, N.P., and Evers, A. (1972) Stabilities of the cyanide complexes of the IB group monovalent metal ions in aqueous solution. *J. Inorg. Nucl. Chem.*, **34** (12), 3747–3751.
13. Rothbaum, H.P. (1957) The composition of copper complexes in cuprocyanide solutions. *J. Electrochem. Soc.*, **104** (11), 682–686.
14. Višomirskis, R.M. (1969) *Kinetics of Electrodeposition of Metals from Complex Electrolytes*, Nauka, Moscow (in Russian).
15. Halley, J.W., Smith, B.B., Walbran, S., Curtiss, L.A., Rigney, R.O., Sutijanto, A., Hung, N.C., Yonco, R.M., and Nagy, Z. (1999) Theory and experiment on the cuprous-cupric electron transfer rate at a copper electrode. *J. Chem. Phys.*, **110** (13), 6538–6552.
16. Sillen, L.G. and Martel, A.E. (1964, 1971) *Stability Constants of Metal-Ion Complexes*. Special Publications No. 17 and 25, Chemical Society, London.
17. Costa, M. (1963) Contribution à l'étiude de la cinétique de la réaction de l'electrode cuivre/cyanure double de cuivre et de potassium. *J. Rech. Centre Nat. Rech.*, **64**, 285–315.
18. Survila, A. and Spudas, L. (1981) On the reversibility of discharge of Cu (II) in

glycine solutions. *Proc. Lithuanian Acad. Sci. Ser. B*, **5** (126), 27–33.

19. Pourbaix, M. (1966) *Atlas of Electrochemical Equilibria in Aqueous Solutions. Part 2*, Pergamon Press, London.
20. Survila, A., Kalinauskas, P., Ivaškevič, E., and Kutner, W. (1997) Simultaneous photoelectrochemistry and piezoelectric microgravimetry, with the use of electrochemical quartz crystal microbalance, of surface layers formed at the Cu/Cu(II), β-alanine interface. *Electrochim. Acta*, **42**, 2935–2941.

3
Mass Transport

The main act of the electrochemical process, charge transfer, is localized in a very thin double electric layer. This process can take place continuously only when electrically active particles, that is, particles that participate in the charge transfer step are transferred toward the electrode, and the products formed move in the opposite direction – from the surface of the metal phase of the electrode to the solution volume. When electrochemical deposition of metal takes place in simple (noncomplex) salt solutions, there may be no transport of the product, because the metal atoms formed do not participate in the diffusion process, and they form a new solid phase – a crystal lattice.

Diffusion, migration, and convection are the three possible mass transport processes accompanying an electrode reaction. In the first case, the particles move due to the formed concentration gradient. The flux in the case of planar (one-dimensional or linear) diffusion can be described by Fick's first law:

$$J_i(x,t) = -D_i \frac{\partial c_i(x,t)}{\partial x}, \tag{3.1}$$

where J_i is the flux of species i, D_i, and c_i are the diffusion coefficient and the concentration of species i, respectively, x is the location, and t is the time. The minus sign shows that the diffusion proceeds from places where the concentration of i is higher toward those of lower concentration. When Fick's first law is combined with the equation of continuum, $\partial c/\partial t = -\partial J/\partial x$, it becomes Fick's second law

$$\frac{\partial c_i(x,t)}{\partial t} = D_i \frac{\partial^2 c_i(x,t)}{\partial x^2}, \tag{3.2}$$

for the diffusion coefficient independent of x.

The electric field, which always exists in electrochemical systems, also has an effect on the charged particles. Hence, they can move in the migration way too, whose driving force is the potential gradient $d\varphi/dx$. Migration of the electrically active species can either enhance (e.g., during the reduction of cations) or diminish (e.g., during the reduction of anions) the current flowing at the electrode.

When diffusion is coupled with migration, the appropriate form of the Nernst–Planck equation has to be solved. For instance, when the ion with charge ze is distributed at concentration c and the potential φ, a one-dimensional flux of

Electrochemistry of Metal Complexes: Applications from Electroplating to Oxide Layer Formation, First Edition.
Arvydas Survila.

the ion is described by the relationship:

$$J_i(x,t) = -D_i \frac{\partial c_i(x,t)}{\partial x} - \frac{zF}{RT} Dc \frac{\partial \phi(x,t)}{\partial x}. \tag{3.3}$$

The intensity of migration mass transport can be significantly reduced by adding an excess of indifferent electrolyte whose ions are electrically inactive within a wide range of the potentials, that is, they do not participate in the charge transfer process. These ions create the electric field of the opposite direction, which compensates for the aforementioned potential gradient to a great extent. This simplifies the theoretical description of the current.

Contrary to diffusion or migration when transport of the species occurs by a molecular mechanism, in the case of convection the movement of whole volume elements of solution takes place. The intensity of this process is determined by the flowing rate of fluid. Convection may occur due to density gradients (natural convection) that arise for different reasons, which are sometimes difficult to control. In the first place, changes in the solution density near the electrode surface should be assigned to them. The latter, in their turn, depend on the electrode orientation in the gravitational field, the thermal effect of the electrochemical process, and so on.

Forced convection is often applied to enhance the rate of the mass transport process. It can be achieved by stirring the solution with the help of a separate stirrer, or the electrode itself can rotate, vibrate, or even simply expand its volume (which is a movement of its surface against the solution) as the dropping mercury electrode does. In the case of forced convection, the fluid flow can be laminar flow or turbulent flow. The flux of species i driven by one-dimensional motion along the x-axis can be given as follows:

$$J_i(x) = c_i v(x), \tag{3.4}$$

where $v(x)$ is the velocity with which a volume element in the solution moves.

The exact solution of the convection–diffusion equations is complicated, because the theoretical treatments involve solving a hydrodynamic problem, that is, the determination of the solution flow velocity profile by using Navier–Stokes equation. For the calculation of a velocity profile, the solution viscosity, densities, rotation rate, or stirring rate, as well as the shape of the electrode should be considered. Exact solution has been derived for the rotating disc electrode (RDE):

$$\delta = 1.61 \nu^{1/6} D^{1/3} \Omega^{-1/2}, \tag{3.5}$$

where ν is the kinematic viscosity of the solution and Ω is the angular velocity of the rotation. It was established that the thickness of the fictitious diffusion layer is uniform over the entire surface of the disc. This made it possible to simplify the mathematical apparatus of mass transport that is taking place in the conditions of forced convection, assuming that diffusion of particles is taking place in the immovable layer whose thickness is expressed through various hydrodynamic parameters.

As diffusion always exists, main attention should be paid to this way of mass transport.

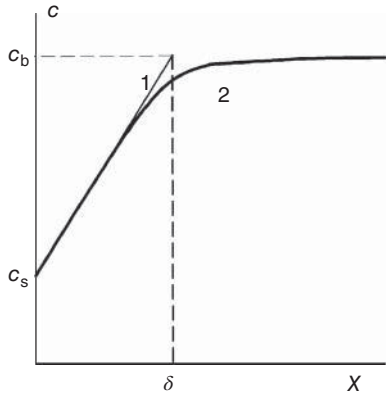

Figure 3.1 Linear approximation (1) and real (2) concentration profile in the diffusion layer.

3.1 Two Models of Linear Mass Transport

A quantitative description of mass transport is related to certain model images. Let us consider a flat metal electrode of unlimited dimensions, which is in electrochemical equilibrium with the salt solution of the same metal containing an excess of indifferent electrode. In these conditions, the concentration gradient outside of the double electrode layer is equal to zero, that is, M^{n+} ion concentration is constant and equals the bulk one (c_b). After switching on, for example, the cathodic current, M^{n+} ions reduction starts, their surface concentration[1] (c_s) decreases, and the concentration gradient appears in a thin layer close to the electrode/solution interface. The boundary, which arises between the solution layer with the decreased concentration and the region where concentration is still equal to c_b, is often called the *diffusion front*. The concentration profile (c dependence on x), which forms at a certain time, is shown in Figure 3.1 by a thick line. Generally, there is a linear profile close to the electrode surface, and at longer distances from the electrode surface, the concentration asymptotically approaches the bulk concentration. The effective thickness (δ) of such a diffusion layer is determined according to the equation

$$\delta = \left(c_b - c_s\right) / \left.\frac{\mathrm{d}c}{\mathrm{d}x}\right|_{x=0} \tag{3.6}$$

that is, it is obtained by extrapolation of the linear part of the concentration profile to the bulk concentration, as shown in Figure 3.1.

In the case of non-steady-state diffusion, the diffusion layer becomes thicker with time because ions are transported from ever more distant areas. Then, the diffusion front gradually moves from the electrode surface to the bulk of the solution. Two main images are used in modern theories. According to semi-infinite diffusion model, the diffusion front is allowed to move from the electrode surface

1) We have in mind the region outside of the double electric layer where the condition of electroneutrality is already obeyed.

without any restrictions. This means that with time, the effective δ can grow to infinity. Similar conditions can be created during the experiment too by arranging special cells where diffusion takes place in sufficiently thin and long capillaries.

Conventional electrochemical cells have no such arrangement; therefore, spontaneous convection flows, which limit the diffusion front shift, can form in them. One of the simplest models, which can evaluate this phenomenon, was proposed by Nernst. According to it, diffusion takes place in a layer of stagnant solution close to the electrode/solution interface. As mentioned earlier, the thickness of the Nernst layer increases with time until natural convection sets in, after which it remains constant. In the presence of forced convection (stirring, electrode rotation), the Nernst layer thickness depends on the intensity of convection that can be controlled, for example, by controlling the rotation speed of an RDE. Hence, the diffusion front can move only as far as to the boundary of the Nernst-type layer. Then, $c(x)$ no longer depends on time and the so-called steady state is reached.

Despite the fact that the Nernst model is rather rough, it has been used in electrochemical kinetics up till now due to its simplicity and obviousness. It has been established by means of different methods that similar structures actually form in the conditions of natural convection. Their thickness makes up 0.01 – 0.03 cm; however, it is rather difficult to strictly define δ_N because it depends on various factors, including the current density *i*. The empirical regularity $\delta_N i^{0.2} \approx$ const has been established experimentally under the steady-state conditions [1]. It should be mentioned that δ_N varies with the potential sweep rate ν when a linear variation of potential $E = E_{eq} - \nu t$ is applied. The regularity of $\delta_N \sqrt{\nu} \approx$ const was previously determined for the $Fe(CN)_6^{4-}/Fe(CN)_6^{3-}$ system [2] and was found to be also valid for Cu(II) solutions containing glycolic and gluconic acids [3, 4]. Slopes of linear $\delta_N - \nu$ plots, presented in logarithmic coordinates (Figure 3.2), range from 0.48 to 0.54.

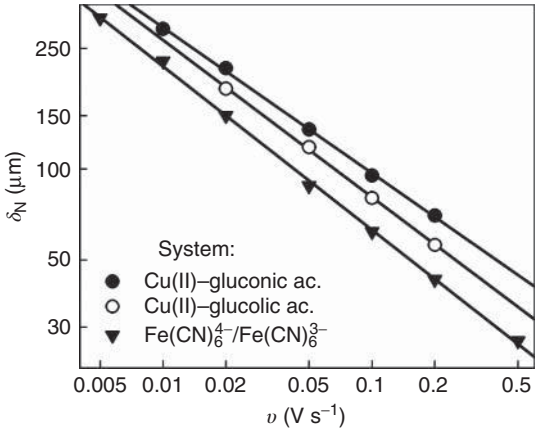

Figure 3.2 Effective thickness of diffusion layer versus potential sweep rate in logarithmic coordinates. The data obtained under natural convection conditions for different redox systems as indicated.

The attempts have been made to substantiate this regularity theoretically [5–8]. Though the models used support a linear dependence between δ and $1/\sqrt{\nu}$, nevertheless the δ values following from these theoretical models are 1 order of magnitude lower than experimental quantities. More realistic data follow from another approach [9] based on Levich's view of microscopic chaotic motion that takes place in the viscous sublayer adjacent to any wall or electrode surface. The $\delta = 230\,\mu m$ was found from analysis of chronoamperometric transients obtained for one-electron reversible oxidation of $Fe(CN)_6^{4-}$; this result is in line with the respective data in Figure 3.2.

Both the semi-infinite diffusion and Nernst's steady diffusion layer concept produce the same results when the diffusion front shift is not yet large as compared to δ_N. In these conditions, the semi-infinite diffusion model, which is simpler from the mathematical point of view, is to be applied. However, the Nernst model is more general because the regularities of the first model follow from it at $\delta_N \to \infty$.

The analysis of diffusion transport is made, first of all, seeking to establish surface concentrations of reactants and products, which are included in the equations of electrochemical kinetics. Such procedures are described in literature sufficiently fully. There are fewer data about the concentration profiles, which form in more complicated systems. Information about it is necessary, for example, in studying the possibilities for the formation of insoluble compounds in the diffusion layer [10, 11].

Now, we shall pass over to the simplest mathematical expressions, which distinguish themselves by universality and can be applied to the solution of more complicated problems. Let us assume that the process $M^{n+} + ne \to M$ during which a metal M crystal lattice forms takes place in the M^{n+} solution containing an excess of indifferent electrolyte. In a general case, the current density i depends on time, whereas M^{n+} concentration is the function of the coordinate x and time t. The concentration profile $c(x,t)$ can be calculated after solving the differential equation representing Fick's second law Eq. (3.2) with corresponding initial and boundary conditions.

When the system is in the initial equilibrium state ($t = 0$), the following condition applies

$$c(x, 0) = c_b, \tag{3.7}$$

meaning that there is no diffusion gradient at the initial moment. The form of one of the boundary conditions depends on the diffusion model type. As regularities of semi-infinite diffusion can be determined from the more general Nernst model, having found the solution limit at $\delta \to \infty$, we shall consider it next. It follows from the Nernst model that

$$c(\delta_N, t) = c_b. \tag{3.8}$$

The second boundary condition follows from Fick's first and Faraday's laws:

$$\left.\frac{\partial c\,(x, t)}{\partial x}\right|_{x=0} = -\frac{i(t)}{nFD}. \tag{3.9}$$

When solving this problem, it is convenient to use the Laplace transform. Following a series of rearrangements, we obtain that the surface concentration of M^{n+} ions is expressed in terms of the equation

$$c(0,t) = c_b + \frac{1}{nF\sqrt{\pi D}} \int_0^t \frac{i(t-u)}{\sqrt{u}} \Psi(u) \mathrm{d}u, \tag{3.10}$$

In this equation, u is the auxiliary variable having the time dimension. The variable t is replaced with the variable $(t-u)$ in the current density function $i(t)$. Function

$$\Psi(u) = 1 + 2\sum_m^\infty (-1)^m \exp\left(-\frac{m^2\delta^2}{Du}\right) \tag{3.11}$$

accounts for the existence of the Nernst-type layer. The nature of its change is represented in Figure 3.3 from which it is seen that the time of transfer into the steady state depends to a great extent on the thickness of the diffusion layer and is proportional to its square. When $\delta \to \infty$, $\Psi(u) \to 1$. Hence, semi-infinite diffusion and Nernst models give the same result when $\Psi(u)$ is close to unity. On the other hand, steady state is achieved when $\Psi(u) \to 0$, or when $t \to \infty$. Then, Eq. (3.10) is transformed into the analog of Eq. (3.9):

$$c(0,\infty) = c_b + i\delta_N/nFD, \tag{3.12}$$

which is well known in electrochemical kinetics.

Though in the general case, mathematical expressions of the Nernst model are more complicated than of those semi-infinite diffusion, stationary mass transport is described by a rather simple Eq. (3.12). In this connection, there occurs an interesting possibility to use superposition of both models, which is convenient to apply when i is the periodic time function. Perturbation signals of this type are considered in the theory of electrochemical impedance spectroscopy. In this case, $i(t)$

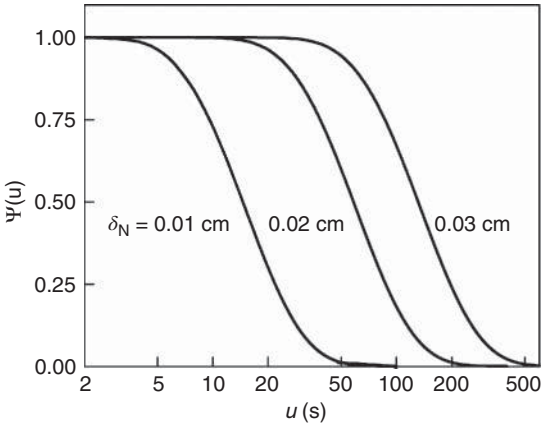

Figure 3.3 Values of $\Psi(u)$ obtained at different thickness of diffusion layer $D = 5 \times 10^{-6}\mathrm{cm}^2\ \mathrm{s}^{-1}$.

can be divided into two parts: steady i_s and alternating $\Delta i(t)$ components:

$$i(t) = i_s + \Delta i(t). \tag{3.13}$$

It follows from the equations that the expression of the surface concentration $c(0,t)$ will have an analogous structure. Within a certain period of time when the condition $\Psi(u) \to 0$ has been reached (see Figure 3.3), the expression Eq. (3.12) yields the steady $c(0,t)$ component. Provided that periodical concentration changes, which are caused by $\Delta i(t)$, are localized in a rather thin layer (as compared with δ_N), regularities of semi-infinite diffusion can be applied to them. This method allows the mathematical apparatus of mass transport to be simplified.

In conclusion, it should be noted that in case of the controlled current density, that is, when the function $i(t)$ is specified, no assumptions about the charge transfer mechanism and its kinetic parameters are to be used in calculating concentration profiles. The situation, however, changes when the electrode potential is controlled, that is, when the system is perturbed by the signal $E(t)$ of a defined shape. This case requires a separate analysis.

3.2
Other Cases of Diffusional Mass Transport

A (hemi)spherical electrode has been applied to estimation of charge transfer kinetics, effect of electric migration, and kinetics of chemical steps. Spherical diffusion takes place through an increasing area as the radial coordinate *r*, measured from the center of the spherical electrode, increases. The main differential equation for three-dimensional mass transport is given in Table 3.1. On substitution of $c = y/r$, this relationship can be reduced to the one-dimensional mass transport yielding

$$\frac{\partial y}{\partial t} = D\frac{\partial^2 y}{\partial r^2}. \tag{3.14}$$

In contrast to the semi-infinite diffusion at a plane electrode, this diffusion equation has the steady-state solution

$$c_s = c_b(1 - r_0/r), \tag{3.15}$$

where r_0 is the radius of the spherical electrode. The expression for limiting diffusion current is obtained when the surface concentration $c_s \to 0$. Spherical diffusion has often been employed for a model of the microelectrode behavior, when the radius of the electrode is much larger than the shift of diffusion front estimated as $\sim \sqrt{Dt}$. Sometimes, it was also used for description of diffusion at an edge of a planar electrode. Besides, diffusion at an expanding sphere has been analyzed as applied to polarography.

Solid electrodes utilized in electrochemical investigations are often made of wire and present a small cylinder with radius r_0 and height *h*. It is commonly assumed that symmetric diffusion flows are directed toward side surface, whereas

Table 3.1 Differential equations for various electrode geometries.

Electrode	Equation
Planar	$\frac{\partial c(x,t)}{\partial t} = D\frac{\partial^2(x,t)}{\partial x^2}$
(Hemi)sphere	$\frac{\partial c(r,t)}{\partial t} = D\left(\frac{\partial^2 c(r,t)}{\partial r^2} + \frac{2}{r}\frac{\partial c(r,t)}{\partial r}\right)$
Cylinder	$\frac{\partial c(r,t)}{\partial t} = D\left(\frac{\partial^2 c(r,t)}{\partial r^2} + \frac{1}{r}\frac{\partial c(r,t)}{\partial r}\right)$
Inlaid disk	$\frac{\partial c(r,t)}{\partial t} = D\left(\frac{\partial^2 c(r,t)}{\partial r^2} + \frac{1}{r}\frac{\partial c(r,t)}{\partial r} + \frac{\partial^2 c(z,t)}{\partial z^2}\right)$
Inlaid band	$\frac{\partial c(r,t)}{\partial t} = D\left(\frac{\partial^2 c(r,t)}{\partial r^2} + \frac{\partial^2 c(z,t)}{\partial z^2}\right)$

small disks at the bottom or/and at the top are ignored. The relation obtained is somewhat similar to that derived for spherical diffusion (Table 3.1).

Electrodes of different shapes (disk, ring, cylinder, sheet, spiral, etc.) shielded by insulator are referred to as *inlaid electrodes*. The inland disc, for instance, is characterized by the radial distance, r, measured from the center of the disk and distance z, normal to the disk. When the radius of such electrode is large, diffusion occurs predominantly linearly in the z direction to the center of the disk with a small radial diffusion contribution from the edges of the disk. In the case of ultramicroelectrodes, where the diameter is on the order of 20 μm or smaller, the diffusion is predominantly radial to the edges leading to a steady-state current. Under steady-state conditions, the left-hand side of the differential equation (Table 3.1) is zero. This is also true for spherical, hemispherical, ring, and conical geometries but not for cylindrical or band geometries, which do not reach a steady state.

Inlaid electrodes can be arranged in groups using lithographic procedures or electrochemical or electroless template deposition methods. Modern technologies make it possible to manufacture electrodes of very small dimensions (down to 0.2 – 1 μm of order) [12], by using different materials. Microelectrodes and their ensembles (arrays) have been investigated from both theoretical and experimental point of view; a comprehensive review of papers is given in Ref. [13].

The behavior of array electrodes depends on the ratio of the diameter of the individual electrode to the spacing between electrode features. High diffusion current densities conditioned by radial flows and low values of ohmic potential drop are most prominent in the case of ultramicroelectrodes [13, 14]. By replacing a single macroelectrode by an array of ultramicroelectrodes, the current density can be increased by orders of magnitude as well as the ratio of faradaic to capacitive currents.

The so-called partially blocked electrodes containing active and passive sites can be also treated as microelectrode arrays, when the charge transfer is utterly impossible at the passive area. Simulations of their electrochemical behavior under linear potential sweep conditions showed [15] that a good agreement

between experimental and numerical results can be obtained with precise formulation of boundary conditions.

3.3 Mass Transport of Chemically Interacting Particles

Chemical interactions, which take place not only in the solution volume but also in the diffusion layer, are characteristic of the systems of metal complexes. Electrically active complex (EAC), which directly participates in the charge transfer step, can be formed from other complex particles upon their dissociation, or, on the contrary, when a certain quantity of ligand is attached to them. After EAC reduction takes place, released ligand can also chemically interact with other components of the solution. Hence, in a general case, electrochemical changes take place in accordance with the so-called CEC mechanism (chemical step + electrochemical step (charge transfer reaction) + chemical step). Some cases of this mechanism were considered earlier [16]; however, analytical solutions are possible only when a chemical reaction is of the first (or pseudo-first) order. In case of higher degrees, such solutions no longer exist.

To evaluate the influence of chemical stages on mass transport, we shall consider a simple complex system containing M^{n+}, ML^{n+}, ML_2^{n+}, and L particles. The charge of free ligand L is conditionally assumed to be equal to zero. As the solution is considered to contain an excess of indifferent electrolyte, the migration influence is insignificant and the assumption made has no impact on the conclusions being drawn. Moreover, the increase in the number of the particles under investigation does not change the results either.

Chemical interactions taking place in the system under discussion can be written in the following way:

$$M^{n+} + L \underset{k_{-1}}{\overset{k_1}{\rightleftharpoons}} ML^{n+}, \tag{3.16}$$

$$ML^{n+} + L \underset{k_{-2}}{\overset{k_2}{\rightleftharpoons}} ML_2^{n+}, \tag{3.17}$$

where k is the rate constants of direct (positive indexes) and reverse (negative indexes) reactions. Rates of these processes (w) are described by means of orthodox equations of chemical kinetics:

$$w_1 = k_1[M^{n+}][L], \tag{3.18}$$

$$w_{-1} = k_{-1}[ML^{n+}], \tag{3.19}$$

$$w_2 = k_2[ML^{n+}][L], \tag{3.20}$$

$$w_{-2} = k_{-2}[ML_2^{n+}]. \tag{3.21}$$

Concentrations of species indicated in the square brackets are functions of the coordinate x and time t. In solving the diffusion problem, Fick's second law with

kinetic terms, reflecting changes in the particles concentration caused by chemical interaction, must be written for each particle. Then, in the case of one-dimensional diffusion at planar electrode,

$$\frac{\partial[\mathrm{M}^{n+}]}{\partial t} = D\frac{\partial^2[\mathrm{M}^{n+}]}{\partial x^2} - w_1 + w_{-1}, \tag{3.22}$$

$$\frac{\partial[\mathrm{ML}^{n+}]}{\partial t} = D\frac{\partial^2[\mathrm{ML}^{n+}]}{\partial x^2} + w_1 - w_{-1} - w_2 + w_{-2}, \tag{3.23}$$

$$\frac{\partial[\mathrm{ML}_2^{n+}]}{\partial t} = D\frac{\partial^2[\mathrm{ML}_2^{n+}]}{\partial x^2} + w_2 - w_{-2}, \tag{3.24}$$

$$\frac{\partial[\mathrm{L}]}{\partial t} = D\frac{\partial^2[\mathrm{L}]}{\partial x^2} - w_1 + w_{-1} - w_2 + w_{-2}. \tag{3.25}$$

Having added Eqs. (3.22), (3.23), and (3.25), we obtain:

$$\frac{\partial c_{\mathrm{M}}(x,t)}{\partial t} = D\frac{\partial^2 c_{\mathrm{M}}(x,t)}{\partial x^2}, \tag{3.26}$$

where c_{M} is the total (analytical) metal concentration ($c_{\mathrm{M}} = [\mathrm{M}^{n+}] + [\mathrm{ML}^{n+}] + [\mathrm{ML}_2^{n+}]$). Similarly, a linear combination of Eqs. (3.23)–(3.25) gives the following:

$$\frac{\partial c_{\mathrm{L}}(x,t)}{\partial t} = D\frac{\partial^2 c_{\mathrm{L}}(x,t)}{\partial x^2}, \tag{3.27}$$

where c_{L} is total (analytical) ligand concentration ($c_{\mathrm{L}} = [\mathrm{ML}^{n+}] + 2[\mathrm{ML}_2^{n+}] + [\mathrm{L}]$). The obtained expressions (3.26) and (3.27) no longer contain kinetic members. This result is obtained without any assumptions about rate constants of chemical transformations and is valid for both labile and inert complexes.

Having in mind the fact that it is only the particles containing metal that can reduce and that ligand is regarded to be electrically inactive, initial and boundary conditions are specified by Eqs. (3.7)–(3.9) in which the value c is replaced with concentration c_{M}.

Two main conclusions follow from the aforementioned fact:

- the total metal concentration varies in the same way as the concentration of "free" metal ions in the absence of ligand;
- the total concentration of electrically inactive ligand is constant throughout the entire diffusion layer and beyond it.

Let us consider another system, which also contains protonated ligand forms. We shall assume that they are unable to form coordination bonds with M^{n+} ions for the reason that a proton, when bound to the donor atom of ligand, blocks the free electron pair. For the sake of simplicity, we shall limit ourselves to only one of such particles, namely to LH^+. Then, the above-listed chemical interactions Eqs. (3.16) and (3.17) are to be supplemented with the following reactions: $\mathrm{L} + \mathrm{H}^+ \rightleftarrows \mathrm{LH}^+$ and $\mathrm{H}^+ + \mathrm{OH}^- \rightleftarrows \mathrm{H_2O}$. An analogous analysis shows that the

same dependencies Eqs. (3.26) and (3.27) are obtained in this case too. However, regularity appears, which can be expressed by means of the following equation:

$$\frac{\partial c_{\mathrm{H}}(x,t)}{\partial t} = D\frac{\partial^2 c_{\mathrm{H}}(x,t)}{\partial x^2}, \tag{3.28}$$

where c_{H} is the total concentration of proton donors and acceptors. Contrary to analytical concentrations c_{M} or c_{L}, the value c_{H} is formed artificially. It is a formal quantity composed of the concentrations of the particles that release protons (with a positive sign) and of those that are able to join protons (with a negative sign). Hence, it can also be negative in alkaline media. In the present case, $c_{\mathrm{H}} = [\mathrm{H}^+] + [\mathrm{LH}^+] - [\mathrm{OH}^-]$. If H^+ or OH^- ions are electrochemically inactive, c_{H} is constant throughout the entire diffusion layer and beyond it.

It was accepted in the above-presented equations that diffusion coefficients of all the particles were equal. If the size of complexes or ligands is similar, such an assumption is justified. However, it is known that H^+ and OH^- ions distinguish themselves from other by their greater mobility, which is determined by the so-called structural diffusion (Grotthuss mechanism) involving a shift of structural units as a result of rearrangement of the protons without a considerable shift of water molecules themselves.

Theories of various electrochemical analysis methods (polarography, chronopotentiometry, RDE, etc.) state that the thickness of the diffusion layer depends on *D*. Hence, if diffusion coefficients of certain particles differ, thickness of their diffusion layers must be different. When applying such images to the systems of metal complexes, contradictions arise, which are especially obvious in the case of labile complexes. Individual δ_j with its own D_j should exist for each particle. Let us imagine that particles of one kind have an increased mobility. Then, with diffusion mass transport going on, their excess will appear in a certain region of the solution, which will bring about respective shifts of chemical equilibria. As a result, some part of more mobile particles will have to react with other components of the solution. Formally, the same result can be obtained by assigning a lesser D_j to these particles. If we investigate the particles of the reduced mobility, on the contrary, their D_j should be increased. Thus, the mechanism that allows one and the same effective *D* to be assigned to all the particles appears in the systems of sufficiently labile complexes. This mechanism was studied in more detail in [17]; similar conclusions were reached in investigating combined H^+ and HSO_4^- diffusion [18, 19].

The value of the effective *D* of complexes can be obtained from the equation

$$\sum_{j=0}^{N} D_j \frac{\partial[\mathrm{ML}_j^{n+}]}{\partial x} = D\sum_{j=0}^{N} \frac{\partial[\mathrm{ML}_j^{n+}]}{\partial x} = D\frac{\partial c_{\mathrm{M}}}{\partial x}, \tag{3.29}$$

where *N* is the maximum number of ligand in the complex molecule. Then,

$$D = \frac{\sum_{j=0}^{N} D_j \beta_j [L]^j}{\sum_{j=0}^{N} \beta_j [\mathrm{L}]^j}. \tag{3.30}$$

When ML_N^{n+} complexes prevail in the system, the earlier published [20] equation

$$D = \frac{D_0 + D_N \beta_N [L]^N}{1 + \beta_N [L]^N}. \tag{3.31}$$

is obtained from Eq. (3.30). It should be noted that the analysis of D dependence on [L] was used to determine β_N.

Thus, in describing mass transport of complexes, one can use the value of the effective D, which depends on the composition of the solution and the individual D_j, which are not always known. Therefore, it is most convenient to obtain D from the experimental data (limiting currents, transition times, etc.), which are determined by the diffusion process characteristics. Then, classical equations, which were derived for simple systems, can be used by replacing the value c with c_M in them.

3.4 Concentration Profiles

Various methods were proposed for the investigation of the composition of diffusion layers (for brief reviews see Refs. [1, 21]). Some data concerning the thickness of the layers formed under the natural convection conditions (about 0.03 cm) was obtained by means of the interferometry. Brenner used fast freezing of the solution during electrolysis. Then, the frozen layer at the electrode surface was cut into layers as thin as possible, which were further analyzed. Samples for the chemical analysis were taken in other ways too, for example, by sucking off the electrolyte layer from the electrode surface. The electrode made of a net and other ways were used to study the structure of the diffusion layers. All these methods are not easy to be realized technically. They enable approximate and averaged data about the surface concentrations of the components in simple systems to be obtained. Speaking about complex systems only the total metal and ligand concentrations can be determined by means of such methods. Sometimes, it is possible to obtain more detailed information using electrode probes. They are miniature electrodes of the size of the micrometer order, which are reversible with respect to M^{n+} or H^+ ions. Currently, concentration profiles can be mapped with a micrometric resolution when a microelectrode is used as a chronoamperometric probe within the diffusion layer of a larger electrode [22]. However, this method gives somewhat averaged results. Furthermore, when distances between the tip of the microprobe and the surface of the electrode under study are too short, the screening effect occurs. Due to this, the current density decreases and the investigation results are distorted in the region under study.

In connection with the drawbacks of the listed experimental methods, the role of theoretical calculations increases. In a general case, the system of differential equations is to be solved, an example of which is presented earlier

(see Eqs. (3.22)–(3.25)). Also, the initial and boundary conditions have to be formulated in a proper form.

3.4.1 Concentration Profiles in Ideally Labile Systems

The usage of simple relationships Eqs. (3.26) and (3.27) is very tempting, because the solutions of such equations supplemented with corresponding initial and boundary conditions have been well-expounded in literature. However, no information concerning individual components of the system follows from these equations. Therefore, to obtain such data, it is necessary to formulate extra interrelations between their concentrations.

When the chemical interactions between complexes and ligands proceed with "a sufficiently high" rate, it is common to treat their concentrations as "close to equilibrium ones." Assumptions of such kind have been of frequent use and can be found in different problems of electrochemical kinetics. Then, the relations between concentrations might be determined by cumulative (β_j) or stepwise (K_j) stability constants of complexes and protonated ligands. An expression for β_j is given in Chapter 1; stepwise equilibria, such as (3.16) and (3.17), can be characterized by

$$K_j = \frac{k_j}{k_{-j}} = \frac{[\mathrm{ML}_j^{n+}]}{[\mathrm{M}_{j-1}^{n+}][\mathrm{L}]}. \tag{3.32}$$

Further, we shall designate such systems as "ideally labile" (IL systems).

On the basis of the aforementioned conclusions, equations adapted to the diffusion layer acquire the following expression:

$$\sum_{j=0}^{N} \beta_j [\mathrm{M}^{n+}][\mathrm{L}]^j \equiv c_{\mathrm{M}}(x,t) = c_{\mathrm{M}} + F(i,x,t), \tag{3.33}$$

$$\sum_{j=0}^{N} j\beta_j [\mathrm{M}^{n+}][\mathrm{L}]^j + \sum_{m=0}^{M} \beta_m^H [\mathrm{L}][\mathrm{H}^+]^m = c_{\mathrm{L}}, \tag{3.34}$$

$$\sum_{m=0}^{M} m\beta_m^{\mathrm{H}} [\mathrm{L}][\mathrm{H}^+]^m + [\mathrm{H}^+] - [\mathrm{OH}]^- = c_{\mathrm{H}}, \tag{3.35}$$

where all concentrations, with the exception of bulk c_{M}, c_{L}, and $c_{\mathrm{H,}}$ depend on the coordinate x and time t. The function $F(i,x,t)$ evaluates the fact that a certain c_{M} gradient is formed during electrolysis. As bulk c_{M} and c_{L} are known, the total concentration of proton donors and acceptors c_{H} has to be determined from the data obtained after calculating the distribution of the components in the bulk of solution and using the known pH value. The c_{H} obtained in this way is further used assuming it to be constant, like the value c_{L}. This enables pH changes in the diffusion layer to be evaluated.

Steady-state problems are simplest, because i values, like concentration profiles, are independent of t. Then the analog of Eq. (3.6) applies

$$\frac{c_M(x) - c_M(0)}{c_M - c_M(0)} = \frac{x}{\delta}. \tag{3.36}$$

It is known that in the case of steady-state voltammetry, the surface concentration

$$c_M(0) = c_M(1 - i/i_d), \tag{3.37}$$

where i_d is the limiting current density.

We shall present several examples of calculations obtained for the aforementioned model system, assuming that $c_M = 0.01$ M, and the values of stability constants are as follows: $\log \beta_1 = 8$, $\log \beta_2 = 14$. An example of distribution of these particles in the diffusion layer, when there is an excess of ligand in the solution, is presented in Figure 3.4. Concentration of each particle therein $c_j(x)$ is normalized with respect to a corresponding bulk c_j.

Strictly speaking, none of the concentration gradients is constant. Profiles of concentrations of the particles, which dominate in the solution, are close to straight lines. The dependencies presented have a number of useful properties, which are worth mentioning. The results obtained when $i = i_d$ can be used in case of other current densities. For that reason, the origin must be moved to the point $x/\delta = 1 - i/i_d$, leaving the abscissa $x/\delta = 1$ in the same place. The system of coordinates obtained, which satisfies the condition $i = i_d/2$, is represented by a dotted line. It is clear that the data remaining to the left of the new ordinate loses the physical meaning. The analysis of equations used to calculate the concentration profiles also shows that having replaced the argument x/δ with the value $(1 - i/i_d)$, values of functions shall correspond to the normalized surface concentrations $c_j(0)/c_j$. Then, the surface concentrations of the species, which are

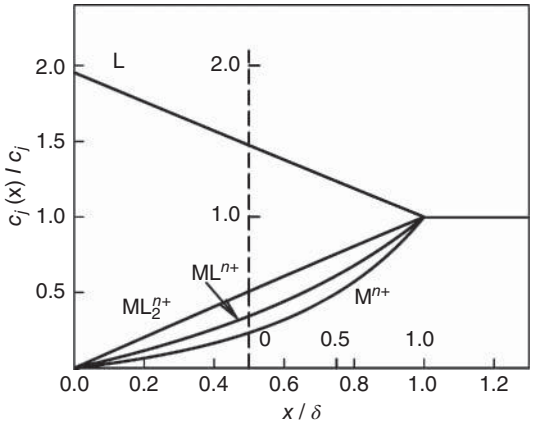

Figure 3.4 Steady-state concentration profiles at $i = i_d$, $c_M = 0.01$, and $c_L = 0.04$ M. When $i = i_d/2$, ordinate should take up the position indicated by a dotted line.

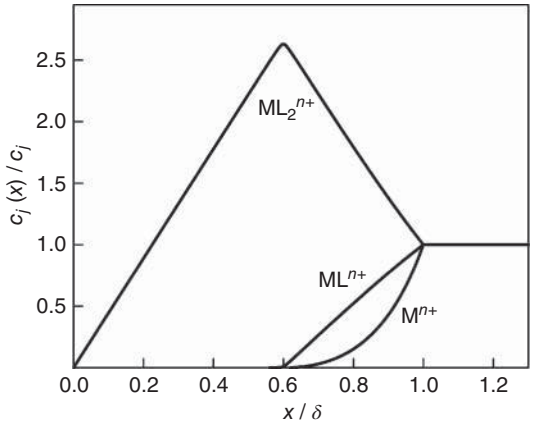

Figure 3.5 Concentration profiles obtained at $i = i_d$ for ligand-deficient system $c_M = c_L = 0.01$ M.

necessary to establish kinetic parameters of the process, can be obtained from the same figure.

Ligand-deficient systems deserve special mention. This state can be realized in several ways: by reducing c_L or by increasing acidity of the solution containing protonated ligands. In the latter case, the bulk concentration of the active form (L) decreases considerably and the amount of protonated LH^+ increases, which, according to the assumption made, does not form coordination compounds with metal ions.

The data in Figure 3.5 show that concentration profiles of some particles have the maximum. They are determined by interaction of two processes – diffusion and a chemical reaction. This state is impossible in the ligand-free systems.

Finally, it should be noted that pH changes also occur in the diffusion layer of the systems containing protonated ligands. They are caused by the shifts of equilibria in which H^+ ions take part. The data presented in Figure 3.6 were obtained for the aforementioned model including LH^+ species with $\log \beta^H = 9$ and the activity coefficient of H^+ ions $\gamma = 0.5$. The curves presented can be easily transformed into concentration profiles of H^+ ions. As can be seen, considerable pH changes are expected at a certain distance from the electrode surface x'. It is possible to discover this effect in real systems when using pH-sensitive electrodes. One of them is $Sb|Sb_2O_3$ microelectrode with redox reaction

$$Sb_2O_3 + 6H^+ + 6e \rightleftarrows 2Sb + 3H_2O. \tag{3.38}$$

To make a pH-measuring microprobe, a thick-walled capillary (~1 mm in diameter) is filled with melted antimony using suction and oxidized. Details for its fabrication and use have been published earlier [23]. Its potential is reversible with respect to H^+ and obeys the Nernst equation

$$E = \text{const} - 0.058 \ \text{pH} \tag{3.39}$$

over a rather wide range of pH (Figure 3.7).

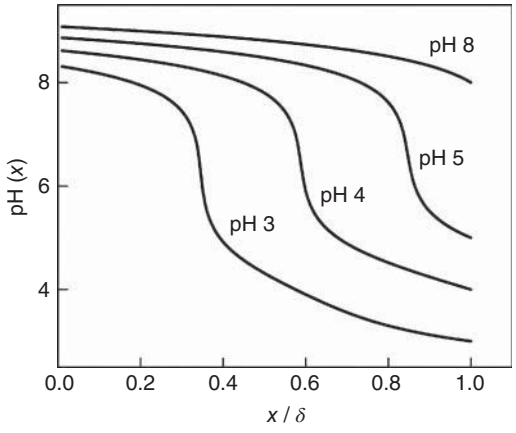

Figure 3.6 pH changes in the diffusion layer formed at $i = i_d$ in the system containing LH^+ species. Bulk pH values are indicated at the respective curves. $c_M = 0.01$ and $c_L = 0.04$ M.

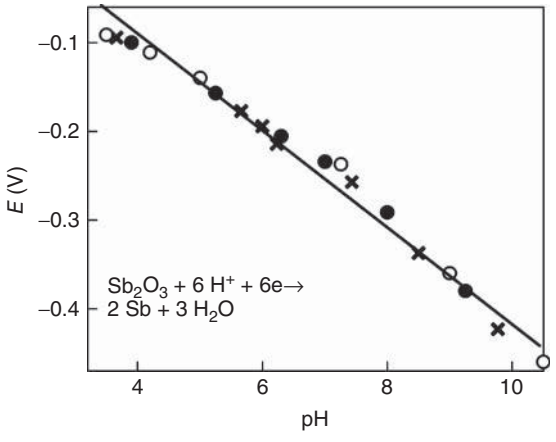

Figure 3.7 Calibration graph of $Sb|Sb_2O_3$ microprobe. Results obtained for three individual samples (different symbols) are approximated with one general line.

Experimental results obtained in investigating reduction of Cu(II)–glycine complexes [24] are shown in Figure 3.8. According to the theory, $x^{/}$ must decrease with the increase in acidity of the solution. In fact, in case of bulk pH = 5, a rather significant change in pH is seen. Features of this change are also seen in case of more acidic (pH 4.5) solution ($x^{/} \approx 0.25$ mm); however, it was impossible to register it at pH 4. A used probe with ~0.8 mm in diameter most probably was not a delicate enough device, which disturbed the hydrodynamic regime near the electrode surface and caused the aforementioned screening effects, which strengthen when approaching the probe to the electrode surface. Despite these drawbacks, it can be maintained that pH changes really exist in the diffusion layers of real complex systems.

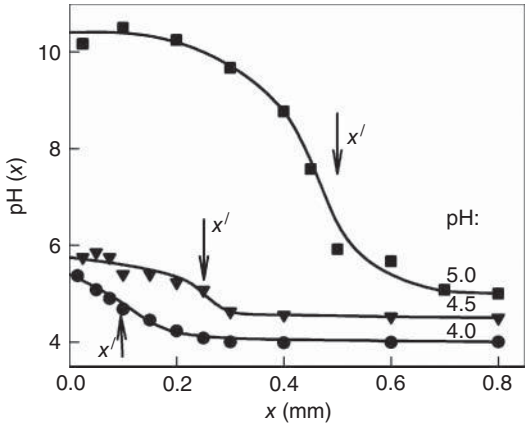

Figure 3.8 pH changes in the diffusion layer of Cu|Cu(II), glycine system. Cathodic $i = 2.5\ \text{mA cm}^{-2}$, $c_M = 0.01$ M, $c_L = 0.04$ M. Bulk pH values are given at the respective curves. Arrows show the position of pH drop according to theoretical predictions.

Table 3.2 Expressions of $F(i,x,t)$ function for $i(t)$ signals of different forms.

Method	$i(t)$	$F(i,x,t)$
Chronopotentiometry	$i = 0,\ t = 0;\ i = \text{const},\ t > 0$	$\frac{2i\sqrt{t}}{nF\sqrt{\pi D}} \exp\left(-\frac{x^2}{4Dt}\right) - \frac{ix}{nFD} erfc\left(\frac{x}{2\sqrt{Dt}}\right)$
Linear current sweep	$i = \nu t$	$\frac{\nu}{nF\sqrt{D}}\left[\left(\frac{4t^{3/2}}{3\sqrt{\pi}} + \frac{x^2\sqrt{t}}{3D\sqrt{\pi}}\right)\exp\left(-\frac{x^2}{4Dt}\right) - \left(\frac{xt}{\sqrt{D}} + \frac{x^3}{6D^{3/2}}\right) erfc\left(\frac{x}{2\sqrt{Dt}}\right)\right]$
Faradaic impedance	$i = i_A \sin \omega t,\ t \to \infty$	$\frac{i_A \exp\left(-x\sqrt{\frac{\omega}{2D}}\right)}{nF\sqrt{\omega D}} \sin\left(\omega t - x\sqrt{\frac{\omega}{2D}} - \frac{\pi}{4}\right)$

To deal with problems concerning non-steady-state processes, the function $F(i,x,t)$ in the Eq. (3.33) should be specified. When the current density is controlled, that is, when the system is perturbed by the specified signal $i(t)$, the usual equations obtained for simple (noncomplex) systems can be used with substitution of c_M for $[M^{n+}]$ in these equations. Some expressions for $F(i,x,t)$ are presented in Table 3.2.

When the sinusoidal perturbation

$$i(t) = i_s + I_0 \sin \omega t, \tag{3.40}$$

is applied, a quasi-steady state is attained after the certain transition period. Then, concentration changes repeat themselves during every subsequent period. From the theoretical point of view, this occurs at $t \to \infty$, but practically several tens of periods are enough for that. Let us assume that during the experiment, a rotating

disk electrode is used. Using expression (3.5) for δ, we shall apply the Nernst model to the steady-state component i_s. When studying periodical changes in concentrations arising at the RDE surface in simple salt solutions, the following approaches were used: (i) semi-infinite diffusion model, (ii) the Nernst model, and (iii) the model evaluating convection flows [25, 26]. It was established that they all give practically the same results if the penetration depth of the concentration wave $x_0 = \sqrt{2D/\omega}$ does not exceed 10–20% of δ_N. On this basis, it is not difficult to determine the limits within which the semi-infinite diffusion model can be applied to the alternating component $i(t)$. The evaluation made shows that the alternating current frequency should be higher than tens of Hertz, when the Schmidt number Sc = 2000, and the RDE rotating rate does not exceed 1000 rpm. Then, the following equation applies:

$$c_M(x,t) = c_M - \frac{i_s(x-\delta)}{nFD} + \frac{I_0 \exp(-x\sqrt{\omega/2D})}{nF\sqrt{\omega D}} \sin(\omega t - x\sqrt{\omega/2D} - \pi/4). \quad (3.41)$$

When measuring impedance, the sinusoidal electrode potential

$$E(t) = E_s + V_0 \sin \omega t. \quad (3.42)$$

is applied and the current density is analyzed as a response. If the amplitude of alternating voltage $V_0 \ll RT/nF$, the system may be regarded as linear. Then,

$$i(t) = i_s + a \sin \omega t + b \cos \omega t = i_s + \sqrt{a^2 + b^2} \sin(\omega t + \psi), \quad (3.43)$$

where the shift of the electric phase

$$\psi = \arctan(b/a), \quad (3.44)$$

and the values a and b depend on the kinetic parameters of the electrode process. The expression of the concentration profile $c_M(x,t)$ is rather complicated. Therefore, we shall present only the equation, which describes the surface concentration. Having inserted the alternating component of Eq. (3.42) in Eq. (3.10) where the upper integration limit t is replaced with the infinity, after a number of rearrangements, we obtain the following:

$$c_M(0,t) = c_M(0) + \frac{(a+b)\sin\ \omega t + (b-\ a)\cos\ \omega t}{nF\sqrt{2\omega D}}, \quad (3.45)$$

where $c_M(0)$ is the steady-state surface concentration defined by Eq. (3.37). Expression (3.45) will be used below in analyzing impedance under the forced convection conditions.

It follows from the last example that when controlling the potential, its value is to be related to i and surface concentration of EAC. The latter term appears in the kinetic equation. For this purpose, it is necessary to know mechanism and kinetic parameters of the charge transfer process. However, this complicated way may be avoided, if the experimentally obtained $i(t)$-function is utilized. Then, to find concentration profiles, the Laplace transform of this function is to be obtained:

$$i(s) = \int_0^\infty i(t) e^{-st} \mathrm{d}t, \quad (3.46)$$

where s is a complex variable. It can be shown that transformed Eqs. (3.2), (3.7) – (3.9) yield the following relationships. In the case of semi-infinite diffusion,

$$c_{\mathrm{M}}(x,s) = \frac{c_{\mathrm{M}}}{s} + \frac{i(s)\exp\left(-x\sqrt{s/D}\right)}{nF\sqrt{sD}}, \tag{3.47}$$

and when applying the Nernst model we obtain that

$$c_{\mathrm{M}}(x,s) = \frac{c_{\mathrm{M}}}{s} + \frac{i(s)}{nF\sqrt{sD}} \frac{\exp\left[\sqrt{s/D}\,(\delta - x)\right] - \exp\left[-\sqrt{s/D}\,(\delta - x)\right]}{\exp\left(\delta\sqrt{s/D}\right) - \exp\left(-\delta\sqrt{s/D}\right)}. \tag{3.48}$$

Having inserted Eq. (3.46) in Eq. (3.47) or in Eq. (3.48) and having made the inverse Laplace transform, the function $c_{\mathrm{M}}(x,t)$ is obtained, which can be used in Eq. (3.33). If we limit ourselves to the evaluation of surface concentrations only, we may not use these procedures. Then, it is enough to substitute the variable t in the function $i(t)$ for the variable $(t-u)$ and insert it into Eq. (3.10).

To conclude, we shall discuss several simpler cases that apply to reversal electrode processes, that is, when the exchange current density $i_0 \to \infty$. Under these conditions, the Nernst equation applies to the electrode potential. If the potential step perturbation is used (a constant E is applied at $t > 0$), the surface concentration of aqua-ion M^{n+} will change and become equal to:

$$[\mathrm{M}^{n+}]_s = \exp(nF\eta_0/RT), \tag{3.49}$$

where $\eta_0 = E - E^{0/}$, and $E^{0/}$ is the formal potential of $\mathrm{M}|\mathrm{M}^{n+}$ electrode. The $[\mathrm{M}^{n+}]_s$ value will remain constant during the entire perturbation. As surface concentrations of all other particles can be determined by means of material balance equations, the total metal concentration $c_{\mathrm{M}}(0)$ at the electrode surface becomes available. Using analogy between total metal mass transportation in complex systems and M^{n+} ion transport in the systems without ligand, we obtain:

$$\frac{c_{\mathrm{M}}(x,t) - c_{\mathrm{M}}}{c_{\mathrm{M}}(0,t) - c_{\mathrm{M}}} = erfc\left(\frac{x}{2\sqrt{Dt}}\right), \tag{3.50}$$

$$\left.\frac{\partial c_{\mathrm{M}}(x,t)}{\partial x}\right|_{x=0} = \frac{c_{\mathrm{M}} - c_{\mathrm{M}}(0,t)}{\sqrt{\pi Dt}}, \tag{3.51}$$

$$i(t) = [c_{\mathrm{M}}(0,t) - c_{\mathrm{M}}]\sqrt{D/\pi t}. \tag{3.52}$$

As in case of controlled current density, i dependence on t can further be found using Eqs. (3.50) – (3.52). If the electrode potential is changed according to the law $E = E_{\mathrm{eq}} - \nu t$ (linear potential sweep), Eq. (3.49) is to be changed into

$$\eta = -\nu t = \frac{RT}{nF} \ln \frac{[\mathrm{M}^{n+}]_s}{[\mathrm{M}^{n+}]}. \tag{3.53}$$

The way of a further analysis remains unchanged.

It should be noted that concentration profiles arising under the controlled potential conditions cannot be obtained in isolation from kinetics and mechanism of the electrochemical process. All these tasks must be solved jointly.

What is provided by the IL approach?

Let us return to the examples of concentration profiles presented in Figures 3.4 and 3.5. A characteristic feature of the results obtained is that certain concentration gradients of metal-containing species arise at the electrode surface and none of them is equal to zero. By analogy with Eq. (3.9), this means that all without distinction complexes take part in the charge transfer processes producing their own partial currents. This result is in the certain contradiction with reality. The most objectionable feature of IL model consists in the fact that the electrochemical activity of complexes is associated with their stability, because the shapes of concentration profiles and partial currents depend mainly on β_j. Certainly, thermodynamics allows us to treat any metal-containing species as possible EAC, because the same equilibrium potential should be attributed to any charge transfer process (see Chapter 2). However, there is a lot of experimental data (see, e.g., [1]) testifying that the EAC is liable to contain less ligand particles than the more stable species predominating in the solution. Special methods applied for establishing the EAC composition are considered in the following section. At the same time, the model of IL system leaves no freedom in choosing the EAC. Therefore, the alternatives free from such limitations should be considered.

3.4.2
Concentration Profiles in Systems of Limited Lability

As metal ions in aqueous solutions form hydrated aqua complexes, complex-formation processes should be considered as reactions involving replacement of water molecules by ligand particles. Kinetic data for the formation of metal complexes obtained by various methods showed [27] that the formation of ML complexes proceeds via a rapid pre-equilibrium, resulting in the formation of an outer sphere complex $M(H_2O)L$. Then, this intermediate loses water in the rate-determining step of inner sphere complex (ML) formation.

Rates of chemical reactions vary within a wide region of magnitude. Due to diffusion limitations, the rate constant of bimolecular reaction cannot exceed 10^{10} mol^{-1} dm^3 s^{-1} [28]; therefore, this value can be used as an upper limit of k_1. Reactions whose half-times are less than l0 s are considered fast [29]; then, the rate constant for monomolecular reaction should exceed ~0.1 s^{-1}. In accordance with the reaction rate, metal complexes are classified as labile and inert, but it is not possible to draw a sharp boundary line between the two groups.

The rate of complex formation depends on various factors, such as the nature of the bond, the constitution of the electronic shells of the central metal atom, stereochemistry of the complex, and so on [29]. It has been suggested [30] that the rate constant for ligand penetration is characteristic of the metal ion alone. However, the exceptions are possible for chelation reactions in which steric effects,

Table 3.3 Rate constants for $CuL_{n-1}^{3-n} + L^- \rightleftarrows CuL_n^{2-n}$ (25 °C) [30, 31].

Ligand (LH)	n	k_n ($mol^{-1}\ dm^3\ s^{-1}$)	k_{-n} (s^{-1})	k_{aq} (s^{-1})
Glycine	1	4.0×10^9	34	2.0×10^9
	2	4.0×10^8	50	5.0×10^9
α-Alanine	1	1.3×10^9	12	—
	2	1.5×10^8	33	—
β-Alanine	1	2.0×10^8	11	—
	2	8.0×10^6	19	—

such as chelate ring formation, can reduce the overall complexation rate. Unfortunately, kinetic data are incomparably weaker than vast databases of stability constants. We were able to find some more exhaustive data on the formation of Cu(II)–amino acid complexes [30–32]; some of them are listed in Table 3.3. It was found that the release of a water molecule from the inner hydration sphere of the metal ion is the rate-determining step. The monomolecular rate constants for glycine penetration into the inner hydration sphere, k_{aq}, were also estimated. Forward rate constants for glycine and α-alanine were found to be of the same order of magnitude, but those for β-alanine are substantially smaller. This effect was interpreted on the basis of ring closure as the rate-determining step. It was supposed that the five-membered chelate ring undergoes the transformation into six-membered configuration.

To reveal the effect of the rate of chemical steps, we consider concentration profiles simulated for the certain model system. To make the mathematics simpler, we explore only a limited number of components emphasizing that an increase in their number has no effect on general conclusions. Thus, the system to be analyzed would contain only "free metal ions" (aqua complexes) M^{n+}, monoligand complexes ML^{n+}, and uncharged ligand L. Then, a single chemical reaction Eq. (3.16) occurs both in the bulk of solution and in the δ-thick diffusion layer.

When chemical interactions are not infinitely fast, to determine concentration profiles, it is necessary to solve the set of differential equations containing kinetic terms. Hereinafter the results, obtained with the parameters listed in Table 3.4, are referred to the *system of limited lability* (LL system). The rate constants were varied so that the relation (3.32) was always obeyed. Current densities applied are given next as fractions of the steady-state limiting current density, that is,

$$i_d = \frac{nFDc_M}{\delta}. \tag{3.54}$$

The initial condition of the system (at $t = 0$) is commonly treated as an equilibrium state with constant (bulk) concentrations of species over the whole area of the system. The same is valid for the respective boundary conditions at $x \geq \delta$, because the electrochemical process, which starts at $t > 0$, gives rise to the formation of certain concentration gradients only within the diffusion layer (at $0 < x < \delta$).

Table 3.4 The main set of parameters used in simulations.

Parameter	Symbol	Main values	Dimension
Total metal concentration	c_M	0.01	mol dm^{-3}
Total ligand concentration	c_L	0.02, 0.1	mol dm^{-3}
Stability constant of ML^+ species	K_1	100	mol^{-1} dm^3
Rate constant of complex formation	k_1	Varied	mol^{-1} dm^3 s^{-1}
Rate constant of complex dissociation	k_{-1}	Varied	s^{-1}
Diffusion coefficient	D	5×10^{-6}	cm^2 s^{-1}
Diffusion layer thickness	δ	0.02	cm
Number of electrons transferred	n	1	—
Limiting current density	i_d	2.4125×10^{-4}	A cm^{-2}

Another boundary condition follows from the first Fick's law and correlates the flux of the EAC with the current density *i*.

In the case of IL system, differential equations contain only total concentrations; therefore, there is no necessity to preset which species (M^{n+} or ML^{n+}) is the EAC taking part in the respective charge transfer processes

$$M^{n+} + ne \rightarrow M, \tag{3.55}$$

$$ML^{n+} + ne \rightarrow M + L. \tag{3.56}$$

In any case

$$i = -nFD\left.\frac{\partial c_M}{\partial x}\right|_{x=0}. \tag{3.57}$$

As the ligand is supposed to be electrochemically inert,

$$\left.\frac{\partial c_L}{\partial x}\right|_{x=0} = 0. \tag{3.58}$$

The latter condition does not mean that [L] is also constant; the certain gradient of free ligand L follows from the material balance of the total ligand. However, in the case of LL system, the boundary conditions (3.57) and (3.58) should be rewritten and specified for each species. For electrically active species, this condition takes a shape of Eq. (3.57), the concentration gradient of electrically inert component is set equal to zero.

The data, presented in Figure 3.3 for $\delta = 0.02$ cm, show that a steady state is attained in ~200 s, where $\Psi(u) \rightarrow 0$. This conclusion is supported by simulation data, an example of which is presented in Figure 3.9. Hence, the data obtained for LL system at sufficiently long times can be compared with the respective steady-state data simulated for IL system.

When the rate of chemical interactions is sufficiently high, concentration profiles are the same for both systems (Figure 3.10). However, we shall see from the following discussion that the certain discrepancy can be observed at lower reaction rates.

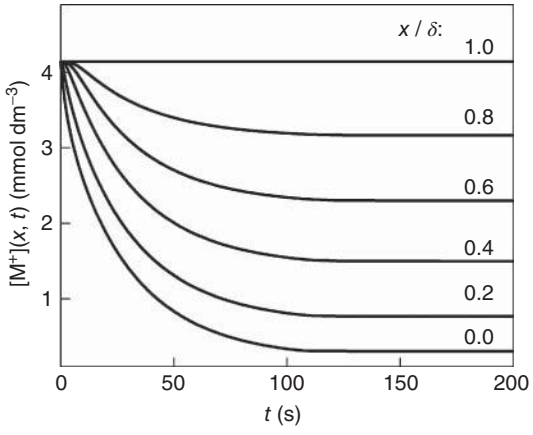

Figure 3.9 Dynamics of concentration profiles of M^+ ions. Simulation with $c_M = 0.01$ M, $c_L = 0.02$ M, $\log K_1 = 2$, $k_1 = 100\ \text{mol}^{-1}\ \text{dm}^3\ \text{s}^{-1}$.

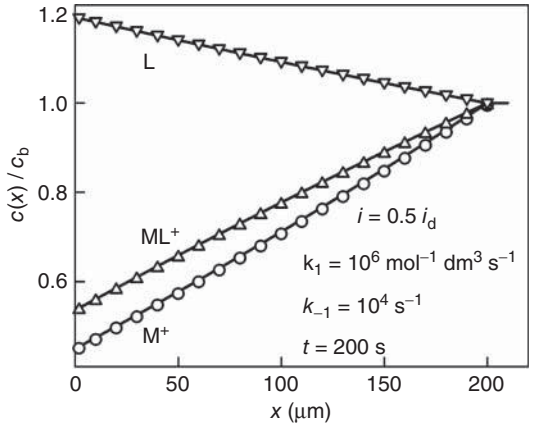

Figure 3.10 Comparison of normalized steady-state concentration profiles simulated at $i = 0.5\ i_d$ for IL (solid lines) and LL (circles) systems. The concentration gradients, obtained for IL system at $x = 0$, were used as boundary conditions for LL system. $c_M = 0.01$ M, $c_L = 0.02$ M.

Analysis of CE mechanism (chemical step + electrochemical step) is often based on the concept that a thin reaction layer is formed at the electrode surface where the certain nonequilibrium distribution of the system components occurs (see e.g., [33]). In the case of preceding reactions of the first (or pseudo-first) order, the thickness of such layer was estimated by the relationship

$$\delta_r = \sqrt{\frac{D}{k_{-1}}}. \tag{3.59}$$

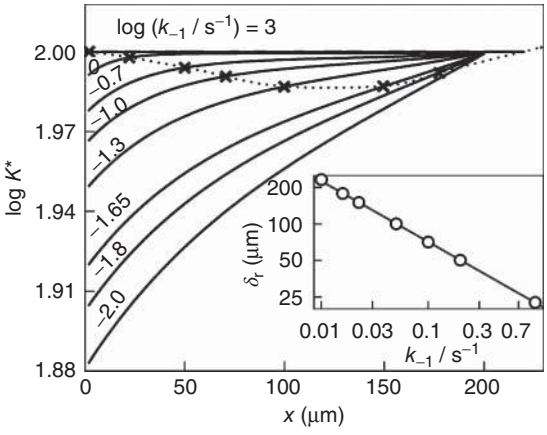

Figure 3.11 Effective stability constants K^*, as functions of coordinate x. The thickness of the hypothetical reaction layer, δ_r, is indicated with crosses. Its dependence on k_{-1} determined by Eq. (3.38) is shown in the inset (logarithmic presentation).

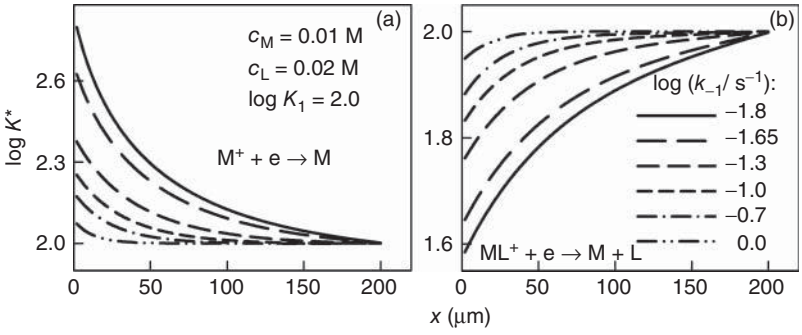

Figure 3.12 Effective stability constants K^* in the case of different charge transfer reactions: the reduction of M^+ aqua complexes (a) and that of ML^+ species (b).

To check whether this concept is suitable in the case of the system under consideration, we calculated effective K^* values substituting simulated $c(x)$ functions in Eq. (3.32). The data obtained at constant ratio of $k_1/k_{-1} = 100(\log K_1 = 2)$ are shown in Figures 3.11 and 3.12. An obvious divergence of K^* from the specified K_1 quantity should occur in the reaction layer. However, there is no indication that such layer actually exists as a part of diffusion layer. This conclusion holds true when both metal-containing species are electrochemically active (Figure 3.11) or one of them is electrochemically inert (Figure 3.12). Close inspection of the respective concentration profiles gives no evidence on this matter as well. Hence, when the amounts of both metal species M^+ and ML^+ are of the same order, moderate deviations from equilibrium, depending on the rate constants, are observed over the whole diffusion layer. In other words, the concept of reaction layer is not working in this case. However, the situation changes significantly,

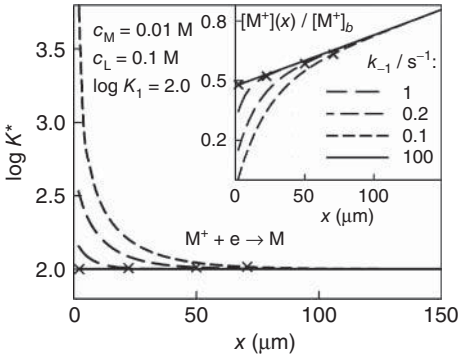

Figure 3.13 Effective stability constants β^* and concentration profiles of M^+ ions (inset). The thickness of the reaction layer is indicated with crosses. The thickness of the hypothetical reaction layer, δ_r, is marked with crosses. The case of M^+ reduction at a large excess of ligand.

when M^+ ions are reduced in the solution containing an excess of ligand. In this case, an amount of EAC is by one order lower than that of ML^+ complexes and the role of electrically inert ML^+ species, as EAC donors, becomes considerable. The conditions that are created in this case are rather similar to those which the concept of reaction layer was suggested for. The reaction layer can be detected from both the concentration profiles and $K^*(x)$ values (Figure 3.13). It can be seen from these data that the Eq. (3.59) is a good approximation for the reaction layer thickness.

It is responsible to suppose that the regularities established for very simple model could serve as a guide to more complex cases. The results obtained for model system show that at least two parameters, namely the rate constant, k_{-1}, and the complexation degree, Φ (see Eq. (1.12)), are responsible for deviations from the equilibrium distribution. This effect is most pronounced at low concentrations of electrically active complexes that are generated by the preceding reaction. Of course, any preliminary premise on system lability should be validated or disproved by the respective simulations.

The aforementioned results show that the condition $k_{-1} \gtrsim 1$ may serve as a criterion of sufficient lability. From this point of view, the data in Table 3.3 give grounds to expect that Cu(II) complexes are referable to labile compounds. This circumstance makes it possible to use the IL model for determining the surface concentrations of species with an acceptable error. On the other hand, the presence of thin nonequilibrium layer offers the prospect to operate with concentration gradients in compatibility with the active current density.

The aforementioned conclusions follow mainly from the regularities of linear diffusion under the steady-state conditions. In the case of other electrode geometry (Table 3.3), an account of chemical steps can be performed in the same manner. The differential equations, written for each component that takes part in the diffusional mass transport, should be supplemented with the respective kinetic terms.

Again, the described linear combinations of the differential equations yield the relationships that contain no kinetic terms and operate with total concentrations of metal and ligand. Further, limits of IL or LL applications can be evaluated.

These cases seem to be more complicated and need further investigations. Because of the nonuniform distribution of diffusional flows, it is likely that the effects of chemical interactions would be also different in various regions of the solution adjacent to an electrode surface.

References

1. Vetter, K.J. (1967) *Electrochemical Kinetics*, Academic Press, New York.
2. Survila, A., Stasiukaitis, P.V., and Kanapeckaitė, S. (1998) Concept of Nernst-type diffusion layer in linear potential sweep voltammetry. *Chemija*, **9** (2), 138–142.
3. Survila, A., Mockus, Z., Kanapeckaitė, S., and Stalnionis, G. (2012) Kinetics of Sn(II) reduction in acid sulphate solutions containing gluconic acid. *J. Electroanal. Chem.*, **667**, 59–65.
4. Survila, A. and Kanapeckaitė, S. (2012) Kinetics of cathodic processes in Cu(II) gluconate solutions containing an excess of sulphate. *Electrochim. Acta*, **78** (3), 359–364.
5. González Velasco, J. (1994) The linear sweep voltametric method: an application to the study of reversible and irreversible processes. *Electroanalysis*, **6** (9), 711–724.
6. Arun Prasad, M. and Sangaranarayanan, M.V. (2004) Analysis of the diffusion layer thickness, equivalent circuit and conductance behaviour for reversible electron transfer processes in linear sweep voltammetry. *Electrochim. Acta*, **49** (3), 445–453.
7. Arun Prasad, M. and Sangaranarayanan, M.V. (2004) Formulation of a simple analytical expression for irreversible electron transfer processes in linear sweep voltammetry and its experimental verification. *Electrochim. Acta*, **49** (16), 2569–2579.
8. González Velasco, J. (2006) On the dependence of the Nernst diffusion layer thickness on potential and sweep rate for reversible and of the thickness of the charge transfer layer for irreversible processes studied by application of the linear potential sweep method. *Electrochim. Acta*, **51** (14), 2971–2976.
9. Amatore, C., Szunerits, S., Thouin, L., and Warkocz, J.-S. (2001) The real meaning of Nernst's steady diffusion layer concept under non-forced hydrodynamic conditions. A simple model based on Levich's seminal view of convection. *J. Electroanal. Chem.*, **500** (1–2), 62–70.
10. Šarmaitis, R. and Survila, A. (1998) Mass transfer of components of the zinc chromating solutions. Part 1: mass transfer of species containing Cr(VI), Cr(III) and Zn(II). *Plat. Surf. Finish.*, **85** (10), 64–68, 76.
11. Šarmaitis, R., Survila, A., Dikinis, V., and Stasiukaitis, P.V. (1999) Mass transfer of zinc chromating solutions components. Part 2: formation of low-solubility substances at the zinc/chromating solution interphase. *Plat. Surf. Finish.*, **86** (7), 53–57.
12. Lee, C., Miller, C.J., and Bard, A.J. (1991) Scanning electrochemical microscopy: preparation of submicrometer electrodes. *Anal. Chem.*, **63** (1), 78–83.
13. Aoki, K. (1993) Theory of ultramicroelectrodes. *Electroanalysis*, **5** (8), 627–639.
14. Scharifker, B.R. (1988) Diffusion to ensembles of microelectrodes. *J. Electroanal. Chem.*, **240** (1), 61–76.
15. Baronas, R., Ivanauskas, F., and Survila, A. (2000) Simulation of electrochemical behaviour of partially blocked electrodes under linear potential sweep conditions. *J. Math. Chem.*, **27** (4), 267–278.
16. Macdonald, D.D. (1977) *Transient Techniques in Electrochemistry*, Plenum Press, New York.

17. Kačena, V. and Matoušek, L. (1953) Proteins and aminoacids. XVIII. The effect of electrolytes on proteins. *Collect. Czech. Chem. Commun.*, **18** (2), 294–301.
18. Hilbert, F. (1969) Die elektrolytische Abscheidung von Eisen und Wasserstoff. Habilitationsschrift. Universität Graz.
19. Miyoshi, Y. and Lorenz, W.J. (1970) For proton transport in sulfuric acid solutions. *Berichte Phys. Chem.*, **74** (4), 412–416.
20. Koryta, J. (1962) in *Progress in Polarography*, vol. **1** (ed. P. Zumann), Interscience, New York, pp. 291–302.
21. Kravtsov, V.I. (1969) *Electrode Processes in Solutions of Metal Complexes*, Leningrad State University, Leningrad (in Russian).
22. Amatore, C., Szunerits, S., Thouin, L., and Warkocz, J.S. (2000) Mapping concentration profiles within the diffusion layer of an electrode: part III. Steady-state and time-dependent profiles via amperometric measurements with an ultramicroelectrode probe. *Electrochem. Commun.*, **2** (5), 353–358.
23. Matulis, J. and Sližys, R. (1964) On some characteristics of cathodic processes in nickel electrodeposition. *Electrochim. Acta*, **9** (9), 1177–1188.
24. Milevičius, R., Spudas, L., and Survila, A. (1987) pH effects in the diffusion layer of the Cu(II)- glycine system. *Proc. Lithuanian Acad. Sci. Ser. B*, **2** (159), 16–24.
25. Levart, E. and Schuhmann, D.J. (1975) Comparison of some solutions for the Warburg impedance of a rotating disk electrode. *J. Electrochem. Soc.*, **122** (8), 1082–1083.
26. Scherson, D.A. and Newman, J. (1980) The Warburg impedance in the presence of convective flow. *J. Electrochem. Soc.*, **172** (1), 110–113.
27. Eigen, M. and Wilkins, R.G. (1965) *Mechanisms of Inorganic Reactions*, Chapter 3, Advances in Chemistry, Vol. **49**, Max-Planck Institut für Physikalische Chemie, Göttingen, Germany State University of New York at Buffalo, Buffalo, NY, pp. 55–80.
28. Gerischer, H. (1964) Kinetik der Metallabscheidung aus Lösungen komplexgebundener Ionen. *Chem. Ing. Tech.*, **36** (6), 666–671.
29. Alimarin, P.I. (1973) Kinetics of complex formation of metals with organic ligands in analytical chemistry. *Pure Appl. Chem.*, **34** (1), 1–12.
30. Makinen, W.B., Pearlmutter, A.F., and Stuehr, J.E. (1969) Copper(II) chelation kinetics. α- alanine, β-alanine and histidine. *J. Am. Chem. Soc.*, **91** (15), 4083–4088.
31. Pearlmutter, A.F. and Stuehr, J.E. (1968) Kinetics of copper(II)-glycine interactions in aqueous solution. *J. Am. Chem. Soc.*, **90** (4), 858–862.
32. Pearson, R.G. and Lanier, R.D. (1964) Rates of rapid ligand exchange reactions by nuclear magnetic resonance line broadening studies. *J. Am. Chem. Soc.*, **86** (5), 765–771.
33. Galus, Z. (1994) *Fundamentals of Electrochemical Analysis*, 2nd edn, Ellis Horwood, New York.

4
Peculiarities of Electrochemical Processes Involving Labile Complexes

The earlier formulated regularities of mass transport of complexes enable the composition of the system at the electrode|solution boundary of phases to be determined and valuable information about surface concentrations of components, which are one of the main factors determining the rate of the electrochemical process, to be obtained.

The peculiarities of electrode processes considered next have no analogs among the so-called noncomplex systems. In their case, the same species (M^{n+} solvate-complexes) participate in both diffusion mass transport and the charge transfer step.[1)] On the contrary, in the solutions containing complexes, mass transport is determined by the flows of *all particles* including M^{n+}, whereas the electrode potential depends only on *some components* within the system: electrically active complexes (EACs) and products of their reduction (ligands).

When considering regularities of these processes, two main alternatives are to be distinguished, depending on which of the electric parameters (i or E) are controlled during the experiment. However, under steady-state conditions, these differences disappear. Moreover, according to the hypothesis put forward in Ref. [1], selection of the controlled electric parameter has no significance in the case of quasi-stationary states, which, for example, are reached in the impedance spectroscopy or in the electrolysis of periodic impulses of small amplitude.

In case of quasi-reversible processes when the rate of the reaction is controlled by both diffusion and the charge transfer steps, it is necessary to assess the influence of such kinetic parameters as the exchange current density (i_0) and the charge transfer coefficient (α). Furthermore, additional variants to be considered appear related to different mechanisms of the electrochemical process. Therefore, in the simplest case, it is most convenient to analyze reversible processes when $i_0 \to \infty$ and only the diffusion overvoltage η_d is observed in the system. Despite the fact that characteristics of the latter processes differ quantitatively from the first one, general peculiarities remain the same.

As the characteristics of the reversible process do not depend on the charge transfer mechanism, the latter can be chosen freely. For the sake of simplicity, let us assume that the process $M^{n+} + ne \to M$ is taking place in the interphase.

1) Partial desolvation of metal ions attributable to the characteristics of the mechanism may take place in the double electric layer.

Electrochemistry of Metal Complexes: Applications from Electroplating to Oxide Layer Formation, First Edition. Arvydas Survila.

Then, Eq. (3.49), which contains surface concentration $[M^{n+}]_s$, is valid for the diffusion overvoltage. This value, used as a parameter, allows the current density to be related to overvoltage through the material balance equations written for the electrode surface.

4.1 Steady-State Voltammograms

When considering this case, from our point of view, an interesting analogy between the potentiometric titration curves and reversible voltammograms appears. It should be reminded that under the conditions of steady-state electrolysis, according to Eq. (3.37), the surface concentration $c_M(0)$ is the linear function of the current density. With the increase in cathodic i, $c_M(0)$ decreases proportionally, whereas $c_L(0)$ and $c_H(0)$ remain unchanged. Thus, the states imitating changes in surface concentrations during the electrolysis can be realized in the volume of ligand solution by changing the total metal concentration therein and leaving c_L constant. As in this case, as well as in the case of electrolysis, the electrode potential is described by the Nernst equation, the potentiometric titration curve can be treated as a voltammogram analog assuming that *the current plays the role of titrant at the electrode surface.*

We modified titration curves (Figure 2.1) assuming that a certain amount of simple metal salt containing M^+ ions is added to the solution containing ligand L. As this takes place, M^+ ions (aqua complexes) and ML^+ species are formed whose total concentration is equal to c_M. Some examples of simulated curves are presented in Figure 4.1 where the shift of the equilibrium potential (ΔE_{eq}) versus c_M is plotted. A sharp decrease in E_{eq} is observed at the equivalent point, the depth of which depends on the stability constant (K) of ML^+ complex.

Again, the potential drop displays the demarcation between two different states of the system that are related to transitions from the state with ligand deficiency into the state with ligand excess, or vice versa. Analogous transitions are also possible at the electrode surface in two cases:

- when increasing cathodic polarization in the system with ligand deficiency;
- when increasing anodic polarization in the system with ligand excess.

In both cases, corresponding (cathodic or anodic) overvoltage increases abruptly in a narrow range of current densities.

Reversible cathodic voltammograms simulated for ligand-deficient system at different stability of ML^+ complex are shown in Figure 4.2. Pronounced potential changes observable in Figure 4.1 manifest themselves in voltammograms as prewaves at $i/i_d = 0.5$ when the ratio $r \equiv c_L/c_M = 0.5$.[2)] It can be also seen from the comparison of Figures 4.1 and 4.2 that E changes in the region of prewave are

2) To achieve a full analogy, it is necessary to image that the total metal concentration is being decreased in Figure 4.1.

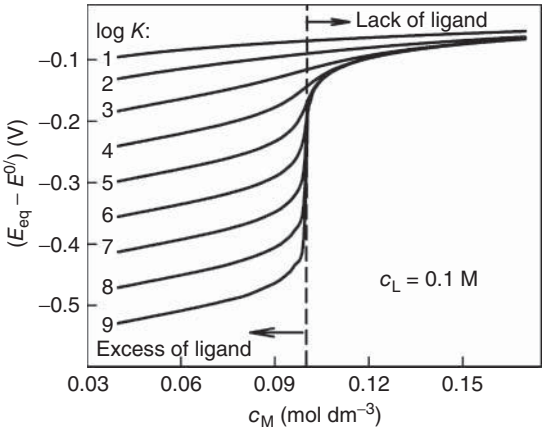

Figure 4.1 Variations of equilibrium potential on addition of simple metal salt to 0.1 M ligand solution. It is supposed that ML^+ complexes of different stability can be formed. log K values are given at the respective curves.

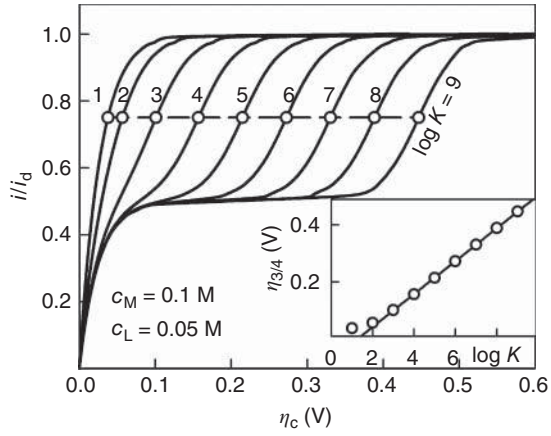

Figure 4.2 Normalized reversible cathodic voltammograms simulated at different stability of ML^+ complexes (log K values are given at the respective curves). Variations of the overvoltage at $i/i_d = 0.75$ with log K (see dotted lines) are given in the inset.

of the same order as these in Figure 4.1 at the equivalent point. In the region over prewave, η increases linearly with log K (inset in Figure 4.2) and its shift is equal to $2.303RT/nF$ per decade of K.

The effect of ligand concentration is shown in Figure 4.3. Curves were obtained for reduction of bivalent metal ions M^{2+} that form two (mono- and diligand) complexes. Hence, the equivalent point corresponds to the ratio $r = 2$. The curve obtained for the ligand-free solution ($r = 0$) has a usual classical form. Upon the

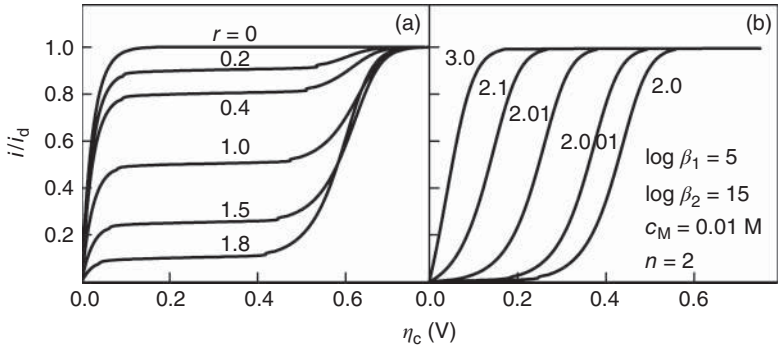

Figure 4.3 Normalized reversible cathodic voltammograms simulated at different ratios $r = c_L/c_M$ that are indicated at the respective curves.

introduction of ligand into the system, a prewave appears at $\eta_c < 0.5\,\mathrm{V}$. Its density (i_{lim}) decreases when increasing ligand concentration (Figure 4.3a). The analysis shows that independently of ligand bulk concentration and, consequently, of the value i_{lim}, the equivalent ratio of ligand and metal surface concentrations, that is, $r = c_L(0)/c_M(0) = 2$, is formed at i_{lim}.

The prewave disappears when the same ratio $r = 2$ is in the bulk of the solution; further, the overvoltage begins to decrease. Finally, with a sufficiently large excess of ligand, cathodic overvoltages practically coincide with these obtained for the ligand-free solution (cf. the curves at $r = 0$ and $r = 3$). It should be noted that the shift of the equilibrium potential (ΔE_{eq}) toward more negative E values takes place when c_L is increased. Therefore, decrease in η (Figure 4.3b) is in essence determined by ΔE_{eq}. If currents are plotted versus E, difference in their position becomes significantly lesser.

Thus, cathodic prewaves are characteristic of the systems with ligand deficiency. Formulating this statement more strictly, the active form of ligand L, which forms complex compounds with M^{n+}, should be kept in mind. The deficiency of this form can also be realized by decreasing pH of the solutions if they contain inactive protonated ligands, though it could seem that the total excess of ligand is sufficiently large. An example of this could be reversible voltammograms, which are calculated for the system Cu|Cu(II), glycine with the following complexation characteristics: $\log \beta_1 = 8.46, \log \beta_2 = 15.3, \log \beta_1^{\mathrm{H}} = 9.68, \log \beta_2^{\mathrm{H}} = 12.05$ (Figure 4.4).

With the increase in cathodic polarization, due to a shift of corresponding equilibria, pH at the electrode surface (pH_s) increases. Its changes are especially significant in slightly acidic media. Due to this, the shape of polarization curve depends on the nature of the supporting electrolyte. If the latter (such as SO_4^{2-}) is able to interact with protons, it plays a role of buffer and reduces pH_s changes to a certain extent (cf. continuous and dotted curves in Figure 4.4).

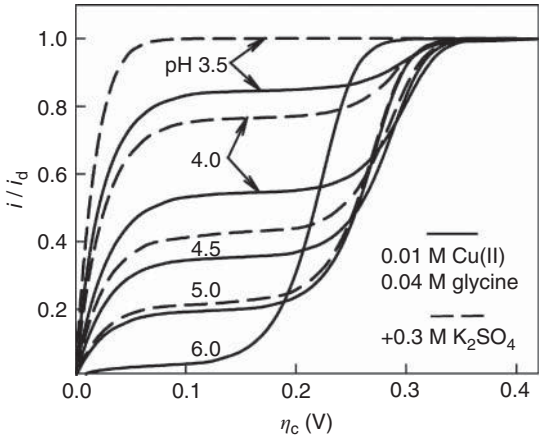

Figure 4.4 Normalized reversible cathodic voltammograms simulated for Cu|Cu(II), glycine system with $c_M = 0.01$ M, $c_L = 0.04$ M. Bulk pH is indicated at the respective curves. The effect of sulfate (0.3 M) is presented by dotted lines.

For the systems where the amount of protonated ligand forms is insignificant, the equation defining such pseudo-limiting current (prewave) can be obtained [2]:

$$i_{\lim} = \frac{nFD}{\delta}\left(c_L \frac{\sum_{j=0}^{N} j\beta_j [\mathrm{L}]^j}{\sum_{j=0}^{N} j^2 \beta_j [\mathrm{L}]^j} - c_M \right). \tag{4.1}$$

If species ML_N^{n+} prevails in the system, it follows from Eq. (4.1) that

$$i_{\lim} = \frac{nFD(c_L - Nc_M)}{N\delta}. \tag{4.2}$$

It is seen from this equation that $i_{\lim} > 0$, when $c_L > Nc_M$ (anodic pseudo-limiting currencies) and $i_{\lim} < 0$, when $c_L < Nc_M$ (cathodic prewaves).

Prewaves under discussion should be distinguished from kinetic limiting currents that are observed when equilibrium is established between an electrically active form and a species, which is not reduced or oxidized within the certain potential range. If the rate of conversion of the electrically inactive species into active is slower than the transport by diffusion, a kinetic limiting current results. This current can be used to calculate the rate constant of the chemical reaction, generating the electrically active species. By contrast, prewave emerges regardless of the mechanism of the charge transfer step, when chemical interactions are fast. Besides, it should have much lower temperature coefficient than the kinetic current.

The effects following from theory were confirmed experimentally. In this connection, voltammetric data obtained for Au|Au(I), CN^- system are worthy of notice. When no extra cyanide is added to the $KAu(CN)_2$ solution and it contains

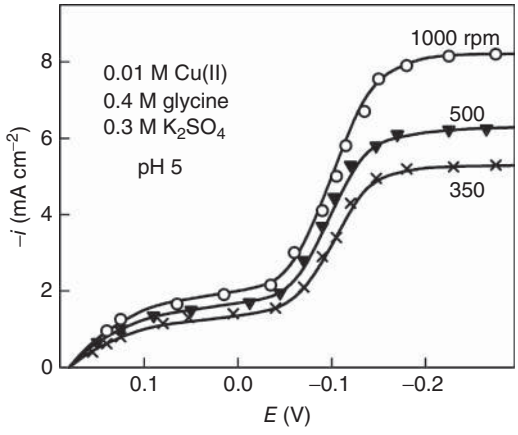

Figure 4.5 Cathodic voltammograms obtained for Cu|Cu(II), glycine system at different rotating velocities of RDE as indicated. Comparison between experimental (symbols) and simulated (lines) data.

equivalent amounts of metal and ligand, a rise of voltammogram is observed at rather high cathodic overvoltages ranging up to 1.2–1.4 V [3, 4]. Such large overvoltage is conditioned by high stability of dicyanoaurate ($\log \beta_2 \sim 39$ [4]).

Cathodic prewaves were discovered in reducing Cu(II)–glycine complexes [5]. Simulation procedures involving the determination of surface concentrations and the use of experimentally established kinetic parameters make it possible to obtain voltammograms that nicely coincide with experimental data (Figure 4.5). Analogous shapes of voltammograms were also observed for Sn(II)–citrate solutions [6] (see Section 8.3.2).

Investigating of cathodic processes in ligand-deficient Cu(II)–ethylenediamine system [7] showed that only a prewave can be observed during the experiment. The system Co|Co(II), citrate [8] could serve as a typical example of such a case. The current density plateau was found in experimental voltammograms (Figure 4.6) whose height decreases with an increase in citrate concentration. By means of rotating disc electrode (RDE), it was established [2] that i_{lim} dependencies on $\sqrt{\Omega}$ are well approximated by lines that pass the origin. This shows that the main factor controlling Co(II) reduction rate is diffusion. The analysis of the composition of the system showed that monoligand complexes ($N = 1$) prevail in the solution, when there is no excess of ligand. It follows from Eq. (4.2) in this case that i_{lim} must be proportional to the value ($c_{\text{OB}} - c_{\text{LB}}$) and this is confirmed by experimental data (inset in Figure 4.6). The slope of this linear dependence and Eq. (4.2) yield the value of $\delta = 0.019$ cm. Such thickness of the diffusion layer is typical under the natural convection conditions. As Co(II) reduction is accompanied by H_2 evolution, which begins to dominate at $E < -1$ V, it is impossible to observe the real (diffusion) limiting current (i_{d}) that is masked by reduction of hydrogen ions. Such effect must be taken into consideration when the standard potential of the metal being reduced is sufficiently negative.

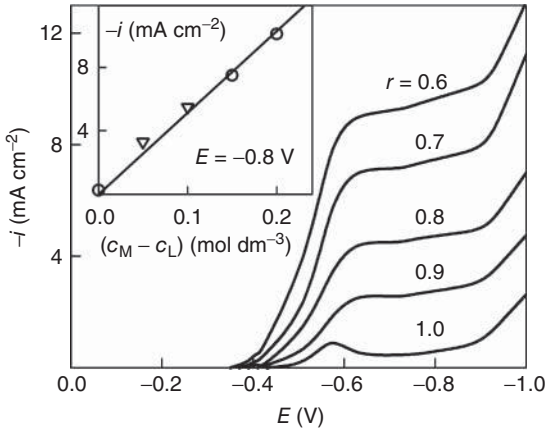

Figure 4.6 Cathodic voltammograms obtained for Co|Co(II), citrate system [8] at different ratios $r = c_L/c_M$ and $c_M = 0.5$ M, pH 7.2, 25 °C. Variation of prewave height versus overequivalent ligand concentration is shown in the inset. Triangular symbols indicate i values obtained with elimination of hydrogen evolution current.

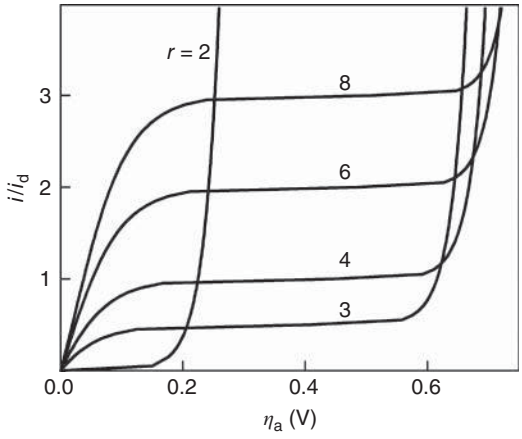

Figure 4.7 Anodic voltammograms simulated for model system at different ratios $r \equiv c_L/c_M$. Anodic i is normalized with respect to the cathodic limiting current density i_d.

Voltammograms simulated at anodic polarizations are presented in Figure 4.7. Anodic "limiting" currents are possible in the systems with the excess of ligand. The reasons for their appearance are the same: with the increase in anodic polarization, that is, with the surface $c_M(0)$ growing, the ratio $r \equiv c_L(0)/c_M(0)$ at the electrode surface falls till the equivalent r value is achieved. Unlike the case of cathodic processes, transfer from the state with the excess of ligand into the state with ligand deficiency is taking place on the electrode surface. A further increase in anodic current is not related to the beginning of the new process. Its nature

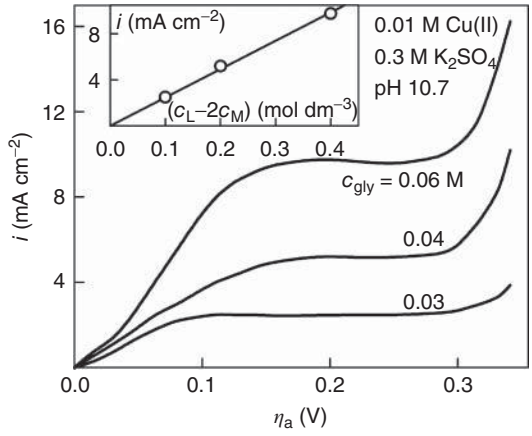

Figure 4.8 Anodic RDE voltammograms obtained for Cu(II)–glycine solutions at 300 rpm and different glycine concentrations as indicated. Inset contains i_{lim} values determined at $\eta_a = 0.2$ V and plotted versus overequivalent ligand concentration.

remains the same, and only M^{n+} ions, which are generated during the anodic process, do not form complex compounds at the electrode surface due to the deficiency of ligand. Like in the case of cathodic processes, pH of the solutions containing protonated ligand also is of significance. While increasing the acidity of the solution, the amount of active ligand L and the complexation degree of the system decrease. Then, transfer from the state with the excess of ligand into the state with ligand deficiency on the electrode surface becomes impossible and the plateau of the anodic current disappears.

Well-reproducible data, which are not distorted due to passivation, are obtained for the Cu|Cu(II), glycine system in a certain area of the composition of solutions ($c_M = 0.01\,M, c_L \leq 0.06\,M, 8 < pH < 11$) [9]. Experimental anodic voltammograms also have analogous properties (Figure 4.8). Experimental i_{lim} obtained using an RDE increases with increasing ligand concentration; it obeys Eq. (4.2) with $N = 2$, $D = 6.4 \times 10^{-6}\,cm^2\,s^{-1}$ and δ obtained with Eq. (3.5) (see inset in Figure 4.8).

4.2 Potential Transients

According to the material presented in Chapter 3, the value of convolution integral (see Eq. (3.10)) determines surface concentrations. Its analysis allows certain analogies between steady-state and non-steady-state processes to be found. Having inserted the condition $x = 0$ in the expressions of functions $F(i,x,t)$ (Table 3.2) and having compared them with Eq. (3.37), the criteria of similarity can be formulated, which allow transforming the above-discussed voltammograms into other non-steady-state characteristics.

Let us consider chronopotentiometry (CPM), which is a controlled-current technique in which the potential variation with time is measured following a current step. When the system is perturbed by the current pulse, Eq. (3.37) acquires the following form:

$$c_M(0) = c_M(1 - \sqrt{t / \tau}), \tag{4.3}$$

where τ is the transition time. A similar equation can be obtained when a linear current sweep is applied, that is, when $i = \nu t$. Then,

$$c_M(0) = c_M[1 - (t/\tau)^{3/2}] . \tag{4.4}$$

Having compared Eqs. (3.37) and (4.3), one can see that voltammograms can be easily transformed into chronopotentiograms upon replacing the value i/i_d by $\sqrt{t / \tau}$ and interchanging abscissa and ordinate. Analogous procedures can be carried out using Eqs. (3.37) and (4.4).

It follows from the aforementioned details that within the framework of the model under study, a certain congruence between the voltammograms and non-steady-state transients is possible. This allows foreseeing peculiarities of the latter. For example, the above-discussed cathodic prewaves should be also reflected in chronopotentiograms in the form of additional transition time. The conditions and reasons for its appearance remain the same.

However, it should be noted that under the conditions of non-steady-state electrolysis, additional effects can become pronounced too. First and foremost, non-faradaic currents, which can increase considerably in the case of high ν, should be attributed to them. Transition time related to reduction of the adsorption layer can have no analogous in steady-state voltammograms. On the whole, the lability criteria of complex systems under the conditions of non-steady-state electrolysis should be formulated more strictly. Therefore, the influence of kinetics of chemical interactions on the electrochemical process rate can reveal itself. A comparison of transformed voltammograms with the corresponding experimental E, t-dependencies can be of use in interpreting the data obtained. Figure 4.9 demonstrates the congruence of characteristics obtained for Cu(II)–glycine system by RDE voltammetry and CPM.

4.3 Current Transients

When investigating the behavior of labile complex systems under the potentiodynamic conditions, certain simplifications are usually made, which are grounded in the case of large excesses of ligand only. Mention should be made of work [10], which belongs to those rarer investigations where there are no such restrictions, in which cyclic voltammograms are analyzed when the number of complex species does not exceed two. Later, this problem was investigated in a more general form [11–13], assessing kinetics of simple [12] and stepwise [13] charge transfer.

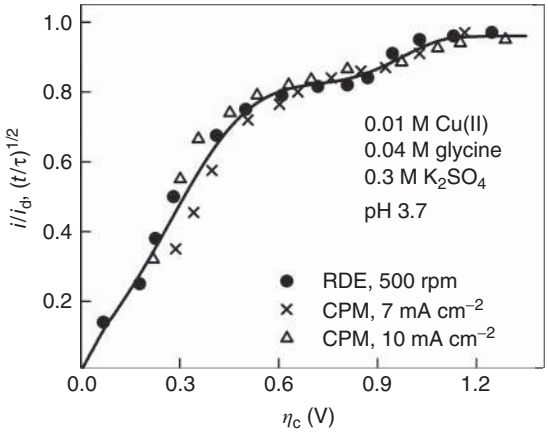

Figure 4.9 Comparison of RDE voltammogram and CPM transients obtained for Cu(II)–glycine solutions of indicated composition.

Seeking to quantitatively describe potentiodynamic characteristics, information about the composition of complex compounds and their distribution is necessary in the first stage already. Response of the complex system to perturbation by the potential signal $E(t)$ can be determined after solving material balance Eqs. (1.18)–(1.19) written for the solution bulk, and their analogous Eqs. (3.33)–(3.35), adapted for the electrode surface together with the kinetic equation of charge transfer (see Chapter 5). The latter acquires the form of the Nernst equation (3.53) when charge transfer is regarded as reversible (the exchange current density $i_0 \to \infty$).

A mathematical description of this problem is more complicated than that in the current perturbation when the analytical expression of the convolution integral can be used in Eq. (3.10). On the contrary, when the system is perturbed by $E(t)$, the desired current density function in various equations has different forms: $i(t)$ – in the kinetic equation and $i(t-u)$ in the mass transport equation. When solving such problems, various mathematical procedures have to be used (see [12–14]).

Peculiarities of a response to potentiodynamic perturbation are determined in a more simple way when the charge transfer process is reversible and Eq. (3.49) applies. However, before starting the analysis of such processes, several notes should be made. First of all, it should be noted that concentrations $[M^{n+}]$ and c_M coincide in the system that contain no ligand. In this case, the surface concentration of M^{n+} is the only parameter relating dependencies of overvoltage η of the current density i on time. According to [14], when $\eta = vt$, equation:

$$i(t) = 2nFc\sqrt{\frac{nFvD}{\pi RT}}\Phi\left(\sqrt{\frac{nFvt}{RT}}\right), \tag{4.5}$$

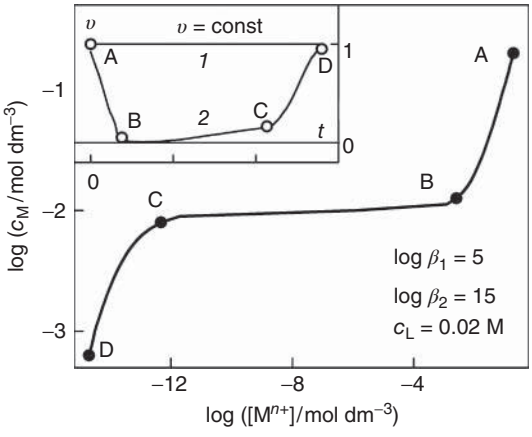

Figure 4.10 Relationship between the concentration of free metal ions M^{n+} and that of total metal c_M (simulated at constant c_L). Variations of real (1) and effective (2) potential sweep rate with time are shown in the inset.

applies to the reversible process where Φ is the integral function of the specified argument (the Dawson integral):

$$\Phi(\alpha) = \exp(-\alpha^2) \int_0^{\alpha} \exp(u^2) \mathrm{d}u. \tag{4.6}$$

In the case of complex systems, the situation is different. Here, as before, the value of the potential is related to M^{n+} concentration; however, the current density depends already on concentration of all particles containing M^{n+}, that is, on the c_M value. In this connection, it is useful to analyze the relationship between these two concentrations calculated for the model system when c_L = const. It should be remembered that the latter condition applies to the diffusion layer in which mass transport of the components of complex systems is taking place. The dependence shown in Figure 4.10 can be conditionally divided into three approximately linear parts. AB reflects complex solution with ligand deficiency, CD – with ligand excess, whereas BC is the transitional zone analogous to the potential leaps shown in Figure 2.1. Any point on the curve can reflect the state within specific solution bulk. Let us imagine that A is such a point. However, let us assume that the potential of the electrode within the solution of the specified composition is linearly decreased at the constant rate v, represented by the line 1 in the insert in Figure 4.10.

According to Eq. (3.49), surface concentration of M^{n+} will decrease from the point A to, say, the point D in accordance with the exponential law

$$[M^{n+}]_s = [M^{n+}] \exp\left(-\frac{nFvt}{RT}\right). \tag{4.7}$$

If c_M changed according to the same law too (the case of a noncomplex system), the voltammograms should have one maximum. It is determined by two opposite phenomena. The first one is related to the fact that with the increase in overvoltage

(time), the current density increases too. However, at the same time, the diffusion layer develops whose effective thickness increases. Diffusion processes more and more influence the current density. According to the regularities of semi-infinite diffusion, due to the second effect, the current, with time, must fall to zero; within the frame of the Nernst model, it decreases approaching to the steady-state value. The latter effect, with time, becomes dominant. Hence, the said current maximum is determined by the superposition of these two effects.

However, at the electrode surface, c_M changes in a quite different manner in a complex system. Only within AB and CD intervals $[M^{n+}]$ and c_M variations are approximately similar, whereas between B and C the total metal concentration determining the current density practically remains unchanged. To obtain this change in the surface c_M in a noncomplex system, the electrode potential should be swept at a different rate whose dependence on time is represented by curve 2 in the inset of Figure 4.10. In the initial BC part, the effective ν is close to zero and only later it increases again. It is clear that the shape of the voltammograms will be quite different. It will depend on the ratio of ligand and metal concentrations ($r = c_L/c_M$) in the bulk of solution.

More detailed information about linear potential sweep (LPS) voltammograms of quasi-reversible processes is presented in our articles [12, 13] where systems with protonated ligand forms are analyzed. Here (Figures 4.11 and 4.12) we present two graphs regarding the model system whose complexation parameters are close to the respective Cu(II)–glycine characteristics (see Figure 1.1), namely $\log \beta_1 = 8$, $\log \beta_2 = 15$, $\log \beta_1^H = 10$, $\log \beta_2^H = 12$. To define the thickness of the diffusion layer, it was assumed that the RDE is used with the rotation velocity of 1000 rpm. Therefore, the current maxima become evident unless and until the potential sweep rate is sufficiently high ($\nu \gtrsim 0.1\,V\,s^{-1}$).

The analysis of simulated reversible voltammograms shows that in the case of sufficiently high excesses of active ligand L^-, voltammograms practically coincide

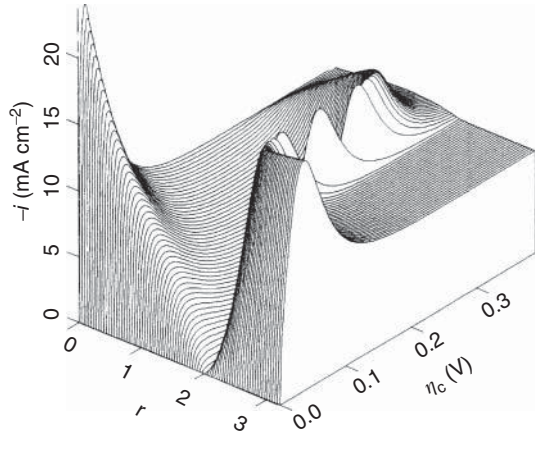

Figure 4.11 Reversible cathodic RDE chronovoltammograms simulated at $\nu = 1\,V\,s^{-1}$, pH 11, 1000 rpm. Effect of the ligand/metal ratio.

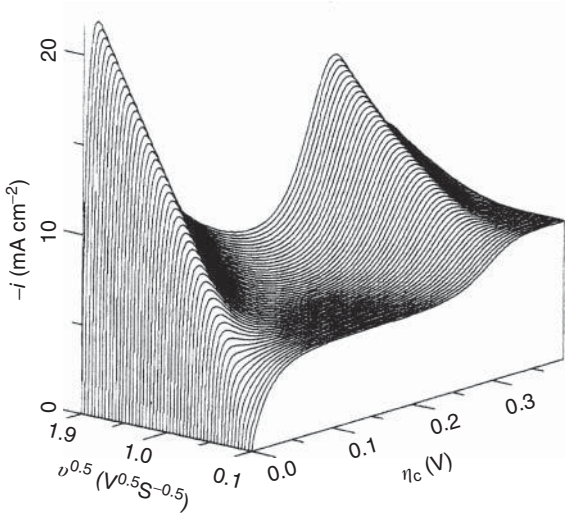

Figure 4.12 Reversible cathodic RDE chronovoltammograms simulated at $r = 4$, pH 4, 1000 rpm. Effect of the potential sweep rate.

with these obtained for ligand-free systems. It is necessary to emphasize that the protonated ligands LH and LH_2^+ are considered as inert species that are not capable of forming complexes with metal ions. Therefore, the complexation degree depends not only on the concentration of total ligand but also on solution pH. At high pH, the fraction of inactive ligands is low and the complexation degree depends on the ratio $r = c_L/c_M$ (Figure 4.11).

When decreasing ligand concentration, the height of the current peak i_p also decreases, and overvoltage η_p, which corresponds to this current maximum, increases to a great extent. When r becomes smaller than the equivalent ratio, which is equal to two in this case, two current maxima i_{p1} and i_{p2} (Figure 4.12) appear in the voltammogram. Overvoltage η_{p1} of the first peak is close to the η_p value of a noncomplex system that is equal to 0.021 V, as follows from Eq. (4.5). Moreover, as the analysis shows, i_{p1} values in ligand-deficient systems are approximately described by Eq. (4.5), if the value c in it is replaced with free metal ion concentration $[M^{n+}]$. The second current maximum is in the region of considerably higher cathodic overvoltages and has no clear relation with concentration of any of the components.

As before, two current maxima appear when there is lack of the active (nonprotonated) ligand form: that is, when c_L or pH values are sufficiently small. The latter case is demonstrated in Figure 4.12. It can be also seen that approximately linear dependence between the peak height and $\sqrt{\nu}$ is obeyed for both current maxima.

On the whole, the shape of voltammograms depends on various factors: the composition of the solution, stability of complexes and protonated ligands, charge transfer mechanism and its kinetic parameters, and so on. Therefore, in a general case, the shape of voltammogram is rather difficult to forecast.

References

1. Smith, D.E. (1964) Theory of the faradaic impedance. Relationship between impedances for various small amplitude. Alternating current techniques. *Anal. Chem.*, **36** (6), 962–970.
2. Survila, A. (1989) *Electrode Processes in Systems of Labile Complexes of Metals*, Mokslas, Vilnius (in Russian).
3. Molčadskytė, O.A. (1979) Kinetics of gold electrodeposition from acid solutions. Institute of Chemistry, PhD thesis. Vilnius.
4. McIntyre, J.D.E. and Peck, W.F. Jr., (1976) Electrodeposition of gold depolarization effects induced by heavy metal ions. *J. Electrochem. Soc.*, **123** (12), 1800–1813.
5. Survila, A. and Uksienė, V. (1992) The electroreduction kinetics of Cu(II)-glycine complexes in aqueous solution. *Electrochim. Acta*, **37** (4), 745–749.
6. Survila, A., Mockus, Z., and Kanapeckaitė, S. (2000) Kinetics of Sn and Co codeposition in citrate solutions. *Electrochim. Acta*, **46** (4), 571–577.
7. Survila, A., Kanapeckaitė, S., and Survilienė, A. (2001) Cathodic processes in ligand-deficient Cu|Cu(II), ethylenediamine system. *J. Electroanal. Chem.*, **501** (1-2), 151–159.
8. Mikučionis, K.S. (1980) Investigation of electrodeposition Co and Ni-Co alloy from citrate electrolytes. Institute of Chemistry, PhD thesis. Vilnius.
9. Spudas, L. and Survila, A. (1983) Electrochemical properties of the Cu(II)-glycine system under anodic polarization. *Proc. Lithuanian Acad. Sci. Ser. B*, **2** (135), 17–23.
10. Spell, J.E. and Philp, R.H. (1980) Voltammetric characterization of complexes in low concentrations of ligand. *J. Electroanal. Chem.*, **112** (2), 281–293.
11. Survila, A. (1987) Response of the labile complex system to the potential perturbation. Reversible processes. *Proc. Lithuanian Acad. Sci. Ser. B*, **4** (161), 27–34.
12. Survila, A. and Stasiukaitis, P.V. (1997) Linear potential sweep voltammetry of electroreduction of labile metal complexes. I. Back-ground model. *Electrochim. Acta*, **42** (7), 1113–1119.
13. Survila, A. and Stasiukaitis, P.V. (1997) Linear potential sweep voltammetry of electroreduction of labile metal complexes. The mechanism of consecutive charge transfer. *Chemija*, **9**, 212–217.
14. Berzins, T. and Delahay, P. (1953) Oscillographic polarographic waves for the reversible deposition of metals on solid electrodes. *J. Am. Chem. Soc.*, **75** (3), 555–559.

5
Quantitative Modeling of Quasi-Reversible Electrochemical Processes Involving Labile Complexes of Metals

Systems of metal complexes are noted for a greater variety of mechanisms of electrochemical processes than solutions of solvate complexes. One of the main reasons determining this feature is that by their composition alone, these complex solutions are more complicated. The material presented at the beginning of this book shows that such solutions can contain a large number of complex and ligand species. In studying the mechanism of electrochemical processes, first and foremost, one must determine the composition of the complex, which directly participates in the charge transfer step, or, in other words, its chemical formula. Hereinafter, this species shall be termed as an *electrically active complex* (EAC).

Analysis of equilibrium electrode potentials (Chapter 2) has shown that any modification of the Nernst equation gives the same E_{eq} value. Consequently, thermodynamics enables any complex species to be reduced at $E < E_{eq}$. However, only kinetics of partial charge transfer processes gives grounds to make an estimate of the contribution of each possible EAC to the net electrochemical process. The main parameter responsible for this could be the activation energy.

Complexes ML_N^{n+} with a saturated inner coordination sphere usually prevail in the systems with the excess of ligand. However, it is due to this property that the bond of such complexes with the metal phase of an electrode is weak, and the activation energy of electron transfer is rather high. The latter can decrease in the case of absorbed complexes when certain interaction between the metal surface and the complex being reduced occurs. Such interaction can be realized by making use of vacancy bonds, which form when a certain amount of ligand is eliminated from the coordination sphere. Hence, EAC is often formed in complex systems in the course of a reaction, for example,

$$ML_N^{n+} \rightarrow ML_p^{n+} + (N-p)L, \tag{5.1}$$

then it becomes reduced:

$$ML_p^{n+} + ne \rightarrow M + pL. \tag{5.2}$$

This electrochemical process consists of two steps – chemical and electrochemical one, and is said to be going on by the chemical step + electrochemical step (CE) mechanism (the acronym is formed of the first letters of the names of the steps). Quantitative description of electrochemical processes involving metal complexes becomes simpler when the single EAC stands out because of

Electrochemistry of Metal Complexes: Applications from Electroplating to Oxide Layer Formation, First Edition.
Arvydas Survila.

significantly lower activation energy. Then, the contribution of other complex species may be neglected.

It should be noted that in making assumptions about the EAC composition, the criterion that was used by Vetter [1], Gerischer [2], and other investigators [3] may be of value. It allows the minimum bulk concentration of the possible EAC to be evaluated. If the discharging complex ML_q^{n+} is formed during the chemical stage when one particle of ligand L is eliminated from the complex ML_p^{n+} (here $p = q + 1$), according to [2], the cathodic current density cannot exceed the value

$$i_{\max} = nF\sqrt{Dk_2[L]}[ML_q^{n+}], \tag{5.3}$$

where k_2 is the rate constant of the process:

$$ML_q^{n+} + L \rightarrow ML_p^{n+}. \tag{5.4}$$

Usually, due to diffusion limitations, the bimolecular reaction rate constant k_2 does not exceed 10^{10} dm^3 mol^{-1} s^{-1} and then the ratio $i_{\max}/[ML_q^{n+}]$ is of the order of 10^7 A cm mol^{-1}.

5.1 Kinetic Equations

Within the framework of formal electrochemical kinetics, the rate of the process (Eq. (5.2)) is described by equations that can have several forms. If the double-layer effects (Chapter 7) are assumed to be insignificant, and the conventional overvoltage $\eta = E - E_{eq}$ is used, the kinetic Butler–Volmer equation shall have the following form:

$$i = i_0 \left\{ \left(\frac{[L]_s}{[L]_b} \right)^p \exp\left(\frac{\alpha^a nF}{RT}\eta \right) - \frac{[ML_p^{n+}]_s}{[ML_p^{n+}]_b} \exp\left(-\frac{\alpha_c nF}{RT}\eta \right) \right\}, \tag{5.5}$$

where subscripts s and b denote the surface and bulk concentrations of the species given in square brackets. The exchange current density i_0, the anodic α_a and cathodic α_c charge transfer coefficients ($\alpha_c + \alpha_a = 1$) are kinetic parameters of the process (Eq. (5.2)).

Another alternative of the kinetic equation is:

$$i = nFk_s \left\{ [L]_s^p \exp\left(\frac{\alpha_a nF}{RT}\eta_0 \right) - [ML_p^{n+}]_s \exp\left(-\frac{\alpha_c nF}{RT}\eta_0 \right) \right\}, \tag{5.6}$$

where k_s is the standard rate constant, and the standard overvoltage η_0 is reckoned from the formal potential of the process (Eq. (5.2)), that is, $\eta_0 = E - E_p^{0/}$ (see Eqs. (2.6) and (2.7)). Both Eqs. (5.2) and (5.6) are equivalent and can be counterchanged using the relation between the exchange current density and the standard rate

constant:

$$i_0 = nFk_s[\mathrm{ML}_p^{n+}]^{\alpha_a}[\mathrm{L}]^{p\alpha_c} \tag{5.7}$$

It should be noted that i_0 depends on the composition of the solution, whereas k_s should be constant for the given system. If the process (Eq. (5.2)) is nonstationary, the current density and the surface concentrations become time dependent. Then, the relationship analog to Eq. (3.10)

$$c_{\mathrm{M},s} = c_{\mathrm{M},b} + \frac{1}{nF\sqrt{\pi D}}\int_0^t \frac{i(t-u)}{\sqrt{u}}\Psi(u)\mathrm{d}u, \tag{5.8}$$

can be used in addition to the aforementioned equations.

Probability that n electrons are at once transferred to EAC is very low when n exceeds 2. Then, processes are to be considered where the net charge transfer process consists of several consecutive steps with the formation of the intermediate species. A typical example could be the case of transfer of two electrons, which can be represented by the following general equations:

$$\mathrm{ML}_p^{2+} + \mathrm{e} \rightarrow \mathrm{ML}_q^{+} + (p-q)\mathrm{L}, \tag{5.9}$$

$$\mathrm{ML}_q^{+} + \mathrm{e} \rightarrow \mathrm{M} + q\mathrm{L}. \tag{5.10}$$

Current density of the total process, i, consists of current densities of separate steps $-i_1$ and i_2, respectively:

$$i = i_1 + i_2. \tag{5.11}$$

Kinetic equations can be obtained using Fick's first and Faraday's laws as described in Chapter 3. Diffusion flows of both M(II) and M(I) should be accounted for:

$$\frac{\partial c_{\mathrm{M(II)}}}{\partial t} = D_2\frac{\partial^2 c_{\mathrm{M(II)}}}{\partial x^2}, \tag{5.12}$$

$$\frac{\partial c_{\mathrm{M(I)}}}{\partial t} = D_1\frac{\partial^2 c_{\mathrm{M(I)}}}{\partial x^2}. \tag{5.13}$$

When formulating the initial conditions, it is thought that the system is totally equilibrated at $t = 0$ and the respective concentration of the intermediate, $c_{\mathrm{M(I),b}}$, is formed in the bulk of solution (see Section 2.2). Boundary conditions are as follows:

$$\left.\frac{\partial c_{\mathrm{M(II)}}}{\partial x}\right|_{x=0} = -\frac{i_1}{FD_2}, \tag{5.14}$$

$$\left.\frac{\partial c_{\mathrm{M(I)}}}{\partial x}\right|_{x=0} = \frac{i_1 - i_2}{FD_1}. \tag{5.15}$$

The following equations for surface concentrations of M(II) and M(I) species ($c_{\mathrm{M(II)},s}$ and $c_{\mathrm{M(I)},s}$ respectively) are obtained:

$$c_{\mathrm{M(II)},s} = c_{\mathrm{M(II)},b} + \frac{1}{F\sqrt{\pi D_2}} \int_0^t \frac{i_1(t-u)}{\sqrt{u}} \psi(u)\mathrm{d}u, \tag{5.16}$$

$$c_{\mathrm{M(I)},s} = c_{\mathrm{M(I)},b} + \frac{1}{F\sqrt{\pi D_1}} \int_0^t \frac{i_2(t-u) - i_1(t-u)}{\sqrt{u}} \psi(u)\mathrm{d}u. \tag{5.17}$$

Assuming that D_1 and D_2 related to species M(I) and M(II), respectively, do not differ significantly ($D_1 \approx D_2 = D$), it is possible to obtain the expression involving the net current density i that is controlled experimentally. Then, Eqs. (5.11), (5.16), and (5.17) yield

$$c_{\mathrm{M(II)},s} + \frac{c_{\mathrm{M(I)},s}}{2} = c_{\mathrm{M(II)},b} + \frac{c_{\mathrm{M(I)},b}}{2} + \frac{1}{nF\sqrt{\pi D}} \int_0^t \frac{i(t-u)}{\sqrt{u}} \psi(u)\mathrm{d}u. \tag{5.18}$$

Here, the stoichiometric number of electrons involved in an electrode reaction $n = 2$. Similarly to Eq. (5.2), the partial current densities are expressed by

$$i_1 = i_{01} \left\{ \frac{\left[\mathrm{ML}_q^+\right]_s [\mathrm{L}]_s^{p-q}}{[\mathrm{ML}_q^+]_b [\mathrm{L}]_b^{p-q}} \exp\left(\frac{\alpha_{a1}F}{RT}\eta\right) - \frac{[\mathrm{ML}_p^{2+}]_s}{[\mathrm{ML}_p^{2+}]_b} \exp\left(-\frac{\alpha_{c1}F}{RT}\eta\right) \right\}, \tag{5.19}$$

$$i_2 = i_{02} \left\{ \frac{[\mathrm{L}]_s^q}{[\mathrm{L}]_b^q} \exp\left(\frac{\alpha_{a2}F}{RT}\eta\right) - \frac{[\mathrm{ML}_q^+]_s}{[\mathrm{ML}_q^+]_b} \exp\left(-\frac{\alpha_{c2}F}{RT}\eta\right) \right\}, \tag{5.20}$$

where the extra subscripts 1 and 2 refer to the relevant parameters of the processes (Eqs. (5.9) and (5.10)), respectively.

According to Vetter [4], the steady-state partial currents might be assumed to be equal: $i_1 = i_2 = i/2$. Such an assumption is reasoned when the intermediate product ML_q^+ remains within the reaction zone, that is, its amount transferred by diffusion from the electrode surface to the bulk of the solution is negligible. To check this assumption, we carried out the special investigation [5] using the data simulated for the stepwise process $\mathrm{M}^{2+} + \mathrm{e} \rightarrow \mathrm{M}^+ + \mathrm{e} \rightarrow \mathrm{M}$, proceeding under linear potential sweep (LPS) conditions. According to the results obtained, two limiting cases can be easy considered. In the region of the plateau of limiting current, the relationship

$$\frac{i_2}{i_1} = 1 + \frac{[\mathrm{M}^+]_b D_1 \delta_2}{[\mathrm{M}^{2+}]_b D_2 \delta_1} \tag{5.21}$$

is obtained, which shows that the ratio of i_2/i_1 is determined mainly by the ratio of concentrations $[\mathrm{M}^+]_b/[\mathrm{M}^{2+}]_b$ that establish in the system $\mathrm{M}|\mathrm{M}^{2+}$ after equilibration. In its turn, the latter ratio depends on the difference $\Delta E^{0/} = E_1^{0/} - E_2^{0/}$ in formal potentials of the $\mathrm{M}|\mathrm{M}^+$ and $\mathrm{M}|\mathrm{M}^{2+}$ electrodes (see Eq. (2.17)). Hence, the higher the value of $\Delta E^{0/}$, the lower the ratio of $[\mathrm{M}^+]_b/[\mathrm{M}^{2+}]_b$ and the difference of $(i_1 - i_2)$. For example, $\Delta E^{0/} = 0.183\,\mathrm{V}$ in the case of Cu^{2+} solutions, and partial current densities will differ by the value of some per cent only. It should be noted

that the ratio of i_2/i_1 does not depend on kinetic parameters of the consecutive charge transfer processes in this case.

Another limiting case concerns the region of low cathodic overvoltages where voltammograms can be linearized. It follows at $[M^+]_b/[M^{2+}]_b \ll 1$ that $i_1 \approx i_2$, if $i_{01} \approx i_{02}$.

The region of moderate η_c is more complicated for analysis and certain conclusions become available after examination of simulated LPS voltammograms. The results shown in Figure 5.1 have been obtained for a model system with characteristics closely approximating those for $Cu|Cu^{2+}$ one: $\Delta E^{0/} = 0.183\,V, D_1 = D_2 = 7 \times 10^{-6}\,cm^2\,s^{-1}$. We fixed the initial concentration of Cu^{2+} ions to be equal to 0.01 M; ~1% of this amount was converted into Cu^+ in the course of equilibration. As the transfer of the first electron to $Cu^{2+}$is known as the *rate-determining step* ($i_{01} \ll i_{02}$), we set $i_{01} = 0.1$ and $i_{02} = 50\,mA\,cm^{-2}$.

An inspection of the region of limiting current shows that i_1/i_2 is close to 1. Besides, this ratio does not depend on the exchange current density and the charge transfer coefficient. Thus, we have an evidence to support the conclusion that the ratio of i_2/i_1 is independent of kinetic parameters of consecutive charge transfer.

The highest deviations of i_1/i_2 from 1 are observed at low overvoltage and high potential sweep rate. Despite the fact that the entire voltammogram corresponds to the steady state at sufficiently low v, the difference $i_1 - i_2$ remains prominent: when $v \to 0$, the value of $i_1/i_2 \approx 0.85$. As the potential sweep rate increases, the ratio of i_1/i_2 approximates that of i_{01}/i_{02}. The same result follows from other data obtained at different i_{01}/i_{02} [5]. Hence, though the attainment of a steady state favors an approach of partial currents, this does not result in complete equalization of i_1 and i_2. Simulations with other $\Delta E^{0/}$ values showed [5] that the diminution of $\Delta E^{0/}$ leads to a decrease in the first partial current due to the corresponding

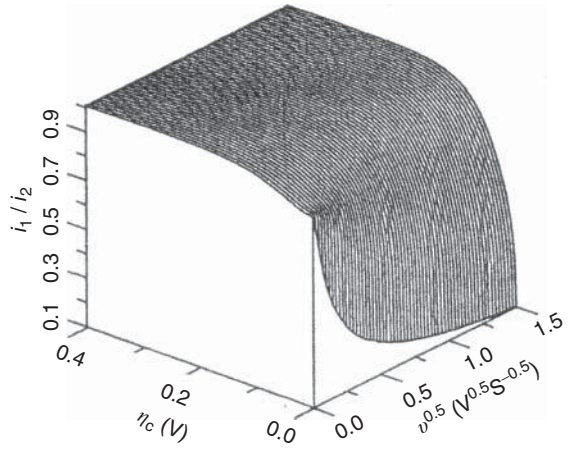

Figure 5.1 The ratio of partial current densities versus the overvoltage at various potential sweep rates.

decrease in the bulk concentration of M^{2+} ions. This current approaches zero at $E^{0/} < 0$.

Hence, the condition of $i_1 \approx i_2$ seems to be obeyed in the Tafel region at sufficiently high $E^{0/}$ under steady-state conditions. Then, it is possible to eliminate concentrations of the intermediate from Eqs. (5.19) – (5.20) and obtain the following relationship:

$$i = \frac{\left(\frac{[L]_s}{[L]_b}\right)^p \exp\left[\frac{(1+\alpha_{a1})F}{RT}\eta\right] - \frac{[ML_p^{2+}]_s}{[ML_p^{2+}]_b} \exp\left(-\frac{\alpha_{c1}F}{RT}\eta\right)}{\frac{1}{2i_{01}} + \frac{1}{2i_{02}}\left(\frac{[L]_s}{[L]_b}\right)^{p-q} \exp\left[\frac{(\alpha_{a1}+\alpha_{c2})F}{RT}\eta\right]}. \tag{5.22}$$

It is necessary to note that mathematical expressions of the kinetic equations are directly related to the shape of relevant charge transfer reactions ((5.2) or (5.9) and (5.10)). Therefore, in quantitatively describing the rate of the electrochemical process, determination of its mechanism poses one of the major problems.

5.2 Employment of Voltammetric Data

At present, voltammetric investigations hold a prominent position among different techniques used for studies of electrochemical behavior of metal complexes. Currently available variations of voltammetry make it possible to accumulate the necessary experimental data readily and handily. The next step involves a quantitative interpretation of the data obtained, which could be modified in response to the respective theoretical relationships intended for application. Some selected transforms of voltammetric data are considered next.

5.2.1 Tafel Plots Normalized with Respect to the Surface Concentration of EAC

One of the oldest methods of determining kinetic parameters is based on the analysis of Tafel plots (log i dependence on η or E). Tafel dependencies are obtained at sufficiently high anodic ($\eta_a \equiv \eta$) or cathodic ($\eta_c \equiv -\eta$) overvoltages where one of the exponents of the kinetic equation becomes close to zero. Having rejected this term, the kinetic equation can be simplified. As kinetic equations always contain surface concentrations (c_s), these terms should be also accounted for. Notice that this procedure amounts to a mass transport correction of voltammetric characteristics. In the case of simple redox systems, this can be performed by straightforward division of current density by $(1 - i/i_d)$ [4]. The conditions under which a mass transport corrected Tafel plot is predicted to be linear were considered by Streeter and Compton [6]. According to them, the linearity of the plot may be predicted with knowledge of the reversible/irreversible nature of the electron transfer and the electrode geometry. The microdisc and tubular flow electrodes were used as examples of nonuniformly accessible electrodes. It was shown by numerical

simulation that the Tafel equation is not valid when axial and radial diffusions are significant. These conclusions seem to be also acceptable for systems involving complexes. However, the means for mass transport correction deserve adequate consideration.

On elimination of anodic or cathodic exponential terms from Eq. (5.5), we shall obtain respectively:

$$\ln \frac{i_a}{[\mathrm{L}]_s^p} = \ln i_0 - p \ln [\mathrm{L}]_b + \frac{\alpha_a nF}{RT}\eta_a, \tag{5.23}$$

$$\ln \frac{i_c}{[\mathrm{ML}_p^{n+}]_s} = \ln i_0 - \ln [\mathrm{ML}_p^{n+}]_b + \frac{\alpha_c nF}{RT}\eta_c, \tag{5.24}$$

where anodic current density $i_a \equiv i$, and cathodic one $i_c \equiv |i|$. As kinetic equations always contain surface concentrations (c_s), which depend on i (and E), they must be moved to the left side of the Tafel expression, as has been done in Eqs. (5.23) and (5.24). In the opposite case, the Tafel dependencies will not be linear. Division of the current density by c_s, or, in other words, its *normalization* with respect to a corresponding surface concentration is necessary in studying processes taking place in the systems of complex compounds, in which changes in surface concentrations can be profound and complicated. A further analysis of such *normalized Tafel plots* (*NTPs*) is simple: charge transfer coefficients α are determined from the slope of the lines obtained, and when extrapolating these lines to $\eta = 0$(or to $E = E_{\mathrm{eq}}$)i_0 are found.

To obtain the NTP in case of consecutive transfer of several electrons, a more complicated kinetic equation (5.22) must be first simplified. This is possible to do having made the assumption about which of the steps, (Eq. (5.9) or (5.10)), determines the rate of the process. If it is transfer of the first electron, the condition that $i_{01} \ll i_{02}$ is satisfied, and the term of Eq. (5.22) with i_{02} can be rejected. Further, as earlier, the NTP expressions can be obtained, which are valid at high anodic or cathodic overvoltages:

$$\ln \frac{i_a}{[\mathrm{L}]_s^p} = \ln 2i_{01} - p \ln [\mathrm{L}]_b + \frac{(1+\alpha_{a1})F}{RT}\eta_a, \tag{5.25}$$

$$\ln \frac{i_c}{[\mathrm{ML}_p^{2+}]_s} = \ln 2i_{01} - \ln [\mathrm{ML}_p^{2+}]_b + \frac{\alpha_{c1}F}{RT}\eta_c. \tag{5.26}$$

The NTP expressions are found in the analogous way when the rate-determining step is transfer of the second electron to EAC, that is, when $i_{02} \ll i_{01}$:

$$\ln \frac{i_a}{[\mathrm{L}]_s^q} = \ln 2i_{02} - q \ln [\mathrm{L}]_b + \frac{\alpha_{a2}F}{RT}\eta_a, \tag{5.27}$$

$$\ln \frac{i_c}{[\mathrm{ML}_q^{2+}]_s} = \ln 2i_{02} - \ln [\mathrm{ML}_q^{2+}]_b + \frac{(1+\alpha_{c2})F}{RT}\eta_c. \tag{5.28}$$

Several properties of the equations obtained should be mentioned. It is natural that they contain kinetic parameters of the rate-determining step only. However,

contrary to the case of the earlier considered mechanism (Eq. (5.2)), these dependencies contain double exchange current densities and multipliers of $(1 + \alpha)$ type at η in Eqs. (5.25) and (5.28). In other words, the value of the effective α determined from the experimental NTP can be larger than 1. This circumstance enables us to determine the transfer of which electron controls the rate of the process. Another thing is that despite the fact that intermediate complex ML_q^+ participates in the second step; Eq. (5.28) contains *concentrations of its double-charged analog* ML_q^{2+}. This makes it easier to construct the NTP because most often there is a lack of information about the composition of intermediate complexes and their stability.

It is seen from the above-presented material that in constructing the NTP, it is necessary to know the composition of the EAC, which is to be determined by means of other methods. Sometimes, we succeed in solving this problem within the framework of the NTP methods by reviewing all possible EAC and making use of several criteria. If the composition of the EAC is defined correctly, the NTP, first of all, must be linear. Second, the NTP obtained for solutions of different composition must coincide if the electrode potential E is plotted on the abscissa axis. One can make sure of that having analyzed modification of the kinetic equation (5.6) in the analogous manner.

No matter what the form of voltamperogram is, it is possible to obtain linear NTP. For example, in the system Cu|Cu(II), glycine, where there is deficiency of the active form of ligand L^-, voltammograms have a prewave, the reasons for appearance of which are described in Chapter 4. As the analysis [7] showed, the surface concentration of one of the Cu(II) complexes, namely that of CuL^+, falls significantly (about 10^4 times) in the prewave region. Figure 5.2 demonstrates a voltammogram and its transform into NTP. It is possible to obtain linear NTP only when this particle is the EAC.

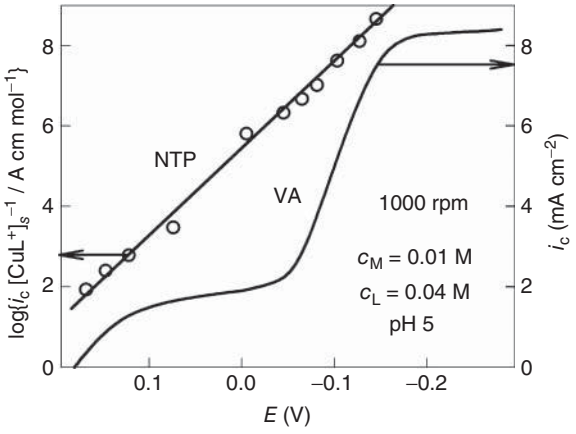

Figure 5.2 RDE voltammogram (VA) and normalized Tafel plot (NTP) obtained for the system Cu|Cu(II), glycine.

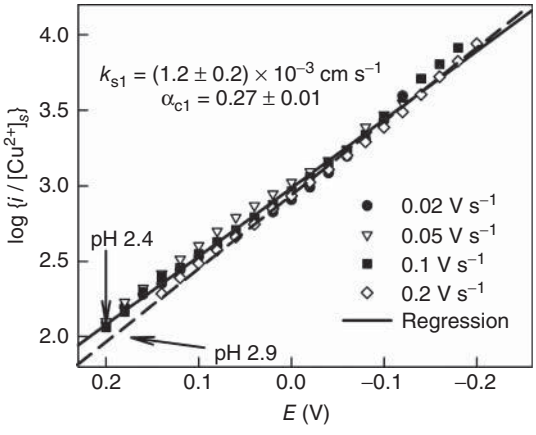

Figure 5.3 NTP obtained for Cu|Cu(II), glycolic acid system at pH 2.4 and different potential sweep rates (symbols). Regression of similar results obtained at pH 2.9 is presented by dotted line. Dimensions: $[i] = \mathrm{mA\,cm^{-2}}$, $[c] = \mathrm{mol\,dm^{-3}}$.

Another example is processes taking place in the system Cu|Cu(II), glycolic acid [8]. Procedures carried out to evaluate surface concentrations in this system are based on the material balance equations written for the surface layer (see [8]). The NTP obtained are shown in Figure 5.3. It can be stated that neither the potential sweep rate nor acidity of the solution (and the composition) has any significant influence on the nature of these dependencies. Thus, the assumption that free Cu^{2+} ions (Cu(II) aqua complexes) are electrically active in this case is quite acceptable. Kinetic parameters of the charge transfer process $Cu^{2+} + e \rightarrow Cu^{+}$ can be determined with reasonable accuracy (Figure 5.3).

In closing, it is necessary to call particular attention to one aspect relating to Tafel plots. To construct, for instance, cathodic Tafel plot, the anodic component of current density should be ignored as negligible. In the case of metal electrodeposition in ligand-free systems, anodic exponent in the kinetic equation contains no multiplier; therefore, it is very easy to estimate this term. However, when metal complexes are reduced, anodic exponent is multiplied by the surface concentration of ligand, $[L]_s$, (see e.g., Eq. (5.2)). As cathodic overvoltage increases, $[L]_s$ increases as well. It is conceivable that an increase in $[L]_s$ will surpass a decrease in anodic exponent retarding the fall of anodic component.[1)] Therefore, a check upon the validity of the procedures applied is highly recommended.

5.2.2
Analysis of LPS Current Maxima

LPS voltammetry employing a linear potential scan $\eta = vt$ is a widely applied technique. The theoretical basis of this method was elaborated for different

1) Such case is possible in the Au|Au(I) CN^{-} system containing no extra cyanide (see Section 8.1.3).

electrochemical processes controlled by diffusion, charge transfer, slow chemical interactions, and so on. Most often, coordinates of LPS current peaks (E_p and i_p) are analyzed. In the case of diffusion-controlled (reversible) process $M^{n+} + ne \rightarrow M$ (the product forms a solid phase), the following relationship for i_p was obtained [9]

$$i_p = 1.082\, nF\sqrt{\frac{nF\nu}{\pi RT}}Dc. \tag{5.29}$$

In this case, the position of current peak does not depend on ν, that is, E_p = const. If the reduction process is irreversible, the latter relationship undergoes a change [10]:

$$i_p = 0.282nF\sqrt{\frac{\pi F}{RT}\alpha n_\alpha \nu Dc}, \tag{5.30}$$

and the peak potential becomes a linear function of $\ln \nu$:

$$\frac{\partial E_p}{\partial \ln \nu} = \frac{RT}{2\alpha n_\alpha F}. \tag{5.31}$$

More complicated dependencies arise when a slow chemical step precedes the charge transfer. To compare the i_p of the reversible redox process with i_r produced by slow first-order chemical reaction, the empiric relation was suggested (see [11]):

$$i_p/i_r = 1.02 + 0.531p, \tag{5.32}$$

where

$$p = \frac{1}{K}\sqrt{\frac{F\alpha n_\alpha \nu}{RT(k_1 + k_{-1})}}. \tag{5.33}$$

Relationships (Eqs. (5.29) and (5.30)) with $c = c_M$ seem to be applicable for labile systems with excess of ligand. This can be seen from the data in Figure 5.4 where

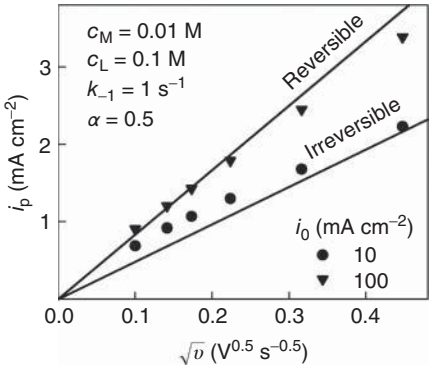

Figure 5.4 Comparison of i_p simulated for model system (symbols) with those obtained by Eqs. (5.29) and (5.30) (lines).

the data, simulated for model system (Section 3.4.2) with given parameters, are compared with dependencies following from Eqs. (5.29) and (5.30). At sufficiently high exchange current densities ($i_0 = 100\,\mathrm{mA\,cm^{-2}}$), simulated data are in line with the relationship (Eq. (5.29)) derived for reversible processes. At lower i_0, the transition to regularity (Eq. (5.30)) is evident. To draw more general conclusions, extensive simulations are required.

5.3
Techniques Based on the Control of the Intensity of Forced Convection

In order to study the mechanism of electrochemical processes, it is necessary to have reliable and correctly determined values of kinetic parameters. As processes involving complex species have peculiarities, the applicability of traditional methods to the investigation of complex systems must be critically reviewed. Main problems are most often related to the evaluation of surface concentrations whose experimental determination is not available. Therefore, for the most part, surface concentrations are obtained by simulation using the certain theoretical model. It is obvious that the reliability of the results obtained depends on the adequacy and precision of the model used.

The difference between surface and bulk concentrations depends on the regularities of mass transport and manifests itself in the fact that the certain diffusion overvoltage arises in the system. Use of the rotating disc electrode (RDE) makes it possible to carry out the experiments under different intensities of forced convection and to control the intensity of diffusive mass transport. This provides the means to eliminate the diffusive part of the overvoltage promoting the determination of kinetic parameters.

5.3.1
Isosurface Concentration Voltammetry

We have already mentioned that linear Tafel plots cannot be obtained by simple elimination of one of the exponents in Eq. (5.2) or (5.6), because the remaining EAC surface concentration still depends on the overvoltage. In this connection, the possibilities to carry out experiments at constant EAC concentration have attracted considerable attention. RDE voltammetry making it possible to realize this condition was suggested by Miller *et al*. [12, 13] and was referred to as *isosurface concentration voltammetry* (ICV). This method was substantiated theoretically for quasi-reversible reduction in relatively simple systems (metal – metal ions and redox systems) for low overpotentials [12 – 14] and for the Tafel regions [15, 16]. Later, complex systems were considered in this respect [17].

Conditions for constant surface concentration can be formulated on the basis of equations describing the mass transport. For instance, it follows from Eq. (3.12) that $i\delta$ should be kept constant under steady-state conditions. This condition

Table 5.1 Conditions for constant surface concentrations.

Method	Constant quantity	c_M (0, t)
RDE voltammetry	$\frac{i}{\sqrt{\Omega}}$	$c_M + \frac{1.61\nu^{1/6}}{nFD^{3/2}} \frac{i}{\sqrt{\Omega}}$
Chronopotentiometry	$i\sqrt{t}$	$c_M + \frac{2}{nF\sqrt{\pi D}} i\sqrt{t}$
Linear current sweep	$\nu t^{3/2}$	$c_M + \frac{4}{3nF\sqrt{\pi D}} \nu t^{3/2}$

together with Eq. (3.37) as well as with other expressions given in Table 3.2 suggests requirements listed in Table 5.1.

An experimental verification of the method under consideration was performed for the Ag|Ag(I), NH_3 system, because certain kinetic data are available in [18]. To prepare working electrodes, silver was deposited on Pt RDE from a cyanide bath. Current density and the rate of rotation varied simultaneously in such way that quantity $i/\sqrt{\Omega}$ remained constant.

In analyzing the RDE voltammograms, the following equilibria were taken into account: $NH_3 + H^+ \rightleftarrows NH_4^+$, $Ag^+ + NH_3 \rightleftarrows Ag(NH_3)^+$, $Ag^+ + 2NH_3 \rightleftarrows Ag(NH_3)_2^+$, for which the logarithms of the constants β_1^H, β_1, and β_2 are, respectively, 9.13, 3.31, and 7.21 [19]. Simulations of distribution of the components showed [17] that a large part of Ag(I) is present as $Ag(NH_3)_2^+$. The expression for $c_M(0, t)$ given in the first line of Table 5.1 made it possible to evaluate the surface concentrations of Ag(I) at the certain $i/\sqrt{\Omega}$ applied in the experiments. These values are listed in Figure 5.5. Calculations with procedures described in Chapter 3 showed that $Ag(NH_3)_2^+$ species predominate at the electrode surface. According to [20], these species take part in the charge transfer step with $\alpha_c = 0.5$.

Linear Tafel plots can be constructed at sufficiently high cathodic overvoltages (Figure 5.5) that obey the equation:

$$\ln|i_c| = \ln(nFk_s) + \ln[Ag(NH_3)_2^+]_s + \frac{\alpha_c nF}{RT}\eta_0, \tag{5.34}$$

where η_0 is reckoned from the formal potential of the charge transfer step. According to Eq. (2.7), the latter is given by $E_2^{0/} = 0.799 - 0.059 \log \beta_2 = 0.374\,V$. It follows from the slopes of Tafel sections that $\alpha_c = 0.44$; extrapolation of these lines to $E = E_2^{0/}$ yields $k_s = 2.9 \times 10^{-3}\,cm\,s^{-1}$.

5.3.2
Determination of the Exchange Current Density from Polarization Resistance

Elimination of diffusion overvoltage becomes readily available when the electrochemical system can be treated as linear. This is true in the neighborhood of the equilibrium potential where the overvoltage is sufficiently low. Let us consider

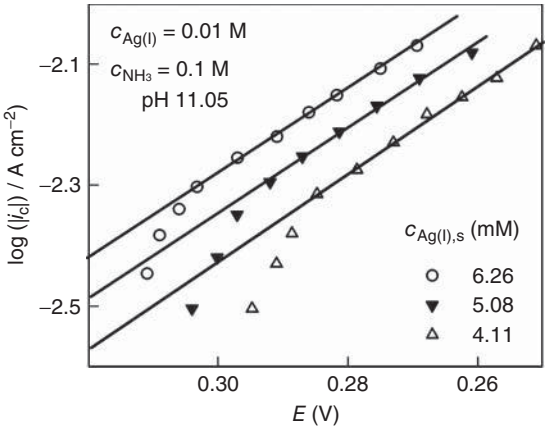

Figure 5.5 Tafel plots obtained for Ag|Ag(I), NH_3 system at pH 11.05 and constant surface concentrations, $c_{Ag(I),s}$, as indicated.

the electrochemical process whose rate is controlled by charge transfer and diffusion; from this point of view, the slope of voltammograms $(\partial\eta/\partial i)_{\eta\to 0}$, which, in a physical sense, can be called *polarization resistance* R_{pol}.

In case of quasi-reversible processes that take place in the redox system, R_{pol} is the sum of resistances of charge transfer R_{ct} and diffusion R_d [4]:

$$R_{pol} = \frac{RT}{nF}\left(\frac{1}{i_0} + \frac{1}{i_{ad}} + \frac{1}{|i_{cd}|}\right), \tag{5.35}$$

where i_{ad} and i_{cd} are, respectively, anodic and cathodic diffuse limiting current densities. If consecutive transfer of two electrons is taking place in the redox system, we obtain

$$R_{pol} = \frac{RT}{2F}\left(\frac{1}{2i_{01}} + \frac{1}{2i_{02}} + \frac{1}{i_{ad}} + \frac{1}{|i_{cd}|}\right). \tag{5.36}$$

Thus, in case of processes being analyzed, the value R_{pol} is determined by i_0 and the parameters of diffusion mass transport. If processes are fully reversible, the terms with the exchange current densities can be eliminated from Eqs. (5.35) or (5.36). In case of the irreversible process, on the contrary, members with limiting current densities may not be written.

When studying polarization resistance of complex systems, kinetic equations must be rearranged accordingly. Here, we shall omit mathematical details, which were published earlier [21]. In case of the (Eq. (5.2)) mechanism, the following equation is obtained:

$$R_{pol} = \frac{RT}{nF}\left(\frac{1}{i_0} + \frac{N}{i_{ad}} + \frac{1}{|i_{cd}|}\right), \tag{5.37}$$

where N is the maximum number of ligand particles in the complex. If we use the RDE during the investigations, limiting current densities will be proportional to

$\sqrt{\Omega}$ (Ω is the angular velocity of the electrode rotation). Then,

$$R_{\text{pol}} = \frac{RT}{nF}\left[\frac{1}{i_0} + \left(\frac{N}{\kappa_a} + \frac{1}{\kappa_c}\right)\frac{1}{\sqrt{\Omega}}\right], \tag{5.38}$$

where κ_a and κ_c are coefficients of proportionality between corresponding limiting current densities and $\sqrt{\Omega}$, which are determined by the RDE theory.

It should be noted that the latter two equations are obtained on condition that $\beta_N \gg \beta_{j\neq N}$. If it does not take place, N is to be treated as the average number of coordinated ligands, but linear dependence between R_{pol} and $1/\sqrt{\Omega}$ remains. In case of consecutive transfer of two electrons, a similar equation is obtained:

$$R_{\text{pol}} = \frac{RT}{2F}\left[\frac{1}{2i_{01}} + \frac{1}{2i_{02}} + \left(\frac{N}{\kappa_a} + \frac{1}{\kappa_c}\right)\frac{1}{\sqrt{\Omega}}\right]. \tag{5.39}$$

In all cases, by extrapolating R_{pol} to infinite intensity of forced convection (to $1/\sqrt{\Omega} = 0$), we obtain charge transfer resistances, which have traditional expressions:

$$R_{\text{ct}} = \frac{RT}{nFi_0} \tag{5.40}$$

or

$$R_{\text{ct}} = \frac{RT}{2F}\left(\frac{1}{2i_{01}} + \frac{1}{2i_{02}}\right). \tag{5.41}$$

In the latter case, we have two unknown parameters. If one of them is significantly higher than the other one, it can be rejected. Hence, in this case, the R_{ct} is determined by the lower exchange current density. Additional information about these two parameters can be obtained from other data, for example, from Tafel dependencies, which were analyzed earlier. Concluding the discussion of this method, we present an example of an experimental research of Cu|Cu(II), glycine system (Figure 5.6).

The electroreduction of Cu(II) on Hg electrode is controlled by diffusion. Addition of glycine has no significant effect on the limiting current and results in the negative shift of the half-wave potential according to the theoretical requirements (see Eq. (2.9)). As Cu^{2+}(aq), CuL^-, and CuL_2 are similar-sized, an average diffusion coefficient in this system ($7.1 \times 10^{-6}\,cm^2\,s^{-1}$) is close to that established for Cu^{2+} aqua-ions ($(7.4/7.8) \times 10^{-6}\,cm^2\,s^{-1}$). Kinetics of CuL^- and CuL_2 formation is considered in Section 3.4.2. Rate constants listed in Table 3.3 are indicative of sufficiently high liability of this system.

Analysis of chronopotentiometric data [22] has shown that the rate of anodic process does not actually depend on the free ligand concentration. This feature gives grounds to consider the i_{02} as constant kinetic parameter making the analysis of polarization resistances easier.

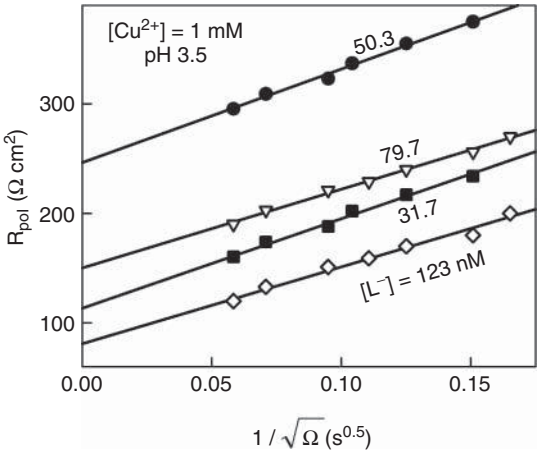

Figure 5.6 Dependencies of polarization resistance on $1/\sqrt{\Omega}$ in the series of isopotential Cu(II)–glycine solutions with constant $[Cu^{2+}] = 1\,\text{mmol}\,\text{dm}^{-3}$ and various L^- concentrations indicated at respective lines.

5.3.3
Electrochemical Impedance Spectroscopy (EIS) under Forced Convection Conditions

When the applied constant potential is superimposed by an alternating (sinusoidal) potential signal of small magnitude (Eq. (3.40)), the certain periodic variations in current density and surface concentrations arise (see Eqs. (3.41)–(3.45)). It is possible to derive expressions for impedance from these equations assuming that the electric properties of the electrode can be represented by the resistance R_s and capacitance C_s in series. Then, the real and imaginary parts of the faradaic impedance are respectively:

$$Z^{/} \equiv R_s = \frac{aV_0}{a^2 + b^2}, \tag{5.42}$$

$$Z^{//} \equiv \frac{1}{\omega C_s} = \frac{bV_0}{a^2 + b^2}, \tag{5.43}$$

where angular frequency $\omega = 2\pi f$. Parameters a and b required for quantitative description of impedance depend on the kinetic parameters of the electrochemical process. To find this relation, it is necessary to formulate the kinetic equation and to compare it identically with Eq. (3.43). The mathematical treatment is rather complicated and details are given elsewhere [18, 23, 24]. The resulting relationships are as follows:

$$R_s = \frac{R_0}{A}\left(1 + \frac{\sqrt{2\omega}}{\lambda}\right), \tag{5.44}$$

$$\frac{1}{\omega C_s} = \frac{R_0}{A}, \tag{5.45}$$

$$\psi = \arctan\left(1 + \frac{\sqrt{2\omega}}{\lambda}\right)^{-1}, \tag{5.46}$$

where

$$R_0 = \lim_{k_s \to \infty} R_s. \tag{5.47}$$

Adequate analytical expressions for λ, R_0, and A are available only in the case of simple redox processes. For instance, in the case of reaction $O + ne \rightarrow R$

$$R_0 = \frac{4RT\cosh^2\left(\frac{nF}{2RT}\eta_{1/2}\right)}{n^2F^2\sqrt{2\omega}(c_O\sqrt{D_O} + c_R\sqrt{D_R})}, \tag{5.48}$$

$$A = 1 - \frac{\alpha_c \exp\left(-\frac{\alpha_a nF}{2RT}\eta_{1/2}\right) - \alpha_a \exp\left(\frac{\alpha_c nF}{2RT}\eta_{1/2}\right)}{c_O\sqrt{D_O} + c_R\sqrt{D_R}} \times \frac{i\sqrt{D}}{i_0^0}, \tag{5.49}$$

where the standard exchange current density

$$i_0^0 = nFk_s, \tag{5.50}$$

$\eta_{1/2}$ is the overvoltage reckoned from the half-wave potential of the reversible process, that is,

$$\eta_{1/2} = E - E_{1/2}, \tag{5.51}$$

and

$$D = D_O^{\alpha_a} D_R^{\alpha_c}. \tag{5.52}$$

When the reduction of metal ions $M^{n+} + ne \rightarrow M$ results in the formation of a solid product, the aforementioned relationships are respectively modified [23]:

$$R_0 = \frac{RT \exp\left(-\frac{nF}{RT}\eta_0\right)}{n^2F^2\sqrt{2\omega D_M}}, \tag{5.53}$$

$$A = 1 - \alpha_c \exp\left(-\frac{\alpha_a nF}{RT}\eta_0\right)\frac{i}{i_0^0}, \tag{5.54}$$

$$\lambda = \frac{k_s}{\sqrt{D_M}} \exp\left(-\frac{\alpha_c nF}{RT}\eta_0\right). \tag{5.55}$$

In the case of processes involving metal complexes, Eqs. (5.42)–(5.47) are valid, but general analytical expressions for λ, R_0, and A are not available and the certain simplifications are necessary [18].

The presented theory is applicable to electrochemical processes whose rate is controlled by charge transfer and diffusion. Based on the relationships obtained,

the following EIS modification can be suggested. It follows from the aforementioned equations that the capacitance C_s and the conductance $1/R_s$ are linear functions of current density, when the electrode potential is kept constant:

$$C_s = C_0 - \frac{\partial C_s}{\partial i} i \equiv ki, \tag{5.56}$$

$$\frac{1}{R_s} = \frac{C_s}{\frac{1}{\omega} + \sqrt{\frac{2}{\omega\lambda^2}}}. \tag{5.57}$$

To obtain such dependencies experimentally, the measurements should be carried out at constant E using RDE and varying its rotation velocity and thereby the current density.

It should be noted that the aforementioned model deals with the semi-infinite diffusion, which is presented by Warburg impedance. As the diffusion layer of finite thickness δ is formed at the RDE surface, it is necessary to meet certain relations between δ, specified by Eq. (3.5), and the depth of penetration of the concentration wave $x_0 = \sqrt{2D/\omega}$. Investigations in this field show [25, 26] that the two aforementioned diffusion models are in harmony when $x_0 < 0.1\delta$. At Schmidt number $\mathrm{Sc} = \nu/D = 2000$, this condition is satisfied when $\omega > 6\Omega$ (or $f > 0.1m$, where m is rotation velocity in rpm).

In the case of real systems, the total impedance Z involves such nonfaradaic elements as the ohmic resistance of the solution R_Ω and the impedance of the double electric layer Z_{dl}. The former quantity is easily obtained as the limit of Z' at $\omega \to \infty$. In the case of smooth homogeneous electrode surface, Z_{dl} can be replaced by the capacitance C_{dl}.

It is necessary to say that the detachment of separate double-layer element in the net equivalent circuit is justified when the faradaic and nonfaradaic currents are independent of one another. This can take place at low EAC concentrations when these species have no pronounced effect on the structure of the double layer. The situation changes in the case of surface-active EAC when these species adsorb at the electrode|solution boundary. Then, according to [27], the equivalent circuit should be supplemented by some extra elements.

At $E = \mathrm{const}$, when the adsorption isotherm is congruent with respect to the electrode potential and the surface coverage is low, the effective standard rate constant may be determined with the *posterior* correction for the double-layer effects. Besides, in some cases (for instance, in the case of $\mathrm{M}|\mathrm{M}^{n+}$ electrode), faradaic elements do not depend on the bulk concentration of M^{n+} [18]. This effect may be useful in studies of C_{dl} in the presence of faradaic process. At last, no surface area of the electrode is required to obtain the parameter k (see Eq. (5.56)). Dependence of directly measured capacitance (unrelated to the surface unit) versus direct current (instead of i) may be used for this purpose.

The method under consideration has been employed in the investigation of $\mathrm{Pt}|\mathrm{K_3Fe(CN)_6}$, $\mathrm{K_4Fe(CN)_6}$ system [28]. The obtained values of $\alpha_c = 0.53 - 0.55$ and $k_s = (0.8 - 1.8) \times 10^{-2}\,\mathrm{cm\,s^{-1}}$ are in agreement with literature data [29, 30].

Predicted by the theory, linear dependencies of C_s versus i, C_0, and b versus $1/\sqrt{\omega}$ have been obtained in the case of Tl(Hg)|Tl^+ system [18, 31].

Here, we would like to present data obtained for the Ag|Ag(I), SCN^- system. Solutions contained 0.05 M $AgNO_3$ and 1.0 or 1.5 M KSCN. Simulations based on the material balance equations have shown that the $Ag(SCN)_4^{3-}$ species predominate at $c_L > 1$ M. This makes it possible to simplify mathematics and to derive the following relationships:

$$C_0 = \frac{n^2F^2\beta_N c_L^N\sqrt{\frac{2D}{\omega}}}{RT}\exp\left(\frac{nF}{RT}\eta_{00}\right), \tag{5.58}$$

$$k = \frac{nF\beta_N c_L^{N-p}\alpha_c\sqrt{\frac{2D}{\omega}}}{RT\beta_p^{\alpha_a}k_s}\exp\left(\frac{\alpha_c nF}{RT}\eta_{00}\right), \tag{5.59}$$

where $p = 2$ [32] and $N = 4$ is the number of coordinated ligand particles in EAC and in dominating complex, respectively, η_{00} is the overvoltage reckoned from the formal potential of the Ag|Ag^+ electrode.

Examples of $C_s - i_c$ dependencies are presented in Figure 5.7. Similar linear plots were also obtained at $c_L = 1$ M. C_s values extrapolated to $i = 0$ are in linear dependence on $1/\sqrt{\omega}$ (Figure 5.8).

Some parameters obtained from the experimental data using Eqs. (5.58) and (5.59) are listed in Table 5.2. In calculations, it was assumed that $\alpha_c = \alpha_a = 0.5$, $\log\beta_2 = 7.6$ [19]; the value of $D = 9.3 \times 10^{-6}$ cm^2 s^{-1} was obtained from the RDE limiting current density using the well-known Levich equation. The values of $\log\beta_4 = 10.1 - 11.3$ are in line with literature data [19]. Comparatively high k_s value points to the fact that the process $Ag(SCN)_2^- + e \rightarrow Ag + 2SCN^-$ is rather fast. This conclusion is supported by the steady-state RDE data: the slope of

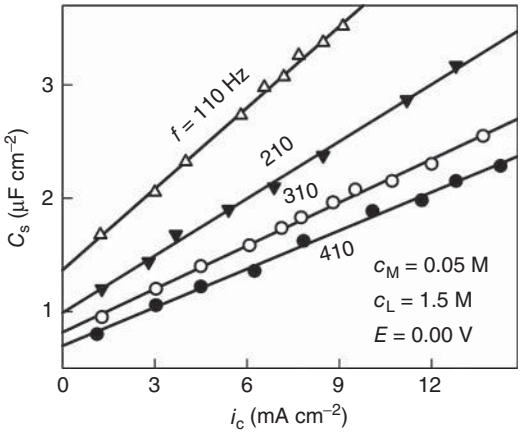

Figure 5.7 Dependencies of C_s on the cathodic current density i at $E = 0.0$ V and different angular frequencies of alternating current indicated at the respective lines.

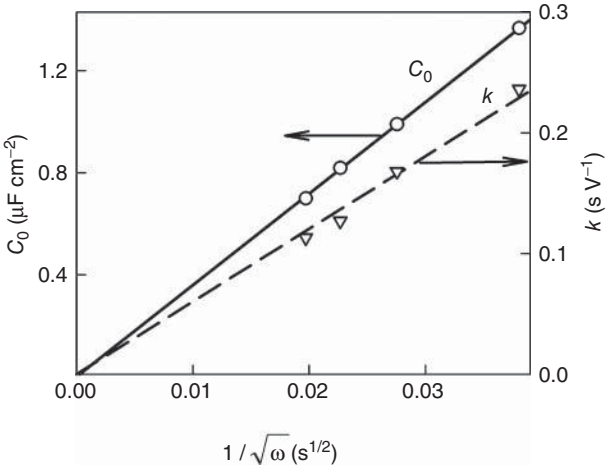

Figure 5.8 C_s values (Figure 5.7) extrapolated to $i = 0$ (left ordinate) and the slope k of $C_s - i$ dependencies (right ordinate) versus $1/\sqrt{\omega}$.

Table 5.2 Values of β_4 and k_s determined for Ag|Ag(I), SCN^- system from impedance data $c_M = 0.05$ M.

E (mV)	c_L (M)	log β_4	k_s (cm s^{-1}) × (mol cm^3)$^{-0.5}$
0	1.5	10.5	0.45
20	1.0	10.8	0.55
24	1.5	10.0	0.67
40	1.0	10.4	0.57
60	1.0	10.1	0.14
80	1.0	9.9	0.11

experimental "$\ln(1 - i/i_d) - E$" line, equal to $(28\,\text{mV})^{-1}$ [24], is close to that $(25\,\text{mV})^{-1}$ typical of reversible processes.

References

1. Vetter, K.J. (1952) The reaction overvoltage. *Z. Elektrochem.*, **56** (10), 931–937.
2. Gerischer, H. (1964) Kinetik der Metallabscheidung aus Lösungen komplexgebundener Ionen. *Chem. Ing. Tech.*, **36** (6), 666–671.
3. Survila, A. and Šironienė, B. (1992) Kinetics of copper deposition from alkaline citrate solutions. *Elektrokhimiya*, **28** (12), 1756–1761.
4. Vetter, K.J. (1967) *Electrochemical Kinetics*, Academic Press, New York.
5. Survila, A. and Stasiukaitis, P.V. (1997) Partial currents of consecutive charge transfer in the processes of metal electrodeposition. *Chemija*, **3**, 31–35.
6. Streeter, I. and Compton, R.G. (2007) Mass transport corrected Tafel analysis of voltammetric waves: when can it be applied? *Electrochim. Acta*, **52** (13), 4305–4311.

7. Survila, A. and Uksienė, V. (1992) The electroreduction kinetics of Cu(II)-glycine complexes in aqueous solution. *Electrochim. Acta*, **37** (4), 745–749.
8. Būdienė, J., Survilienė, A., and Survila, A. (2004) Cathodic processes in acidic Cu(II) solutions containing glycolic acid. *Russ. J. Electrochem.*, **40** (4), 394–399.
9. Berzins, T. and Delahay, P. (1953) Oscillographic polarographic waves for the reversible deposition of metals on solid electrodes. *J. Am. Chem. Soc.*, **75** (3), 555–559.
10. Delahay, P. (1953) Theory of irreversible waves in oscillographic polarography. *J. Am. Chem. Soc.*, **75** (5–6), 1190–1196.
11. Galus, Z. (1994) *Fundamentals of Electrochemical Analysis*, 2nd edn, Ellis Horwood, New York.
12. Miller, B. and Bruckenstein, S. (1970) Hydrodynamic potentiometry and amperometry at ring-disk electrodes. *J. Electrochem. Soc.*, **117** (8), 1032–1039.
13. Miller, B., Bellavance, M., and Bruckenstein, S. (1971) Application of isosurface concentration voltammetry at a rotating disk electrode to simple electron transfer kinetics. *J. Electrochem. Soc.*, **118** (7), 1082–1089.
14. Antropov, L.I., Donchenko, M.I., and Sribnii, L.E. (1976) Application of isosurface concentration voltammetry for study fast reactions of discharge of metal ions or hydrogen. *Elektrokhimiya*, **12** (9), 1347–1351.
15. Antropov, L.I., Donchenko, M.I., and Sribnii, L.E. (1976) Analyse of cathodic polarisation curves of discharge of metal ions or hydrogen in the presence of concentration an ohmic polarization. *Elektrokhimiya*, **12** (7), 1038–1042.
16. Antropov, L.I., Sribnii, L.E., and Donchenko, M.I. (1977) Investigation of the process of electrodeposition of copper from sulfuric acid solutions. Determination of some parameters of the discharge of copper ions. *Elektrokhimiya*, **13** (9), 1349–1354.
17. Survila, A. (1980) Isosurface concentration voltammetry of complex systems under equilibrium conditions in the diffusion layer. *Sov. Electrochem.*, **16** (7), 792–797.
18. Vielstich, W. and Gerischer, H. (1955) Electrolysis at constant potential. II. Kinetics of the deposition of simple zinc and complex silver ions. *Z. Phys. Chem.*, **4**, 10–23.
19. Sillen, L.G. and Martel, A.E. (1964) *Stability Constants of Metal-Ion Complexes*. Special Publication No. 17, Chemical Society, London.
20. Survila, A. (1989) *Electrode Processes in Systems of Labile Complexes of Metals*, Mokslas, Vilnius (in Russian).
21. Survila, A. (1983) Method for determining the exchange current density of quasi-reversible processes in complex systems. *Proc. Lithuanian Acad. Sci.*, **4** (137), 35–39.
22. Jurevičius, D., Spudas, L., and Survila, A. (1983) Mechanism of electroreduction of Cu(II) glycinate complexes in acid medium. *Proc. Lithuanian Acad. Sci.*, **5** (183), 27–34.
23. Krotkus, A. and Survila, A. (1979) Impedance in the system with forced convection. (3. Quasi- reversible discharge of ions). *Proc. Lithuanian Acad. Sci.*, **3** (112), 65–74.
24. Survila, A. (1984) Impedance in the system with forced convection. (6, Quasi-reversible processes in systems of labile complexes). *Proc. Lithuanian Acad. Sci.*, **4** (137), 35–39.
25. Levart, E. and Schuhmann, D. (1975) Comparison of some solutions for the Warburg impedance of a rotating disk electrode. *J. Electrochem. Soc.*, **122** (7–8), 1082–1083.
26. Scherson, D.A. and Newman, J. (1980) The Warburg impedance in the presence of convective flow. *J. Electrochem. Soc.*, **127** (1), 110–113.
27. Grafov, B.M. and Pekar, E.V. (1970) Method of the equivalent multipole in the theory of electrode impedance. *Elektrokhimiya*, **6** (4), 547–556.
28. Krotkus, A. and Survila, A. (1975) Impedance in the system with forced convection. (2. System $K_3Fe(CN)_6/K_4Fe(CN)_6$). *Proc. Lithuanian Acad. Sci.*, **1** (86), 11–17.
29. Daum, P.H. and Enke, C.S. (1969) Electrochemical kinetics of ferri-ferrocyanide couple on platinum. *Anal. Chem.*, **41** (4), 653–656.

30. Tamamushi, R. (1972) *Kinetic Parameters of Electrode Reactions*, Saitame.
31. Krotkus, A. and Survila, A. (1982) Impedance in the system with forced convection. (5. System Tl/Tl^+). *Proc. Lithuanian Acad. Sci.*, **4** (137), 35–39.
32. Brainina, K.Z., Il'in, A.M., Yarunina, G.V., and Neiman, N.Y. (1971) Electrodissolution of metals from the surface of indifferent electrode. VI. Processes complicated by chemical reaction. *Elektrokhimiya*, **7** (6), 888–893.

6
Determination of Mechanism of Electrochemical Processes Involving Metal Complexes

Processes of electrochemical plating that involve metal complexes are always accompanied by chemical steps provided that metal complexes are not absolutely inert. It is the practice to express the mechanism of overall reaction by a certain sequence of symbols "C" (chemical step) and "E" (electrochemical step, i.e., the transfer of electron). For instance, the chemical step + electrochemical step (CE) mechanism means that the certain chemical process generates the particle (the electrically active complex, EAC) that further takes part in the charge transfer. When this symbolism is applied to the complex systems, some comments are necessary. The reduction of metal-containing particles gives rise to the respective shifts in different chemical equilibria that involve complexes, ligands, hydronium ions, and so on. Keeping this in mind, all processes in the systems under consideration should proceed at least by chemical step + electrochemical step (charge transfer reaction) (CEC) mechanism, where "C" represents several simultaneous chemical transmutations. Then, to avoid the certain ambiguity, it makes sense to consider only these chemical stages that are capable of controlling the rate of the overall process.

When revealing the mechanism, it seems expedient to determine the EAC composition first. Outer-sphere and inner-sphere electron transfers to EAC might be distinguished. The first of them takes place when the inner-sphere ligands in EAC are separated from the electrode surface by some molecules of ligand or solvent. The second mechanism involves electron transfer between two metal centers sharing a ligand or atom in their respective coordination shells. In this case, the interaction between the donor and acceptor centers in the transition state can diminish activation energy of the process. Hence, the inner-sphere electron transfer suggests a removal of some ligands from the inner coordination sphere of complex. This promotes adsorption and a decline in the potential barrier of electron transfer.

Though there is no thermodynamic limitation on the EAC composition (the same equilibrium potential is attributed to any charge transfer process), the single electrically active species can be often defined. It is assumed in this case that this species supplies the total current in the system. In our opinion, the predominating in the solution complex does not need to be electrically active. Kinetic factors and the activation energy first of all are responsible for the electrochemical activity of

Electrochemistry of Metal Complexes: Applications from Electroplating to Oxide Layer Formation, First Edition. Arvydas Survila.

complexes. Therefore, special methods should be applied for establishing the EAC composition.

6.1 Determination of the Mechanism by Reaction Orders

The order of the reaction with respect of species S_j is often used in the formal kinetics to elucidate the mechanism of the reaction. Similar approach is also employed in electrochemical kinetics. In so doing, it is necessary to keep in mind that the same component S_j takes part in two, anodic and cathodic, electrochemical processes. Therefore, two orders, $z_{R,j}$ and $z_{O,j+}$, respectively, can be attributed to S_j; besides, these quantities can be and often are different [1–3]. Some methods based on analysis of the reaction orders are considered below.

According to Vetter [1, 3, 4], having determined the orders of electrochemical reactions of all substances S_j that are present in the solution independently of one another, it is possible to unambiguously determine the total formulas S_O, and S_R of the substances, which immediately take part in the charge transfer process. The following relationships are suitable for this purpose:

$$S_O = z_{O,1}S_1 + z_{O,2}S_2 + z_{O,3}S_3 + \ \ldots \ + z_{O,q}S_q, \tag{6.1}$$

$$S_R = z_{R,1}S_1 + z_{R,2}S_2 + z_{R,3}S_3 + \ \ldots \ + z_{R,q}S_q. \tag{6.2}$$

Several methods were proposed for determining the orders of reactions. One of them [3] deals with analysis of the dependence of a steady-state current density on concentration of the component S_j. The necessary condition that is imposed in this case requires keeping constant concentrations of the rest components, when the amount of S_j is varied. The analysis must be carried out at constant potential in the Tafel region. Changing concentration c_k of one of the substances S_k and maintaining all others constant, relevant orders of the reaction can be determined from the changes of anodic i_a or cathodic i_c current densities at $E = \text{const}$:

$$z_{R,k} = \frac{\partial \log i_a}{\partial \log c_k}, \tag{6.3}$$

$$z_{O,k} = \frac{\partial \log |i_c|}{\partial \log c_k}. \tag{6.4}$$

In another case, Vetter [2, 3] proposed to analyze analogous dependencies of the exchange current density i_0. This method requires additional information about the charge transfer coefficients α_c and α_a, as well as stoichiometric coefficients ν_j, involving in the net electrochemical process[1)]

$$\nu_1 S_1 + \nu_2 S_2 + \ \ldots \ + ne \rightleftarrows (-\nu_l)S_l + \ \ldots \ + (-\nu_q)S_q. \tag{6.5}$$

1) Stoichiometric coefficients of the reduced species are regarded to be negative.

Then,

$$z_{R,k} = \frac{\partial \log i_0}{\partial \log c_k} - \alpha_a \nu_k \frac{z}{n}, \tag{6.6}$$

$$z_{O,k} = \frac{\partial \log i_0}{\partial \log c_k} + \alpha_c \nu_k \frac{z}{n}. \tag{6.7}$$

Here, z is the number of electrons participating in the charge transfer step, which might not coincide with the value n in the total reaction (6.5), which reflects the initial and final state of the system.

In investigating systems of metal complexes, the latter method was also used by Gerischer [5–7]. With a sufficient excess of cyanide, Zn(II) complexes containing four cyanide ions prevail in solutions; therefore, the net reaction taking place on the amalgam electrode can be written as follows:

$$Zn(CN)_4^{2-} + 2e \rightleftarrows Zn(Hg) + 4CN^-, \tag{6.8}$$

where stoichiometric coefficients of Zn(II) and CN are equal, +1 and −4, respectively, The exchange current densities [5], which were dependent not only on Zn(II) ir CN^- concentrations, but also on pH, were determined by means of the electrochemical impedance method. The OH^- ions are absent in the net Eq. (6.8); therefore, their stoichiometric coefficient is equal to zero. According to Eq. (6.7), in which $n = z = 2$ and $\alpha_c = 0.45$ [5], the following orders of reactions were obtained: $z_{O,Zn(II)} = +1$, $z_{O,CN^-} = -4$, $z_{O,OH^-} = +2$. Then, the following EAC formula can be derived from Eq. (6.1): $S_O = Zn(CN)_4^{2-} - 4CN^- + 2OH^- = Zn(OH)_2$. Hence, electrochemical process in this system takes place in accordance with the CE mechanism. During the initial chemical step, the aforementioned EAC is formed, which further takes part in the charge transfer process:

$$Zn(CN)_4^{2-} + 2OH^- \rightleftarrows Zn(OH)_2 + 4CN^-, \tag{6.9}$$

$$Zn(OH)_2 + 2e \rightleftarrows Zn(Hg) + 2OH^-. \tag{6.10}$$

If the system contains a clearly dominating complex species, the net reaction is not difficult to specify. However, in opposite cases, where such a species is absent, problems arise. In studying reduction of Zn(II) oxalate complexes [5], two different net reactions were supposed to proceed at different ligand concentrations, However, independently of that, one and the same EAC formula, namely ZnC_2O_4, was obtained.

The opposite result was obtained in analyzing reduction of cyanide complexes [6]. In those cases, one net reaction involving $Cd(CN)_4^{2-}$ was used. However, the EAC formulas, obtained for cyanide solutions of different concentrations, were also different: $Cd(CN)_2$ at smaller and $Cd(CN)_3^-$ at larger cyanide concentrations. A similar situation arose in studying silver electrodeposition from cyanide solutions [7]. One of the main reasons limiting the application of these methods to the reduction of labile complexes is that components of such systems cannot be

regarded as interdependent. For example, in changing the ligand concentration, the concentrations of other components (complex species) also change.

Methods used by Kublanovsky *et al.* [8, 9] are based on similar concepts. It was suggested to determine an average coordination number of EAC, k, by equations

$$k = \frac{\partial \ln(i_c \Phi_s)}{\partial \ln [\mathrm{L}]_s}, \tag{6.11}$$

$$k = \frac{\partial \ln(i_c \Phi_s)}{\partial \ln [\mathrm{L}]_s} + \frac{\alpha z F}{RT} \frac{\partial E_{\mathrm{eq}}}{\partial \ln [\mathrm{L}]_s}. \tag{6.12}$$

The first of them was derived for constant potential; the second one is applicable at constant overvoltage. Both relationships contain surface concentrations, which are to be determined.

6.2 Method of Isopotential Solutions

It has been mentioned in Chapter 2 that a series of solutions of complex compounds with constant M^{n+} concentration, which according to Eq. (2.3) unambiguously determines the electrode potential, can always be prepared. Bulk concentrations of free ligand and complex particles are different in such isopotential solutions (IPSs). The composition of the IPS series can be calculated using material balance equations and setting the same $[M^{n+}]$ but different [L] values. Further, we shall see that the exchange current density measurements in the IPS series enable the EAC composition to be determined in a rather simple manner with no limitations mentioned in Section 6.1.

Let us briefly discuss the theory of the IPS method [10]. In formal electrochemistry, the exchange currency density is the cathodic or anodic component of current density i in the equilibrium state, where $E = E_{\mathrm{eq}}$, and $i = 0$. The following expression can be obtained from the kinetic equation written for the charge transfer process (Eq. (2.5)):

$$i_0 = k_a [\mathrm{L}]^p \exp\left(\frac{\alpha_a n F}{RT} E_{\mathrm{eq}}\right) = k_c [\mathrm{ML}_p^{n+}] \exp\left(-\frac{\alpha_c n F}{RT} E_{\mathrm{eq}}\right), \tag{6.13}$$

where k_a and k_c are rate constants of the anodic and cathodic process, respectively. As has already been mentioned, in the IPS series, E_{eq} and $[M^{n+}]$ are constant. It follows from the expression of ML_p^{n+} stability constant that the ratio of $[ML_p^{n+}]/[L]^p$ in the IPS series also remains constant. All that makes it possible to state that $i_0 = \mathrm{const} \times [L]^p$, or

$$p = \frac{\partial \log i_0}{\partial \log [\mathrm{L}]}. \tag{6.14}$$

If several charge transfer reactions involving different complex species ML_j^{n+} $(j = p, p+1, \ldots, q)$ occur, the exchange current density i_0 consists of

partial i_{0j} and then,

$$i_0 = \sum_{j=p}^{q} b_j [\mathrm{L}]^j, \tag{6.15}$$

that is, in the IPS series, i_0 dependence on [L] shall be described by means of a power series of a certain degree. If kinetic parameters of partial processes differ significantly, linear regions appear in $\log i_0$ dependencies on log[L] with slope equal to the number of ligand particles in the EAC.

If the stepwise charge transfer process proceeds in accordance with the reactions (5.9) and (5.10), the exchange current densities of both steps are to be determined. In this case, the following are valid for the equilibrium state

$$i_{01} = k_{a1}[\mathrm{L}]^{p-q} \exp\left(\frac{\alpha_{a1} F}{RT} E_{\mathrm{eq}}\right) = k_{c1}[\mathrm{ML}_p^{2+}] \exp\left(-\frac{\alpha_{c1} F}{RT} E_{\mathrm{eq}}\right), \tag{6.16}$$

$$i_{02} = k_{a2}[\mathrm{L}]^{q} \exp\left(\frac{\alpha_{a2} F}{RT} E_{\mathrm{eq}}\right) = k_{c2}[\mathrm{ML}_q^{+}] \exp\left(-\frac{\alpha_{c2} F}{RT} E_{\mathrm{eq}}\right). \tag{6.17}$$

Similar analysis shows that the following equations are valid for two consecutive one-electron transfers:

$$p = \frac{\partial \log i_{01}}{\partial \log[\mathrm{L}]}, \tag{6.18}$$

$$q = \frac{\partial \log i_{02}}{\partial \log[\mathrm{L}]}, \tag{6.19}$$

which can be used to determine the EAC composition.

The Cu|Cu(II), glycine system, in which a consecutive transfer of two electrons takes place, can serve as an example. Stability constants of complexes are: $\log \beta_1 = 8.46$, $\log \beta_2 = 15.3$, and relevant protonation constants are: $\log \beta_1^{\mathrm{H}} = 9.68$, $\log \beta_2^{\mathrm{H}} = 12.05$. These values were used in calculating the composition of the IPS series [11]. As protonated ligands prevail in acid solutions, rather low concentrations of deprotonated L^- form must be set (Table 6.1). The open-circuit potentials $0.218 \pm 0.004\,\mathrm{V}$ are in line with equilibrium potential

Table 6.1 Characteristics of Cu(II)–glycine isopotential solutions series (pH 3.5).

Concentration (mol dm^{-3})				E_{eq} (V)	i_{01} (μA cm^{-2})
$[\mathrm{Cu}^{2+}]$	$[\mathrm{L}^-]$	c_{M}	c_{L}		
10^{-3}	1.26×10^{-8}	0.0049	0.0248	0.217	13
	3.17×10^{-8}	0.0121	0.0647	0.212	28
	5.03×10^{-8}	0.0205	0.106	0.218	51
	7.97×10^{-8}	0.0366	0.178	0.220	74
	1.28×10^{-7}	0.0706	0.310	0.224	120

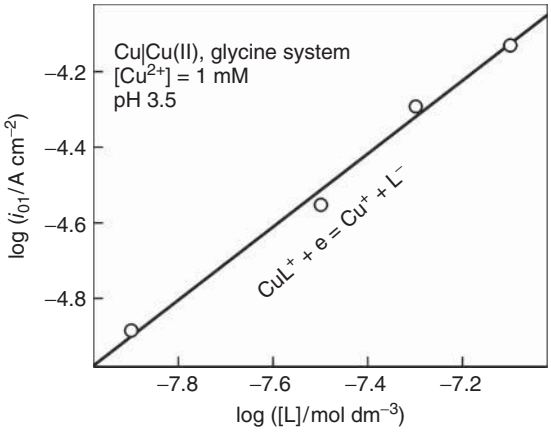

Figure 6.1 Variations of the exchange current density i_{01} with the free ligand concentration in the IPS series.

obtained from the Nernst equation with $\gamma_{Cu}^{2+} = 0.07$ [12]. Polarization resistance obtained under forced convection conditions was used to determine the exchange current density i_{01} (see above Section 5.3.2). The results obtained are presented in Table 6.1. The logarithmic dependence of i_{01} versus $[L^-]$ is linear with unit (0.97) slope (Figure 6.1). This would mean that EAC involves one particle of ligand. Chronopotentiometric data [11] showed that the rate of the cathodic process clearly depends on ligand concentration, whereas the rate of the anodic process does not practically depend on $[L^-]$. The approximately constant i_{02} value shows that the intermediate Cu(I) product is a simple Cu^+ ion whose reduction is more reversible. Consequently, the sequence of cathodic processes might be as follows: the rate-determining step $CuL^+ + e \rightarrow Cu^+ + L^-$ and fast step $Cu^+ + e \rightarrow Cu$.

More IPS applications are given in Chapter 8.

References

1. Vetter, K.J. (1967) *Electrochemical Kinetics*, Academic Press, New York.
2. Vetter, K.J. (1950) The dependence of the initial slope of current density-potential curves on the concentrations: implications for the potential-determining reaction in oxidation-reduction systems. *Z. Phys. Chem.*, **194**, 284–296.
3. Vetter, K.J. (1951) Zur Ermittlung des Reaktionsmechanismus bei der Einstellung von Redoxpotentialen. *Z. Elektrochem.*, **55** (1–8), 121–127.
4. Vetter, K.J. (1955) Unsere Vorstellungen über die Kinetik von Elektrodenprozessen. *Z. Elektrochem.*, **59** (6–10), 596–604.
5. Gerischer, H. (1953) Kinetics of discharge of simple and complex Zinc ions. *Z. Phys. Chem.*, **202** (3–4), 302–317.
6. Gerischer, H. (1953) Zum Entladungsmechanismus von Komplex – Ionen. *Z. Elektrochem.*, **57** (6–10), 604–609.
7. Vielstich, W. and Gerischer, H. (1955) Electrolysis at constant potential. II.

Kinetics of the deposition of simple zinc and complex silver ions. *Z. Phys. Chem. (N.F.)*, **4**, 10–23.

8. Belinsky, V.N., Kublanovsky, V.S., and Glushchak, T.S. (1981) Determination of the electroactive form of zinc in electrolysis complexed zinc solutions. *Ukr. Khim. Zh.*, **47** (11), 1188–1190.
9. Nikitenko, V.N., Litovchenko, K.I., and Kublanovsky, V.S. (1987) Determination of the composition of electrochemically active ions at constant overvoltage. *Ukr. Khim. Zh.*, **53** (3), 265–268.
10. Survila, A. (1981) A method of isopotential solutions for investigating the discharge mechanism in complex systems. *Sov. Electrochem.*, **17** (8), 1014–1015.
11. Jurevičius, D., Spudas, L., and Survila, A. (1983) Mechanism of electroreduction of Cu(II) glycinate complexes in acid medium. *Proc. Lithuanian Acad. Sci.*, **5** (183), 27–34.
12. Survila, A. and Spudas, L. (1981) On the reversibility of Cu(II) discharge in glycine solutions. *Proc. Lithuanian Acad. Sci.*, **5** (126), 27–33.

7
Adsorption

We saw that formal kinetic equations apart from kinetic parameters also contain surface concentrations c_s of electrically active species. It follows from the material presented in previous chapters that c_s differs from the corresponding bulk values because a diffusion layer with certain concentration profiles forms at the electrode surface. Moreover, another reason due to which surface concentrations change is adsorption phenomena, which form a certain structure called a double electrode layer (DEL) at the boundary metal|solution. It is clear that in kinetic equations, it is necessary to use local concentrations of reactants and products, that is, concentrations in that region of DEL where electrically active particles are located. The second effect produced by DEL is related to the fact that a potential ψ_1 in the localization of the electrically active complex (EAC) differs from the electrode potential. Therefore, activation energy of the electrochemical process does not depend on the entire jump of the potential at the boundary but on its part only, which characterizes the change in the potential in the reaction zone. In this connection, the so-called Frumkin correction appears in the electrochemical kinetic equations, which is related to the evaluation of the local potential ψ_1 [1].

It is thought [2] that indifferent (supporting) electrolyte suppresses not only migration mass transport (see Chapter 3) but also the said DEL effects. If electrically active particles do not display high adsorption ability, effective kinetic parameters may be determined using methods that do not take into account double-layer effects. Thereafter, with the data about the DEL structure available, certain corrections can be made [3]. On the whole, adsorption ability of complexes with a saturated coordination sphere should not be larger than that of separate M^{n+} or L species because most chemical or weaker bonds in the complex have already been used. It is clear that the solvation degree of particles also has an impact on their surface activity. Partial dissociation of the complex often takes place prior to the adsorption step; then, the broken bond that connected ligand with the metal ion can be used for adsorptive interaction with the metal surface. However, the works by Anson and others [4–7] showed that ligand is the particle that initiates adsorption of the complex. It was established [5] that bonds between Cd(II) and Hg electrode form only after SCN^- ions specifically adsorb on Hg. Later, it was confirmed [6] that this regularity also applies to adsorption of Zn(II), Cd(II), Pb(II), In(III) complexes with iodide, thiosulfate, thiocyanide, azide, and others.

Electrochemistry of Metal Complexes: Applications from Electroplating to Oxide Layer Formation, First Edition. Arvydas Survila.

Modern theories, when describing adsorption of one or another substance on the substrates of various types, try to evaluate electrostatic and the so-called specific interactions between the adsorbate, on the one hand, and between the adsorbed particles, on the other hand. Most often, ideally polarized electrodes are investigated, assuming that no Faraday process is taking place on them. However, the main property of complex systems, namely, chemical reactions, which take place both in the solution bulk and the diffusion layer and, eventually, in the adsorption state, are not taken into account. In solving this problem, not only thermodynamic properties of the system have to be analyzed but also models of adsorption layers are desirable to be considered. Main model conceptions are presented in more detail in the monograph by Damaskin *et al.* [8].

7.1 Thermodynamic Aspects

Let us form a system of metal complexes $ML_j^{z_0+}$ by dissolving simple metal salt $M_{\nu+}A_{\nu-}$ and uncharged ligand L in solvent W. Let charge numbers of cation and anion be equal to z_0, z_a, and 0, respectively. In the meantime, we are not going to make any model assumptions about the structure of the adsorption layer, and we shall write the basic equation of electrocapillarity:

$$d\sigma = -\varepsilon dE - \frac{\varepsilon}{z_k F} d\mu_k - \sum_{j=0}^{N} \Gamma_j d\mu_j - \Gamma_L d\mu_L - \Gamma_a d\mu_a, \tag{7.1}$$

where σ is the surface energy (the surface tension), μ is the chemical potential of a corresponding component in the solution phase, indexes j and k refer, respectively, to complexes $ML_j^{z_0+}$ and that component of the solution, with respect to which the reference electrode is reversible. In what follows, solvent W is taken as the reference component and adsorption Γ is the surface excess according to Gibbs (for a plane where $\Gamma_W = 0$).

Making use of the expression for the thermodynamic stability constant of the complex (see Eq. (1.2)), we obtain the equation

$$d\mu_j = RT(d \ln a_0 + jd \ln a_L), \tag{7.2}$$

where a is the activity of the respective species. It follows from Eqs. (7.1) and (7.2) that

$$d\sigma = -\varepsilon dE - \frac{\varepsilon}{z_k F} d\mu_k - RT(\Gamma_{MT} d \ln a_0 + \Gamma_{LT} d \ln a_L + \Gamma_a d \ln a_a), \tag{7.3}$$

where Γ_{MT} and Γ_{LT} are total metal and ligand adsorptions, that is,

$$\Gamma_{MT} = \sum_{j=0}^{N} \Gamma_j, \tag{7.4}$$

$$\Gamma_{LT} = \sum_{j=0}^{N} j\Gamma_j + \Gamma_L. \tag{7.5}$$

The charge density ε on the metal face of the DEL is equal to that of the ionic part of the DEL taken with the opposite sign:

$$\varepsilon = -F(z_0\Gamma_{MT} + z_a\Gamma_a). \tag{7.6}$$

After substitution of Eq. (7.6) into Eq. (7.3), we obtain for $E = \text{const}$:

$$\mathrm{d}\sigma = -RT\left(-\frac{z_0\Gamma_{MT} + z_a\Gamma_a}{z_k}\mathrm{d}\ln a_k + \Gamma_{MT}\mathrm{d}\ln a_0 + \Gamma_{LT}\mathrm{d}\ln a_L + \Gamma_a\mathrm{d}\ln a_a\right). \tag{7.7}$$

Depending on the type of the reference electrode, various modifications of Eq. (7.7) can be obtained. If it is the first kind electrode, reversible with respect to metal ions, then $z_k = z_0$, $a_k = a_0$ and, having used the condition that $|z_a|/z_0 = \nu_+/\nu_-$, we obtain:

$$\mathrm{d}\sigma_{E+} = -RT\left(\Gamma_{LT}\mathrm{d}\ln a_L + \frac{\nu_+ + \nu_-}{\nu_-}\Gamma_a\mathrm{d}\ln a_\pm\right), \tag{7.8}$$

where $a_\pm$ is the average activity of the metal salt. In a similar way, for the second kind electrode, which is reversible with respect to the anion, $z_k = z_a$, $a_k = a_a$ and

$$\mathrm{d}\sigma_{E-} = -RT\left(\Gamma_{LT}\mathrm{d}\ln a_L + \frac{\nu_+ + \nu_-}{\nu_+}\Gamma_{MT}\mathrm{d}\ln a_\pm\right). \tag{7.9}$$

Finally, for the reference electrode with constant composition $\mathrm{d}\mu_k = 0$ and

$$\mathrm{d}\sigma_E = -RT(\Gamma_{MT}d\ln a_0 + \Gamma_{LT}d\ln a_L + \Gamma_a d\ln a_a). \tag{7.10}$$

The last equation also describes the decrease in the electrocapillary maximum; it can be obtained from Eq. (7.3), when $\varepsilon = 0$. In this case, the value of $\mathrm{d}\sigma$ does not depend on the nature of the reference electrode. Note that Eq. (7.10) at $\varepsilon \neq 0$ is valid only for sufficiently diluted solutions so that one can assume that $\mathrm{d}E$ reflects the change in the Galvani potentials at the ends of the electrochemical cell [9]. In this case, concentrations can be substituted for activities to a sufficient degree of approximation.

Let us briefly review which of the listed values and in what manner can be determined. It is possible to calculate the distribution of complex species in the solution, that is, bulk concentrations or activities, by means of the methods discussed in Chapter 1. Besides, the composition of solutions can be changed so that Eqs. (7.8)–(7.10) would become simpler. For example, one can use a series of solutions with constant concentration of free ligand for which $d\ln a_L = 0$. In the series of isopotential solutions (see Section 2.1), the condition $d\ln a_0 = 0$ holds. By differentiation of the electrocapillary curve with respect to E for a solution of constant composition, one can obtain the value of the charge density ε and use Eq. (7.6) for the calculation of total adsorptions Γ_{MT} and Γ_{LT}. Thus, electrocapillary measurements, as well as a number of other methods (radioactive indicator, surface stress, piezoelectric, extensometer methods), give information only about the total amounts of adsorbed metal and ligand. Consequently, for further solution of the problem posed, some model images are necessary.

7.2 Model Aspects

In studying adsorption properties of some weak acids, the conclusion was drawn [10–15] that their dissociation–association takes place in the adsorption state. Hence, in the adsorption layer, as in the solution bulk, chemical equilibria can exist, which are characterized by the corresponding equilibrium constants β^{A} in a manner analogous to equilibria in the bulk of solution. These ideas would be convenient to extend to adsorption of complexes.

When the solution contains an excess of supporting electrolyte, the fraction of adsorption entering in the diffusion part of the DEL may, as a rule, be neglected if the components are ions or extremely surface-active organic molecules. Then, the Γ values can be considered to be approximately equal to the surface concentrations. Given β^{A} and total metal and ligand adsorptions, Γ_{MT} and Γ_{LT}, the composition of the adsorption layer could be calculated by means of the same material balance equations as in the case of the solution bulk (see Section 1.1). Besides, equilibria of another type should be mentioned here too, namely between solution and the adsorption layer. Various adsorption isotherms were offered for their description [8]. In some research [10, 13, 15], equilibria of both types were considered together, using the Langmuir or Frumkin isotherms and constants β^{A}.

Let us consider from this aspect the complex system for which we assume the existence of three types of equilibrium: one in the bulk of solution, which can be defined by Eq. (1.2); a second between the solution bulk and the adsorption layer, which is determined by the adsorption isotherm; and a third in the adsorption layer, which can be determined by constants β^{A}. The adsorption stability constant β_j^{A} of the complex ML_j (the charge is omitted) can be expressed by Eq. (1.2) type. If all adsorbed particles are assumed to form a single monolayer of thickness δ, we can write an equation for β_j^{A} similar to Eq. (1.2). Once δ, the relevant surface concentrations Γ and surface coverage $\theta = \Gamma/\Gamma_{max}$ are included in the value of β_j^{A}, the following relationship is obtained:

$$\beta_j^{A} = \frac{\theta_j}{\theta_0 \theta_L^j}. \tag{7.11}$$

Let us assume that Γ_{MT} and Γ_{LT} are established when $E = \text{const}$ and the adsorption isotherms are congruent with respect to the electrode potential [8, 16]. Then, a question arises whether it is possible to combine Eqs. (1.2) and (7.11) with adsorption isotherms. Analysis of a number of isotherms showed that such consistency exists only in the case where the adsorption of the complex species obeys a Freundlich isotherm $B_j c_j^{n} = \theta_j$, going over to a Henry isotherm with $n = 1$, and also in the case of purely electrostatic adsorption. It can be proved that in the case of Freundlich isotherm, there exists the relationship between the three types of constants:

$$\beta_j^{A} = \frac{\beta_j^{n} B_j}{B_0 B_L^j}. \tag{7.12}$$

Analysis in this respect of other isotherms [8] leads to other results. For example, in the case of Langmuir isotherm

$$B_j c_j = \frac{\theta_j}{1 - \sum\limits_{\substack{j=0 \\ j=L}}^{N} \theta_j} \tag{7.13}$$

we obtain the relationship[1)]

$$\beta_j^{\mathrm{A}} = \frac{\beta_j B_j}{B_0 B_{\mathrm{L}}^j \left(1 - \sum \theta_j\right)^j}. \tag{7.14}$$

It is clear that β_j^{A} is not a constant and depends on θ if $B_j = \text{const}$, and, on the other hand, for $\beta_j^{\mathrm{A}} = \text{const}$, the values of B_j cannot be treated as constants. In the case of small θ, the majority of isotherms reduce to the Henry isotherm and then one can use any two of the three types of constants.

Now, we consider isotherms involving the so-called attraction (interaction) coefficient a that evaluates lateral interactions between adsorbed particles. Such parameter was proposed in treating the adsorption layer as the analog of two-dimensional gas ("gas on the plane"). According to van der Waals, who introduced the "internal pressure" in the equation of the state of real gases, an analogous correction was also introduced in the equation of the state of the adsorption layer. Due to this, an additional multiplier $\exp(-2a\theta)$ appeared in adsorption isotherms.

Let us extend this analogy and assume that it is necessary to form the equation of the state of gas mixture, evaluating the fact that reversible chemical reactions take place in the mixture. It is clear that it is inexpedient to use the aforementioned images because in a given case, the factors that determine the rate of chemical reactions become most significant. The latter reflects itself in the reaction rate constant on whose ratio the values of the equilibrium constants depend. It is this adsorption layer that is considered here. Therefore, interactions of all types between the adsorbed particles can reflect themselves to a sufficient degree in the stability constants β^{A} of adsorbed complexes.

The analysis showed that in the case of the adsorption under discussion, such term as $\exp(-2a\theta)$ cannot be inserted separately. Attempts to perform this operation lead to incompatibility of expressions of the constants β, β^{A}, and B.

Having in mind the latter conclusion, we are going to analyze the following model of the boundary layer. Let the concentration of adsorption sites on the metal surface equal to α_m, and on adsorption of one particle of the jth component, n_j of these sites is used. We also assume that at maximum adsorptions (Γ_m), all the sites of surface are occupied. Then,

$$n_0 \Gamma_{0m} = n_j \Gamma_{j_m} = n_{\mathrm{L}} \Gamma_{\mathrm{L}m} = \alpha_m / N_{\mathrm{A}}, \tag{7.15}$$

1) Hereinafter, the ranges of the summation are dropped for reasons of space.

where N_A is the Avogadro number. If Γ_0, Γ_j, and Γ_L are the actual adsorptions, then the concentration of occupied sites

$$\alpha = N_A \sum n_j \Gamma_j, \tag{7.16}$$

and the remaining places, whose concentration is α_v, are vacant. As

$$\alpha_v + \alpha = \alpha_m, \tag{7.17}$$

$$\theta_v + \theta = 1, \tag{7.18}$$

then

$$\theta_v = 1 - \sum \theta_j, \tag{7.19}$$

where $\theta_j = \Gamma_j / \Gamma_{j_m}$. For the quasi-chemical reaction: ML_j in bulk solution + n_j free sites ⇄ adsorbed ML_j; one can obtain the following isotherm:

$$B_j c_j = \frac{\theta_j}{\left(1 - \sum \theta_j\right)^{n_j}}, \tag{7.20}$$

where the fact that adsorbed particles can occupy a different number of adsorption centers has been taken into consideration. If only one component is being absorbed, this expression turned into Flory – Huggins isotherm [17, 18]. If together with Eq. (1.2), one uses Eq. (7.20) written for the respective components, one obtains, after series of transformations:

$$\frac{B_j \beta_j}{B_0 B_L^j} = \frac{(1 - \theta_j)^{n_0 + j n_L - n_j} \theta_j}{\theta_0 \theta_L^j}. \tag{7.21}$$

In order for the right side of this equation to be constant, it is necessary that the following condition should apply

$$n_j = n_0 + j n_L. \tag{7.22}$$

Then, (Eq. (7.21)) transforms into Eq. (7.12), where $n = 1$. The physical meaning of condition (7.22) is as follows: the number of adsorption sites occupied by the complex is the same as the sum of adsorption sites of its fragments. Hence, when the adsorbed complex dissociates, the number of occupied adsorption sites does not vary. If the latter are distributed equitably over the surface, this signifies that the area S_j that can be occupied by the adsorbed complex is equal to the sum of the areas of the species that are formed on its dissociation, that is, $S_j = S_0 + jS_L$. This effect is to be expected with a planar orientation of the adsorbed complexes, when, as noted earlier, all the forms of adsorbed species form a single, common monolayer of uniform thickness. Then, together with (Eq. (7.19)) isotherm, the defined constants β_j^A can be used.

To illustrate the conclusions drawn, we calculated distribution of complexes in the solution bulk and in the adsorption layer (Figure 7.1). It was assumed that $c_M = 0.01\,M$, the maximum amount of coordinated ligand in the complex

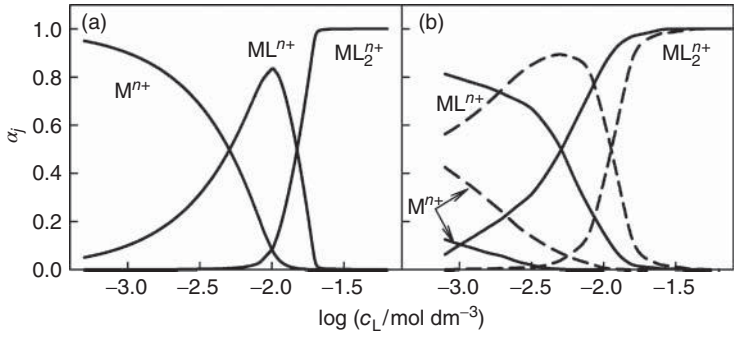

Figure 7.1 Distribution of complexes in the bulk of solution (a) and in the adsorption layer (b) versus the total ligand concentration. The first and the second variants of simulations (see text) are presented by full and doted lines, respectively.

$N = 2$, $\log \beta_1 = 7$, $\log \beta_2 = 12$, and numbers of adsorption sites are as follows: $n_0 = n_L = 1$, $n_1 = 2$, $n_2 = 3$. Two adsorption cases were studied. It was assumed in the first variant that free adsorption energy of complexes ΔG_A consists of the sum of energies of their separate fragments (values of adsorption constants corresponding to that are as follows: $B_0 = 0.1$, $B_1 = 15.5$, $B_2 = 2460$, $B_L = 2.86$), and in the second place ΔG_A increased more slowly ($B_0 = 0.1$, $B_1 = 2.86$, $B_2 = 15.5$, $B_L = 2.86$). Molar parts α_j in the case of the solution bulk (Figure 7.1a) corresponds to the definition (Eq. (1.11)), and for the adsorption layer (Figure 7.1b) $\alpha_j = \Gamma_j/\Gamma_{MT}$. The results of simulation showed that in the adsorption layer, the particles are distributed differently from that in the solution bulk (Figure 7.1). Surface coverage θ_j depends to a great extent on both the number of occupied adsorption places and distribution of adsorption energies; in the second case, θ_j are about five times lower than in the first variant (Figure 7.2).

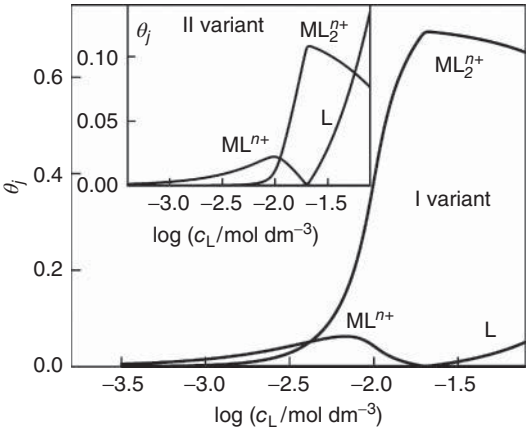

Figure 7.2 Surface coverages versus the total ligand concentration.

If the equilibration in the adsorption layer is fast, the images presented are likely to be applied in those cases when the faradaic process occurs. Then, the adsorption isotherms could be used for interrelation between the adsorption Γ values and the so-called surface concentrations (Chapter 3), which are outside DEL and which are determined by mass transport regularities. A mercury electrode, which has a considerably wider area of ideal polarizability than many solid electrodes, would suit best in such investigations. The adsorption values could be determined quite accurately from electrocapillary data; capacitance measurements could serve as an extra method providing a way of estimating the relations between the constants B_j and the potential E (see Eq. (3.30) in monograph [8]).

In the case of solid electrodes, which are in contact with the solution of complexes, there is practically no area of ideal polarizability. Accuracy of other experimental methods intended for the determination of adsorption (e.g., radioactive indicator method) is considerably lower. Furthermore, crystallographic and other inhomogeneities, which are to be evaluated, are characteristic of solid electrodes. Owing to these complications, thus far, no theory of adsorption of chemically interacting species is suitably developed.

Nonetheless, the conclusion can be drawn that in the case of sufficiently small θ, the impact of adsorption on the orders of electrochemical reaction is not significant, especially if they are determined maintaining the constant electrode potential. However, this cannot be said when speaking about such kinetic parameters as charge transfer coefficients or standard rate constants. It is desirable that their effective values determined without analyzing adsorption phenomena should be corrected for DEL effects.

References

1. Damaskin, B.B., Petrii, O.A., and Tsirlina, G.A. (2001) *Electrochemistry*, Khimiya, Moscow (in Russian).
2. Vetter, K.J. (1967) *Electrochemical Kinetics*, Academic Press, New York.
3. Damaskin, B.B. (1965) *Principles of Modern Methods of the Investigation of Electrochemical Reactions*, Moscow St. Un-ty, Moscow (in Russian).
4. Anson, F.C. and Barclay, D.J. (1968) Anion induced adsorption of cadmium(II) on mercury from iodide and bromide media. *Anal. Chem.*, **40** (12), 1791–1798.
5. Anson, F.C., Christie, J.H., and Osteryoung, R.A. (1969) A study of the adsorption of cadmium (II) on mercury from thiocyanide solutions by double potential-step chronocoulometry. *J. Electroanal. Chem.*, **13** (4), 343–353.
6. Kowalski, Z. and Anson, F.C. (1969) Adsorption of cadmium(II) and zinc(II) on mercury induced by azide anions. *J. Electrochem. Soc.*, **116** (9), 1208–1212.
7. Barclay, D.J. and Anson, F.C. (1970) Some aspects of anion-induced adsorption of white metal cations on mercury. *J. Electroanal. Chem.*, **28** (1), 71–79.
8. Damaskin, B.B., Petrii, O.A., and Batrakov, V.V. (1971) *Adsorption of Organic Compounds on Electrodes*, Plenum Press, New York.
9. Damaskin, B.B. and Petrii, O.A. (1975) *Introduction to the Electrochemical Kinetics*, Vyssh. Shk, Moscow.
10. Galus, Z. and Jeftic, L.J. (1957) Application of differential capacity measurements to the determination of the dissociation constant of acetylacetone. *Bull. Acad. Pol. Sci. Sec. Sci. Chim.*, **15** (7), 285–289.

11. Sanfeld, A. and Steinchen-Sanfeld, A. (1966) Association and dissociation in the electrochemical diffuse layer. *Trans. Faraday Soc.*, **62** (7), 1907–1914.
12. Nürnberg, H.W. and Wolf, G. (1969) Influences of homogeneous chemical reactions in the diffuse double layer. *J. Electroanal. Chem.*, **21** (1), 99–121.
13. Galus, Z., Dojlido, J., and Chojanacka-Kalinowska, G. (1972) Pyridine protonization by adsorption measurements. *Electrochim. Acta*, **17** (2), 265–270.
14. Mairanovskii, S.G. and Gaevskii, Y.K. (1975) On the determination of dissociation constants of adsorbed acids. *Elektrokhimiya*, **11** (10), 1562–1565.
15. Mairanovskii, S.G., Kryukova, G.G., and Kozlova, O.S. (1981) Adsorption some weak uncharged acids and their anions on mercury electrode. *Elektrokhimiya*, **17** (8), 1148–1153.
16. Frumkin, A.N., Damaskin, B.B., and Survila, A.A. (1968) The congruence of the adsorption isotherm with respect to the electrode potential or charge and the choice of an independent electric variable. *J. Electroanal. Chem.*, **16** (4), 493–503.
17. Flory, P.J. (1942) Thermodynamics of high polymer solutions. *J. Chem. Phys.*, **10**, 51–61.
18. Huggins, M.L. (1942) Some properties of solutions of long-chain compounds. *J. Phys. Chem.*, **46**, 151–158.

8
Electrochemical Processes in Real Systems

Any theoretical model deals with a defined and, therefore, limited number of problems, which are considered to be major. All other aspects are recognized as inessential and may be ignored. The question always arises of whether a certain theoretical model is complete enough and adequate. The answer to this question is obtained in studying the processes that take place in real electrochemical systems, which are noted for a great variety of mechanisms. Therefore, we deemed it to be expedient to supplement this book with our experimental data and data from literature about the most popular complex systems, which either are widely used in practical galvanic processes or are interesting from the theoretical point of view and, therefore, are thoroughly investigated. The works cited here have been published during the period of several recent decades, though, if necessary, information about certain earlier works is presented. Main attention is paid to kinetics and mechanisms of electrochemical reduction of complexes and the ways of their determination. More detailed information about other properties of these systems can be found in original works. We, for example, do not consider reliability of complexation characteristics used in the cited articles because a critical analysis of stability constants was made earlier [1].

8.1
Experimental Details

In the chapters that follow, a considerable part is given to the results of investigations performed by the author of this book and his coworkers. As a rule, traditional experimental methods were used; nevertheless, some details are noteworthy.

To prepare the working electrodes, Pt or Au substrates were coated with 5–7–μm-thick smooth layer of the proper metal. Copper was deposited at 10 mA cm^{-2} in a solution containing (g dm^{-3}): $CuSO_4$ $5H_2O$-200, H_2SO_4-50. To prepare tin electrodes, the substrate coated with 0.3–0.4-μm-thick copper sublayer was covered at 10 mA cm^{-2} with tin in a solution containing (g dm^{-3}) $SnSO_4$-50, H_2SO_4-160, surfactant laprol 2402 C-1. Similar procedure was used for the preparation of zinc electrodes. Zn was plated at 20 mA cm^{-2} in the solution containing (g dm^{-3}) $ZnCl_2$-100, ammonia-200, and a brightener Likonda® ZnSR.

Electrochemistry of Metal Complexes: Applications from Electroplating to Oxide Layer Formation, First Edition.
Arvydas Survila.

The active element of the electrochemical quartz crystal microbalance (EQCM) was a gold-coated quartz crystal whose oscillation frequency was equal to 5 or 6 MHz. It was plated in a similar way, but the metal coatings were thinner (0.2 – 0.4 μm). The constant relating the variations in quartz crystal mass with its oscillation frequency was determined by special calibration using EQCM data obtained in acid $CuSO_4$ solutions at a controlled current density.

So, prepared electrodes were rinsed with water, immediately immersed into the solution to be tested, and kept for the controlled time τ under open-circuit conditions. Until then, a pure argon stream was passed through solutions for 0.5 h.

Voltammetric experiments were carried out using a conventional three-electrode cell containing the working electrode, the respective anode, and the Ag|AgCl|KCl(sat) reference electrode ($E = 0.197$ V vs SHE) that was inserted in a Luggin capillary. As mentioned, all values of potentials are given next with respect to the SHE. In the case of impedance measurements, Pt wire of 0.36 cm^2 in area fused into a glass holder, prepared in the same manner, was placed within Pt cylinder that served as an auxiliary electrode for the polarization with an alternating current.

A three-electrode glass cell with a quartz window was utilized in photoelectrochemical measurements. The response of electrochemical systems to a light beam perturbation was investigated in two ways. In the first case, the dynamics of the photopotential under open-circuit conditions were recorded with perturbation by a single pulse of light emission. The second case involved recording voltammograms while perturbing with regularly repeating pulses. Entire electrode surface was illuminated by light beams that were generated by argon laser, light-emitting diodes, xenon lamp, and other light sources. A monochromatic illumination was obtained using special light filters.

pH-probing of the solution at the electrode surface was carried out by means of a $Sb|Sb_2O_3$ microelectrode. Electrochemical characteristics of the antimony microelectrode (AME) are described earlier (Section 3.3). The calibration of the AME was carried out in the solutions under investigation at different pH values that were controlled by means of a glass electrode with an accuracy of ±0.03. The design of the equipment permitted the position of the AME tip to be controlled with an accuracy of 10 μm. The distance of closest approach of the AME to the electrode surface, Δx, was arbitrarily taken as zero. The bulk pH was attributed to the respective value of the AME potential, and pH changes were determined in accordance with the slope of the calibration curve.

All experiments were carried out at 20 °C temperature, unless otherwise noted.

8.2 Cyanide Systems

Cyanide is one of those rarer ligands, which stood a century-long test in functional plating. Despite their toxicity, due to their advantages, cyanide solutions have been used up to date [2]. Coatings obtained in cyanide baths are noted for their high

physical–mechanical properties, are homogenous, and have good adhesion with various substrates. As the complexation degree of most metal cyanide solutions is high, equilibrium potentials are shifted toward more negative values to a great extent. Therefore, steel surfaces in cyanide baths can be directly coated with nobler (electropositive) metals without using sublayers of other metals. Ranges of optimal composition of cyanide baths and exploitation conditions are rather wide. As electrochemical processes are sufficiently stable, control of the composition of solutions, as well as their correction, is not complicated.

When using cyanide systems, broad practical experience was gained; however, studies of kinetics and the mechanism of electrochemical processes were not detailed or fruitful enough for a long time, though certain progress has been achieved in this sphere during recent decades. Most of theoretical and experimental problems arising at the time of carrying out investigations are related to a rather wide variety of cyanide complexes, a high adsorption ability of cyanide and certain other properties of this system. It is natural that various ways of solving these problems, different levels of the experimental and theoretic basis used reflect themselves in inconsistencies or contradictions, which can be detected in different sources in literature.

8.2.1
System Cu|Cu(I), CN^-

A comparatively small number of publications relevant to the investigations into kinetics and the mechanism of reduction of Cu(I) cyanide complexes [3–10] are most likely the result of certain difficulties arising in interpreting experimental data. Most problems are caused by foreign processes that take place alongside Cu(I) reduction, the most important of which is hydrogen evolution. Favorable conditions for this process arise from high stability of Cu(I) cyanide complexes, due to which reduction moves to a region of rather negative potentials. In this connection, the current efficiency of copper reduction in practical processes is rather low (30–60%) [11]. Foreign processes take place not only at cathodic polarizations but also under the open-circuit conditions both in naturally aerated solutions [12] and in solutions from which oxygen was eliminated [13]. The nature of nonpolarized Cu electrode potentials (E_{oc}) in cyanide solutions was considered in Section 2.4.1. Though certain corrosion processes take place in this system, E_{oc} are close to the equilibrium potentials due to a rather high exchange current density [13].

Bek and Shuraeva [8], using material balance equations (see Section 3.3), calculated dependencies of surface concentrations of the components on i/i_d within a wide range of the values (from 2.23 to 8) of the ratio $r = c_L/c_M$ and evaluated the diffusion overvoltage η_d. It was established that regularities of copper deposition depend to a large extent on η_d whose contribution increases with a decrease in r value. Effects of the distribution of the system components taking place on the electrode surface are significant [8]; therefore, in studying experimental data,

it is necessary to evaluate these effects. For example, in analyzing the Tafel plots, the steady-state current density should be normalized according to the surface concentration of an electrically active complex. However, this is not always done [3, 14], and in some works [5, 7], the dependencies of log $(i/(1 - i/i_d))$ versus E are used to make the Tafel plots. This procedure means that the current density is normalized with respect to c_M (see Eq. (3.37)) and is acceptable if the system contains the excess of ligand and one kind of complexes prevails. However, in cyanide Cu(I) solutions, it is not always possible to distinguish one kind of dominating complexes (see, e.g., Figure 2.10) and then problems arise in formulating the overall reaction of the electrochemical process. Attempts were made to avoid these difficulties by introducing stoichiometric coefficients that depend on the composition of solutions and the effective numbers of the electrons being transferred [14] for which fractional values were also allowed.

One of the main objectives of studying the mechanism is to determine the composition of the electrically active complex (EAC). In literature, among the possible EAC, all mononuclear complexes are mentioned: CuCN [3, 5], $CuCN_2^-$ [4, 7, 15], $CuCN_3^{2-}$ [6, 14], and $CuCN_4^{3-}$ [14]. In most cases, statements about the composition of the EAC have a nature of assumptions, which sometimes are reasoned in one or another way. A special analysis was made in work [3] where dependence of the exchange current density on free cyanide concentration was studied. However, the latter value was evaluated roughly without making more accurate calculations of the solution composition. It should be noted that in making assumptions about the EAC composition, the criterion given by Eq. (5.3) may be of value. It allows the minimum bulk concentration of the possible EAC to be evaluated. Calculations of the composition of solutions showed [4, 8] that the bulk concentration of CuCN never exceeds 10^{-11} mol cm^{-3} and, therefore, reduction of this particle can produce current density less than 1 mA cm^{-2}. Hence, the assumption that CuCN could be electrically active is often inconsistent with the condition Eq. (5.3).

On the other hand, the interaction of complexes, which have a saturated coordination sphere, with the metal phase of the electrode is weak, and the activation energy is high. Therefore, the probability of reduction of such complex as $CuCN_4^{3-}$ is low and it should also be eliminated from the list of possible EAC. An analogous conclusion was drawn in Ref. [6].

Surface concentrations were used in the analysis of experimental voltammograms obtained for Cu electrode whose surface was mechanically renewed in the course of measurements [4]. To determine the number of ligand particles in the electrically active complex $CuCN_p^{1-p}$, the following equation was suggested:

$$\frac{\partial \ln(i_c/[Cu^+]_s)}{\partial \ln [CN^-]_s}\Big|_{E,T} = p, \tag{8.1}$$

which is obtained from kinetic equation at sufficiently high cathodic overvoltages. Experimental data obtained at −0.9 V and presented as log $(i_c/[Cu^+]_s)$ versus log $[CN^-]_s$ were approximated by a line with a slope close to 2. This made it possible to state that complexes $CuCN_2^-$ are those species that take part in the charge transfer step. These EAC are formed as a result of dissociation of complexes $CuCN_3^{2-}$

or $CuCN_4^{3-}$ prevailing at $r < 3$ or $r > 4$, respectively. At the same time, it was underlined that only with such mechanism certain irregularities (prewaves) may appear in voltammograms, which, as has already been mentioned, sometimes can be confused with diffusion limiting currents. The authors relate rather low values of the effective α_c and their dependence on the potential to the surface activity of ligand (cyanide).

Rather controversial literature data concerning the composition of possible EAC most likely encouraged Dudek and Fedkiw [10] to analyze the model according to which any complex may be electrically active. Reduction of each of them is described by a separate kinetic equation with individual kinetic parameters, and partial currents are summed. Regularities of mass transport are considered taking into account the fact that the components of the system participate in chemical interactions, and using the principles, which are presented in Chapter 3. For example, the assumption is made that equilibration covers all areas of the solution. It should only be noted that individual diffusion coefficients are assigned to each particle being transferred and migration mass transport is taken into account. The present authors draw the conclusion that the model admitting parallel reduction of several EAC better reflects the peculiarities of kinetics in a real system and any other more convenient analysis of experimental data could hardly be created in case of such a mechanism. However, the theoretical model [10] does not take adsorption phenomena into account and ignores the effects of the double layer. Having in mind the surface activity of cyanide and Cu(I) cyanide complexes [16–20], these effects should be significant enough.

8.2.2
System Ag|Ag(I), CN−

Cyanide-based silver plating baths were put into operation before 150 years and are profitably employed up to now. Throughout the whole period, the main efforts were directed toward perfecting a practical implementation of this process [21, 22]. Thus, to reduce the toxicity of the baths, replacement of cyanide with other ions ($Fe(CN)_6^{4-}$, SCN^-, I^-, SO_3^{2-}, $S_2O_3^{2-}$, $P_2O_7^{4-}$) was suggested. At the beginning, problems regarding the mechanism of Ag(I) reduction remained to be studied more thoroughly, but later the certain progress was attained.

Three complex species containing two, three, and four CN^- ions were detected in the Ag(I)–cyanide system with sufficiently reliable stability constants. Besides, poorly soluble AgCN was also considered, but its dissociation constant is not known yet. An example of distribution of Ag(I) cyanide complexes is given in Figure 1.2.

On investigation of electrochemically deposited Ag coatings, it was established [23] that their open-circuit potentials (E_{Ag}) possess all properties that are characteristic of equilibrium potentials. In contrast with Cu electrodes in cyanide system (see Section 2.4.1), no change in the Ag electrode mass was observed upon its daily exposure to the deaerated Ag(I)–cyanide solution. After the potential step perturbation, the equilibration proceeds rather rapidly and E_{Ag} acquires its initial

value in 1–2 min. This value does not depend on stirring intensity when deaerated solutions are used; besides, the E_{Ag} value does not also depend on the presence of surfactants. Macroscopic chemical changes could not be detected when metallic Ag was brought in contact with cyanide solutions. E_{eq} values calculated by Nernst equation with $\log \beta_2 = 21.1$, $\log \beta_3 = 21.8$, and $\log \beta_4 = 20.7$ [1] are in good agreement with experimental E_{Ag} over a wide range of cyanide solution compositions ($c_M \subset [0.05, 0.25\ \text{M}], c_L \subset [0.01, 1.0\ \text{M}]$). Electrochemical measurements with distinct faces of Ag monocrystals showed [24] that E_{Ag} values depend on the index of the crystal face. It should be noted that the equilibration in the Ag|Ag(I), CN^- system proceeds significantly faster as compared with analogous copper or gold systems [12].

Similar to Cu|Cu(I), CN^- system, all Ag(I) cyanides were mentioned in literature as EAC. In this respect, the research [25] is characteristic. According to it, depending on the solution composition and the potential region, all complexes from AgCN up to $AgCN_4^{3-}$ can take part in the charge transfer step. The main problem arising in the determination of EAC composition consists in the fact that molar fractions of different complexes are of the same order and a single predominating species cannot be distinguished over the certain range of CN^- concentrations. Therefore, sometimes, it becomes impossible to formulate the overall electrochemical reaction using integer stoichiometric coefficients. The research [26] performed by Vielstich and Gerischer should be marked as one of previous efforts to establish the mechanism of electrochemical transformations. The potential-step perturbation was applied and chronoamperometric data were used to obtain exchange current densities. It was established that the dependence of $\log i_0$ on $\log [CN^-]$ passes the minimum. To explain the results obtained, two competitive charge transfer processes were assumed. At comparatively low cyanide concentrations, AgCN acts as EAC, but another charge-transfer process, namely $AgCN + e \rightarrow Ag + 2CN^-$, predominates at higher $[CN^-]$. In both cases, EAC are formed by dissociation of $AgCN_3^{2-}$ complexes that prevail in the bulk of solution. After a while, dependencies of i_0 on $[CN^-]$ were revised and some corrections were made to these data [27].

Exchange current densities were also determined using voltammetric (polarization resistance) and EIS data [28]. Three linear regions were distinguished in $\log i_0$ versus $\log[CN^-]$ dependencies and three different EAC (AgCN, $AgCN_2^-$ or $AgCN_3^{2-}$) were attributed to them. The authors maintain that the solutions with constant concentration of $AgCN_3^{2-}$ were used, but it remains unclear how this condition was realized.

To investigate the kinetics and mechanism of electrochemical processes occurring in the vicinity of the equilibrium potential, the method of isopotential solutions (IPSs) (Section 6.2) was employed [29]. In calculating four series of IPS compositions, we specified four constant values of $[Ag^+]$ and different values of $[CN^-]$. Then, we determined the values of c_M and c_L using material balance equations with stability constants given earlier. As the investigations were carried out in a sufficiently alkaline medium (pH ~ 10.5), protonated ligand was not taken into account. In preparing the solutions, we used salts $KAg(CN)_2$ and KCN,

Table 8.1 Characteristics of isopotential solutions involving Ag(I) cyanide complexes.

Concentration (mol dm^{-3})				E_{Ag} (V)
$[Ag^+]$	$[CN^-]$	c_M	c_L	−0.375
				−0.374
10^{-20}	0.025	0.0088	0.0258	−0.381
	0.035	0.0181	0.0377	−0.376
	0.05	0.0394	0.0569	
	0.1	0.1894	0.5394	

and hence calculated their concentrations (c_1 and c_2) from the following relations: $c_1 = c_M$, $c_2 = c_L - 2c_1$. Variations of concentrations of Ag(I) cyanide complexes in IPS series are shown in Figure 2.4; some examples of the data obtained are presented next.

Table 8.1 contains typical data obtained for one of IPS series. The open-circuit potential of Ag electrode in this IPS series is practically constant. Its average value (−0.376 V) coincides with the theoretical one following from the Nernst equation at the activity coefficient of Ag^+ ions equal to 0.6.

As the stability constants of Ag(I) cyanide complexes are high, we have to deal with rather low concentrations of "free" Ag^+ ions. In the extreme cases, the concentrations of some components can take on the enormously low values devoid of physical sense (this takes place in the Au|Au(I), CN^- system considered next). However, in the calculations of E_{eq}, this is not important, because from a thermodynamic point of view, it does not matter which of the species is regarded as potential dependent. Therefore, any convenient form of the Nernst equation can be used (see Chapter 2).

Exchange currency densities were determined having measured polarization resistance of the rotating Ag electrode. A part of established R_{pol} values are shown in Figure 8.1. When plotted versus $1/\sqrt{\Omega}$, these values can be approximated by lines suitable for quantitatively testing the theory presented in Section 5.3.2. When the complex species ML_N^{n+} predominate in the system and $\beta_N \gg \beta_{j\neq N}$, one can write Eq. (5.38) as

$$R_{pol} = \frac{RT}{nF}\left[\frac{1}{i_0} + \frac{\delta}{nFD}\left(\frac{1}{c_M} + \frac{N^2}{c_L}\right)\right]. \tag{8.2}$$

Though the weaker relation of $\beta_3 > \beta_2 > \beta_4$ holds true for the system under consideration, it seems possible to estimate the value of N in Eq. (8.2) using relation (5.37) and experimental slopes of lines, a part of which is shown in Figure 8.1. A calculation with $D = 10^{-5}$ cm^2 s^{-1}, $\nu = 0.01$ cm^2 s^{-1}, c_M, and c_L, used in experiments, has shown that the average $N \approx 3$. Consequently, Eq. (8.2) is a sufficiently good approximation for a quantitatively description of the system under discussion.

Charge transfer resistance R_{ct} was obtained extrapolating R_{pol} to $1/\sqrt{\Omega} = 0$; then i_0 was calculated with Eq. (5.40). Linear plots of $\log i_0$ versus $\log[CN^-]$ were

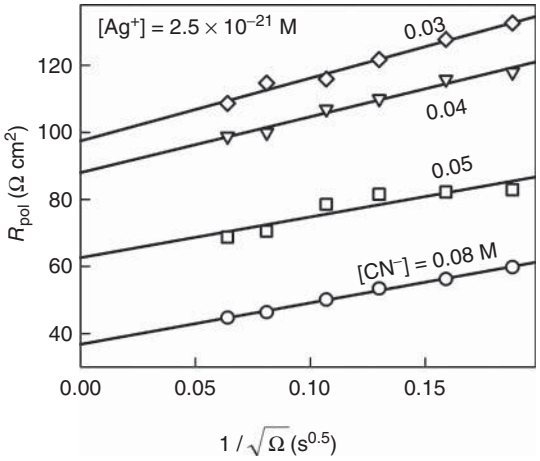

Figure 8.1 Dependencies of polarization resistance on $1/\sqrt{\Omega}$ in the series of isopotential Ag(I) cyanide solutions with constant $[Ag^+] = 2.5 \times 10^{-21}$ M and various CN^- concentrations indicated at respective curves.

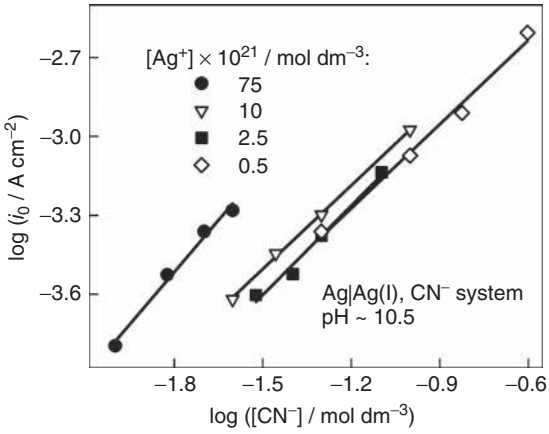

Figure 8.2 Variations of the exchange current density with the free cyanide concentration in the IPS series.

obtained in all the cases (Figure 8.2) with slopes close to 1 (or, more precisely, 1.21, 1.07, 1.08, and 1.04). Thus, the formal kinetic analysis of experimental data leads to the conclusion that AgCN is the electrochemically active species formed by the dissociation of the rest Ag(I) cyanide complexes. Similar conclusion was drawn from the analysis of anodic voltammograms [30]. It was deduced that the charge transfer process $Ag + CN^- \rightarrow AgCN + e^-$ is preceded by the chemical reaction $AgCN + CN^- \rightleftarrows AgCN_2^-$, and the rate of the overall electrochemical process is controlled by both charge transfer and diffusive mass transport. Though the stability of AgCN is not known exactly, its bulk concentration seems to be too low to

obey the criterion (Eq. (5.3)) over the entire region of cathodic polarizations. Nevertheless, such EAC could act at low polarizations, especially when in adsorbed state. We considered this problem appealing to the nonlinear dependence of log i_0 on E_{eq} [29].

According to the data, [26–29] obtained for solutions containing excess of cyanide, $AgCN_2^-$ should be the EAC at higher cathodic polarizations. Bek *et al.* [31–35] also share this judgment appealing to the results obtained for specially cleaned Ag electrodes (their surface was renewed immediately in the solutions under investigation). Nevertheless, exhaustive studies have shown that the reaction order with respect of cyanide is not an integer and falls into a narrow region between 1.2 and 1.4 [27, 36–38].

Most investigators attribute the fractional value of the reaction order to adsorption phenomena. Specifically, the data presented in Figure 8.2 can serve as indirect validity of this approach. If adsorption phenomena are ignored, a linear dependence of $\log i_0$ on E_{eq} follows from Eq. (5.7) at $[CN^-] = \text{const}$ [29]. However, the real dependence obtained from the data of Figure 8.2 is nonlinear. More detailed analysis showed [29] that the deviations between theoretical and experimental plots could arise from a parabolic dependence of adsorption constant B (see e.g., Eq. (7.13)) on the electrode potential. Its maximum is expected to be at $E \approx -0.5\,\text{V}$, that is, near the zero charge potential of Ag electrode [39].

EIS investigations [40–43] are indicative of rather complicated multistep adsorption of cyanide on Ag electrode involving mass transport and adsorption–desorption as the rate-limiting stages. Besides, adsorption regularities depend on electrode potential and obey different isotherms. It became clear from these and previous investigations that the specific adsorption of cyanide involves partial charge transfer from CN^- to Ag. This viewpoint is in line with the data of quantum chemical simulations [44] dealing with the adsorption properties of Ag_4CN^- cluster, whose formation is supported by surface-enhanced Raman spectroscopy (SERS) data [44, 45].

Some authors are of opinion that adsorbed CN^- gives rise to passivation phenomena [37, 46, 47] and, in consequence, Ag might be treated as partially blocked electrode. In this connection, the nature of voltammetric prewave observed at low cathodic polarization is explained differently [35, 37, 38, 46, 48]. A failing effect of the stirring intensity on the prewave height is sometimes taken as a point in favor of the passivation. In this connection, it seems worthy to consider the effect of forced convection in this region using views presented in Chapter 4.

The following relation is valid for the charge transfer process proceeding according Eq. (5.5) at sufficiently high cathodic overvoltages:

$$i_c = i_0 \frac{[ML_p^{n+}]_s}{[ML_p^{n+}]_b} \exp\left(\frac{\alpha_c n F}{RT}\eta_c\right) \equiv B i_0 \frac{[ML_p^{n+}]_s}{[ML_p^{n+}]_b} \tag{8.3}$$

(hereinafter, the exponential term is designated as B). The current density in the system is determined by Eq. (3.37) that contains the ratio of total concentrations of metal at the electrode surface and in the bulk of solution. This ratio can be

replaced by a similar term $[ML_p^{n+}]_s/[ML_p^{n+}]_b$ invoking the respective molar fractions of ML_p^{n+} ($\alpha_{p,s}$ and $\alpha_{p,b}$) defined by Eq. (1.11). Then,

$$\frac{[ML_p^{n+}]_s}{[ML_p^{n+}]_b} = \frac{\alpha_{p,s}}{\alpha_{p,b}}\left(1 - \frac{i_c}{i_d}\right). \tag{8.4}$$

Simple combination of Eqs. (8.3) and (8.4) with $i_d = \kappa\sqrt{\Omega}$ following from the Levich equation yields

$$\frac{1}{i_c} = \frac{1}{i_0 rB} + \frac{1}{\kappa\sqrt{\Omega}}, \tag{8.5}$$

where $r = \alpha_{p,s}/\alpha_{p,b}$. At first, let us consider the case when both right-side terms are of the same order of magnitude. Then, one can see from the equation that the effect of forced convection goes down with increasing rotation velocity Ω. On the other hand, at sufficiently high η_c, this equation transforms into $i_d = \kappa\sqrt{\Omega}$.

Voltammetric data reported in Ref. [49] were used to construct plots shown in Figure 8.3. According to Eq. (8.5), these data are well approximated by lines. It follows from their slopes and Eq. (8.5) that $\kappa = 2.1$ and 1.3 mA $s^{0.5}$ cm^{-2} at $c_M = 0.05$ and 0.025 M, respectively; in the region of limiting current, this parameter is of the same order (2–2.5 mA $s^{0.5}$ cm^{-2}). An increase in the intercept with CN^- concentration is observed (lines 2–4), this being indicative of the respective diminution in the exchange current density (see Eq. (8.5)). This result conforms with the assumption that the EAC is produced by preceding dissociation of Ag(I) complexes prevailing in the system.

The concept of partial charge transfer was employed by Baltruschat and Vielstich [27] for interpretation of the reduction of Ag(I) cyanide complexes.

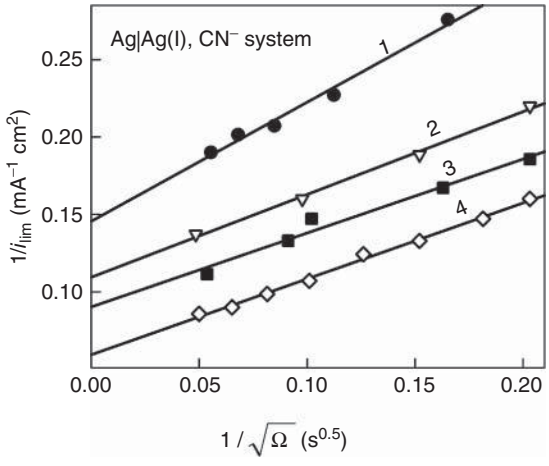

Figure 8.3 Dependencies of $1/i_{lim}$ versus $1/\sqrt{\Omega}$ obtained for Ag|Ag(I), CN^- system. c_M = 0.025 M (1) and 0.045 M (2–4); c_L = 0.05 M (1), 0.22 M (2), 0.18 M (3) and 0.1 M (4); pH 13.

According to them, initial stages of this process might be as follows:

$$\mathrm{Ag} + \mathrm{CN}^- \rightarrow \mathrm{Ag} - \mathrm{CN}_{\mathrm{ad}}, \tag{8.6}$$

$$\mathrm{Ag} - \mathrm{CN}_{\mathrm{ad}} + \mathrm{CN}^- \rightarrow \mathrm{AgCN}_2^{(2-\rho)-} + \rho\mathrm{e}^-, \tag{8.7}$$

$$\mathrm{AgCN}_2^{(2-\rho)-} + (z - 2)\mathrm{CN}^- \rightarrow \mathrm{AgCN}_2^{(z-1)-} + (1 - \rho)\mathrm{e}^-. \tag{8.8}$$

Here, the stoichiometric factor z depends on CN^- concentration and is equal to 2 or 3 at $[CN^-] < 0.05\,M$ and $[CN^-] > 0.4\,M$, respectively. The partial charge ρ depends on potential and varies from 0.7 to 1. Afterward, this mechanism was developed by Bek and Rogozhnikov [36, 37] on the assumption that the formation or destruction of adsorbed complex (process (Eq. (8.7))) is the rate-determining step. CN^- adsorption data were invoked for determining the orders of reactions, provided that the EAC (AgCN) adsorption is significantly weaker. Besides, the potential profile in the double layer was taken into account. For instance, the following kinetic equation was derived for anodic processes:

$$i_a = Fk_a\Gamma_1 c_1 \exp\frac{F\phi_2}{RT}\exp\frac{\alpha F\rho_a\Delta\psi_{01}}{RT} \tag{8.9}$$

where k_a is the anodic rate constant, Γ_1 is the surface excess of specifically adsorbed CN^- ions, c_1 is the concentration of free cyanide, and φ_2 is the local potential. The last quantity refers to the plane where nonadsorbed CN^- ions are placed (it was supposed that this is the outer Helmholtz plane). $\Delta\psi_{01}$ is the potential difference between the electrode surface and the plane where adsorbed species (complexes and ligand) are localized. It was shown that the disregard for CN^- adsorption leads to inexact reaction order that is less than 2. On the basis of the data obtained, the surface $AgCN_2^-$ complex was validated as the EAC. At the same time, it was found that the reaction order with respect to Ag(I) is 0.9 and, therefore, $AgCN_2^-$ adsorption is weak.

8.2.3
System Au|Au(I), CN—

This system is simpler in composition. Especially, stable $AgCN_2^-$ complex was identified. It is supposed that AuCN should also exist, but no information about its stability has been reported, as in the case of analogous monoligand AgCN complex. Despite the widespread use of cyanide gold-plating solutions in electroplating practice, relatively few papers have been published up to now, which deal with the kinetics and mechanism of electrode processes occurring in said system. Anodic processes are discussed in most of these papers [50–55], and it is suggested that the primary product of gold oxidation is adsorbed AuCN, which then passes into the solution to form $AuCN_2^-$ complex.

Similar views were held when investigating cathodic processes [51, 56, 57]. According to [51], at low cathodic polarizations, the reduction of Au(I) proceeds

via two steps involving formation of adsorbed intermediates:

$$AuCN_2^- \rightarrow AuCN_{ads} + CN^-, \tag{8.10}$$

$$AuCN_{ads} + e \rightarrow Au + CN^-. \tag{8.11}$$

At higher polarizations, a direct discharge of $AuCN_2^-$ diffusing from the bulk of solution to the electrode is possible. In Ref. [57], the assumption is made that the electrically active complex is AuCN, which at low η_c is reduced insofar as it is present in the surface layer. It follows from Tafel slopes reported in Ref. [57] that $\alpha_c = 0.5$. More complete kinetic data have been obtained at 60 °C for $AuCN_2^-$ reduction [56]: $\alpha_a = 0.7$, $i_0 = 0.82\,\text{mA cm}^{-2}$, $k_s = 3.9 \times 10^{-3}\,\text{cm s}^{-1}$.

According to [12], the open-circuit potentials of Au electrodes (E_{Au}) immersed into oxygen-containing Au(I) cyanide solutions are corrosion potentials, because products of O_2 reduction react with the Au surface forming surface oxides. These compounds are gradually eliminated during deaeration with nitrogen, but this process takes several hours.

Oxygen-free solutions were used by us for a test of E_{Au} with respect to the Nernst equation. Two values of $AuCN_2^-$ stability constant were found in the available literature [1, 12]: $\log \beta_2 = 36.6$ and 38.3. When calculating E_{eq} of the Au|Au(I), CN^- system, it is convenient to use the following modification of Nernst equation:

$$E_{eq} = E_2^{0/} + \frac{RT}{F} \ln \frac{[Au(CN)_2^-]}{[CN^-]^2}. \tag{8.12}$$

where the formal potential $E_2^{0/} = -0.611\,\text{V}$ as determined by Bodländer (see [58]). The mean E_{Au} values at $c_L = 0.15$, 0.25, and 0.4 M are −0.536, −0.590, and −0.623 V, respectively. The calculation via Eq. (8.12) leads to E_{eq} of −0.5355, −0.5909, and −0.6258 V. Nice agreement between E_{Au} and E_{eq} shows that an equilibrium state is attained under experimental conditions; hence, polarization in this system can be regarded as an overvoltage.

Due to the extremely high stability of Au(I) cyanide complexes, $KAu(CN)_2$ solutions containing no KCN are stable even in rather acid media. Cathodic overvoltage in such solutions is extremely high ranging up to 1.2–1.4 V [59, 60], but an addition of KCN results in significant (up to 0.3 V [59]) diminution of η_c. In our opinion, these phenomena owe to the reasons that are discussed in Chapter 4. An effect of KCN added to $KAu(CN)_2$ solutions is seen from Figure 8.4. In the absence of KCN, the concentration of free CN^- ions is of order of $10^{-14}\,\text{mol dm}^{-3}$. Therefore, very low cathodic currents are sufficient for large changes in the CN^- surface concentration and, according to the Nernst equation (8.12), for large variations in the cathodic overvoltage.

Even very low (less than $1\,\mu\text{mol dm}^{-3}$) amounts of cyanide give rise to significant depolarization of the reversible process. When increasing $[CN^-]$, half-wave potentials of voltammograms do not vary essentially, and all η_c variations result from the respective negative shifts of the equilibrium potential. It is worthy to note

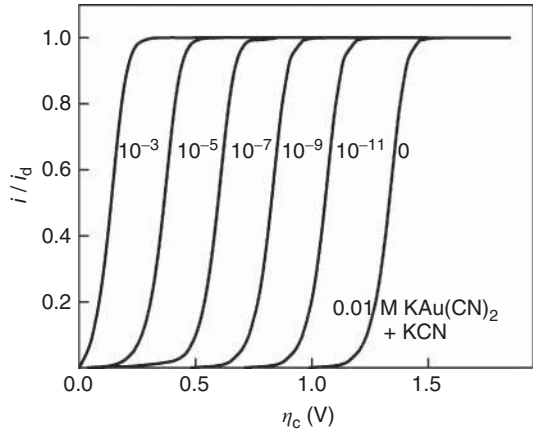

Figure 8.4 Cathodic voltammograms simulated for reversible reduction of Au(I) in 0.01 M $KAu(CN)_2$ solutions containing different amounts of KCN (in mol per cubic decimeter) as indicated.

that these variations can be responsible for bad reproducibility of experiments. If we use, say, the charge of only 0.1 C for $AuCN_2^-$ reduction, a negligible amount of CN^- ions released in the solution is capable of making significant corrections to the results of replicated experiments.

Another noteworthy property lies in the fact that both reversible and irreversible voltammograms obtained for the process

$$AuCN_2^- + e \rightarrow Au + 2CN^- \tag{8.13}$$

by the relationship

$$i = i_0 \left\{ \left(\frac{[CN^-]_s}{[CN^-]_b} \right)^2 \exp\left(\frac{\alpha_a nF}{RT} \eta \right) - \frac{[Au(CN)_2^-]_s}{[Au(CN)_2^-]_b} \exp\left(-\frac{\alpha_c nF}{RT} \eta \right) \right\} \tag{8.14}$$

with $\alpha_c = 0.5$ and $i_0 = 10^{-4}\ i_d$, become hardly distinguishable, if the amount of KCN added is less than 1 μmol dm^{-3}. Besides, Tafel plots are not available at high η_c, because it becomes impossible to simplify the kinetic Eq. (8.14) through the elimination of its anodic component. In this case, the growth with η_c in the $[CN^-]_s/[CN^-]_b$ ratio more than compensates for the decrease in the first exponent. As the diffusion-controlled phenomena prevail in the system, no conclusions on the charge transfer mechanism are also available.

Au(I) – cyanide solutions with an excess of ligand were used by us in experimental investigations. Chronopotentiograms (Figure 8.5) contain potential jumps at τ_1 between 0.2 and 0.5 s in addition to the fundamental transition time, τ, which is of the order of 1 – 10 s when i_c between 5 and 15 mA cm^{-2} is applied. The transition time τ_1 is distinct during the first recording of the chronopotentiogram (Figure 8.5), but vanishes when current pulses are repeated 4 – 5 times.

Product $i_c\tau_1$ for the solutions investigated has a value of 2.3 ± 0.7 mC cm^{-2} and tends to decrease with increasing cyanide concentration. The process occurring

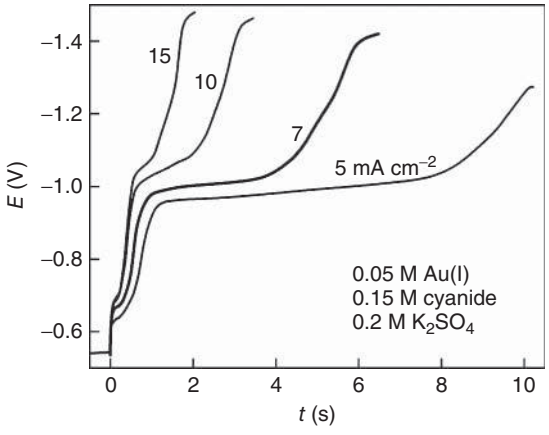

Figure 8.5 Chronopotentiograms obtained at indicated current densities for Au(I) cyanide solutions. $c_M = 0.5\,M$, $c_L = 0.15\,M$.

by the first transition time seems to be associated with the reduction of a chemisorbed layer (most likely of $AuCN_{ads}$). With this assumption, we used the equation analogous to that suggested by Lorenz [61]

$$i_c\tau = nF\Gamma + \frac{n^2F^2\pi D c_M^2}{4i_c}, \tag{8.15}$$

where Γ is the surface excess of adsorbed EAC. In accordance with this relation, the experimental dependence of $i_c\tau$ versus $1/i_c$ is close to linear (Figure 8.6). The values of $\Gamma \sim 20\,nmol\,cm^{-2}$ and $D = 1.2 \times 10^{-5}\,cm^2\,s^{-1}$ follow from the intercept (labeled by a cross in Figure 8.6) and from the slope, respectively.

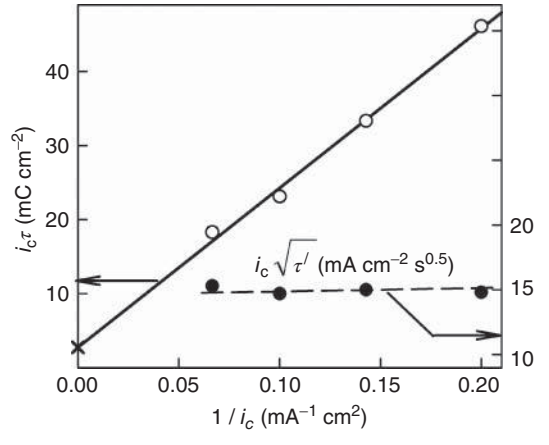

Figure 8.6 Plots of $i_c\tau$ (ordinate to the left) and $i\sqrt{\tau/}$ (ordinate to the right) versus $1/i_c$ obtained for Au|Au(I), CN^- system from chronopotentiometric data.

According to the analysis performed, $i_c\tau_1 \approx nF\Gamma$. Then, one can suggest from this result that the almost whole adsorption layer is reduced up to τ_1 and, at $t > \tau_1$, diffusion of Au(I) complexes to the electrode surface and the removal of liberated ligand species prevails. Under this assumption, Eq. (8.15) can be transformed to the relationship

$$i_c(\tau - \tau_1) \equiv i_c\tau' = \frac{n^2F^2\pi Dc_M^2}{4i_c} \tag{8.16}$$

that is in essence identical to the well-known Sand equation. Then, the product $i\sqrt{\tau'}$ should be constant, and that is the case (Figure 8.6). The mean value of $i\sqrt{\tau'} = 14.9\,\mathrm{mC\,cm^{-2}\,s^{0.5}}$ together with Eq. (8.16) yields $D = 1.2 \times 10^{-5}\,\mathrm{cm^2\,s^{-1}}$, which coincides with D determined earlier and is close to the earlier reported data [57].

The Tafel approximation of Eq. (8.14) is as follows:

$$\ln i_c = \ln i_0 + \ln \frac{[\mathrm{Au(CN)_2^-}]_s}{[\mathrm{Au(CN)_2^-}]_b} + \frac{\alpha_c nF}{RT}\eta_c. \tag{8.17}$$

Surface concentrations of complex species and ligands can be determined by means described in Chapter 3; further, the normalized Tafel plots (NTPs) can be obtained. However, initially, we shall make use of isosurface concentration voltammetry presented in Section 5.3.1. Using experimental data obtained at constant surface concentrations, one can estimate the value of α_c without any tentative assumptions as to the mechanism of the charge transfer step, that is, for unknown composition of the EAC. It follows from Eq. (4.3) that for $t/\tau' = \mathrm{const}$, the surface concentrations of the components do not depend on time. Selected in this way, data (Figure 8.7) are satisfactorily approximated by the lines with similar slopes, which yield $\alpha_c = 0.37 \pm 0.03$ (see Eq. (8.17)). This value can be checked by the analysis of individual transients of the potential, but then the composition of the EAC must be established.

As pointed out earlier, complex species $\mathrm{Au(CN)_2^-}$ are predominant in the system and the concentration of $\mathrm{Au^+}$ aqua complexes is so low that it could not sustain rates of the electrochemical process, which are observed experimentally. Nothing is known concerning the concentration of species AuCN, but the stepwise dissociation of $\mathrm{Au(CN)_2^-}$ should yield a certain amount of AuCN.

NTPs constructed for the case of EAC containing two coordinated cyanide ions are presented in Figure 8.8. Current densities $i_{\mathrm{norm}} = i_c/r$ were normalized with respect to the ratio $r = [\mathrm{Au(CN)_2^-}_s/\mathrm{Au(CN)_2^-}]_b$ at different i_c and the array of the transformed data was approximated by a single line with an acceptable accuracy. The value of $\alpha_c = 0.41$ obtained from its slope is in satisfactory agreement with the value found earlier in a different way. By extrapolating the data presented to $\eta_c = 0$, one can obtain $i_0 = 1.1 \times 10^{-5}\,\mathrm{A\ cm^{-2}}$. Considering the experimental errors and a possible departure of the properties of the real system from the model concepts, the quantities obtained could reasonably be rounded off to $\alpha_c = 0.4$ and $i_0 = 10^{-5}\,\mathrm{A\,cm^{-2}}$.

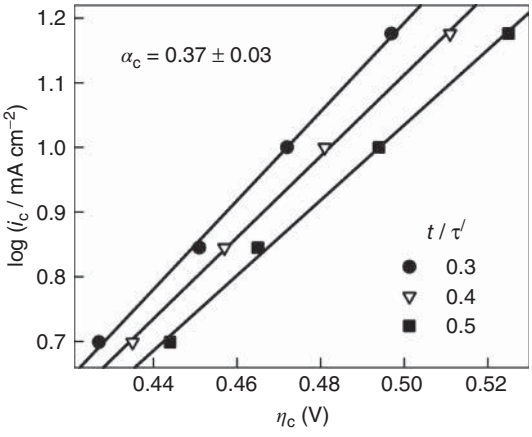

Figure 8.7 Chronopotentiometric data selected at constant ratios of t/τ' as indicated.

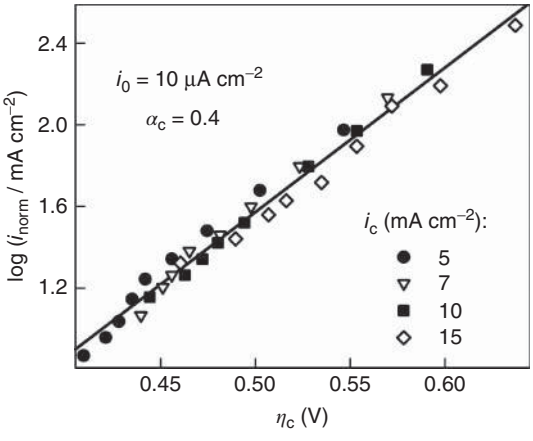

Figure 8.8 Normalized Tafel plots obtained from chronopotentiometric data at cathodic current densities, i_c, as indicated. Determined from this NTP kinetic parameters are also listed.

According to Eq. (6.6),

$$\frac{\partial \log i_0}{\partial \log[\mathrm{CN}^-]} = p + \alpha_a \nu_L, \tag{8.18}$$

where p is the number of ligand particles in the EAC and ν_L is the stoichiometric number of the ligand in the overall electrode reaction (8.13): $\nu_L = -2$. The latter relation provides a way of estimating the effect of CN^- concentration on i_0 at different EAC. For $p = 1$ and 2, the derivative $\partial \log i_0 / \partial \log c_L$ assumes values of -0.2 and 0.8, respectively. Thus, i_0 should decrease with increasing cyanide concentration, when the species AuCN is involved in the charge transfer process, but i_0 should increase with c_L in the case of EAC having the composition of $Au(CN)_2^-$.

Experimental data count in favor of the second mechanism (for details, see our article [62]). Thus, the process following the discharge of adsorption layer should involve the reduction of $Au(CN)_2^-$ diffusing from the bulk of solution.

The standard rate constant k_s can be determined by the Eq. (5.7) that for the charge transfer process (Eq. (8.13)) takes the form of

$$i_0 = nFk_s[Au(CN)_2^-]^{\alpha_a}[CN^-]^{2\alpha_c}. \tag{8.19}$$

For a temperature of 20 °C, we obtained $k_s = 10^{-4}(\mathrm{cm\,s^{-1}})(\mathrm{mol\,cm^{-3}})^{0.4}$. This value is ~39 times lower than the value obtained for 60 °C [56]. One can see when comparing these values that k_s increases on an average by a factor of 2, 5 for each decade of temperature. This is in harmony with the widely known range of temperature coefficients of chemical reactions. The values found for α also are within the range of literature data [58].

8.3 Ecological Systems Containing Hydroxy Acids

Hydroxy acids (HAs) are a class of chemical compounds that contain both a hydroxyl group and a carboxyl group in their molecules. They may be either manufactured in a lab or found in the nature. α-Hydroxy acids are carboxylic acids with one hydroxyl group attached to the α-position of the carboxyl group. The simplest representative of αHA is glycolic acid (chemical name, hydroxyacetic acid). Similarly, β-hydroxy acids have one hydroxyl group attached to the β-position of the carboxyl group. Some of them are also considered αHAs as they contain a hydroxyl group in the α-position to one carboxyl group and in the β-position to the other carboxyl group. Malic acid and citric acid are prominent representatives in this category. Polyhydroxycarbonic acids are abundant in the plant world and play an important role in various processes proceeding in nature.

HA are capable of forming quite stable coordination compounds with metal ions. Considerable recent attention has been focused on such substances, because they can be industrially applied without a negative impact on environment. The most often considered ligands are:

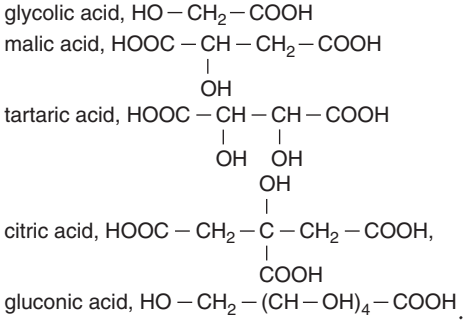

Carboxyl groups contain mobile hydrogen atoms that can be removed as hydronium ions, so liberating unshared electron pairs at oxygen atoms and creating conditions favorable to the formation of coordination bonds. Therefore, deprotonated hydroxy acids are classified as active forms of ligand capable of forming metal complexes. The aforementioned substances are often abbreviated with formulae that reflect the presence of mobile hydrogen. For instance, glycolic acid is abridged as LH, malic and tartaric acids are presented as LH_2, and so on. In alkaline media, H atoms can be detached from OH-groups as well. Then, citric acid is denoted as LH_4 instead of LH_3. To distinguish between carboxylic and hydroxylic hydrogen atoms, the abbreviation HGH_4 was proposed for gluconic acid. Due to the presence of four hydroxyl groups, gluconic acid is an effective ligand in the alkaline medium, where very stable mono- and binuclear chelates can be formed. Most of the aforementioned acids have already found practical use in plating processes and the field of their application is permanently extending. However, the research in this area is, in most cases, of applied character; the problems of the mechanism and kinetics of electrode processes have received less attention. Next, kinetics and mechanism of cathodic processes involving such ligands are considered.

8.3.1 Electroreduction of Cu(II) Complexes

A great variety of Cu(II)–HA complexes was reported [1], and most of them prevail in alkaline media. Acid solutions are simpler in composition. We obtained some distribution data using material balance equations with stability constants taken from available catalogs [1]. It should be noted that the required data were sometimes few in number and discrepant. Nevertheless, some view on complexes predominating at pH < 6 can be inferred from Table 8.2. The species whose molar fraction exceeds 30% are listed in it. Considering that solutions commonly contain an excess of indifferent electrolyte, we tried to select stability constants corresponding to the sufficiently high ionic strength ($I \approx 1$). Perchlorates and nitrates are usual substances that are most often used to maintain the certain I in experiments. However, these components are uncommon in plating baths giving way to other supporting electrolytes, such as sulfates. In this connection, some points regarding the "indifference" of sulfates are worthy of consideration.

A systematic investigation of the thermodynamic quantities associated with the interaction between Cu^{2+} and SO_4^{2-} has been performed by Akilan [63]. According to various authors, the stability constant (K_A) of $Cu^{2+}SO_4^{2-}$ (aq) ionic couple essentially depends both on the ionic strength of solutions and on the method used. It was found that $CuSO_4$ "complexes" can be detected by UV-spectrophotometry at $\lambda = 250$ nm. In the visible region, the spectra of equimolar $CuSO_4$ and $Cu(ClO_4)_2$ solutions virtually coincide [64]. According to [63], in the case of concentrated solutions ($1 < I < 5$ M), K_A only slightly depends on I; on the average, $K_A = 10$. Stability constant of gluconate complex CuL^+ was found to be equal to $10^{2.2}$ (spectrophotometric data [65]). These values

Table 8.2 Complex species predominating in acid Cu(II)–HA solutions containing an excess of ligand ($r = c_L/c_M = 4$) at pH < 6.

Ligand	Symbol	Species	pH range
Glycolic acid	LH	Cu^{2+}(aq)	<4
Malic acid	LH_2	CuL^+	>2.5
Tartaric acid	LH_2	Cu^{2+}(aq)	<3.9
Citric acid	LH_4	CuL	>3.3
Gluconic acid	LH	CuL_2^{2-}	>4.4
		Cu^{2+}(aq)	<3
		CuL	>2.5
		CuL_2^{2-}	>4
		Cu^{2+}(aq)	<3.6
		CuL^{2-}	>3.8
		$CuLH^-$	3.4–4.3
		Cu^{2+}(aq)	<5
		CuL^+	>3

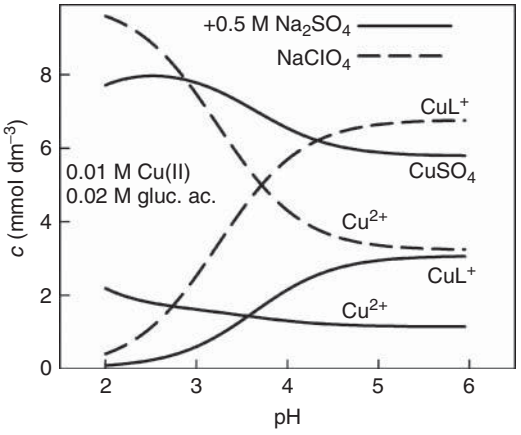

Figure 8.9 Distribution of species in 0.01 M Cu(II) solutions containing 0.5 M Na_2SO_4 and gluconic acid with total concentration of 0.02 M (solid lines) and 0.05 M (dashed lines).

were used in simulations whose results are presented in Figure 8.9. In the case of sulfate-containing solutions, concentrations of three species, namely Cu^{2+}, CuL^+, and $CuSO_4$(aq) are of the same order of magnitude. Simpler distribution of species is observed in perchlorate solutions (dotted lines in Figure 8.9). In the following, we shall see that the shape of voltammograms obtained for perchlorate and sulfate solutions is also different.

Typical linear potential sweep (LPS) voltammograms, obtained at different pH as indicated, are given in Figure 8.10. They contain two well-defined maxima that are indicative of two different cathodic processes. The first current peak (i_{p1}) observed at a relatively low cathodic polarization ($E_{p1} \approx 0.1\,V$) is essentially

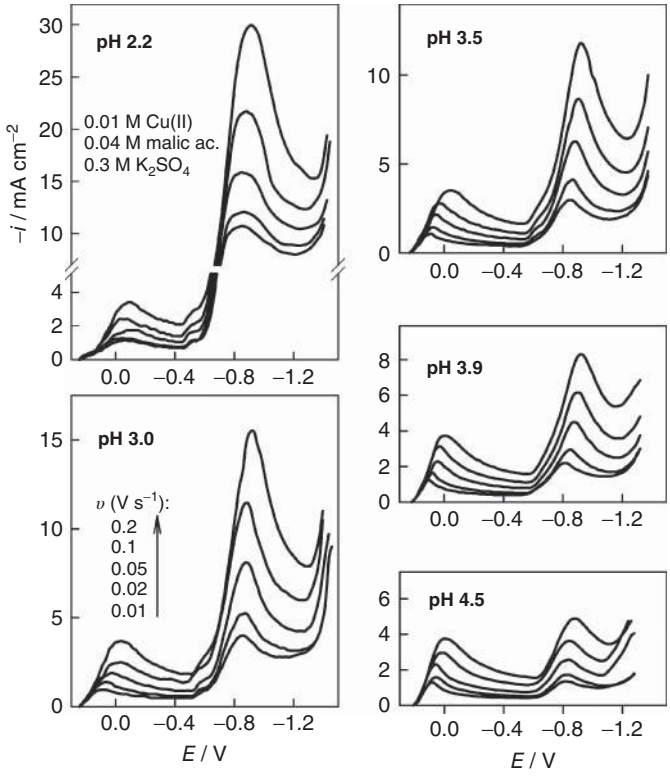

Figure 8.10 LPS voltammograms obtained for Cu(II)–malic acid system at different pH and potential sweep rates as indicated.

pH independent. The further increase in cathodic polarization gives rise to the second process with a distinctive current peak (i_{p2}) located at $E_{p2} \approx -0.9\,V$. Contrary to i_{p1}, the height of the second peak increases with the acidity of solutions. A similar peak is also observed in Cu(II)-free solutions. Moreover, the voltammograms obtained in the latter case and brought to the level of partial Cu(II) reduction current coincide sufficiently well with the data recorded in the presence of Cu(II). This effect, as well as large difference between E_{p1} and E_{p2}, gives grounds to analyze the two processes independently.

Considering the different pH effects, it can be assumed that the first partial process is Cu(II) reduction whereas the hydrogen evolution could be the second process. To verify this supposition, the voltammograms recorded directly were compared with those obtained from EQCM data.

Let us suppose that the electrodeposition of copper is the only process that results in an increase of the electrode mass (Δm). According to the Sauerbrey equation [66],

$$\Delta m = -k\Delta f \tag{8.20}$$

where k is the constant relating the variations in quartz crystal mass with its resonant oscillation frequency f. On the other hand, it follows from Faraday's law that

$$\Delta m = \frac{AM}{nF}\int_0^{\Delta t} i(t)\mathrm{d}t, \tag{8.21}$$

where A is the electrode surface, M is the molar mass of copper, and $n = 2$ is the number of electrons involved in the Cu(II) reduction reaction. The aforementioned equations yield the relation

$$i(t) = -\frac{KnF}{M}\frac{\mathrm{d}\Delta f}{\mathrm{d}t} \tag{8.22}$$

with $K = k/A$, which makes it possible to transform EQCM data into partial current of Cu(II) reduction. Voltammograms recorded directly and calculated from EQCM data are compared in Figure 8.11. The results obtained by the two different methods are very close in the region of the first current maximum that should be attributed to the copper electrodeposition. No additional change in the electrode mass was observed at higher cathodic overvoltages and, therefore, no second current peak follows from EQCM data. The situation remains actually the same in the case of Cu(II)-free solutions as well; only the noisy EQCM response of zero level was detected. The results obtained testify quite unambiguously that the second current maximum is conditioned by hydrogen evolution in sufficiently acidic media.

Consecutive charge transfer steps are typical of Cu(II) reduction. To study processes of this kind, different transient techniques can be applied, including the EIS. Proper analysis of impedance spectra often involves use of adequate equivalent circuits (ECs). However, sometimes they lack substantiation and, as a consequence, the physical meaning of EC elements is treated at random. Preferable

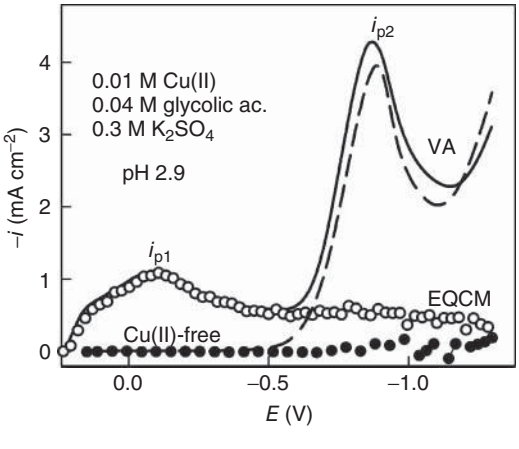

Figure 8.11 Comparison between experimental voltammograms (VAs, lines) and transformed EQCM data (symbols). Data for Cu(II)-free solutions are presented by dotted line and black circles.

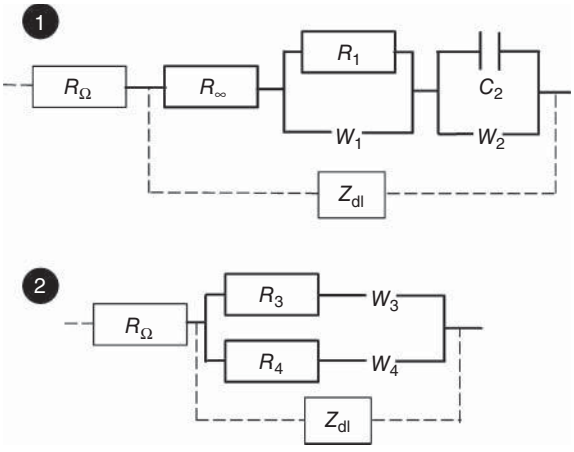

Figure 8.12 Two equivalent circuits for consecutive transfer of two electrons. Faradaic elements are connected with solid lines. The ohmic resistance of the solution, R_Ω, and the double-layer impedance, Q_{dl}, are the non-faradaic elements.

circuits should follow from the mathematical expressions derived for the appropriate theoretical models.

In previous studies, a theoretical analysis of the faradaic impedance has been performed provided that the final product is also soluble [67–69]. Next, the relationships obtained in Ref. [66] have been extended for the case when an insoluble final product (e.g., metal deposit) is formed [69]. No EC was proposed in the previous investigations [67, 68] until it was found [70] that the general impedance expression corresponds to an EC consisting of five elements that, according to the authors, "have no sensible physical meaning." At the same time, we proposed another EC [71], which rigorously followed from analytical expressions and contained less subcircuits. So, two different chemical step + electrochemical step (CE) have been proposed for description of the same mechanism (Figure 8.12). To avoid confusion in this situation, we made an attempt to analyze both EC so as to clarify their possible interrelation.

As has been reported [69], the faradaic admittance, derived by Armstrong and Firman [68] for the mechanism $O + e \rightleftarrows Y$, $Y + e \rightleftarrows R$, can be expressed as

$$Y_F = \frac{1}{Z_F} = \frac{1}{R_\infty} \frac{1 + \frac{b}{\sqrt{s}}}{1 + \frac{c}{\sqrt{s}} + \frac{d}{s}}, \tag{8.23}$$

where the complex variable $s = j\omega$, $j = \sqrt{-1}$, and angular frequency $\omega = 2\pi f$. Notice that the general relationship obtained by Despić *et al.* [67] also takes this form.

The analysis performed shows (for details see Appendix for this Section) that two different EC follow from Eq. (8.23). The faradaic subcircuit of the first CE was composed by Rueda *et al.* [69]. Upon supplementing with non-faradaic elements, the EC N1 takes form shown in the upper part of Figure 8.12. Its description code is

$R_\Omega[R_\infty(R_1W_1)(C_2W_2)]Q_{dl}$, where Q is a constant phase element (CPE). According to the impedance theory, the complex conductivity of CPE (admittance Y) is given by the relationship

$$Y = Y_0(j\omega)^n, \tag{8.24}$$

where the exponent n characterizes the nature of CPE. When n is equal to 1, 0.5, 0, or −1, CPE transforms into the capacitance, Warburg impedance, resistance, or inductance, respectively.

Though the magnitude and the frequency dependence of Y_F are essentially controlled by four parameters (see Eq. (8.23)), the faradaic subcircuit contains more (five) elements. For this reason, the specific link between faradaic EC elements occurs:

$$C_2 = R_1Y_{01}Y_{02}, \tag{8.25}$$

where Y_{01} and Y_{02} are constants of the respective Warburg admittances (see Eq. (8.24)).

The faradaic circuit of EC N2 contains less (four) elements displaced in two parallel $[RW]$ subcircuits. Both foregoing EC yield the same impedance spectra, if and only if the condition 8.25 is satisfied. As this takes place, the interrelation between elements of the two EC is given by Eqs. (A4)–(A8) in the Appendix. The EC N2 is preferable due to more clear physical sense. For instance, in the case of copper deposition, the following relationships are valid under the equilibrium conditions [70, 71]:

$$i_{01} + i_{02} = \frac{RT}{F}\left(\frac{1}{R_1} + \frac{1}{R_2}\right), \tag{8.26}$$

$$\frac{1}{i_{01}} + \frac{1}{i_{02}} = \frac{R_1 + R_2}{\sigma_1 + \sigma_2}\frac{1}{F\sqrt{D}}\left(\frac{1}{[Cu^{2+}]} + \frac{4}{[Cu^{+}]}\right), \tag{8.27}$$

where Warburg coefficients (σ) have their common meaning, namely $\sigma = 1/\sqrt{2}Y_0$.

It can be seen from Eqs. (8.26) and (8.27) that R_1 and R_2 represent the charge transfer kinetics, whereas W_1 and W_2 characterize both the charge transfer and the semi-infinite diffusion. We wish to emphasize particularly that all faradaic elements are interrelated and each of them depends on the characteristics of both steps. Close inspection of mathematics regarding similar but adsorption-complicated processes [72] shows that this conclusion is more general and might be extended to more complex mechanisms.

To determine the composition of the electrically active complex in the Cu(II)–glycolic acid solutions, the EIS and IPS methods (see Section 6.2) were used. The composition of IPS series (Table 8.3) was calculated using material balance equations with $[Cu^{2+}] = 5.3\,mM$, pH 5.3, and different [L]. Copper electrodes in these solutions acquire actually the same equilibrium potential equal to $0.239 \pm 0.001\,V$. Experimental Nyquist plots (the interrelation between real, Z', and imaginary, Z'', components of the impedance) and the EC applied

Table 8.3 Composition of IPS and parameters of the equivalent circuit.

EC elements →			Q_{dl}		R_1	W_1	G	W_2
Parameters →			$10^6\ Y_0$	n	R_1	Y_0	K_a	$10^4\ Y_0$
IPS ↓	c_M	c_L						
A	6.4	10	71	0.92	62.1	0.171	1.43	8.86
B	7.6	20	81	0.84	64.3	0.094	1.23	3.76
C	10.0	40	71	0.86	60.0	0.096	2.02	5.12
D	15.2	80	96	0.85	61.6	0.084	1.38	5.07

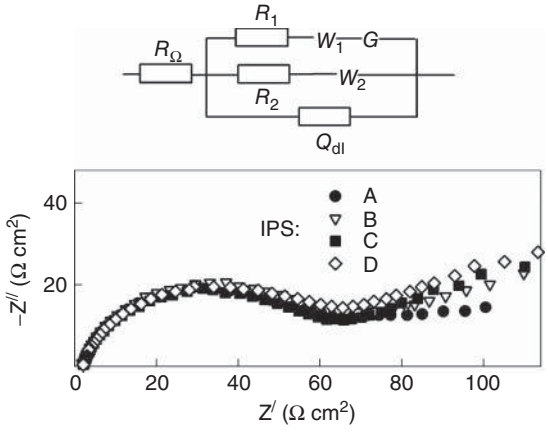

Figure 8.13 Equivalent circuit and experimental Nyquist plots obtained for series of isopotential Cu(II)–glycolic acid solutions.

are shown in Figure 8.13. The analysis performed showed that the EC N1 should be supplemented with G that accounts for the existence of the preceding chemical reaction (PCR). According to the theory developed by Gerischer [73] for the case when electrically active particles O are formed through a first- or pseudofirst-order PCR ($A \rightleftarrows O$ or $A \rightleftarrows O + B$, respectively), the admittance of component G is determined by

$$Y_G = Y_0\sqrt{K_a + j\omega}, \tag{8.28}$$

and the expression for Y_0 takes the form

$$Y_0 = \frac{n^2F^2c\sqrt{D}}{RT}, \tag{8.29}$$

where c and D are the equilibrium concentration and diffusion coefficient of the EAC. If the rate constants of forward and backward reactions shown earlier

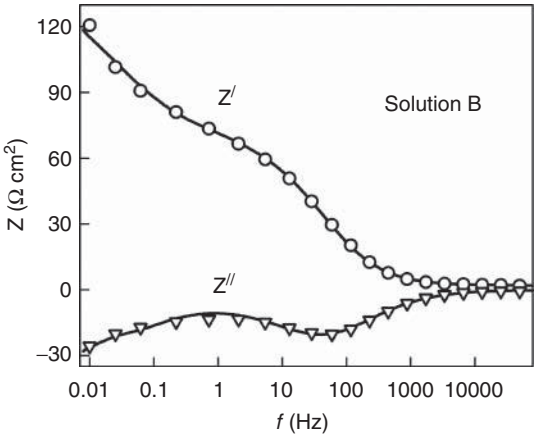

Figure 8.14 Comparison of impedance spectra measured for solution B (symbols) and calculated for the equivalent circuit (solid lines) with pertinent data from Table 8.1.

are designated by k_1 and k_2, respectively, then the quantity K_a in Eq. (8.28) can be expressed as follows: $K_a = k_2$ for a first-order PCR, and $K_a = k_2 c_B$ for a pseudofirst-order PCR. In the latter case, it is also assumed that the concentration of substance B (c_B) can be considered constant.

Using the indicated EC makes it possible to describe the impedance spectra quantitatively with an error not exceeding 3–4% (see the example in Figure 8.14). A preliminary analysis of the experimental data has shown that because of the large number of electrical components, their parameters, which were determined from a fitting procedure, vary in reliability. The values of R_Ω and R_1 are the most accurately determined (with an error of 2–4%) while the relative error amounts to 30–60% for K_a and 10–30% for the remaining parameters. Reliable values of R_2 cannot be obtained; it is only possible to conclude that $R_2 \ll R_1$. In order to increase the degree of certainty of the parameter K_a (EC element G) in determining other parameters, we fixed the value $Y_0 = 0.05\,\Omega^{-1}\,\mathrm{cm}^{-2}\,\mathrm{s}^{0.5}$, which follows from Eq. (8.29) with $c \equiv [Cu^{2+}] = 5.3\,\mathrm{mM}$ and $n = 1$. The results are presented in Table 8.3.

As $R_2 \ll R_1$, the transfer of the first electron is the rate-determining step. The small value of resistance R_2 admits the certain simplifications as has been done previously [74, 75]. Then, component R_1 assumes the meaning of the resistance attributed to the transfer of the first electron, and its value can be used to determine the corresponding exchange current density from the equation

$$i_{01} = \frac{RT}{4FR_1}. \tag{8.30}$$

It follows from the data in Table 8.3 that the values of R_1 determined for all IPS are very close to each other, and according to Eq. (8.30), the average value of i_{01} is equal to 0.1 mA cm^{-2}. From the fact that i_{01} does not depend on the concentration of the free ligand, there follows the important conclusion that the electrically

active particle does not contain the ligand and aqua complexes of Cu^{2+} participate in the charge-transfer step.

As we noted earlier, at $n = 1$, Eq. (8.24) transforms into the relationship for electrical capacitance. The average value of n for Q_{dl} is ~0.9, and this is indicative of the capacitive nature of Q_{dl}, which can be considered the electrical analog to the double layer. Then, it is possible to assume that the parameter Y_0 approximately represents the double-layer capacitance, which amounts to 70–90 μF cm^{-2}. Somewhat higher values of Y_0 were obtained for the Cu|Cu(II) system in the absence of adsorption of organic substances [71, 76]. In the IPS series, the total Cu(II) concentration varied from 6.5 to 15 mM. According to the well-known equation for Warburg impedance [77], it is possible to estimate the value of Y_0, which amounts to about 0.1 Ω^{-1} cm^{-2} $s^{0.5}$ for a 10 mM Cu(II) solution and the transfer of one electron. This agrees with the order of magnitude of Y_0 determined for component W_1. The analogous value for component W_2 is approximately 2 orders of magnitude smaller, and this agrees with the estimated ratio of the equilibrium concentrations $[Cu^+]/[Cu^{2+}]$ in the solutions. Consequently, it is possible to consider W_1 and W_2 as representing the diffusive flows of Cu(II) and Cu(I). In contrast to the aforementioned electrical analogs, component G appears to be a somewhat coarse approximation, because it is difficult to classify the chemical processes occurring in the system under discussion as first- or pseudofirst-order PCR, which could be represented by G impedance.

It seems necessary to estimate to what extent PCR kinetics can be reflected in the LPS voltammograms. According to [78], the empirical equation that defines the ratio of the values of the current peaks in the absence (i_p) and with the occurrence (i_r) of a first-order PCR has the form

$$\frac{i_p}{i_r} = 1.02 + \frac{0.531}{K}\sqrt{\frac{b}{l}}, \tag{8.31}$$

where $b = \alpha n_\alpha F v/RT$. $K = k_1/k_2$ is the equilibrium constant of the PCR; k_1 and k_2 are the rates constants of forward and backward reactions, respectively, and $l = k_1 + k_2$. The effect of the PCR can be considered as negligible, when $i_r \approx i_p$. This case corresponds to the condition

$$\frac{1}{K}\sqrt{\frac{b}{l}} < 0.1. \tag{8.32}$$

If the process $CuL^+ \rightarrow Cu^{2+} + L^-$ is taken as the PCR, the condition Eq. 8.32 is satisfied when $v < 0.02\,V\,s^{-1}$ [79]. However, even for larger values of v, there were no indications suggesting the presence of such limiting PCR (see next). Therefore, this process must be considered sufficiently fast to be consistent with the well-known liability of Cu(II) complexes. Another probability could be the dissociation of weak Cu(II)–sulfate complexes [63] that can be formed when K_2SO_4 is used as a supporting electrolyte. From our point of view, a more realistic PCR, which is suggested by the impedance data, may be the dissociation of LH. However, to reveal the nature of PCR, further investigations should be performed.

To check the validity of the earlier assumptions, it is of interest to establish to what extent Cu(II) is reduced over the region preceding the onset of hydrogen evolution. Let us assume that the solution with the total Cu(II) concentration equal to $c^*_{\mathrm{Cu(II)},b}$ is prepared for experiments. When it comes into contact with the Cu electrode, certain amount of Cu(I) is produced due to the interactions between the Cu and Cu(II)-containing species. This process holds on until the equilibrium is achieved and certain total concentrations $c_{\mathrm{Cu(II)},b}$ and $c_{\mathrm{Cu(I)},b}$ are established. It follows from the material and charge balance regularities that

$$c_{\mathrm{Cu(II)},b} + \frac{c_{\mathrm{Cu(I)},b}}{2} = c^*_{\mathrm{Cu(II)},b} \tag{8.33}$$

As Cu(II) reduction involves two consecutive one-electron transfers, the rate of the overall process involves current densities of both steps, that is, $i = i_1 + i_2$. According to Eqs. (5.18) and (8.33), a decrease in the total Cu(II) concentration at the electrode surface is expressed by the equation

$$\Delta c_{\mathrm{Cu(II)}} \equiv c^*_{\mathrm{Cu(II)},b} - \left(c_{\mathrm{Cu(II)},s} + \frac{c_{\mathrm{Cu(I)},s}}{2} \right) = -\frac{1}{nF\sqrt{\pi D}} \int_0^t \frac{i(t-u)}{\sqrt{u}} \psi(u) \mathrm{d}u \tag{8.34}$$

that requires no assumptions on the composition of the electrically active complex. An example of results obtained with this equation is shown in Figure 8.15. According to Ref. [80], hydrogen evolution becomes detectable at $E \approx -0.6\,\mathrm{V}$ (at $\eta_c \approx -0.8\,\mathrm{V}$). At this point, $\Delta c_{\mathrm{Cu(II)}} \approx c^*_{\mathrm{Cu(II)},b}$ and, according to Eq. (8.34), the surface concentration of copper-containing species approaches zero. The result obtained shows that Cu(II) complexes are sufficiently labile under LPS conditions and permits the use of $\Delta c_{\mathrm{Cu(II)}}$ for evaluation of the solution composition at the electrode surface, as described in Chapter 3.

NTPs for glycolic acid system were presented in Figure 5.3. Similar data obtained from transform of LPS (malic and tartaric acid systems) and rotating

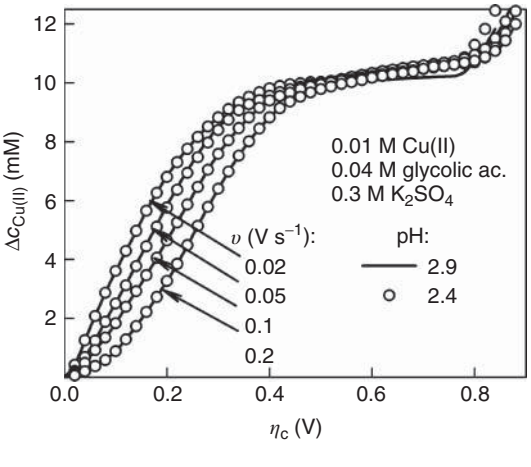

Figure 8.15 Changes in Cu(II) surface concentration under linear potential sweep conditions. Transform of the LPS voltammograms by Eq. (8.14).

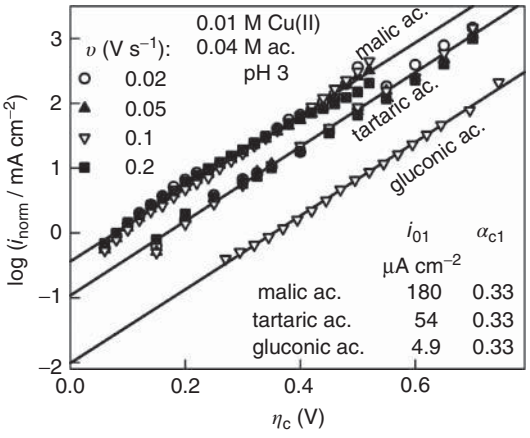

Figure 8.16 Normalized Tafel plots obtained by transformation of LPS (malic and tartaric acid systems) and RDE (gluconic acid system) voltammograms. 0.3–0.5 M sulfate was used as a supporting electrolyte.

disc electrode (RDE) (gluconic acid system) voltammograms are shown in Figure 8.16. Here, $i_{\text{norm}} = -i/r$, where $r = [Cu^{2+}]_s/[Cu^{2+}]_b$. In this case, extrapolation of NTP to $\eta = 0$ yields the value of 2 i_{01} (see Eq. (5.26)). The plots for different ligands are compared at the same c_L and pH, because kinetic parameters depend on these quantities [80]. The exchange current density decreases with the molar mass of ligand, whereas the cathodic charge transfer coefficient remains the same.

Such profound alterations in the i_{01} cannot be attributed to the respective differences in the complexation degree of the systems. Distribution data for pH 3 show that Cu^{2+} concentrations are of the same order of magnitude, whereas i_{01} values for malic and gluconic acid systems differ by ~40 times. Specifically, we have found [65] that an addition of gluconic acid significantly inhibits the cathodic process. This effect is noticeable at rather low concentrations of ligand and cannot be caused only by the variation in the state of Cu(II) in the bulk solution. XPS and morphological studies of the deposits have shown [65] that the chemisorption of gluconic acid could be responsible for the phenomena observed. This surface process involves a partial destruction of gluconic acid with subsequent incorporation of the ligand fragments into Cu deposits.

Transient techniques including an LPS voltammetry are often more sensitive than the steady-state measurements. To extend the scale of information on the system, an analysis of LPS voltammetric maxima is desirable. Unfortunately, analytical expressions for LPS voltammograms are not available for circumstances discussed in Chapter 4. Nevertheless, it is of interest to use for this purpose some relationships derived for simple redox systems replacing the concentration of the oxidant by the total concentration of metal. Certain grounds for such operation follow from the regularities of mass transport of labile complexes (Section 3.2).

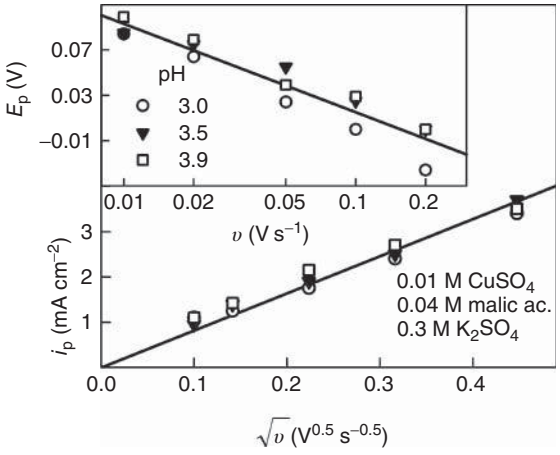

Figure 8.17 Variations of the peak current density with the square root of potential sweep rate. Variations of the peak potential with *v* are shown in the inset in semilogarithmic coordinates. The data obtained for Cu|Cu(II), malic acid system at different pH as indicated.

At first, we shall deal with the data concerning the malic acid system. As the pH effect on i_p is weak, the dependencies of i_p versus $\sqrt{\nu}$ obtained at different pH were approximated by a single general line passing the origin, as shown in Figure 8.17. Its slope of 8.2 mA cm^{-2} V$^{-0.5}$ s$^{0.5}$ was substituted in Eq. (5.30) and the product of $\alpha_c D_{ef} = 1.82 \times 10^{-6}$ cm^2 s^{-1} was obtained. When performing transforms of LPS voltammograms according Eq. (8.34), the value of $D_{ef} = 5.7 \times 10^{-6}$ cm^2 s^{-1} was established. Then, $\alpha_c = 0.32$. At the same time, the value of $\partial E_p / \partial \log \nu = -78$ mV per decade follows from the experimental data (inset in Figure 8.16) and, according to Eq. (5.31), $\alpha_c = 0.37$ is obtained. The last two α_c values conform acceptably with the quantity obtained from NTP (Figure 8.16).

Similar and yet somewhat different data were obtained for gluconic acid system. As earlier, the effect of pH on the peak current is weak, but its position shifts noticeably toward more negative potentials when pH is increased (Figure 8.18). Experimental value of $\partial i_p / \partial \sqrt{\nu} = 8.15$ mA cm^{-2} V$^{-0.5}$ s$^{0.5}$ yields $\alpha_c D_{ef} = 1.8 \times 10^{-6}$ cm^2 s^{-1}. It follows from RDE data [65] that the effective diffusion coefficient decreases with increasing the complexation degree of the system (increasing pH or ligand concentration) and, as judged from these data, $D_{ef} = 4.4 \times 10^{-6}$ cm^2 s^{-1} for the solutions under discussion; then, $\alpha_c = 0.40$. An average value of α_c obtained from E_p data is 0.43. In this case, the reconciliation of LPS and NTP data is worse.

More close inspection of LPS data shows that current maxima are not even and contain some irregularities (Figure 8.19). It is presumable that they are composed of several peaks that become more evident at higher *v*. Some reasons can be responsible for such a feature. According to Ref. [81], two current maxima can arise on LPS voltammograms when process $A + n_1 e \rightarrow B + n_2 e \rightarrow C$ occurs,

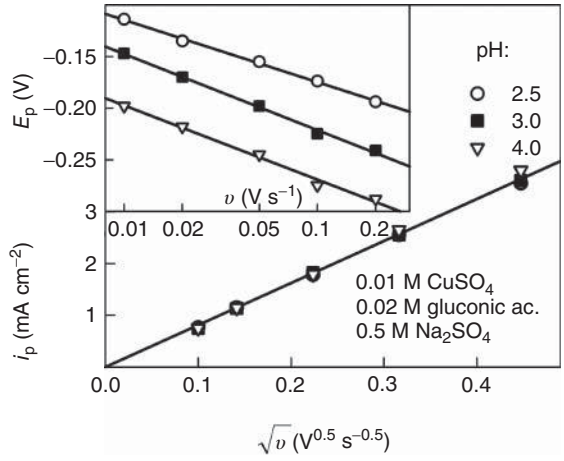

Figure 8.18 The same as in Figure 8.17 for Cu|Cu(II), gluconic acid system.

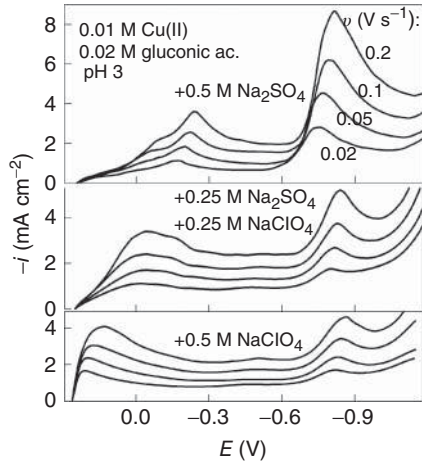

Figure 8.19 LPS voltammograms obtained for Cu(II) gluconate solutions containing different supporting electrolytes: sulfate (upper part), mixture of sulfate and perchlorate (middle part), perchlorate (lower part).

provided that A and B are reduced at rather different potentials. However, when this potential difference is less than $100/\alpha n_\alpha$ mV, both peaks overlap producing one deformed maximum.

Theoretical behavior of labile metal complexes under LPS conditions was considered in Chapter 4. It was established [82] that irregular or bifurcated current maxima are possible in the case of consecutive charge transfer. However, it is necessary to note that a stepwise charge transfer is not an essential condition for duplex structure of current peaks; similar shapes are also possible in the case of

complex systems with a lack of ligand. Finally, a simultaneous electroreduction of several EAC should not be overlooked.

To reduce the number of possible EAC species, we carried out extra experiments using perchlorate as a supporting electrolyte. Distribution of complex species in solutions is presented (Figure 8.9). The effect of supporting electrolyte can be seen from Figure 8.19. Even one-half substitution of perchlorate for sulfate results in significant reduction of cathodic polarization involving ~0.24 V shift of the first current peak (cf. the upper and middle parts of Figure 8.19); however, some irregularities of current maxima still persist. When sulfate is fully replaced by perchlorate (the lower part of Figure 8.19), E_p is located at relatively low cathodic polarizations and the current maxima become smooth and even.

It is clearly seen that E_p becomes more negative at a higher pH, that is, when CuL^+ concentration increases; therefore, the gluconate complex of Cu(II) cannot be electrochemically active over a wide region of potentials. Then, it is reasonable to suppose that "free" Cu^{2+} ions (aqua complexes) could be the single EAC in perchlorate media. A similar conclusion has been also drawn for sulfate solutions on the basis of voltammetric RDE data [65]. It remains to be seen whether the Cu(II)–sulfate complex can be also reduced over the same range of potentials. To elucidate the mechanism of Cu(II) reduction in more detail, special further investigations are required.

It is evident that the rate of cathodic process is significantly lower in the presence of sulfate. Among the factors responsive for such an effect, different adsorption behavior of ions should be mentioned. In contrast to ClO_4^-, chemisorbed (specifically adsorbed) SO_4^{2-} ions were identified on copper by SERS [83]. The most intense adsorption was observed at ~−0.20 V with following progressive diminution and desorption occurring at ~−0.4 V. It is common knowledge that most organic compounds are adsorbed near the zero charge potential (E_{zc}), where the surface charge density is not too high. Different E_{zc} values of copper electrode have been reported up to date. More positive values (close to 0 V) seem to be preferred for copper electrodes prepared by electrolysis (see Ref. [84]). Then, the gluconate desorption is expected at sufficiently negative potentials. According to impedance data [85], this takes place at~−0.25 V where the double-layer admittance approaches values that are typical of additive-free Cu(II) solutions. Hence, the discussed current maxima fall into the range of potentials involving adsorption phenomena.

At the same time, adsorption of Cu(II) complexes in themselves seems to be weak. It can be seen from chronopotentiometric data that are plotted in Figure 8.20 in coordinates adjusted to Eq. (8.15). Zero intercepts of fitting lines observed at pH ≤ 4 suggest the absence of reduction processes involving the adsorbed Cu(II) complexes. Then, the $i\sqrt{\tau}$ product should be constant and this is approximately obeyed (inset in Figure 8.20). It follows from the foregoing that Cu^{2+}(aq) species is electrically active in acid media. However, at higher pH, the mechanism of electrode reaction can vary, because complexes formed in alkaline media are competitive with the aforementioned EAC. The Cu|Cu(II), citric acid system is characteristic in this respect [86, 87].

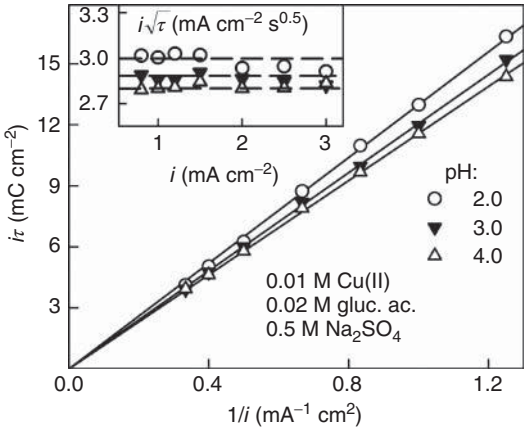

Figure 8.20 The $i\tau$ products plotted versus 1/i at different pH as indicated. Respective $i\sqrt{\tau}$ values are given in the inset.

Generally, a citric acid can be denoted by the symbol LH_4. According to Nurnberg *et al.* [88], the release of the first two protons from a citric acid molecule is rather fast, whereas the rate of the third proton elimination is noticeably lower. The same seems to be true for the forth proton, that is, for the dissociation of LH^{3-} species. We found no data indicating the inertness of Cu(II) citrate complexes. Their lability is supported to a certain extent by a diffusive nature of a limiting current. This can be seen from the data presented in Figure 8.21. As different Cu(II) concentrations were used, the limiting current density is normalized to the total Cu(II) concentration. The data obtained at different c_M and pH fall on the single line whose slope yields $D = 3.7 \times 10^{-6}$ cm^2 s^{-1}. This value is close to $D = 4.1 \times 10^{-6}$ cm^2 s^{-1} found by us from polarographic data.

To account for the distribution of system components, we used the material balance equations described in Chapter 1. Appropriate stability constants selected from the reference books [1] are listed in Table 8.4. Cumulative stability constants β_{pq} and β_m^H refer to the complete dissociation of $CuL_pH_q^{2+q-4p}$ and LH_m^{m-4} species, respectively. The values of β_{pq} depend, to some extent, on the nature of supporting anion and on the ionic strength of solutions. However, they do not differ as much as the data for β_m^H. The comparison of the data taken from Refs. [1] and [89] shows that the primary source of β_m^H variations results from the uncertainty of the β_1^H value obtained for LH^{3-} species, because stepwise protonation constants for other species (LH_2^{2-}, LH_3^-, LH_4) coincide quite well.

Cu(II) citrate complexes and protonated ligands prevailing at pH < 8 are shown in Figure 8.22. At pH < 3, the complexation degree is low and Cu^{2+} aqua complexes predominate. At pH > 4, their concentration becomes low and the main Cu(II)-containing species are $CuLH^-$ and CuL^{2-}. Higher affinity of Cu^{2+} ions to ligand than that of protons results in the formation of deprotonated CuL^{2-} complex yet at pH > 3, while the respective free ligand L^{4-} species appear only at pH > 10 (see inset).

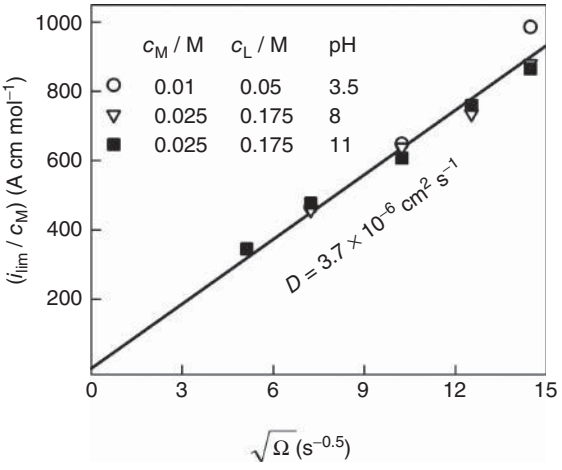

Figure 8.21 Limiting current densities normalized to the total Cu(II) concentration in Levich coordinates.

Table 8.4 Stability constants used in simulations.

Species	i	j	$\log \beta_{pq}$	Species	m	$\log \beta_m$
CuL^{2-}	1	0	13.0	LH^{3-}	1	11.8
$CuLH^{-}$	1	1	16.8	LH_2^{2-}	2	17.5
$CuLH_2$	1	2	19.5	LH_3^{-}	3	21.9
$CuLH_3^{+}$	1	3	22.1	LH_4	4	24.8
$CuL_2H_2^{4-}$	2	2	29.7			
$CuL_2H_4^{2-}$	2	4	36.6			

To determine the composition of the electrically active complex in acid media, we resorted to the method of IPSs. Concentrations of free Cu^{2+} and L^{4-} ions were kept constant ($[Cu^{2+}] = 2 \times 10^{-5}$, $[L4^{-}] = 2 \times 10^{-11}$ M) and pH varied from 4 to 4.75. The polarization resistances, R_{pol}, were determined from slopes of RDE voltammograms and the charge transfer resistance, R_{ct}, was obtained by extrapolating the R_{pol} to infinite intensity of forced convection as described in Section 5.3.2. In the case of two consecutive one-electron transfers, R_{ct} is defined by both exchange current densities, i_{01} and i_{02}, according to Eq. (5.41). By analogy with other Cu(II) systems, it might be assumed that $i_{01} \ll i_{02}$. Then

$$R_{ct} = \frac{RT}{4Fi_{01}}. \tag{8.35}$$

The values of $\log i_{01}$, when plotted versus pH, can be approximated by line (inset in Figure 8.23) whose slope of ~1.2 can be rounded off to unity. By analogy with Eq. (6.18), this means that EAC should contain one mobile proton. An inspection of the component distribution in the solutions shows (Figure 8.22)

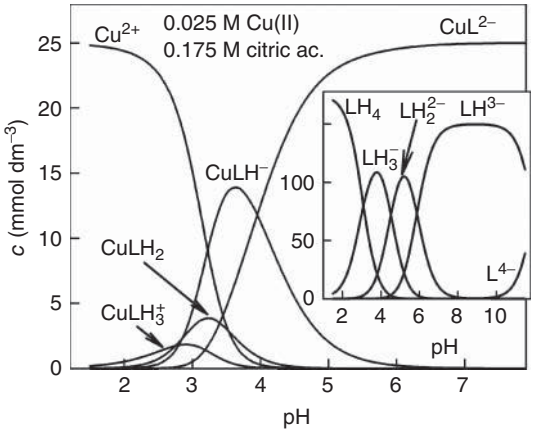

Figure 8.22 Distribution of complexes and protonated ligands (inset) in the Cu(II)–citric acid system versus pH.

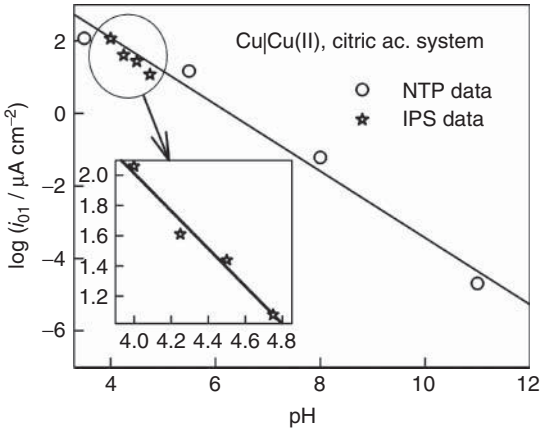

Figure 8.23 Plots of $\log i_{01}$ versus pH obtained from NTP (circles) and IPS (stars) data.

that there is one complex species that corresponds to the condition $q = 1$ and can be viewed as the electrically active complex. The species in question is $CuLH^-$.

It is of interest to verify this conclusion invoking other methods. With this aim, the RDE voltammograms were normalized to the ratio $r = [CuLH^-{}_s/CuLH^-]_b$, that is, the values of $i_{norm} = i_c/r$ were obtained. Surface concentrations were calculated, using procedures described in Chapter 3 and stability constants listed in Table 8.4. Simulations have shown that an alkalization of surface layer occurs under cathodic polarization conditions. The difference between bulk and surface pH becomes significant in weakly acidic solutions that do not contain an excess

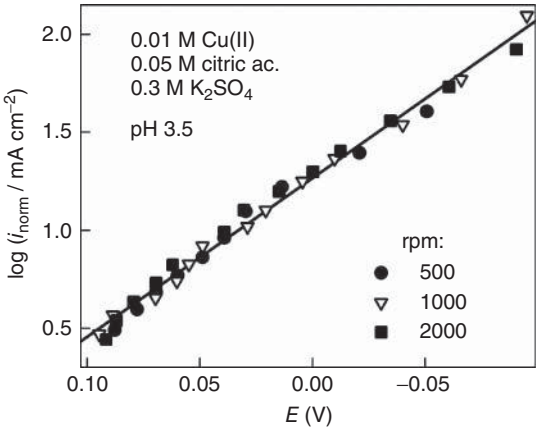

Figure 8.24 Normalized Tafel plots obtained by transformation of RDE voltammograms. $CuLH^-$ species is treated as the EAC.

of ligand. In such cases, the composition of surface layers formed at the same current density does not actually depend on the bulk pH. Its value markedly affects the position of the equilibrium potential, but the position of reversible voltammograms relative to the potential axis remains actually the same.

As seen from a typical example (Figure 8.24), the dependence of $\log i_{norm}$ on E is linear. Moreover, such parameter as, for example, the intensity of forced convection, makes no impact on this dependence. In a wide range of E, the experimental data obtained at different rotation velocities of RDE are satisfactorily approximated with a single line. Its slope yields $\alpha_{c1} = 0.47$. Similar NTPs were also obtained for alkaline 0.025 M Cu(II) solutions containing 0.175 M citrate and 0.3 M K_2SO_4 at $8 < pH < 11$. Exchange current densities were determined by extrapolating the i_{norm} values to the equilibrium potential. These data are given in Figure 8.23. It can be seen that both, IPS and NTP, methods yield consistent results. Diminution of i_{01} with pH can be easily explained by the respective decrease in EAC bulk concentration.

Hence, the mechanism involving $CuLH^-$ as EAC formally describes the reduction kinetics over a wide range of pH. However, some extra comments are desired. According to the data presented in Figure 8.22, the $CuLH^-$ species predominates in the moderate acidic medium, and its amount rapidly falls with the solution pH: $[CuLH^-]$ ranges from several μmol dm^{-3} (pH 8) up to several nmol dm^{-3} (pH 11). If it is the $CuLH^-$ species that is considered as an electrically active complex in alkaline media, its formation from the predominating complexes should occur via scheme:

$$CuL^{2-} + H^+ \underset{k_2}{\overset{k_1}{\rightleftharpoons}} CuLH^-. \tag{8.36}$$

The rate of $CuLH^-$ formation depends on the product of $[CuL^{2-}][H^+]$ that is rated low in alkaline media (at pH 11, this quantity approximates to

10^{-20} mol^2 dm^{-6}). In this connection, let us estimate the contribution of this PCR making use of the concept of reaction layer as was done by Gerischer [90]. The thickness of the reaction layer, δ_r, can be obtained from the relationship

$$D\frac{[\mathrm{CuLH}^-]}{\delta_r} = k_1[\mathrm{CuL}^{2-}][\mathrm{H}^+]\delta_r = k_2[\mathrm{CuLH}^-]\delta_r. \tag{8.37}$$

Then,

$$\delta_r = \sqrt{\frac{DK}{k_1}} = \sqrt{\frac{D}{k_2}}, \tag{8.38}$$

where

$$K = \frac{k_1}{k_2} = \frac{[\mathrm{CuLH}^-]}{[\mathrm{CuL}^{2-}][\mathrm{H}^+]}. \tag{8.39}$$

The maximum current density

$$i_{\max} = nFD\frac{[\mathrm{CuLH}^-]}{\delta_r} = nF[\mathrm{CuLH}^-]\sqrt{\frac{Dk_1}{K}}. \tag{8.40}$$

Putting the maximum value of the bimolecular reaction rate constant ($k_1 \sim 10^{10}$ dm^3 mol^{-1} s^{-1} [90]) and making use of the equilibrium constant $K = \beta_{11}/\beta_{10} = 10^{3.8}$ mol^{-1} dm^3 (see Table 8.4), we obtain with $D \approx 4 \times 10^{-6}$ cm^2 s^{-1} [86] that $i_{\max} \approx 5 \times 10^5$ [CuLH$^-$]/mA cm^{-2} when [CuLH$^-$] is given in mol dm^{-3}. Though the data presented in Figure 8.23 appear quite reasonably at a glance, in the case of alkaline media, they come into collision with the condition 8.40 that restricts the $i_{\max}$ to several mA cm^{-2} at pH 8 and to several μA cm^{-2} at pH 11. The change of the charge transfer mechanism in the alkaline solutions might be responsible for such discrepancies.

In this connection, we extended the analysis of RDE voltammograms obtained for alkaline solutions [86]. The CuL^{2-} complex was treated as the EAC and the respective NTPs were constructed. The same mechanism was also applied to acid medium. Again, linear NTPs were obtained at different pH, and the intensity of forced convection showed no impact on these dependencies (Figure 8.25). Subsequent analysis showed that, within the experimental errors, the voltammograms pertaining to electroreduction of Cu(II) citrate complexes can be quantitatively described by two different mechanisms, by properly selecting the kinetic parameters (Table 8.5). Both mechanisms suppose very low exchange current densities in alkaline media. This factor is responsible for some instability in the open-circuit potential and for emergence of a characteristic delay of current density, which extends up to −0.8 V, until a pronounced rise of voltammogram is observed (Figure 8.26). Differences between the voltammograms simulated for two different mechanisms (lines) are within the reproducibility of the experimental curves (symbols).

It seems likely that both EAC mentioned earlier could take part in the charge transfer process contributing to the total current density. However, the separation of their partial current densities is a problem yet to be solved.

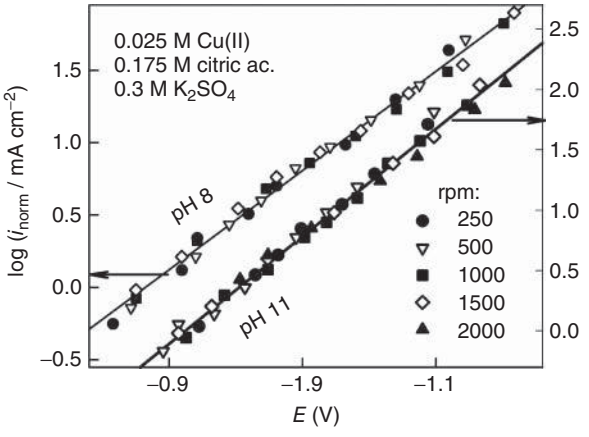

Figure 8.25 Normalized Tafel plots obtained from RDE voltammograms at different pH. CuL^{2-} species is treated as the EAC.

Table 8.5 Kinetic parameters for two mechanisms of Cu(II) reduction in the solutions containing 0.025 M Cu(II), 0.175 M citrate, and 0.3 M K_2SO_4 as a supporting electrolyte.

EAC →	$CuLH^-$		CuL^{2-}	
pH ↓	α_{c1}	i_{01} (μA cm^{-2})	α_{c1}	i_{01} (μA cm^{-2})
3.5	0.46	116	0.36	400
5.5	0.42	14.5	0.34	0.32
8.0	0.46	0.06	0.42	2.9×10^{-4}
11.0	0.49	2×10^{-5}	0.49	1.7×10^{-5}

8.3.2
Electroreduction of Sn(II) Complexes

Electrochemical deposition of tin and its alloys has found extensive application in modern electroplating. Some outstanding properties of tin such as nontoxicity, high corrosion resistance, and good solderability are characteristic of tin coatings. The most common acid sulfate or sulfonate and alkaline stannate solutions have certain shortcomings that restrict their application in some fields. For instance, acid solutions are unacceptable for plating of Mo-coated soda-lime glasses that are used as substrates in solar cells. At the same time, stannate solutions operate at elevated (60–70 °C) temperatures with rather low (65–80%) current efficiency. Consequently, slightly acid or neutral Sn(II) solutions offer more promise in modern tin plating.

A great variety of compositions were tested. One group of solutions contained only simple inorganic salts such as sulfates, fluorides, chlorides, fluoborates, pyrophosphates, and cyanides, which may be treated as weak ligands with the

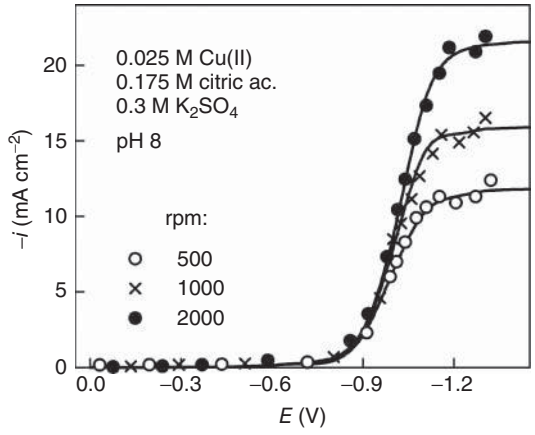

Figure 8.26 Comparison of experimental (symbols) and simulated (lines) voltammograms.

exception of the last two. Solutions containing simple Sn(II) salts are stable only in highly acid media and their electrolysis produces loosely adhering acicular tin growths rather than uniform coatings.

Thus, to improve deposit morphology, various organic additives are used. At present, much attention is given to substances that can be industrially applied without compromising the environment. Gluconate, glucoheptonate, tartrate, and citrate are among them. The use of ligands makes it possible to extend the pH region of the solutions used and, in the certain cases, to inhibit the oxidation of Sn(II) to Sn(IV). To make coatings brighter, various surfactants are usually used, such as butinediol, sintanol, and formaldehyde. It should be noted that it is possible to obtain bright tin coatings even in the absence of special brighteners in solutions containing complexes (e.g., with gluconate as a ligand [91]).

Voltammograms obtained for weakly acid Sn(II) citrate solutions show some peculiarities that are typical of ligand-deficient complex systems. Special attention must be given to the diminution of current density with solution pH that is observed at moderate cathodic polarizations ($-0.6 < E < -0.45$ V) (Figure 8.27). Similar effects are also observed at constant pH with decreasing citrate concentration.

To consider the reasons responsible for such behavior, the distribution of species at the electrode surface should be analyzed. Procedures appropriate for this purpose are described in Section 3.3. They require the stability constants of metal complexes and those of protonated ligands to be employed. According to the potentiometric data [92] that were improved in Ref. [93], at least two Sn(II) citrate complexes, namely SnL^{2-} and $SnLH^{-}$, should be taken into account at $3.5 <$ pH5.5 with $\log\beta$ equal to 15.35 and 19.5, respectively. Stability constants of protonated ligand species are given in Table 8.4. Simulations have shown that the surface concentrations of Sn(II) citrate complexes vary differently with cathodic current density (Figure 8.28). Despite the fact that the total surface concentration of Sn(II) decreases with cathodic i, the surface concentration of

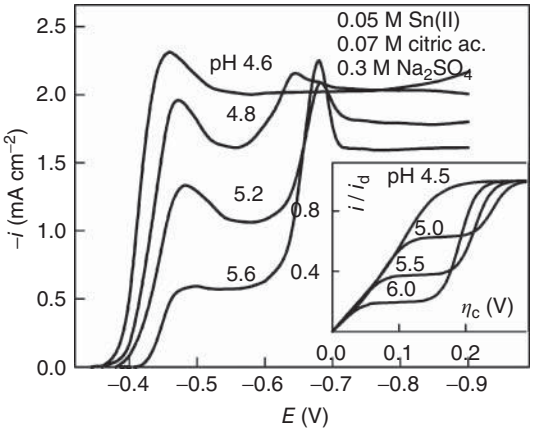

Figure 8.27 Experimental voltammograms of Sn(II) reduction obtained under natural convection conditions at various pH. Simulated reversible voltammograms are given in the inset.

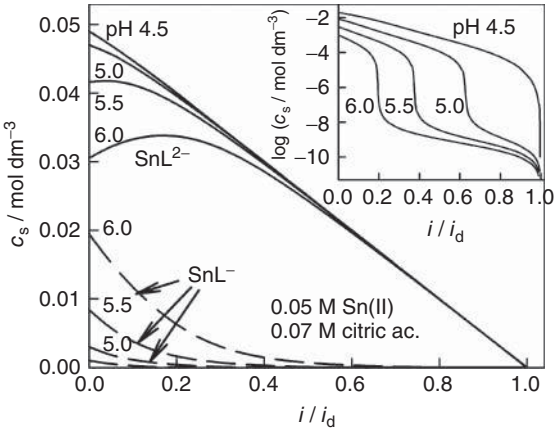

Figure 8.28 Distribution of Sn(II) citrate complexes versus normalized cathodic current density. The data for the $SnLH^-$ species are given in the inset in semilogarithmic coordinates.

SnL^{2-} increases up to $i/i_d \approx 0.2$. Such an effect results from the respective shifts in chemical equilibria and is impossible for simple ligand-free systems. A sharp change in $[SnLH^-]_s$ is observed at the certain i/i_d. It becomes most obvious when presenting the data in semilogarithmic coordinates (inset in Figure 8.28). The surface concentration of "free" Sn^{2+} ions varies in the same manner. The data obtained makes it possible to construct reversible voltammograms. As in the case of real system, simulated curves contain prewaves whose height varies with pH in the similar manner.

It should be emphasized that reversible voltammograms are independent of the choice of reaction mechanism and any Sn(II)-containing particle may be treated

as EAC. In accordance with Nernst equation, the following equations are valid for reversible reduction of Sn^2, SnL^{2-}, or $SnLH^-$ species, respectively:

$$\eta_c = \frac{RT}{nF} \ln \frac{[Sn^{2+}]_s}{[Sn^{2+}]_b}, \tag{8.41}$$

$$\eta_c = \frac{RT}{nF} \ln \frac{[SnL^{2-}]_s[L^{4-}]_b}{[SnL^{2-}]_b[L^{4-}]_s}, \tag{8.42}$$

$$\eta_c = \frac{RT}{nF} \ln \frac{[SnLH^-]_s[L^{4-}]_b[H^+]_b}{[SnLH^-]_b[L^{4-}]_s[H^+]_s} = \frac{RT}{nF} \ln \frac{[SnLH^-]_s[LH^{3-}]_b}{[SnLH^-]_b[LH^{3-}]_s}. \tag{8.43}$$

The identity of logarithmic terms follows from the expressions of the respective stability constants.

In the case of Sn^{2+} or $SnLH^-$ reduction, the occurrence of prewaves is evident, because the surface concentrations of Sn^{2+} or $SnLH^-$ species vary with a sharp fall as shown in the inset of Figure 8.28. Variations of $[SnL^{2-}]_s$ with i did not display such property (Figure 8.28); however, this feature is characteristic of surface concentration of L^{4-} (Figure 8.29) that is present in Eq. (8.42).

Somewhat different situation arises, when the reduction of Sn(II) complexes is irreversible. To construct cathodic NTP, the anodic component of the total current density should be ignored as negligible. In so doing, the products of cathodic process, whose concentrations are multiplies at the anodic exponent, are excluded from consideration. Thus, prewave-containing cathodic voltammograms can be transformed to linear NTP, if special requirements on the possible EAC are imposed. The main of them consists in the occurrence of a sharp fall in EAC surface concentration within the narrow range of current density. $SnLH^-$ complexes satisfy this condition and linear NTPs are obtained for this

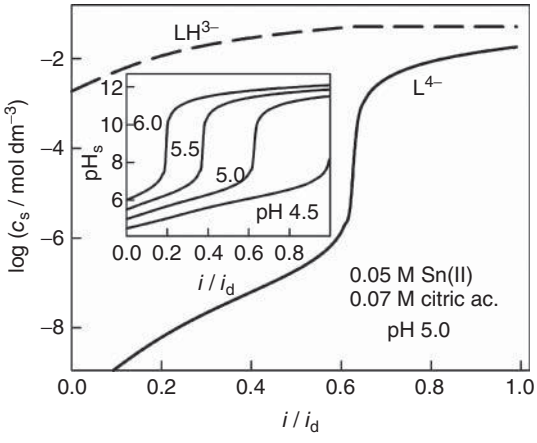

Figure 8.29 Variations of LH^{3-} and L^{4-} surface concentrations with normalized cathodic current density. The inset contains similar data for surface pH.

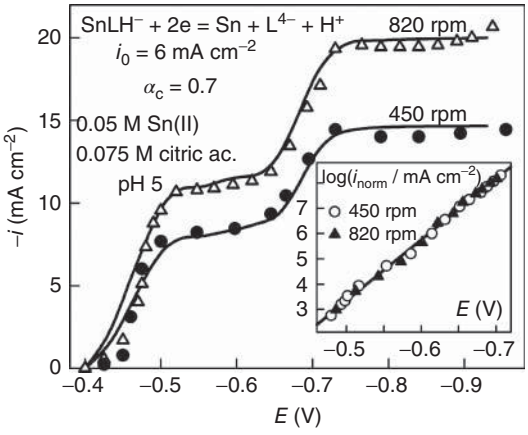

Figure 8.30 Comparison between experimental RDE voltammograms (symbols) and theoretical curves simulated with the indicated kinetic parameters. Tafel plots normalized to the ratio $r = [SnLH^-]_s/[SnLH^-]_b$ are shown in the inset.

mechanism (Figure 8.30). Kinetic parameters obtained from NTP were used in simulating voltammograms that are in a good agreement with the experimental data (Figure 8.30).

We have already mentioned that the surface concentration of SnL^{2-} increases with cathodic i over the certain range of current densities (Figure 8.28). This means that the possibility exists for an abnormally high slope of experimental voltammograms obtained for complex systems. In the certain cases, curves of this kind occur in the system under consideration [93].

It follows from model simulations that the surface pH increases significantly with cathodic current density. In the region of limiting current, pH_s ranges up to ~12 (Figure 8.29), whereas only a weakly acid media is created in the bulk of solution. This effect results from corresponding shifts in equilibria and occurs even when hydrogen evolution does not occur. Then, the $[Sn^{2+}][OH^-]^2$ product simulated for the electrode surface may exceed that determined by the solubility constant of $Sn(OH)_2$. This give grounds to draw the conclusion about the possibility of forming Sn hydroxide at certain current densities and bulk pH. For instance, at pH 5, formation of $Sn(OH)_2$ becomes possible at the electrode surface, when $i/i_d > 0.6$. Hydroxide may form colloidal species and act as a brightener. Nevertheless, oversaturation of the surface layer should not be too high.

The electroreduction of Sn(II) gluconate complexes is characterized by some peculiarities. Due to various chemical interactions between the components of Sn(II) and gluconic acid solutions, their composition can become rather complex. As was mentioned earlier, it is a good approach to symbolize gluconic acid as LH, when only an acid medium is considered. Then, L^- can be treated as the active form of ligand that forms complexes with different metal ions, whereas LH and lactones do not exhibit this property. In order to better understand the nature of electrochemical processes, a clear knowledge on the distribution of Sn(II) and

other species is desirable first. To obtain such data, reliable stability constants of complexes and protonated ligands are required. Unfortunately, the data concerning Sn(II) complexes are few in number; we were able to find only two articles containing quantitative characteristics of Sn(II) gluconate [94] and sulfate [95] complexes. The latter compounds can be also formed, because 0.5 M Na_2SO_4 was used as a supporting electrolyte. Finally, the Sn(II) hydrolysis processes should be also considered.

These interactions were taken into account in our article [96]. As the adopted equilibrium constants were determined by different authors using different methods, it is not improbable that used β values are somewhat self-inconsistent. Therefore, the results of simulations [96] could be treated as tentative, but they showed that the system under discussion is rather complicated. Three complex species may be present in comparable amounts. Sulfate complexes prevail in more acidic media and, as pH increases, they are replaced by SnL_2. Finally, products of Sn(II) hydrolysis, $Sn(OH)^+$, and $Sn(OH)_2$, are thermodynamically stable at pH > 4. However, the formation of these species seems to be kinetically impeded, because we observed no precipitation of hydroxide.

The comparison of simulated and experimental potentials showed [96] that they correlate satisfactorily. The best fit was observed at low pH where the open-circuit potential of tin electrode is very stable and is reproducible with a high accuracy (±1 mV at pH 2). The situation deteriorates in a weakly acidic media where the 30–50 mV shift of E_{oc} can last 30–40 min until a steady state is achieved. The phenomena observed are indicative of slow equilibration of the system at insufficiently low pH.

The position of E_{eq} values calculated for $H_2|H^+$ electrode showed that the Sn(II) reduction can be preceded by hydrogen evolution, which is thermodynamically probable over a wide range of pH. To estimate the contribution of this side process, EQCM experiments were performed. These data were transformed to voltammograms as described in Section 8.2.1. Curves recorded directly (Figure 8.31) contain two current peaks located at −0.35 and −0.85 V. Transformed EQCM data reproduce only the first maximum and the further potential sweep results only in the progressively diminishing current. This gives grounds to attribute the second current peak to hydrogen evolution. Such peculiarities of voltammograms are typical of the systems involving weak acids as proton donors (see Section 10.2). It should be concluded that Sn(II) reduction in weakly acid media predominates up to −0.6 V and the hydrogen evolution is negligible in this region. Such an effect seems to be conditioned by a high hydrogen overvoltage on the tin electrode that is also responsible or a high corrosion resistance of tin in strong acid solutions. Previous EQCM experiments have shown [97] that the corrosion current density in 1 M H_2SO_4 solutions is about 10 μA cm^{-2}. Respectively, the exchange current density for H^+ reduction is very low (~10^{-11} A cm^{-2}) [98].

Voltammograms obtained by the RDE technique are of common shape (Figure 8.32). They contain a well-defined plateau of limiting current that is observed over a wide region of cathodic potentials ($-1.2 < E < -0.6$ V). Foremost, the limiting current density (i_{lim}) depends on solution composition, and

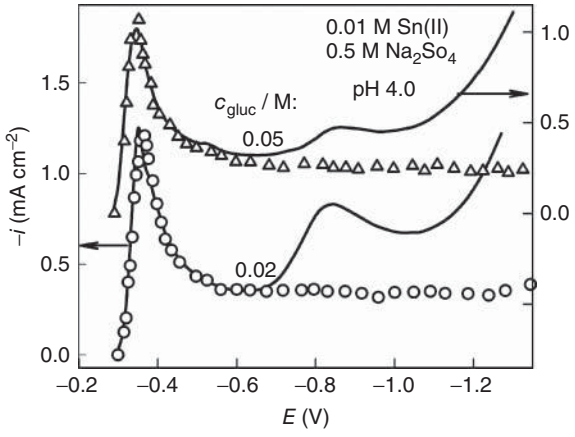

Figure 8.31 Cathodic voltammograms obtained for 0.01 M Sn(II) solutions containing 0.02 M (lower curve, ordinate to the left) and 0.05 M (upper curve, ordinate to the right) of gluconate at pH 4.0. Direct measurements (solid lines) are compared with transformed EQCM data (symbols).

pH should be treated as the main factor that is responsible for electrochemical behavior of the system under discussion. The rate of Sn(II) reduction falls with pH to a great extent and, at pH 5, i_{lim} makes only 1/3 part of the quantity that is observed at pH 2. Nevertheless, the effect of intensity of forced convection still persists and the dependencies of i_{lim} on $\sqrt{\Omega}$ (Ω is the angular rotation velocity of RDE) can be approximated by lines at different pH (Figure 8.33). Various reasons might be responsible for such effects. It should be mentioned primarily that similar phenomena are possible in inert systems with slow chemical interactions. Then, i_{lim} should depend on the concentration of an EAC that directly takes part in the charge transfer step. It follows from the distribution data [96] that Sn^{2+}, $SnSO_4$, and $Sn(SO_4)_2^{2-}$ could be the species whose amount decreases with solution pH. However, none of them is consistent with another observation, according to which i_{lim} increases with gluconate concentration at constant pH (see data for pH 4 in Figures 8.32 and 8.33). Hence, the model of inert Sn(II) system lacks the experimental validation.

In the case of simple Sn^{2+} solutions, the limiting current is of diffusion nature and obeys Levich equation with $D = 6.2 \times 10^{-6}\,cm^2\,s^{-1}$. An application of this relationship to the experimental data, obtained for 0.01 M Sn(II) and 0.05 M gluconate solutions (Figure 8.33), yields D_{ef} equal to 4.6×10^{-6}, 2.3×10^{-6}, and $0.63 \times 10^{-6}\,cm^2\,s^{-1}$ at pH 2.0, 4.0, and 5.0 respectively. Noticeably different values of individual D of aqua and gluconate complexes may be responsible for D_{ef} variations with solution composition. As the content of large SnL_2 complexes increases with pH, this should result in the decrease of D_{ef} that is in agreement with experimental results. However, the effect of ligand is opposite and does not support this point of view. D_{ef} obtained at pH 4 for 0.01 M Sn(II) and 0.02 M gluconate solution is lower ($1.5 \times 10^{-6}\,cm^2\,s^{-1}$) than that established for a similar solution containing a higher

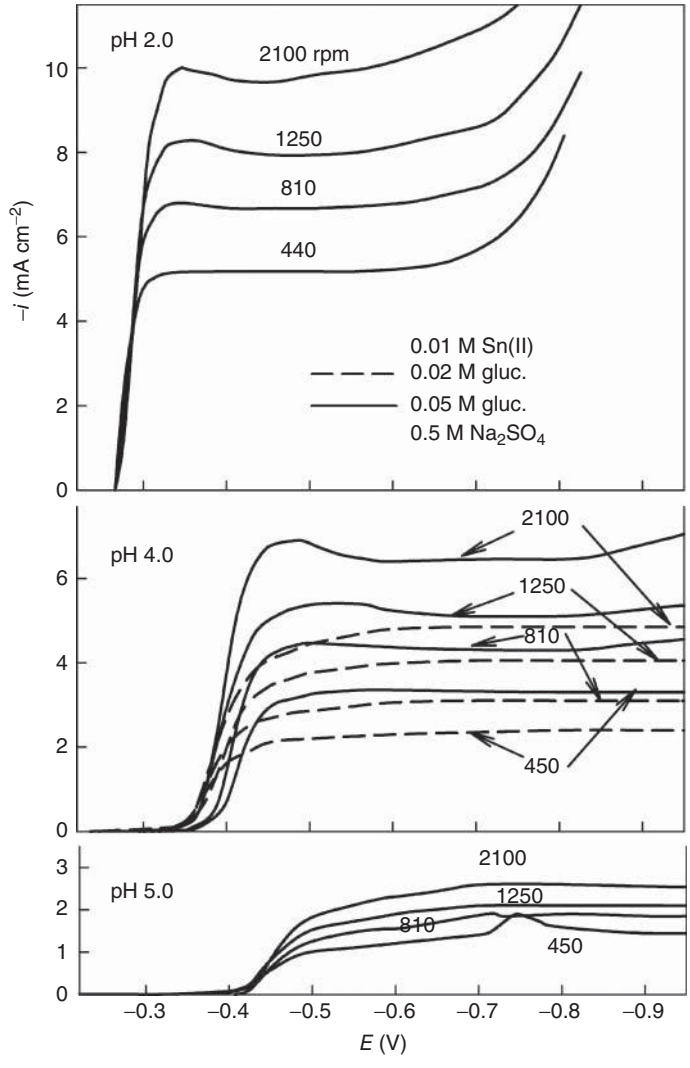

Figure 8.32 RDE voltammograms obtained for 0.01 M Sn(II) solutions containing 0.02 M (dotted lines) or 0.05 M (solid lines) of gluconate at indicated pH. The RDE rotating velocity (revolutions per minute) is indicated at the curves.

(0.05 M) concentration of ligand. Thus, it should be concluded that the redistribution of complex species cannot be of decisive importance, though it can play a certain role. Therefore, other physical phenomena should be found and invoked. However, before we proceed further, we shall consider some voltammetric results obtained under non-steady-state conditions (Figure 8.34).

The aforementioned tendencies are still retained and one of them consists in the pronounced decay of current density with solution pH (cf. Figures 8.32 and 8.34).

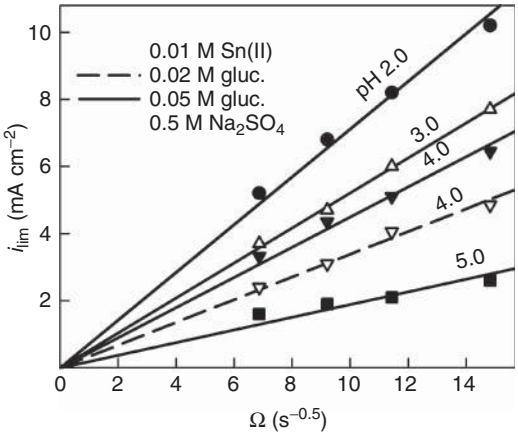

Figure 8.33 Levich plots obtained for 0.01 M Sn(II) solutions containing 0.02 M (dotted line) or 0.05 M (solid lines) of gluconate at indicated pH.

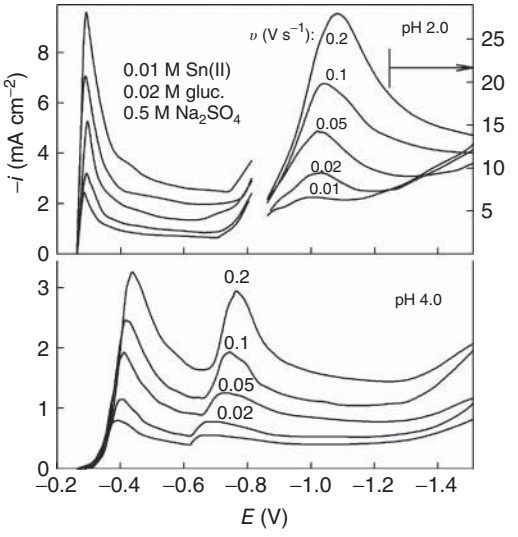

Figure 8.34 LPS voltammograms obtained for 0.01 M Sn(II) solutions containing 0.02 M of gluconate. The region of the second current peak (pH 2.0, upper part) is shown in a reduced scale (ordinate to the right). Potential sweep rates *v* are indicated at the curves.

Two current peaks (i_p) are observed on LPS voltammograms. The one on the left is located at $-0.45 < E < -0.3$ V, and as follows from EQCM data, it is conditioned by Sn(II) reduction. The second one is observed at more negative potentials and results from hydrogen evolution.

We start our discussion assuming again that the Sn(II)–gluconate system is labile and the Sn(II) reduction is controlled by charge transfer and diffusive mass

transport. Then, Eq. (5.8), which requires no assumptions on the EAC composition, is useful for analysis. At pH 2.0, the values of $\Delta c = c_{\mathrm{Sn(II)},b} - c_{\mathrm{Sn(II)},s}$ obtained by this equation for different potential sweep rates, are close; this being indicative of a rather reversible character of charge transfer. According to Eq. (5.8), at $c_{\mathrm{Sn(II)},s} \to 0$, the changes in surface concentration should attain the limit that is equal to the bulk concentration of Sn(II). At pH 2.0, the value of $\Delta c = 10\,\mathrm{mM}$ is achieved with $D_{\mathrm{ef}} = 5.9 \times 10^{-6}\,\mathrm{cm^2\,s^{-1}}$, but at pH 4.0, D_{ef} depends on the potential sweep rate and amounts to an average of $2 \times 10^{-6}\,\mathrm{cm^2\,s^{-1}}$.

If the model of a labile complex system is valid, the most orthodox relationships, relating the current density, and the concentration of reactant (c), could be applicable with the proviso that c is treated as the total concentration of metal-containing species ($c_{\mathrm{Sn(II)}}$ in this case). Then, the coordinates of voltammetric maxima (E_{p}, i_{p}) should obey the relations (5.29) – (5.31). Having no evidence that the charge transfer proceeds via two consecutive one-electron steps, thereafter we assume that $n\alpha = n = 2$. Analysis of experimental data shows that i_p dependencies on $\sqrt{\nu}$ can be approximated by lines passing the origin (Figure 8.35). Their slopes are equal to 22, 18, and 7.9 mA $\mathrm{cm^{-2}\,V^{-0.5}\,s^{0.5}}$ at pH 2.0, 3.0, and 4.0, respectively.

Some specific information regarding the reversibility of Sn(II) reduction can be obtained from the data shown in Figure 8.36. In the case of sufficiently acid solutions (pH 2.0), E_p is actually independent of ν. The effect of potential sweep rate develops with solution pH and, at pH 4.0, E_p varies linearly with $\log \nu$ that is in agreement with Eq. (5.31). It follows from the slope of this line (−34.2 mV per decade) and Eq. (5.31) that $\alpha = 0.42$. Then, Eq. (5.30) yields $D_{\mathrm{ef}} = 2.0 \times 10^{-6}\,\mathrm{cm^2\,s^{-1}}$, whereas $D_{\mathrm{ef}} = 4.4 \times 10^{-6}\,\mathrm{cm^2\,s^{-1}}$ is obtained with Eq. (5.30) at pH 2.0. Thus, the diminution of D_{ef} with pH follows from the analysis of current peaks as well.

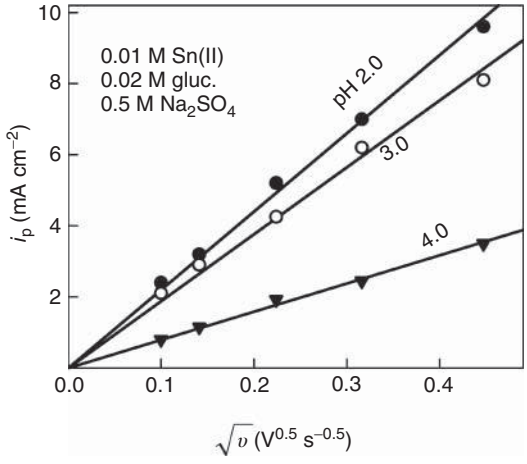

Figure 8.35 Variations of the peak current density with the square root of potential sweep rate. The data obtained for 0.01 M Sn(II) and 0.02 M gluconate solution at different pH as indicated.

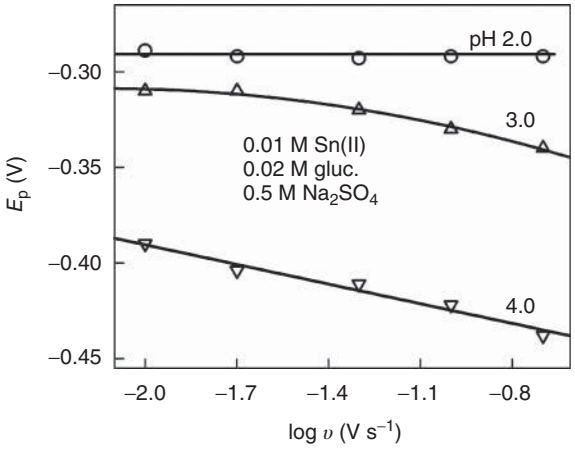

Figure 8.36 Dependencies of the peak potential on the potential sweep rate in the semilogarithmic coordinates obtained for 0.01 M Sn(II) and 0.02 M gluconate solution at different pH as indicated.

The results obtained by three different methods are summarized in Table 8.6. While the general tendency of D_{ef} variations remains the same in all cases, nevertheless, the certain quantitative differences occur. It should be emphasized that different areas of potentials were taken for analysis: entire voltammograms (convolution procedures), i_{lim} at sufficiently negative potentials (RDE data) and single points on LPS voltammograms (i_p analysis). As the main properties of the system are potential-dependent, it is quite possible that this may have an impact on the results obtained. Specifically, surface pH (pH_s) may be quite different at low overvoltage (here, $pH_s \approx pH_b$) and in the region of limiting current where the certain alkalization is expected due to the release of ligands from the discharged Sn(II) complexes. An estimation of pH_s shows that pH_s changes are not pronounced at $pH < 4$ (when $pH_b = 4$, pH_s increases up to 4.2–4.3), but they can become very significant when the Sn(II) hydroxo-complexes are formed in the solution (Figure 8.29). It might be supposed that the inhibition effects gain an advantage over other factors in this case. It is reasonable to assume that electroreduction

Table 8.6 Effective diffusion coefficients evaluated by different methods.

pH	$10^6 D_{ef}$ (cm^2 s^{-1})		
	RDE	Convolution	LPS
2.0	4.6	5.9	4.4
3.0	3.8	3.9	~3.2
4.0	2.3	1.8–2.2	2.0
5.0	0.63		

of Sn(II) in gluconate solutions is accompanied by adsorption phenomena whose inhibitive character enhances with solution pH.

More definite conclusions may be drawn on the basis of exhaustive analysis of impedance spectra that carry information not only on the kinetics of faradaic processes but also on the characteristics of a double electric layer. As for gluconate systems, such investigations are scarce. A great variety of Nyquist plots (relationships between real, $Z^{/}$, and imaginary, $Z^{//}$, components of impedance) are demonstrated in Ref. [99] that deal with the deposition of tin from neutral gluconate baths, but no quantitative analysis is presented. As we established earlier [100, 101], Nyquist plots obtained at open-circuit potentials for surfactant-free solutions are nothing else than lines that were observed over an entire range of applied frequencies. This means that Sn(II) reduction is mainly controlled by diffusive mass transport.

Before the detailed analysis of impedance is presented, brief mention should be made of the equilibration processes occurring at the interface. We found that impedance spectra recorded at the open-circuit potential (E_{oc}) vary with exposure time τ and these variations crucially depend on solution pH. Fast equilibration of the system is observed in sufficiently acidic media and, at $\tau > 5$ min, impedance data show good reproducibility. At higher pH, the transition process takes more time and is accompanied by a certain shift in the open-circuit potential to more negative values. For the most part, a steady state is achieved within ~15 (pH 4) or 15–20 min (pH 4.5 and 5). On this basis, steady-state data were selected to be presented below.

As follows from voltammetric data, the acidity of solutions is the main factor governing the kinetics of Sn(II) reduction over a wide range of potentials. A considerable (approximately fourfold) decrease in limiting current density was observed when solution pH increased from 2 to 5 (Figure 8.32). At E_{oc}, respective variations in impedance spectra are still larger and amount to 2 orders of magnitude. To show better such a wide scale of impedance variations, it is expedient to present Nyquist plots in logarithmic coordinates (Figure 8.37), although this is inconsistent with common practice. When plotted in linear scale, two arcs can be detected on Nyquist plots obtained for moderately acidic media. However, when the acidity of Sn(II) solutions is sufficiently high (pH $\leq$ 2), Nyquist plots become linear nearly over the entire range of applied frequencies. Their slope is close to 1, which is typical of diffusion controlled processes. A high exchange current density (i_0) of Sn(II) reduction is responsible for such behavior. According to different literature data [100–104], the i_0 is in the range from 50 to 250 mA cm^{-2}. Unfortunately, it is impossible to compare the data at higher pH, because pH 2 is the limit of stable gluconate-free Sn(II) solutions containing an excess of sulfate. At pH > 2, Sn(II) hydrolysis originates. The aforementioned peculiarities of Nyquist plots, obtained at pH 2 for gluconate-containing solutions, complicate an inclusive analysis of impedance spectra. Only one reliable kinetic characteristic was available in this case. It was Warburg parameter Y_0 (see below Eq. (8.44)) that was found to be equal to 0.34 Ω^{-1} cm^{-2} s$^{0.5}$. Further, the effective diffusion coefficient, D_{ef}, was determined using the well-known relationships [2]. The established

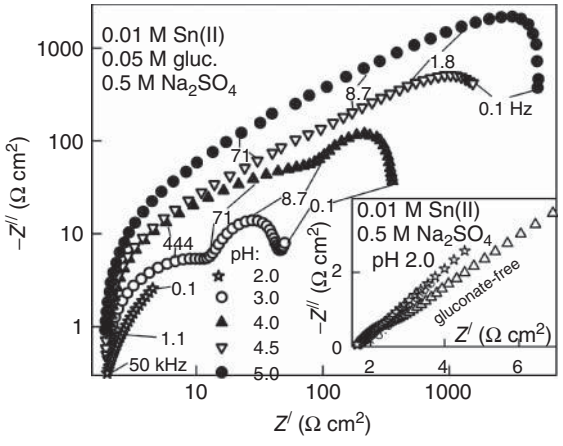

Figure 8.37 Nyquist plots obtained at open-circuit potentials (see Table 8.6) for the Sn electrode exposure for 20 min under open-circuit conditions to 0.01 M Sn(II) and 0.05 M gluconate solutions at different pH. Some characteristic frequencies are given at certain points. Impedance data obtained for the gluconate-free and gluconate-containing solutions at pH 2 are shown in the inset.

value of $4.8 \times 10^{-6}\,\mathrm{cm^2\,s^{-1}}$ is in line with D_{ef} obtained from voltammetric data. In the case of gluconate-free solutions (inset in Figure 8.37), Z values are somewhat higher and a rudiment of arc is visible on Nyquist plots at high frequencies. Accordingly, lower $i_0 \approx 10\,\mathrm{mA\,cm^{-2}}$ follows from the analysis of this Z spectrum. As will be apparent next, i_0 values are significantly lower in less acidic gluconate-containing solutions.

To perform a quantitative analysis of impedance data, an appropriate EC should be selected. For this purpose, a retrieval of literature data was carried out preferring the ECs that yield plots containing two arcs. Such a shape is typical of electrochemical processes that involve adsorption of reacting species. Some EC described in different references are shown in Figure 8.38. Ibidem, their description codes are also presented.

One of the simplest cases, which were analyzed by Koper [105], considers an electrocatalytical mechanism for which a single species first adsorbs onto the electrode and then it is either oxidized or reduced. Faradaic subcircuits following from this analysis have numbers 1 and 2 in Figure 8.38. They contain the charge transfer resistance (R_{ct}) and elements that characterize the adsorption process. When adsorption and desorption rates are independent of potential, the faradaic subcircuit takes the form of $R_{ct}(R_aC_a)$. Another structure, namely ($R_{ct}[R_aL]$), follows from the analysis when adsorption exhibits a stronger potential dependence than electron transfer [105]. It should be noted that similar subcircuits were also proposed for processes involving one or more adsorbed intermediates [106–111]. It is remarkable that similar impedance characteristics are peculiar to electrochemical processes that involve ion transport through compact monolayers or very thin films [112, 113]. The EC that follows from the relationships given in Ref. [112] is

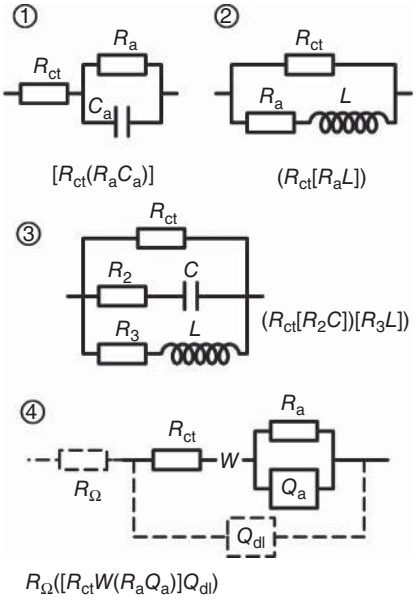

Figure 8.38 Faradaic equivalent circuits (full lines) and their description codes. The first three EC are taken from the literature (see text). The 4th EC is used in this book; the non-faradaic subcircuit is depicted with dashed lines.

shown in Figure 8.38 as N3. The element R_{ct} is a charge transfer resistance of metal reduction; subcircuits $[R_2C]$ and $[R_3L]$ describe, respectively, anion and cation transport through this film. The latter circuit can be treated as the most general one, because it transforms into the first EC, when anions are not transferred (the subcircuit $[R_2C]$ is absent). Similarly, the second EC follows from N3 when the subcircuit $[R_3L]$ can be ignored. The latter conclusion is based on the fact that two subcircuits, $R_{ct}(R_aC_a)$ and $(R_1[R_2C])$, can display identical impedance spectra, when a proper choice of their parameters is performed. It is necessary to note that the EC N3 represents only the main steps of faradaic process. Specifically, no account of the diffusive mass transport is taken in it. Besides, this subcircuit should be supplemented with such non-faradaic elements as the double-layer capacitance (C_{dl}) and the ohmic resistance of the solution (R_Ω). As the ultimate circuit gains too many adjustable parameters, its fit to the experimental data encounters a number of problems. Therefore, certain simplifications of EC are inevitable regardless of some loss in fitting accuracy.

Considering the surface roughness and inhomogeneities of Sn electrodes, capacitances C_a and C_{dl} were replaced by the respective CPEs Q_a and Q_{dl}. To account for diffusive mass transport, we tested two elements: the Warburg impedance W that represents a semi-infinite diffusion and the element O that follows from the description of the so-called transmissive boundary [106]. It is supposed in the latter case that diffusion occurs in the δ-thick layer. Their impedances are, respectively [106]:

$$Z_W = \frac{1}{Y_0\sqrt{j\omega}}, \tag{8.44}$$

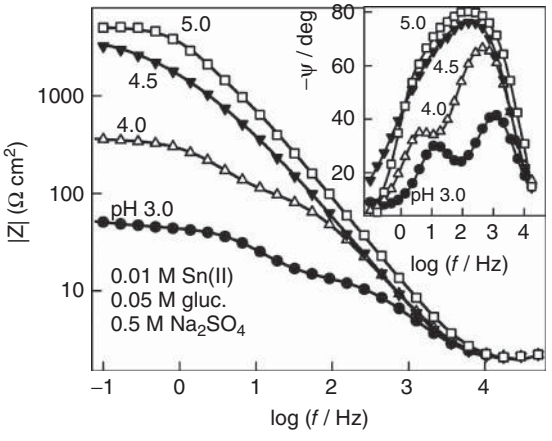

Figure 8.39 Bode plots of impedance (|Z|) and phase shift (ψ), obtained under open-circuit conditions at different pH as indicated. Experimental data (symbols) are compared with the data (solid lines) simulated for EC whose parameters are listed in Table 8.7.

$$Z_{\mathrm{O}} = \frac{\tanh(B\sqrt{j\omega})}{Y_0\sqrt{j\omega}}, \tag{8.45}$$

where $B = \delta/\sqrt{D}$. However, both elements gave actually the same Y_0 at vague $B \gtrsim 2\,\mathrm{s}^{-0.5}$.

Thus, over the entire range of the frequencies applied, the element *O* showed Warburg-like behavior and offered no definite indication of the thickness of diffusion layer. The modified and supplemented with non-faradaic elements ultimate EC is shown in Figure 8.38. This EC was found to fit quite well (with 2% error) the experimental data obtained at pH 3, 4, and 5. At pH 4.5, the error was somewhat higher and averaged between 3 and 4%. The fitting results are shown in Figure 8.39 and the EC parameters are listed in Table 8.7. The double layer capacitance was calculated by the equation [114]:

$$C_{\mathrm{dl}} = Y_0^{1/n}\left[\frac{1}{R_\Omega} + \frac{1}{R_{\mathrm{ct}}}\right]^{(n-1)/n}, \tag{8.46}$$

and the exchange current density was obtained by the well-known relationship.

$$i_0 = \frac{RT}{nFR_{\mathrm{ct}}}, \tag{8.47}$$

A notable decrease in i_0 with pH is observed. At pH 5.0, they are 4 orders of magnitude lower than those observed in surfactant-free solutions. At the same time, C_{dl} also goes down with solution pH. Clear correlation between these faradaic and non-faradaic parameters (Figure 8.40) deserves more exhaustive consideration. As can be seen from Figure 8.40, the dependence of log i_0 versus C_{dl} is near-linear. According to the well-known parallel-capacitor model suggested by Frumkin, C_{dl} decreases linearly with the surface coverage θ. On the other hand, i_0 can be considered as a parameter proportional to the heterogeneous rate constant (k). Then,

Table 8.7 Parameters of the equivalent circle $R_\Omega([R_{ct}W(R_aQ_a)]Q_{dl})$ and related parameters determined for nonpolarized Sn electrode in 0.01 M Sn(II) solution containing 0.05 M gluconate and 0.5 M Na_2SO_4 at different pH. $R_\Omega = 1.87 \pm 0.04\,\Omega\,cm^2$.

		R_{ct}	W	R_a	Q_a		Q_{dl}		C_{dl}	i_0
pH	E_{oc}		Y_0		$10^4\,Y_0$	n	$10^5\,Y_0$	n		
	V	$\Omega\,cm^2$	$\Omega^{-1}\,cm^{-2}\,s^{0.5}$	$\Omega\,cm^2$	$\Omega^{-1}\,cm^{-2}\,s^n$		$\Omega^{-1}\,cm^{-2}\,s^n$		$\mu F\,cm^{-2}$	$\mu A\,cm^{-2}$
3.0	−0.275	12.9	0.114	27.5	12.1	0.899	12.3	0.843	25.3	970
Relative error, %		2	5	2	4	1.5	6	1		
4.0	−0.320	106	0.054	237	4.61	0.880	5.68	0.898	20.0	118
Relative error, %		2	30	3	4	2	3	0.5		
4.5	−0.326	380	0.0024	590	1.90	1.0	7.4	0.847	14.9	33
Relative error, %		6	20	7	9	4	6	0.8		
5.0	−0.31	2480	2590	0.229	1.0	3.16	0.929	11.8	4.7	
Relative error, %		10	10	16	7	3	0.5			

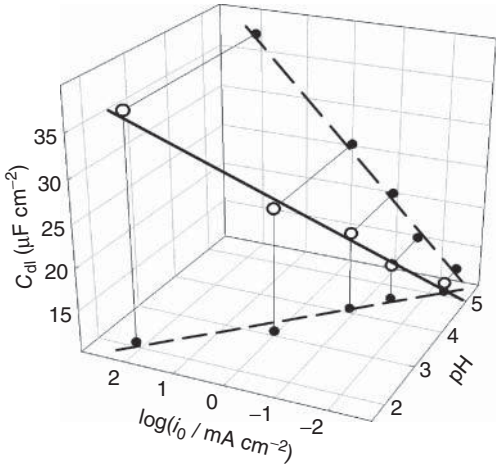

Figure 8.40 Correlation between the pH, the exchange current density, and the capacitance of charged interface. Open-circuit conditions.

the result shown in Figure 8.40 means that k should be an exponential function of θ. Such an approach is rather common in the theory dealing with the role of organic surfactants in electrode kinetics [115].

As already noted, the Warburg conductivity $Y_0 = 0.34\,\Omega^{-1}\,cm^{-2}\,s^{0.5}$, established at pH 2, is consistent with the theoretical model of semi-infinite diffusion. However, it can be seen from Table 8.7 that Y_0 falls with pH and becomes

undetectable at pH 5. It seems likely that this parameter represents, in some way, a more complex mass transport occurring at pH > 2. It involves a semi-infinite diffusion of chemically interacting complex species with subsequent penetration of some of them into a more compact surface layer. An account of D_{ef} changes with pH (voltammetric data) yields Y_0 values decreasing with pH, but the real effect is stronger (Table 8.7). This suggests that the concentration of species that penetrate into the surface layer should also fall with pH. The distribution data show that Sn^{2+} ions meet the latter requirement best. The interpretation of other EC elements (R_a, Q_a) needs more detailed information on the structure of adsorption layer. According to [116], the zero-charge potential of tin in 0.01 M Na_2SO_4 is −0.43 V. Supposing that its position only slightly depends on pH, it can be deduced that the surface charge density is not high in the region of $-0.6 < E < -0.25$ V, where Sn(II) reduction occurs as a main faradaic process. If so, conditions created at sufficiently low cathodic polarizations are quite favorable for gluconate adsorption. Besides, other inorganic ions might also be the components of adsorption layer. As the inhibition increases with solution pH, OH^- should play an important role. In this connection, the probability of surface oxide formation should be also taken into consideration. According to [117], the standard potential of the redox couple: $SnO(s) + 2H^+ + 2e^- \rightleftarrows Sn + H_2O$ is equal to −0.077 V. It follows from the analysis of E_{oc} (Table 8.7) that SnO could be thermodynamically stable only at pH > 4.5.

Some inferred data, regarding the role of Sn^{2+} ions in the absorption processes, can be taken from the comparison of the impedance spectra obtained in the presence and in the absence of Sn(II). Impedance characteristics in Sn(II)-free solutions (Figure 8.41) are far from those typical of ideally polarizable electrodes and large frequency dispersion is observed. Similar behavior was also observed in tin systems involving specific adsorption of polyethers and other surfactants [100, 101, 103, 118, 119]. It was concluded that the adsorption is controlled by the rate of diffusion and electrosorption [103, 118]. It seems possible to assume a similar approach for gluconate systems and to make use of the concept that was proposed by Frumkin and Melik-Gaikasian [120, 121] and further developed in subsequent works, some of which are generalized in [122–124]. The EC ($C_{dl}[R_a W_a C_a]$) that follows from these elaborations was used as a basis for quantitative interpretation of impedance data. Without going into details, we would like to note that relatively high C_{dl} values, namely ~36 and ~27 μF cm^{-2}, were obtained at pH 3.0 and 5.0, respectively. Besides, it can be seen from Figure 8.41 that the effect of pH in Sn(II)-free solutions is quite moderate; moreover, Z decreases with pH over the wide range of the frequencies applied. The effects observed suggest that Sn^{2+} ions are directly implicated in the inhibition processes, which result in a significant decrease in both i_0 and C_{dl} in less acidic media.

Impedance characteristics vary with the potential applied and depend to some extent on gluconate concentration as well as on the structure of tin coatings. We found [125] that some main types of Sn surface morphology might be distinguished.

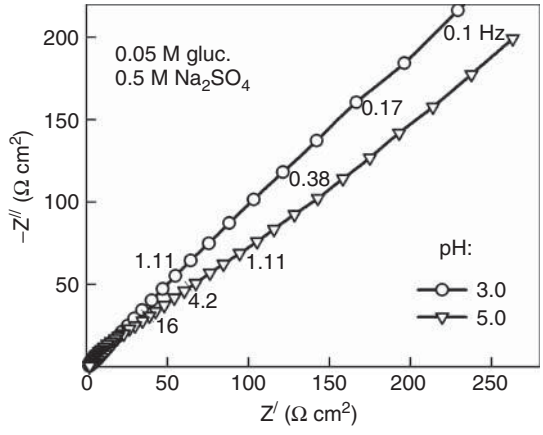

Figure 8.41 Nyquist plots obtained for Sn(II)-free solutions at E_{oc} equal to −0.354 V (pH 3) and −0.392 V (pH 5). Some characteristic frequencies are given at certain points.

Smooth deposits (Figure 8.42, type A) were prepared for further investigations in the solution containing 0.01 M Sn(II), 0.05 M gluconate, and 0.5 M Na_2SO_4 at pH 4. Next, the prepared electrode was supercoated at −0.4 or −0.7 V and the impedance spectra were recorded at the respective potentials. Spongy deposits are formed at low cathodic polarizations and/or at comparatively low gluconate concentrations, when separate grains grow under spherical diffusion control. The nuclei dimensions and their surface density depend on duration and deposition of overpotential. When c_{gluc} is increased from 0.02 to 0.1 M, the growth of spongy deposits is suppressed and they are replaced by coral-like deposits (type B). The latter could be treated as the spongy ones with significantly increased diameters of whisker formatives. Suppression of spongy deposition or an increase in whisker diameter becomes even more evident at more negative potentials. Ultimately, compact boulder-like deposits (type C) are formed in gluconate-rich solutions or at sufficiently negative potentials. Grain dimensions vary from 3 to 5 μm and depend on both the solution composition and electrolysis parameters.

Variations in surface morphology are also embodied in impedance characteristics (Figure 8.42). A freshly prepared Sn electrode, when immersed into a Sn(II)–gluconate solution, acquires the open-circuit potential $E_{oc} = -0.32$ V, and its impedance does not exceed several hundred Ω cm^2. When a low cathodic polarization is applied ($E = -0.4$ V), spongy deposits are formed and Z values decrease about fourfold due to a significant development of the real surface of tin electrode. At the same time, certain changes in the shape of Nyquist plots are observed. The semicircles supplemented with a linear part are typical of the processes proceeding under the mixed (charge transfer and diffusive mass transport) control. Furthermore, when the potential is shifted up to −0.5 V and boulder-like deposits are built up, Z increases by 1 order of magnitude and accounts for several kΩ cm^2. It is remarkable that both the impedance and morphology cease to depend on E at $E < -0.5$ V. Hence, to obtain compact,

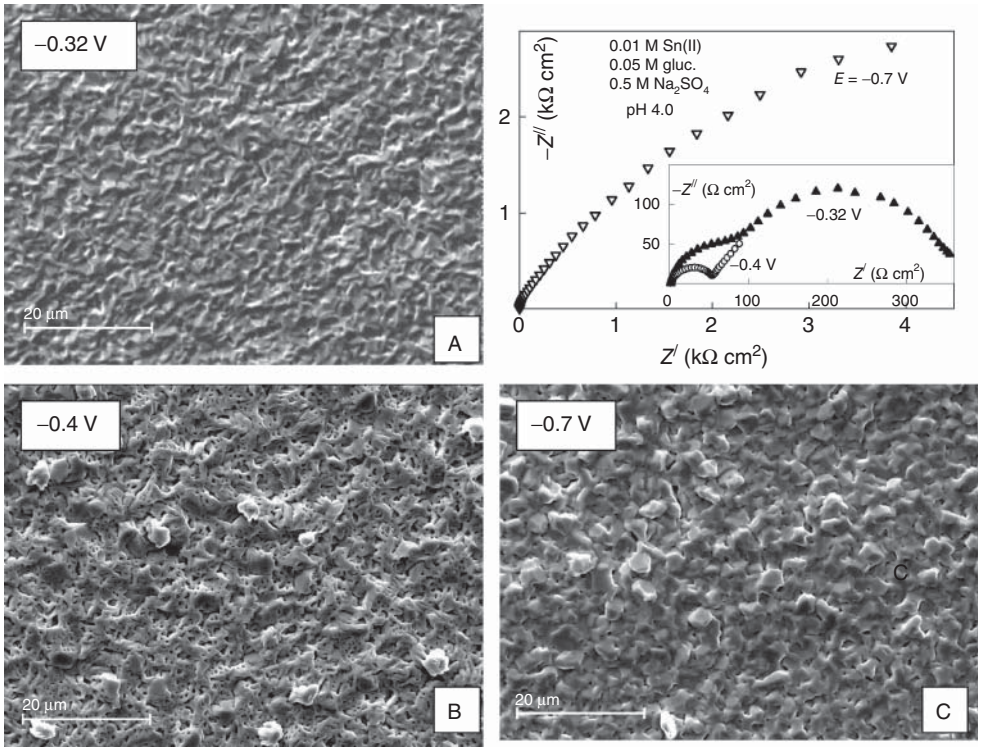

Figure 8.42 Selected types of the morphology of tin coatings and the respective impedance data.

fine-grained deposits, the conditions for high inhibition of tin surface should be established.

The data obtained suggest that the adsorption processes in the system under discussion are complicated. To reveal their nature in more detail, further investigations including surface spectrometry are required. Nevertheless, some inferences based on impedance data seem to be available. A comparison between the data presented in Figures 8.37 and 8.41 shows that a profound effect of pH is observed only in the presence of Sn(II). Then, the overall impedance increases drastically with pH (Figure 8.37), whereas only a weak opposite effect can be seen in the absence of Sn(II) (Figure 8.41). This means that the Sn^{2+} ions are of crucial importance for the formation of adsorption layer. The same should be extended to OH^- ions that possess the ability to form Sn(II) hydroxo-complexes, which can be adsorbed immediately on the hydrophobic surface of tin. The inhibitive character of the surface layer gives grounds to suggest that Sn^{2+} and Sn surfaces do not contact directly and are separated by other species. It is necessary to mention that such foreign elements as carbon and oxygen were detected on the surface of electrodeposited samples. In the case of boulder-like deposits, carbon was found in the amounts of 2.5–4.3 at%, whereas the content of oxygen is somewhat higher

(3–6.5 at%). This may be associated with the ligand chemisorption proceeding with the subsequent incorporation of the fragments of its destruction into the deposits. Similar effects are also observed in the case of copper electrodeposition in gluconate-containing Cu(II) solutions.

8.3.3 Electroreduction of Zn(II) Complexes

Gluconic acid came into use even 60 years ago in zinc plating baths to give a semi-bright and smooth deposits of zinc [126]. At a later date, electroplating of zinc and its alloys has been explored under different electrolysis conditions and gluconate bath compositions [127–132]. Most of these investigations are of applied character; however, the article [127] deals with kinetics of Zn(II) gluconate reduction. The mechanism proposed therein is rather complicated and involves a consecutive charge transfer with adsorption of Zn(I) intermediates.

Available literature data on the Zn(II)–gluconate complexes are also weak. We managed to find quantitative characteristics of two species: ZnL^+ [132] and ZnLOH [133]. According to various authors [1], SO_4^{2-} anions are also capable of interacting with Zn^{2+} ions. Variations of $ZnSO_4$ stability with ionic strength are very similar to those observed for $CuSO_4$ [63].

Stability constants used in the simulations are listed in Table 8.8. They were obtained from spectrophotometric data [65] or selected from literature as best-matched to the ionic strength of the solutions used. To obtain the concentration of hydronium ions from pH measurements, the activity coefficient $\gamma_H+ = 0.7$ [65] was used. Some examples of the distribution are given in Figure 8.43. They show that Zn(II) sulfate complexes prevail in sufficiently acidic media. In weakly acidic solutions (pH > 5), gluconate anions L^- become predominant and this results in the increase of ZnL^+ molar fraction. Formation of OH^--containing ZnLOH complexes becomes tangible at pH > 5. Special simulations showed that the quantities of other hydroxo-complexes are negligible and they can be omitted from consideration.

Table 8.8 Quantitative characteristics of equilibria in Zn(II) sulfate solutions containing gluconic acid (LH).

Equilibrium	Logarithm of equilibrium constant	References
$H^+ + L^- \rightleftarrows LH$	3.7	[1]
$LH \rightleftarrows Lac + H_2O$	−1.25	[134]
$H^+ + SO_4^{2-} \rightleftarrows HSO_4^-$	1.48	[1, 82]
$Zn^{2+} + L^- \rightleftarrows ZnL^+$	1.7	[135]
$ZnL^+ + OH^- \rightleftarrows ZnLOH$	8.14	[136]
$Zn^{2+} + SO_4^{2-} \rightleftarrows ZnSO_4$	1.0	[1]

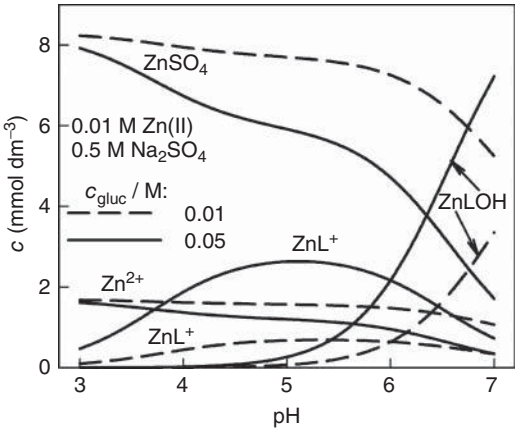

Figure 8.43 Distribution of complex species in 0.01 M Zn(II) solutions containing 0.5 M of Na_2SO_4 and gluconic acid (LH) with total concentration of 0.01 M (dashed lines) and 0.05 M (solid lines).

It is characteristic that the complexation degree of the system slightly varies over the wide pH range ($3 < pH < 6$). Therefore, the equilibrium potentials (E_{eq}) of $Zn|Zn^{2+}$ electrodes remain actually on the same level. Besides, their values are lower than E_{eq} of $H_2|H^+$ electrode; therefore, Zn(II) is reduced along with hydrogen evolution. The rate of the latter partial process falls with solution pH and with decrease in gluconate concentration. Then, the RDE voltammograms also show a well-defined plateau of the limiting current (Figure 8.44) that increases with the

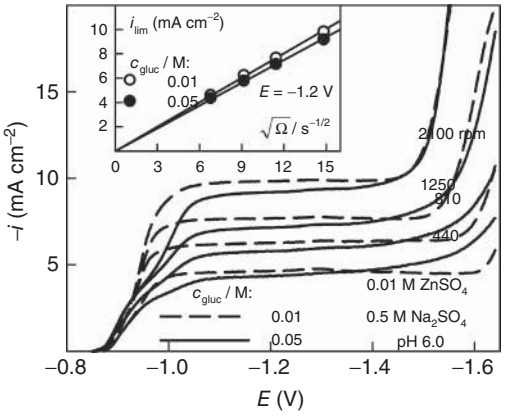

Figure 8.44 RDE voltammograms obtained for 0.01 M Zn(II) solutions containing 0.01 M (dashed lines) or 0.05 M (solid lines) of gluconate at pH 6. RDE rotating velocities (revolutions per minute) are indicated at the curves. Limiting current densities (i_{lim}) versus $\sqrt{\Omega}$ (Ω is an angular rotating velocity) are plotted in the inset.

intensity of forced convection and obeys Levich equation with D_{ef} that depends to some extent on gluconate concentration.

D_{ef} is equal to 4.2×10^{-6} and 3.8×10^{-6} cm^2 s^{-1} when $c_{gluc} = 0.01$ and 0.05 M, respectively. Similar diminution of D_{ef} with ligand concentration was also observed in the case of Cu(II) gluconate solutions [65]. Substitution of simulated $[Zn^{2+}]$ values into Nernst equation yields $E_{eq} = -0.868$ V, which is very close to the origin of cathodic voltammograms (−0.86 −0.87 V).

According to Gerischer [136], $Zn(OH)_2$ is the electrochemically active complex that takes place in the charge transfer processes occurring in sufficiently alkaline solutions. This EAC can be formed not only in zincate solutions but in cyanide solutions as well. Similar mechanism was also postulated for Zn(II) reduction in alkaline D-mannitol solutions [134]; however, this view seems to be unacceptable for acidic media. It follows from the data obtained at $3.7 < pH < 5$ [127] that both Zn^{2+} and ZnL^+ might be electrically active. This leaves the question of the EAC structure open.

In the case of Cu(II) gluconate complexes, similar problem was solved in favor of Cu^{2+} aqua-ions [65]. Similarly, we have assumed that "free" Zn^{2+} ions are discharged whereas other Zn(II) complexes are electrochemically inert, but they can act as species producing EAC. As a first approximation, we assume that Zn^{2+} reduction is controlled by diffusive mass transport and charge transfer. Then, the kinetic equation should be written as follows:

$$i = i_0 \left\{ \exp\left(\frac{\alpha n F}{RT}\eta\right) - \frac{[Zn^{2+}]_s}{[Zn^{2+}]_b} \exp\left[-\frac{(1-\alpha)\, nF}{RT}\eta\right] \right\}. \tag{8.48}$$

Surface concentrations of EAC and other species can be obtained using regularities of diffusive mass transport involving chemical interactions, as described in Chapter 3. In so doing, the pH changes at the electrode surface are estimated. They are especially significant in a slightly acidic medium: for example, pH_s can be changed from 6 up to 11, when cathodic i increases (Figure 8.45). It should be emphasized that the hydrogen evaluation was ignored in simulations. Such high pH variations arise from the redistribution of complexes and protonated ligands at the electrode surface where the dissociation of ZnLOH species is of considerable importance. The current density, at which the pH_s jump is observed, depends on the concentration of gluconate. When the amount of the ligand is sufficiently low (0.01 M or less), the main alkalization of the surface layer occurs in the vicinity of the limiting current.

As mentioned earlier, the hydrogen evolution is low at pH 6 and can be neglected. Then, at sufficiently high cathodic overvoltage, experimental data can be transformed into NTP with normalized current density $Y = |i|/([Zn^{2+}]_s/[Zn^{2+}]_b)$. An example of voltammogram and its transform into NTP are shown in Figure 8.46. The values of $\alpha_c = 0.65$ and $i_0 = 0.1$ mA cm^{-2} were obtained from the NTP slope and intercept, respectively. To simulate a full voltammogram, these kinetic parameters were substituted into Eq. (8.48), and in consequence, a good agreement with experimental data was observed (Figure 8.46). However, this is not obeyed at a large excess of gluconate ($c_{gluc} = 0.05$ M),

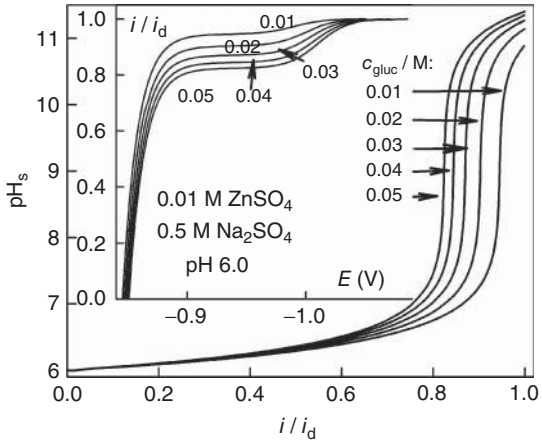

Figure 8.45 Surface pH versus i/i_d simulated at different gluconate concentrations indicated at the respective curves. Reversible cathodic voltammograms are plotted in the inset.

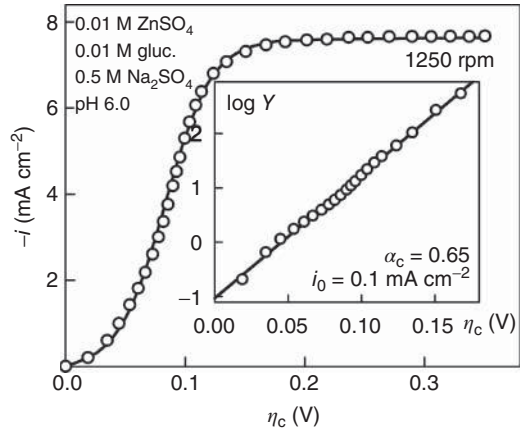

Figure 8.46 Comparison of the experimental voltammogram (circles) with that (solid line) simulated by Eq. (8.51) with kinetic parameters obtained from the NTP presented in the inset.

though some analogies can be drawn between the simulated and experimental voltammograms. Some irregularities observed on experimental curves at low η_c (Figure 8.44) could be from pH_s changes that form the shape of simulated reversible voltammograms (Figure 8.45). Undoubtedly, other phenomena, such as EAC or ligand adsorption [65, 125], hydrogen evolution, and insufficient lability of some complexes, can play a certain role. Admittedly, a disclosure of the mechanism of Zn(II) reduction in gluconate solutions remains an outstanding problem.

Appendix

It follows from Eq. (8.4) that

$$Z_F = R_\infty + \frac{1}{1/R_1 + Y_{01}\sqrt{s}} + \frac{1}{C_2 s + Y_{02}\sqrt{s}}, \tag{A1}$$

where $R_1 = R_\infty(c-b)/b$, $Y_{01} = 1/R_\infty(c-b)$, $C_2 = 1/R_\infty d$, $Y_{02} = b/R_\infty d$. Equation (A1) shows that the faradaic circuit should include the resistance R_∞ that is in series with two other subcircuits whose admittances are given by two respective denominators in this equation. The terms $1/R_1$ and $Y_{01}\sqrt{s}$ testify that the first subcircuit contains R_1 and W_1 in parallel. Similarly, another term in the parenthesis suggests the parallel connection of C_2 and W_2 in the second subcircuit.

At the same time, another form of Eq. (8.4) is possible:

$$Y_F = \frac{1}{R_3 + 1/Y_{03}\sqrt{s}} + \frac{1}{R_4 + 1/Y_{04}\sqrt{s}}. \tag{A2}$$

It follows from the identity of Eqs. (9.8) and (A2) that

$$b = \frac{1/Y_{03} + 1/Y_{04}}{R_3 + R_4}, c = \frac{1}{R_3 Y_{03}} + \frac{1}{R_4 Y_{04}}, d = \frac{1}{R_3 R_4 Y_{03} Y_{04}} \tag{A3}$$

Equation (A2) shows that alternative faradaic EC, namely ($[R_3W_3][R_4W_4]$), is possible. It contains two parallel $[RW]$ subcircuits. The next relationship follows from EC structures, as the limiting case when $\omega \to \infty$:

$$1/R_\infty = 1/R_3 + 1/R_4. \tag{A4}$$

Both EC yield the same impedance spectra, when their elements are chosen according to the following equations:

$$R_1 = R_\infty \frac{R_3^2 Y_{03} + R_4^2 Y_{04}}{R_3 R_4 (Y_{03} + Y_{04})} = \frac{R_3^2 Y_{03} + R_4^2 Y_{04}}{(R_3 + R_4)(Y_{03} + Y_{04})}, \tag{A5}$$

$$Y_{01} = \frac{R_3 R_4 (R_3 + R_4) Y_{03} Y_{04}}{(R_3^2 Y_{03} + R_4^2 Y_{04}) R_\infty} = \frac{(R_3 + R_4)^2 Y_{03} Y_{04}}{R_3^2 Y_{03} + R_4^2 Y_{04}}, \tag{A6}$$

$$Y_{02} = \frac{R_3 R_4 (Y_{03} + Y_{04})}{(R_3 + R_4) R_\infty} = Y_{03} + Y_{04}, \tag{A7}$$

$$C_2 = R_3 R_4 Y_{03} Y_{04} / R_\infty = (R_3 + R_4) Y_{03} Y_{04}. \tag{A8}$$

References

1. (a) Sillen, L.G. and Martel, A.E. (1964) *Stability Constants of Metal-Ion Complexes*, vol. **1**, Special Publications N 17 and 25, Chemical Society, London, (1971) vol. **2**;(b) Smith, R.M. and Martel, A.E. (1974–1977) *Critical Stability Constants*, vol. **1–4**, Plenum Press, New York and London;(c)

Serjeant, E.P. and Dempsey, B. (eds) (1979) *Ionisation Constants of Organic Acids in Aqueous Solutions*, Pergamon Press, Oxford.
2. Horner, J. (1997) Cyanide copper plating. *Plat. Surf. Finish.*, **84** (8), 52–57.
3. Costa, M. (1963) Contribution à l'étiude de la cinétique de la réaction de l'electrode cuivre/cyanure double de cuivre et de potassium. *J. Rech. Centre Nat. Rech.*, **64**, 285–315.
4. Bek, R.Y. and Zhukov, B.D. (1976) Mechanism and kinetics of copper electrodeposition from cyanide electrolytes. *Sov. Electrochem.*, **12** (9), 1291–1295.
5. Sinitski, R.E., Srinivasan, V., and Haynes, R. (1980) Electrode kinetics of copper deposition from copper cyanide solution. *J. Electrochem. Soc.*, **127** (1), 47–51.
6. Chu, D. and Fedkiw, P.S. (1993) The electrochemistry of a cuprous cyanide strike-plating bath. *J. Electroanal. Chem.*, **345** (1-2), 107–120.
7. Steponavičius, A., Radžiūnienė, B., Ivaškevič, E., and Girdauskas, B. (1996) On the mechanism of the cathodic reaction in Cu (I) cyanide solution. *Chemija*, **2**, 48–54.
8. Bek, R.Y. and Shuraeva, L.I. (1997) The near-electrode layer composition and diffusion polarization inherent in electrolysis of copper-plating cyanide solutions with a mild excess of the ligand. *Russ. J. Electrochem.*, **33** (2), 114–118.
9. Katagiri, A., Inoue, H., and Ogure, N. (1997) Cathodic polarization of copper electrode in CuCN– KCN solutions and the current distribution for copper deposition on grooved substrates. *J. Appl. Electrochem.*, **27** (5), 529–538.
10. Dudek, D.A. and Fedkiw, P.S. (1999) Electrodeposition of copper from cuprous cyanide electrolyte: I. Current distribution on a stationary disk. *J. Electroanal. Chem.*, **474** (1), 16–30.
11. Sato, A. and Barauskas, R. (1997) in *Metal Finishing Guidebook and Directory Issue*, 65th edn (ed M. Murphy), Elsevier Science, Tarrytown, NY, p. 230.
12. Hancock, P.D., Finkelstein, N.P., and Evers, A. (1972) Stabilities of the cyanide complexes of the monovalent group IB metal ions in aqueous solution. *J. Inorg. Nucl. Chem.*, **34** (12), 3747–3751.
13. Sabonienė, E., Mikučionis, G., and Survila, A. (1987) Unpolarized Cu electrode potentials in Cu(I) cyanide solutions. *Proc. Lith. Acad. Sci. Ser. B*, **6** (163), 26–33.
14. Cheng, S.C., Gattrell, M., Guena, T., and MacDougall, B. (2002) The electrochemical oxidation of alkaline copper cyanide solutions. *Electrochim. Acta*, **47** (20), 3245–3256.
15. Raub, E. and Muller, K. (1967) *Fundamentals of Metal Deposition*, Elsevier, Amsterdam.
16. Laufer, G., Schaaf, T.F., and Huneke, J.T. (1980) Surface enhanced Raman scattering from cyanide adsorbed on copper. *Chem. Phys.*, **73** (6), 2973–2976.
17. Benner, R.E., Von Raben, K.U., Dornhaus, R., Chang, R.K., Laube, B.L., and Otter, F.A. (1981) Correlation of SERS with cyclic voltammetry for cyanide complexes adsorbed on Cu electrodes. *Surf. Sci.*, **102** (1), 7–17.
18. Loo, B.H. (1982) Surface enhanced Raman spectroscopy-vibrational spectroscopy of adsorbates at the metal-electrolyte interface. *Spectrosc. Lett.*, **15** (2), 85–111.
19. Mahoney, M.R. and Cooney, R.P. (1985) Chemical origins of surface-enhanced Raman scattering by cyanide on copper electrodes. *J. Chem. Soc., Faraday Trans. 1*, **81** (9), 2123–2130.
20. Lee, K.A.B., Kunimatsu, K., Gordon, J.G., Golden, W.G., and Seki, H. (1987) A study of the copper/cyanide solution interphase by polarization modulated FT-IR spectroscopy. *J. Electrochem. Soc.*, **134** (7), 1676–1678.
21. Burkhardt, W. (1990) Eigenschaften und Einsatz galvanisch abgeschiedener Kontaktschichten. *Galvanotechnik*, **81** (9), 3089–3102.
22. Bersirova, O.A., Byk, S.V., and Kublanovsky, V.S. (2013) *Silver Electrodeposition*, Medinform, Kiiv.
23. Survila, A. (1989) *Electrode Processes in Systems of Labile Complexes of Metals*, Mokslas, Vilnius.

24. Nikulin, V.N. and Cypin, M.Z. (1960) Electrode potentials of silver monocrystal. *Zh. Obshch. Khim.*, **34** (12), 2814–2816.
25. Saito, A., Shibata, T., Ohura, H., and Migita, Y. (1998) Mechanism of silver electrodeposition from silver-cyanide complex solutions. *Denki Kagaku.*, **66** (11), 1128–1134.
26. Vielstich, W. and Gerischer, H. (1955) For electrolysis at constant electrode potential. II. Studies on the kinetics of the deposition of zinc simple and complex silver ions. *Z. Phys. Chem. (N.F.)*, **4**, 10–23.
27. Baltruschat, H. and Vielstich, W. (1983) On the mechanism of silver dissolution and deposition in aqueous KCN-KCl electrolytes. *J. Electroanal. Chem.*, **154** (1-2), 141–153.
28. Ashiru, O.A. and Farr, J.P.G. (1995) Application of frequency response analysis to the determination of cathodic discharge mechanism during silver electroplating. *J. Electrochem. Soc.*, **142** (11), 3729–3734.
29. Survila, A.A., Morkevičius, E.I., and Dikčius, A.A. (1985) *Sov. Electrochem.*, **21**, 1351.
30. Li, J. and Wadsworth, M.E. (1993) Electrochemical study of silver dissolution in cyanide solutions. *J. Electrochem. Soc.*, **140** (7), 1921–1927.
31. Nechaev, E.A., Bek, R.Y., and Kudryavcev, N.T. (1967) Investigation of silver electrodeposition from complex electrolytes. II. *Elektrokhimiya*, **1** (9), 1325–1331.
32. Nechaev, E.A. and Bek, R.Y. (1966) Investigation of silver electrodeposition from complex electrolytes. III. *Elektrokhimiya*, **2** (2), 150–154.
33. Bek, R.Y., Nechaev, E.A., and Kudryavcev, N.T. (1967) Investigation of silver electrodeposition from complex electrolytes. IV. *Elektrokhimiya*, **3** (9), 1121–1123.
34. Bek, R.Y., Nechaev, E.A., and Kudryavcev, N.T. (1967) Chronopotentiometric study of electrolytic evolution of silver from cyanide electrolytes. *Elektrokhimiya*, **3** (12), 1465–1467.
35. Nechaev, E.A., Bek, R.Y., and Kudryavcev, N.T. (1968) On the nature of kinks on the polarization curve in the electrodeposition of silver from cyanide electrolytes. *Elektrokhimiya*, **4** (5), 545–549.
36. Bek, R.Y. and Rogozhnikov, N.A. (1995) Adsorption of cyanide ions and the mechanism of anodic silver dissolution in cyanide electrolytes. *Russ. J. Electrochem.*, **31** (11), 1125–1130.
37. Bek, R.Y. and Rogozhnikov, N.A. (1998) Kinetics of electrochemical processes in the system: silver/cyanide solutions. *J. Electroanal. Chem.*, **447** (1-2), 109–115.
38. Baltrūnas, G. (2003) The mechanism of electrode process in the system silver/silver cyanide complexes. *Electrochim. Acta*, **48** (24), 3659–3664.
39. Valette, G. and Namelin, A. (1973) Structure and properties of electrochemical double film on interphase of aqueous sodium-fluoride solutions and silver. *J. Electroanal. Chem.*, **45**, 301.
40. Rogozhnikov, N.A. (1997) Impedance of a silver electrode in cyanide solutions. *Russ. J. Electrochem.*, **33** (6), 668–670.
41. Rogozhnikov, N.A. (1998) Impedance of silver dissolution in cyanide solutions. *Russ. J. Electrochem.*, **34** (1), 61–67.
42. Rogozhnikov, N.A. and Bek, R.Y. (1997) Thermodynamics and kinetics of adsorption of cyanide ions on silver. Part I. *J. Electroanal. Chem.*, **434** (1-2), 19–30.
43. Rogozhnikov, N.A. and Bek, R.Y. (1998) Thermodynamics and kinetics of adsorption of cyanide ions on silver. Part II. *J. Electroanal. Chem.*, **457** (1-2), 31–34.
44. Lin, W.F., Tian, Z.Q., Sun, S.G., and Tian, Z.W. (1992) Quantum chemistry studies on electronic properties of CN adsorbed on silver electrodes. *Electrochim. Acta*, **37** (2), 211–213.
45. Daujotis, V. and Kairys, V. (1997) The mechanism of electroreduction of silver cyanide complexes in aqueous electrolytes—II. Interpretation of SERS data. *Electrochim. Acta*, **42** (9), 1345–1350.
46. Baltrūnas, G., Drunga, V., and Švedas, D. (1994) Phenomena limiting the rate of electroreduction of cyanide silver

complexes at low electrode polarizations. *J. Electroanal. Chem.*, **369** (1–2), 93–96.
47. Daujotis, V., Jasaitis, D., and Raudonis, R. (1997) The mechanism of electroreduction of silver cyanide complexes in aqueous electrolytes—I. Time-resolved EQCM study. *Electrochim. Acta*, **42** (9), 1337–1344.
48. Ashiru, O.A. and Farr, J.P.G. (1992) Kinetics of reduction of silver complexes at a rotating disk electrode. *J. Electrochem. Soc.*, **139** (10), 2806–2810.
49. Baltrūnas, G. (1984) Chemical limitations of electroreduction of silver cyanide complexes. Vilnius University, PhD Thesis. Vilnius.
50. Cathro, K.J. and Koch, D.F.A. (1964) The anodic dissolution of gold in cyanide Solutions. *J. Electrochem. Soc.*, **111** (12), 1417–1420.
51. MacArthur, D.M. (1972) A study of gold reduction and oxidation in aqueous solutions. *J. Electrochem. Soc.*, **119** (6), 672–677.
52. Kirk, D.W., Foulkes, F.R., and Graydon, W.F. (1978) A study of anodic dissolution of gold in aqueous alkaline cyanide. *J. Electrochem. Soc.*, **125** (9), 1436–443.
53. Pan, T.P. and Wan, C.C. (1979) A study of the anodic dissolution of gold in concentrated KCN solution. *J. Chem. Technol. Biotechnol.*, **29** (7), 427–432.
54. Kirk, D.W. and Foulkes, F.R. (1980) Anodic dissolution of gold in aqueous alkaline cyanide solutions at low overpotentials. *J. Electrochem. Soc.*, **127** (9), 1993–1997.
55. Thurgood, C.P., Kirk, D.W., and Foulkes, F.R. (1981) Activation energies of anodic gold reactions in aqueous alkaline cyanide. *J. Electrochem. Soc.*, **128** (8), 1680–1685.
56. Cheh, H.Y. and Sard, R. (1971) Electrochemical and structural aspects of gold electrodeposition from dilute solutions by direct current. *J. Electrochem. Soc.*, **118** (11), 1737–1747.
57. Harrison, J.A. and Thompson, J. (1972) The reduction of gold cyanide complexes. *J. Electroanal. Chem.*, **40** (1), 113–120.
58. Bard, A.J. (ed) (1975) *Encyclopedia of Electrochemistry of the Elements*, vol. **4**, Marcel Dekker, Inc., New York.
59. Molčadskytė, O.A. (1979) Kinetics of gold electrodeposition from acid solutions. Institute of Chemistry, PhD Thesis. Vilnius.
60. McIntyre, J.D.E. and Peck, W.F. Jr., (1976) Electrodeposition of gold depolarization effects induced by heavy metal ions. *J. Electrochem. Soc.*, **123** (12), 1800–1813.
61. Lorenz, W. (1955) Über den Einfluß von Oberflächenrauhigkeit und potentialbestimmender Ionen-adsorption on Elektroden auf das Anklingen der diffusions polarisation bei konstantem Strom. *Z. Elektrochem.*, **59** (7-8), 730–736.
62. Survila, A., Mockevičius, V., and Višomirskis, R. (1987) Chronopotentiometric study of gold electrodeposition from cyanide solutions. *Sov. Electrochem.*, **23** (6), 769–774.
63. Akilan, Ch. (2008) Thermodynamic and related studies of aqueous copper(II) sulfate solutions. PhD Thesis. Murdoch University.
64. Uljanionok, J., Jagminienė, A., and Survila, A. (2009) Spectrophotometric investigation of formation of Cu(II)-maleic acid complexes. *Chemija*, **20** (2), 89–92.
65. Survila, A., Mockus, Z., Kanapeckaitė, S., Pileckienė, J., and Stalnionis, G. (2011) Cathodic processes in copper(II) solutions containing gluconic acid. *Russ. J. Electrochem.*, **47** (2), 129–135.
66. Sauerbrey, G. (1959) Use of vibrating quartz for thin film weighing and microweighing. *Z. Phys.*, **155** (2), 206–222.
67. Despić, A.R., Jovanović, D.R., and Bingulac, S.P. (1970) Kinetics and mechanism of electron exchange at the Cd^{2+}/Cd(Hg) interface. *Electrochim. Acta*, **15** (3), 459–472.
68. Armstrong, R.D. and Firman, R.E. (1973) Impedance plane display of a reaction with a solution soluble intermediate. *J. Electroanal. Chem.*, **4** (1), 3–10.
69. Rueda, M., Sluyters-Rehbach, M., and Sluyters, J.H. (1987) Analysis of the

interfacial admittance in the case of a two-step two-electron electrode reaction with a diffusing intermediate, with application to the reduction of pyrazine. *J. Electroanal. Chem.*, **222** (1-2), 45–68.

70. Survila, A. and Katkus, A. (1980) The impedance of nonpolarized tin electrodes in acid sulfate solutions. *Sov. Electrochem.*, **16** (12), 1483–1487.
71. Survila, A. and Baliukienė, V. (2001) Equivalent circuit of electrochemical processes involving two consecutive charge transfer steps. *Chemija*, **12** (3), 195–198.
72. Gabrielli, C., Moçotéguy, P., Perrot, H., Nieto-Sanz, D., and Zdunek, A. (2006) A model for copper deposition in the damascene process. *Electrochim. Acta*, **51** (8-9), 1462–1472.
73. Gerischer, H.Z. (1951) Bestimmung der Austauschgeschwindigkeit beim Gleichgewichtspotential durch polarisationsmessungen mit Gleich und Wechselstrom. *Elektrochemistry*, **55** (2), 98–104.
74. Slivka, R.A., Aleksandrova, D.P., Grafov, B.M., and Leikis, D.I. (1977) Determination the kinetic parameters based on the theory of kinetics impedance multistage processes. *Elektrokhimiya*, **13**, 888–892.
75. Maslii, A.I., Pirogov, V.Y., and Medvedev, V.Z. (1986) Kinetics of electrodeposition of copper from sulfate solutions. Analysis of the frequency dependence of the impedance for model of step-wise discharge without crystallization limitations. *Elektrochimiya*, **22** (2), 164–169.
76. Survila, A., Mockus, Z., Kanapeckaitė, S., and Samulevičienė, M. (2002) Adsorption behaviour of laprol 2402 C on copper electrode. *Pol. J. Chem.*, **76** (7), 983–991.
77. Macdonald, J.R. (1987) *Impedance Spectroscopy: Emphasizing Solid Materials and Systems*, John Wiley & Sons, Inc., New York.
78. Nicholson, R.S. and Shain, I. (1964) Theory of stationary electrode polarography. Single scan and cyclic methods applied to reversible, irreversible, and kinetic systems. *Anal. Chem.*, **36** (4), 706–723.
79. Būdienė, J., Survilienė, A., and Survila, A. (2007) Impedance of copper electrode in the isopotential solutions containing Cu(II) complexes of glycolic acid. *Russ. J. Electrochem.*, **43** (11), 1294–1298.
80. Būdienė, J., Survilienė, A., and Survila, A. (2004) Cathodic processes in acidic Cu(II) solutions containing glycolic acid. *Russ. J. Electrochem.*, **40** (4), 394–399.
81. Polcyn, D.S. and Shain, I. (1966) Multistep charge transfers in stationary electrode polarography. *Analyt. Chem.*, **38** (3), 370–375.
82. Survila, A. and Stasiukaitis, P.V. (1998) Linear potential sweep voltammetry of electroreduction of labile metal complexes. The mechanism of consecutive charge transfer. *Chemija*, **3**, 212–217.
83. Niaura, G. and Malinauskas, A. (1998) Surface-enhanced Raman spectroscopy of ClO_4^- and SO_4^{2-} anions adsorbed at a Cu electrode. *J. Chem. Soc., Faraday Trans.*, **94** (15), 2205–2211.
84. Survila, A., Mockus, Z., Kanapeckaitė, S., Bražinskienė, D., and Juškėnas, R. (2012) Surfactant effects in Cu-Sn alloy deposition. *J. Electrochem. Soc.*, **159** (5), D296–D302.
85. Pileckienė, J., Grigucevičienė, A., and Survila, A. (2011) Impedance of copper electrode in Cu(II) solutions containing gluconic acid. *Chemija*, **22** (2), 85–90.
86. Survila, A. and Šironienė, B. (1992) Kinetics of electrodeposition of copper from alkaline citrate solutions. *Elektrokhimiya*, **28** (12), 1756–1761.
87. Uksienė, V., Survila, A., and Žukauskaitė, A. (1996) The electroreduction mechanism of copper(II) citrate complexes. *Russ. J. Electrochem.*, **32** (8), 884–888.
88. Nurnberg, H.W., Riesenbeck, G., and Stackelberg, M. (1961) For the polarographic determination of the dissociation and recombination of weak acids. *Collect. Czech. Chem. Commun.*, **28** (1), 126–140.
89. Ishikawa, M. and Enomoto, H. (1989) Complexation of Ni (II) with citrate

in nickel–citrate plating baths. *J. Surf. Finish. Soc. Jpn.*, **40**, 1266.

90. Gerischer, H. (1964) Kinetik der Metallabscheidung aus Lösungen komplexgebundener Ionen. *Chem. Ing. Tech.*, **36** (6), 666–671.

91. Hemsley, J.D.C. and Roper, M.E. (1979) Tin--cobalt alloy plating from a sulphate electrolyte. *Trans. IMF*, **57** (2), 77–80.

92. Survila, A., Mockus, Z., and Kanapeckaitė, S. (2000) Kinetics of Sn and Co codeposition in citrate solutions. *Electrochim. Acta*, **46** (4), 571–577.

93. Survila, A., Mockus, Z., Juškėnas, R., and Jasulaitienė, V. (2001) Electrodeposition of Sn and Co coatings in citrate solutions. *J. Appl. Electrochem.*, **31** (10), 1109–1116.

94. Maskin, T.N., Zmbova, B.Ž., and Veselinović, D.S. (1991) Investigation of Sn(II) gluconate complexes by potentiometric titrations. *J. Serb. Chem. Soc.*, **56**, 337–359.

95. Pettine, M., Millero, F.J., and Macchi, G. (1981) Hydrolysis of tin (II) in aqueous solutions. *Anal. Chem.*, **53** (7), 1039–1043.

96. Survila, A., Mockus, Z., Kanapeckaitė, S., and Stalnionis, G. (2012) Kinetics of Sn(II) reduction in acid sulphate solutions containing gluconic acid. *J. Electroanal. Chem.*, **667**, 59–65.

97. Bražinskienė, D., Pautienienė, V., and Survila, A. (2007) Tin corrosion in highly acidic solutions containing ethylene glycol oligomers and halides: An electrochemical quartz crystal microbalance study. *Russ. J. Electrochem.*, **43** (1), 64–69.

98. Quintin, M. and Hagymas, G. (1964) Contribution à l'étiude de la corrosion electrochimique de l'etain en milieu sulfurique. *J. Chim. Phys.*, **61** (4), 541–547.

99. Sonoda, T., Nawafune, H., and Mizumoto, S. (1992) Electrodeposition of bright tin from neutral gluconate baths. *Plat. Surf. Finish.*, **79** (10), 78–81.

100. Survila, A., Mockus, Z., and Kanapeckaitė, S. (2002) Adsorption behaviour of laprol 2402 C on a tin electrode. *Trans. IMF*, **80** (3), 85–87.

101. Survila, A., Mockus, Z., and Kanapeckaitė, S. (2003) Effect of halides on adsorption properties of polyether laprol 2402 C on copper and tin electrodes. *J. Electroanal. Chem.*, **552**, 97–103.

102. Kostryukova, G.G., Ratkov, O.I., Kozakov, V.A., Ginberg, A.M., and Vagramyan, A.T. (1969) On the application of relaxation methods to the study of processes of electrodeposition of metals I. Electrode Sn / Sn^{2+}. *Elektrokhimiya*, **5** (5), 571–574.

103. Survila, A., Mockus, Z., Kanapeckaitė, S., and Samulevičienė, M. (2005) Effect of sintanol DS-10 and halides on tin(II) reduction kinetics. *Electrochim. Acta*, **50** (14), 2879–2885.

104. Galus, Z. (1975) in *Encyclopedia of Electrochemistry of the Elements*, vol. **4** (ed A.J. Bard), Marcel Dekker, Inc., New York, pp. 223–271.

105. Koper, M.T.M. (1996) Stability study and categorization of electrochemical oscillators by impedance spectroscopy. *J. Electroanal. Chem.*, **409** (1), 175–182.

106. Lasia, A. (1999) Electrochemical impedance spectroscopy and its applications, in *Modern Aspects of Electrochemistry*, vol. **32** (eds B.E. Konway, J. Bocris, and R.E. White), Kluwer Academic Publishers, New York.

107. Armstrong, R.D. and Henderson, M. (1972) Impedance plane display of a reaction with an adsorbed intermediate. *J. Electroanal. Chem.*, **39** (1), 81–90.

108. Cao, C.-N. (1990) On the impedance plane displays for irreversible electrode reactions based on the stability conditions of the steady-state – I. One state variable besides electrode potential. *Electrochim. Acta*, **35** (5), 831–836.

109. Bai, L. and Conway, B.E. (1993) Three-dimensional impedance spectroscopy diagrams for processes involving electrosorbed intermediates, introducing the third electrode-potential variable—examination of conditions leading to pseudo-inductive behavior. *Electrochim. Acta*, **38** (14), 1803–1415.

110. Cao, C.-N. (1990) On the impedance plane displays for irreversible electrode reactions based on the stability conditions of the steady-state—II. Two state variables besides electrode potential. *Electrochim. Acta*, **35** (5), 837–844.

111. Diard, J.-P., Le Gorrec, B., Montella, C., and Montero-Ocampo, C. (1993) Calculation, simulation and interpretation of electrochemical impedance diagrams: part IV. Second-order electrochemical impedances. *J. Electroanal. Chem.*, **352** (1), 1–15.

112. Armstrong, R.D. and Edmondson, K. (1973) The impedance of metals in the passive and transpassive regions. *Electrochim. Acta*, **18** (12), 937–943.

113. Baril, G., Galicia, G., Deslouis, C., Pébère, N., Tribollet, B., and Vivier, V. (2007) An impedance investigation of the mechanism of pure magnesium corrosion in sodium sulfate solutions. *J. Electrochem. Soc.*, **154** (2), 108–113.

114. Brug, G.J., van den Eeden, A.L.G., Sluyters-Rehbach, M., and Sluyters, J.H. (1984) The analysis of electrode impedances complicated by the presence of a constant phase element. *J. Electroanal. Chem.*, **176** (1), 275–295.

115. Damaskin, B.B. and Afanasyev, B.N. (1977) The current state of the theory of influence of adsorption of organic substances on the kinetics of electrochemical reactions. *Elektrokhimiya*, **13** (8), 1099–1117.

116. Bartenev, V.Y., Sevast'yanov, E.S., and Leikis, D.I. (1970) The structure of the double layer on the tin in dilute solutions. *Elektrokhimiya*, **6** (12), 1868–1870.

117. Séby, F., Potin-Gautier, M., Giffaut, E., and Donard, O.F.X. (2001) A critical review of thermodynamic data for inorganic tin species. *Geochim. Cosmochim. Acta*, **65** (18), 3041–3053.

118. Survila, A. and Bražinskienė, D. (2007) Inhibition activity of ethyleneglycol and its oligomers on tin electrode. *J. Solid State Electrochem.*, **11** (1), 65–70.

119. Survila, A., Mockus, Z., Kanapeckaitė, S., Samulevičienė, M., and Jasulaitienė, V. (2009) Electrodeposition of tin from acidic sulphate solutions containing benzaldehyde. *Prot. Met.*, **45** (4), 455–460.

120. Frumkin, A. and Melik-Gaikasian, V.I. (1951) Determination of the kinetics of adsorption of organic substances by measuring the capacitance and conductivity of the electrode-solution boundary by alternating current. *Dokl. Akad. Nauk SSSR*, **77** (5), 855–858.

121. Melik-Gaikasian, V.I. (1952) The kinetics of adsorption of surface-active substances on the mercury electrode. *Zh. Fiz. Khim.*, **26** (4), 560–580.

122. Armstrong, R.D., Race, W.P., and Thirsk, H.R. (1968) The kinetics of adsorption of neutral organic compounds at a mercury electrode. *J. Electroanal. Chem.*, **16** (4), 517–529.

123. Sluyters-Rehbach, M. and Sluyters, J. (1970) in *Electroanalytical Chemistry*, vol. **4** (ed A. Bard), Marcel Dekker, Inc., New York, p. 75.

124. Retter, U. and Jehring, H. (1973) Untersuchungen der adsorptionskinetik an der phasengrenze quecksilber/elektrolyt durch analoge sessung der doppelschichtadmittanz. *J. Electroanal. Chem.*, **46** (2), 375–380.

125. Survila, A., Mockus, Z., Kanapeckaitė, S., Grigucevičienė, A., and Stalnionis, G. (2012) EIS characterization of Sn|Sn(II), gluconic acid system. *Electrochim. Acta*, **85**, 594–599.

126. Sawyer, D.T. (1964) Metal-gluconate complexes. *Chem. Rev.*, **64** (6), 633–643.

127. Vasantha, V.S. and Muralidharan, V.S. (1994) Electrochemical behaviour of zinc gluconate complexes. *Proc. Indian Acad. Sci. (Chem. Sci.)*, **106** (4), 825–836.

128. Vasantha, V.S., Pushpavanam, M., and Muralidharan, V.S. (1995) Electrodeposition and dissolution of Sn-Zn alloy films on glassy carbon. *Proc. Indian Acad. Sci. (Chem. Sci.)*, **107** (5), 581–591.

129. Vasantha, V.S., Pushpavanam, M., Kamaraj, P., and Muralidharan, V.S. (1996) Role of peptone in the electrodeposition of tin and tin-zinc alloys from neutral gluconate bath. *Trans. IMF*, **74**, 28–32.

130. Guaus, E. and Torrent-Burgu'es, J. (2003) Tin-zinc electrodeposition from sulphate-gluconate baths. *J. Electroanal. Chem.*, **549**, 25–36.

131. Ortiz-Aparicio, J.L., Meas, Y., Trejo, G., Ortega, R., Chapman, T.W., Chainet, E., and Ozil, P. (2011) Effect of aromatic aldehydes on the electrodeposition of ZnCo alloy from cyanide-free alkaline-gluconate electrolytes. *J. Appl. Electrochem.*, **41** (6), 669–679.

132. Cannan, R.K. and Kibrick, A. (1938) Complex formation between carboxylic acids and divalent metal cations. *J. Am. Chem. Soc.*, **60** (10), 2314–2320.

133. Eby, G.A. (2004) Zinc lozenges: cold cure or candy? Solution chemistry determinations. *Biosci. Rep.*, **24**, 23–39.

134. Juškėnas, R., Karpavičienė, V., Pakštas, V., Selskis, A., and Kapočius, V. (2007) Electrochemical and XRD studies of Cu–Zn coatings electrodeposited in solution with D-mannitol. *J. Electroanal. Chem.*, **602** (2), 237–244.

135. Escandar, G.M. and Sala, L.F. (1992) Complexes of Cu (II) with d-aldonic and d-alduronic acids in aqueous solution. *Can. J. Chem.*, **70** (7), 2053–2057.

136. Gerisher, H. (1953) Kinetics of discharge of simple and complex zinc ions. *Z. Phys. Chem.*, **202** (3-4), 302–317.

137. Survila, A. and Žukauskaitė, A. (1995) Codeposition of copper and tin in the electrolysis of solutions of citrate complexes. *Elektrokhimiya*, **31** (11), 1254–1260.

9
Electrochemical Deposition of Alloys

Alloy plating is as old as the deposition of individual metals. Extensive studies have shown that the coatings obtained by codeposition of metals can show properties that are not obtained by employing single metals. It was also asserted that alloy deposits can have different properties in certain composition ranges. They can be harder, more corrosion or wear resistant, more protective of the underlying basis metal, superior with respect to magnetic properties, and better in antifriction applications. Nowadays, there is a strong trend toward replacing the individual metals by their alloys that offer wider spectrum of useful properties.

Though alloy deposition is subject to the same scientific principles as individual metal plating, thermodynamics and kinetics of codeposition processes are more complicated than that of the deposition of a single metal. Electrochemical deposition of more than one metal often results in formation of different microstructures and phases. Moreover, electrodeposited binary alloys may or may not be the same in phase structure as those formed by simple melting. Besides, electrodeposited phases are not always in the thermodynamic equilibrium.

The position of metals in the standard electrode potential series is one of the main factors that are responsible for the metal codeposition. When two metals of significantly different standard (or formal) potentials are deposited, the composition of the resulting alloy usually strongly depends on the deposition potential. The more noble metal will be usually reduced first. However, the ad-atoms of one metal that appear on the plated surface in the early stages of the deposition process can act as inhibitors for the deposition of the other metal ions. In this case, when the deposition of a more noble metal is inhibited, an anomalous codeposition is observed. For example, in the case of Zn–Co alloy deposition, preferential deposition of Zn occurs even though Co is nobler, and it should deposit preferentially. Such codeposition can be explained using a hydroxide suppression model. It assumes that $Zn(OH)_2$ is formed during deposition as a consequence of hydrogen evolution that raises the pH in the vicinity of the cathode. Zinc would deposit via an intermediate $Zn(OH)_2$ layer that is transient and not constant, whereas cobalt deposition takes place by discharge of Co^{2+} ions through the $Zn(OH)_2$ layer.

When the deposition of one metal makes possible the deposition of another metal, which cannot be reduced alone, the so-called induced codeposition is observed (e.g., deposition of W and Mo in the presence of an iron-group metal).

Electrochemistry of Metal Complexes: Applications from Electroplating to Oxide Layer Formation, First Edition.
Arvydas Survila.

Favorable conditions for codeposition of two metals, M_1 and M_2 (M_1 is assumed to be more noble), are usually achieved when their equilibrium potentials are close. Both $M_1|M_1^{n+}$ and $M_2|M_2^{n+}$ couples[1)] acquire the same equilibrium potential when the concentrations of M_1^{n+} and M_2^{n+} ions meet the condition:

$$\frac{[M_1^{n+}]}{[M_2^{n+}]} = \exp\left(-\frac{nF}{RT}\Delta E^{0/}\right), \tag{9.1}$$

where $\Delta E^{0/}$ is the difference between formal potentials of the aforementioned couples. Optimal concentrations of free metal ions can be adjusted using properly selected ligands. It is essential that the degree of complexation of more noble metal was respectively higher. For instance, in a mixed copper–zinc solution containing cyanide, the Cu^+ ion concentration can be reduced to the order of 10^{-18} mol dm^{-3} and the concentration ratio $[Zn^{2+}]/[Cu^+]$ will be made very large.

If this is impossible, codeposition of metals will proceed at sufficiently negative potentials falling into the region of limiting current of M_1^{n+} reduction. However, codeposition can be optimized bringing into play kinetic factors that enable to increase selectively the cathodic polarization of more noble metal M_1. This can be realized in the ligand-deficient solutions (see Chapter 4). When M_1^{n+} complexes are reduced, a certain amount of ligand is released at the electrode surface. This increases the complexation degree of other (less noble) metal, but its cathodic polarization remains sufficiently low.

Certain depolarization of M_2^{n+} reduction is expected, which is consistent with the energetic effects of alloy formation. A shift in the equilibrium potential value can be obtained from the thermodynamic relationship

$$\Delta E = -\frac{\Delta G}{nF}, \tag{9.2}$$

where ΔG is the partial Gibbs energy of the metal in the alloy, which is directly related to the change in activity of the metal when the alloy is formed. In general, the activity of a metal in an alloy is determined not only by the composition of the latter but also by the nature of the interaction between the components accompanying alloy formation. Hence, alloys having the same proportions of the components but different types of interaction may show different depolarization.

9.1 Mass Transport during the Codeposition of Metals

If mixed complexes containing metals to be codeposited are not formed in the solution, regularities of mass transport remain the same as considered in Chapter 3:

- the changes in total concentration of metal (c_M) subjected to reduction obey the same laws that are valid for M^{+n} ions in the absence of ligand;

1) It is assumed for simplicity that the charge numbers of both metal ions are the same.

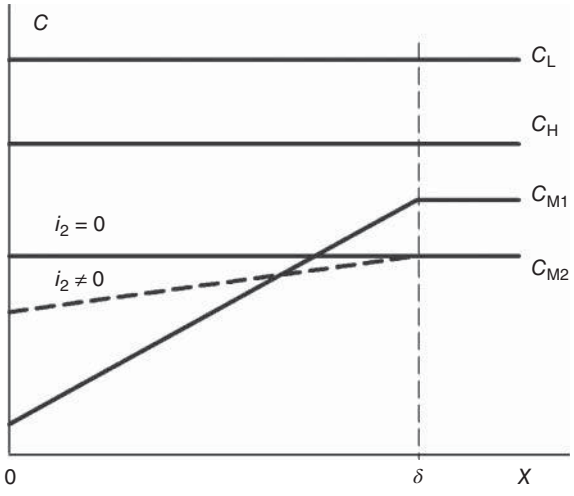

Figure 9.1 Concentration profiles in the steady-state diffusion layer under codeposition conditions. Two cases are shown: (a) less noble metal is not deposited ($i_2 = 0$) and (b) both metals are codeposited ($i_2 \neq 0$, dashed line).

- the total concentration of electrochemically inactive ligand (c_L) remains constant within the entire diffusion layer;
- the latter regularity is also valid for the total concentration of proton donors and acceptors (c_H).

An example of concentration profiles that are formed under steady-state conditions is presented in Figure 9.1. The total current consists of two partial currents whose densities (i_1 and i_2) are determined by gradients of the respective concentrations (c_{M1} and c_{M2}) at the electrode surface. Figure 9.1 reflects a situation when the reduction of more noble metal approaches a limiting current, because its surface concentration (c_{M1} at $x = 0$) is close to zero. The second partial process can be unavailable ($i_2 = 0$), or it can also take place (dashed line for c_{M2}).

When chemical interactions are sufficiently fast (labile complex system), concentration profiles of each component can be obtained from a set of four material balance equations written for both metals, ligand, and proton donors. Besides, partial current densities as functions of the overvoltage are required. When the surface concentrations are determined, partial normalized Tafel plots (NTPs) can be constructed and analyzed as described earlier (Section 5.2). Details of procedures used in the investigations of distinct systems are presented in the following sections.

9.2
Codeposition of Cobalt and Tin

Electrolytic deposition of tin and cobalt alloys has found extensive applications in modern electroplating. Some outstanding properties of tin such as nontoxicity,

high corrosion resistance, and good solderability are characteristics of most tin alloys. Cobalt and its alloys are widely used as typical magnetic materials applicable in various fields such as microelectromechanical system devices, magnetic recording head, reading heads, and data storage media. Codeposition of tin with another metal makes it possible to obtain coatings with additional useful properties. One example is Sn–Co alloy, which is noted for its increased hardness, color, and luster, similar to those of chromium coatings [1–5]. Though the first experiments of Sn–Co codeposition were performed in 1951 [6], it was until 20 years later that a commercially viable bath was produced [7, 8].

A great variety of compositions was tested. One group of solutions contained only simple inorganic salts such as sulfates, fluorides, chlorides, fluoroborates, pyrophosphates, and cyanides, which may be treated as weak ligands with the exception of the last two. Although fluoride forms comparatively weak complexes with Sn^{2+}, this effect inhibits the oxidation of Sn(II) to Sn(IV) [9]. Stronger complexes give rise to some undesirable phenomena. The use of cyanides, for example, those that are able to form stable complexes with Co(II), leads to a significant decrease in the Co content of the coatings [1].

Gluconate, glucoheptonate, tartrate, citrate, and some amines are organic ligands used in the plating baths [1–5, 10, 11]. To make coatings brighter, various additives, such as butynediol, sintanol, and formaldehyde, have been used [12–14]. It should be noted that it is possible to obtain bright coatings even in the absence of special brighteners [8, 10].

Attention in the investigations cited was focused on problems of an applied nature, underlining the influence of the solution composition and electrolysis conditions on the phase and elemental composition of coatings. A theoretical analysis of kinetics and the mechanism of electrode processes were often omitted. In this connection, we present next the main results of our investigations concerning the kinetics of codeposition of tin and cobalt in the solutions containing citric acid (LH_4) [15, 16].

When modeling codeposition of Sn and Co, the distribution of complexes and protonated species of ligand should be primarily estimated. Such data may be obtained through the solution of material balance equation as described in Chapter 1. In the case of acid solutions (pH < 7), the following basic equilibria should be taken into account first:

$$Sn^{2+} + pL^{4-} + qH^{+} \rightleftarrows SnL_pH_q^{2+q-4p}, \tag{9.3}$$

$$Co^{2+} + pL^{4-} + qH^{+} \rightleftarrows CoL_pH_q^{2+q-4p}, \tag{9.4}$$

$$L^{4-} + mH^{+} \rightleftarrows LH_m^{m-4}. \tag{9.5}$$

Constants of these equilibria are simply cumulative stability constants of the species given on the right side of Eqs. (9.3)–(9.5) (β_{pq}^{Sn}, β_{pq}^{Co}, and β_m^H, respectively). The data concerning Sn(II) and Co(II) citrate complexes are listed in Table 9.1; characteristics of different citrate anions are given in Table 8.4.

Table 9.1 Cumulative stability constants of Sn(II) and Co(II) citrate complexes used in simulations.

Equilibrium	Constant	log β
$Sn^{2+} + L^{4-} \rightleftarrows SnL^{2-}$	β_{10}^{Sn}	15.35 [17]
$Sn^{2+} + L^{4-} + H^{+} \rightleftarrows SnLH^{-}$	β_{11}^{Sn}	19.5 [17]
$Co^{2+} + L^{4-} + H^{+} \rightleftarrows CoLH^{-}$	β_{11}^{Co}	16.3 [18]
$Co^{2+} + L^{4-} + 2H^{+} \rightleftarrows CoLH_2$	β_{12}^{Co}	20.1 [18]

The stability of Sn(II)–citrate complexes was determined experimentally and was improved by means of potentiometry [17]. The values of β_{pq}^{Co} available in literature [18] depend, to some extent, on the nature of the supporting anion and on the ionic strength of solutions; however, they do not differ very much. The following analysis also showed that the content of other possible species ($Co(LH_2)_2^{2-}$, $Co(OH)^{+}$) does not exceed 0.01 mol% in the pH range from 3 to 7. This fact gives grounds to exclude them from consideration.

Stability constants of Sn(II) and Co(II) complexes form the following sequence: $\beta_{10}^{Sn} < \beta_{11}^{Co} < \beta_{11}^{Sn} < \beta_{12}^{Co}$ (Table 9.1). To predict the complexation levels of the two metals, model calculations are necessary, an example of which is presented in Figure 9.2. Equilibrium concentrations were obtained on the basis of the equations

$$[M^{2+}]\left(1 + \sum_{p} \beta_{pq}\left[L^{4-}\right]^{p}[H^{+}]^{q}\right) = c_M, \tag{9.6}$$

$$[M^{2+}]\sum_{p} p\beta_{pq}[L^{4-}]^{p}[H^{+}]^{q} + [L^{4-}]\left(1 + \sum_{m} \beta_{m}^{H}\left[H^{+}\right]^{m}\right) = c_L, \tag{9.7}$$

and were normalized to the total concentrations of respective metals. Thus, α_j represents the molar fraction of the complex, that is, $\alpha_j = [ML_pH_q^{2+q-4p}]/c_M$, where c_M is the total concentration of the metal (Sn(II) or Co(II)). In the case of ligand

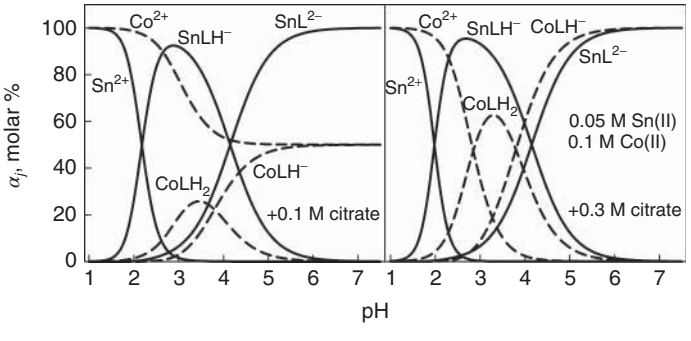

Figure 9.2 Distribution of Sn(II) (solid lines) and Co(II) (dashed lines) citrate complexes at low (a) and high (b) concentration of ligand.

deficit (Figure 9.2a), Sn(II) (its concentration is twice as low as that of Co(II)) is far better complexed, while the amount of Co^{2+} aqua-ions remains considerable. In the system with the excess of ligand (Figure 9.2b), most of Co(II) is also complexed at a sufficiently high pH. It is of interest to note that the increase in the ligand concentration has but inconsiderable impact on the distribution of Sn(II) complex species.

The data presented can be used to optimize the electrolyte composition. To bring the equilibrium potentials of Sn and Co closer, the concentration of the ligand (citrate) has to be chosen properly. In the limiting case, with these potentials being equal, it follows from Eq. (9.1) that $[Co^{2+}]/[Sn^{2+}]$ is of the order of 10^5. Though such a condition cannot be fulfilled for the citrate system, the potentials mentioned come close in solutions in which Sn(II) is complexed well and the major part of Co(II) exists in the form of aqua-ions. Such solutions should contain no excess of ligand in a slightly acid media (Figure 9.2a). Alkaline solutions are unstable due to the precipitation of hydroxides.

Two limiting currents are usually observed on voltammograms (Figure 9.3). First of them (attributable to the reduction of Sn(II)) contains a well-defined plateau, the height of which linearly depends on Sn(II) concentration (inset in Figure 9.3). A limiting current of Co(II) reduction is less pronounced under natural convection conditions (Figure 9.3), but it is well defined when the rotating disc electrode (RDE) is used (see Figure 9.6). It follows from the microanalysis of coatings (XPS data [16]) that Sn(II) reduction dominates up to its limiting current and Co(II) reduction starts at $E = -0.62\,\mathrm{V}$ when $c_{\mathrm{Sn(II)}} = 0.05\,\mathrm{M}$, $c_{\mathrm{Co(II)}} = 0.1\,\mathrm{M}$, and $c_{\mathrm{cit}} = 0.075\,\mathrm{M}$. The equilibrium potential of Co|Co(II) electrode, $E_{\mathrm{eq}}^{\mathrm{Co}}$, obtained with Nernst equation and the distribution data at $i = 0$, is equal to $-0.32\,\mathrm{V}$. Thus, the onset of Co(II) reduction is observed at E that is more negative by about 0.3 V as compared with $E_{\mathrm{eq}}^{\mathrm{Co}}$. In other words, Co(II) electroreduction starts with a significant polarization. Besides, experiments performed by recording reverse voltammograms of Co(II) reduction on the Sn substrate showed that potentials conforming to the condition of $i = 0$ do not coincide with those obtained during the reverse E sweeping. The latter potential corresponding to the cobalt-containing substrate is more positive by some hundred millivolts.

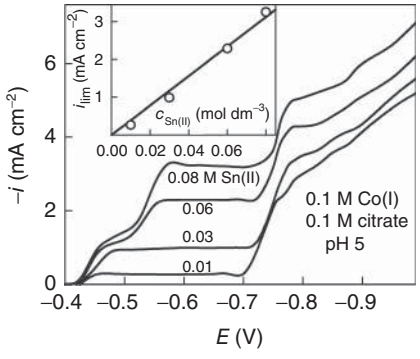

Figure 9.3 Voltammograms of Sn and Co codeposition recorded under natural convection conditions. $c_{\mathrm{Co(II)}} = 0.1\,\mathrm{M}$, $c_{\mathrm{cit}} = 0.1\,\mathrm{M}$, pH 5. Total concentration of Sn(II) (mol dm^{-3}) is indicated on the curves. Limiting currents of Sn(II) reduction versus Sn(II) concentration are plotted in the inset.

One reason for this effect could be the redistribution of system components at the electrode surface. Let us imagine that a small crystal of cobalt is inserted into a tin coating under open-circuit conditions. The comparison of equilibrium potentials with Nernst equations involving simulated $[Sn^{2+}]_b$ or $[Co^{2+}]_b$ yields that $E_{eq}^{Sn} > E_{eq}^{Co}$. As the open-circuit potential $E = E_{eq}^{Sn}$ (the surface area of tin is supposed to be much larger than that of cobalt), the cobalt crystal is polarized anodically and should be dissolved. A decrease in electrode potential E gives rise to Sn deposition and to release of a certain amount of ligand, which, in turn, reacts with Co^{2+} ions decreasing their surface concentration. Similarly, E_{eq}^{Co} may be determined by the Nernst equation involving $[Co^{2+}]_s$ as a function of current density i. According to the results of the simulation, the equality $E = E_{eq}^{Co} = -0.32\,V$ becomes valid at the certain i, which accounts for about 80% of limiting current of Sn(II) reduction. Consequently, Co(II) reduction is possible at the potentials that are more negative than E_{eq}^{Co} estimated for open-circuit conditions. Nevertheless, the effect under discussion seems to be weaker than the polarization of Co(II) reduction observed experimentally. We shall see next (Figure 9.4) that the changes in Co^{2+} surface concentration that determine the E_{eq}^{Co} value are not high.

Surface concentrations can be obtained making use of modified Eq. (9.3) (with $c_M(1 - i/i_d)$ instead of c_M) and unchanged Eq. (9.4) together with the relationship

$$[M^{2+}]\sum_q q\beta_{pq}[L^{4-}]^p[H^+]^q + [L^{4-}]\sum_m m\beta_m^H[H^+]^m + [H^+] - [OH^-] = c_H \quad (9.8)$$

(for details see Section 3.3). An example of the simulated data is given in Figure 9.4. As Sn(II) reduction is supposed to occur, changes in the surface concentrations of Sn(II)-containing species are evident. Release of free ligand particles, increase in the surface pH due to partial protonation of ligand, increase in the complexation degree at the electrode surface, and so on are the main phenomena associated with the Sn(II) reduction. Though the total surface concentration of Co(II) remains constant until Co(II) is reduced, the redistribution of particles containing Co(II) also takes place on the surface of the electrode.

As in the absence of Co(II) (Section 8.3.2, Figure 8.28), an abrupt decrease in $[Sn^{2+}]_s$, $[SnLH^-]_s$, and $[CoLH_2]_s$ also takes place. We have seen (Chapter 4) that

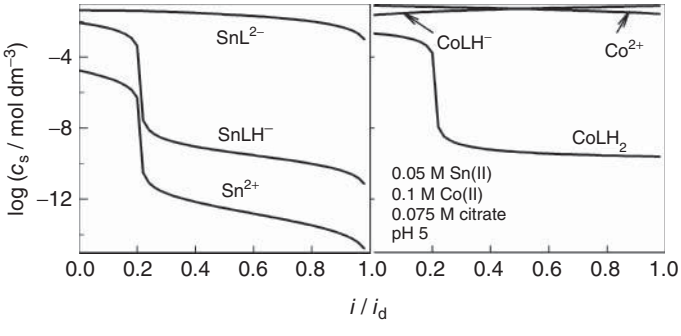

Figure 9.4 Distribution of complex species at the electrode surface versus normalized cathodic current density of Sn(II) reduction ($i_{Co} = 0$).

sharp c_s variations give rise to the emergence of prewaves; however, such regions were not detected in the total voltammograms of Sn and Co codeposition. We have pointed out in Chapter 5 that there is a limitation on electrically active complex (EAC) concentration caused by a finite rate of its generation. As seen from Figure 9.4, the concentrations of some species can fall to a rather low level. Then, the overlow amount of EAC will fail to yield current densities observed in the system. From this point of view, a change of the mechanism of Sn(II) reduction is possible.

SnL^{2-} species are predominant in the solution under discussion (Figure 9.4). When the cathodic current density is normalized to the ratio of $[SnL^{2-}]_s/[SnL^{2-}]_b$, the NTP obtained may be well approximated by the lines. Analysis of the partial process of the Co(II) reduction by means of the same procedures leads to the similar result: linear NTP can be also obtained for $CoLH^-$ reduction (Figure 9.5). Kinetic parameters (α_c and i_0) were obtained from the NTP slope and intercept, respectively. In the case of Co(II) reduction, the effective exchange current density ($i_0^{\text{eff}} = 0.5\,\text{mA cm}^{-2}$) was defined at $E = -0.62\,\text{V}$. These data were used in the calculation of the total voltammogram. In so doing, the limiting current of Sn(II) reduction served as a baseline for the voltammogram of Co(II) reduction. Simulation results are in good agreement with the experimental data (Figure 9.6).

As mentioned earlier, the degree of Sn(II) complexation should be much higher than that of Co(II) in the optimum case. Such condition can be reached in the system with ligand deficit where Sn(II) is properly complexed and most of the Co(II) is in the form of aqua-ions. This conclusion is substantiated by the elemental composition of Sn–Co coatings. For example, when ligand concentration is increased twofold (from 0.2 to 0.4 M) in the solution containing 0.05 M of Sn(II), 0.1 M of Co(II) at pH 5, the amount of Co in coatings decreases 10-fold (from 35 to 3.4 mass%). Moreover, coatings formed in the latter case are uneven and incompact. That is why 0.1 M concentration citrate may be chosen as optimum.

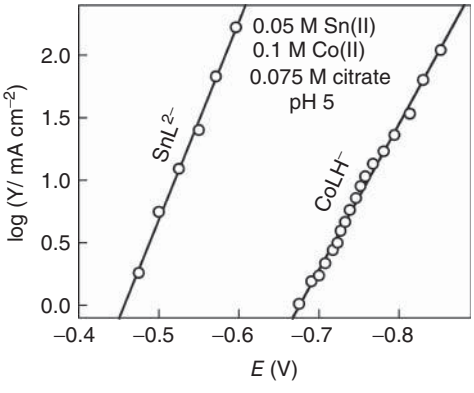

Figure 9.5 Tafel plots normalized to the ratio of c_s/c_b, where c is the respective concentration of the electrically active complex given at the plots. Transformation of RDE voltammetric data at 450 rpm.

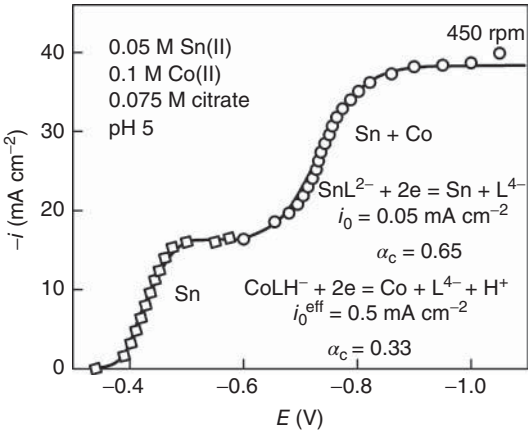

Figure 9.6 Comparison of RDE voltammogram obtained experimentally at 450 rpm (symbols) with that simulated with given kinetic parameters of Sn(II) and Co(II) codeposition.

It is important that the degree of Co(II) complexation should be low, because otherwise the evolution of hydrogen starts to dominate within the region of codeposition.

In this respect, pH is also of importance. If pH is too low, the effects of complexation become weaker. For example, the amount of a more negative component (Co) in coatings was found to decrease at pH 3 due to significant depolarization of H_2 observed in the acid medium. According to our evaluation, optimal pH varies from 4 to 5.9. Then, the amount of Co is stable within a rather large range of current densities.

It follows from model simulations that the surface pH increases notably with the cathodic current density. This effect results from corresponding shifts in the aforementioned equilibria and emerges even when hydrogen evolution does not occur. Then, $[Sn^{2+}][OH^-]^2$ or $[Co^{2+}][OH^-]^2$ products simulated for the electrode surface may exceed those determined by the stability constant (K_{so}) of $Sn(OH)_2$ and $Co(OH)_2$, respectively. Such data are presented in our article [17]. They give sufficient grounds to draw the conclusion about the possibility of forming metal hydroxides at certain current densities and the bulk pH. Hydroxides may form colloidal species and act as brighteners. Oversaturation of the surface layer should not be too high. This may be achieved by using H_3BO_3 as a buffer, which improves the structure of coatings.

The influence of Sn(II) concentration on the coating composition is seen from the data presented in Figure 9.7. Contents of Sn and Co vary almost linearly with $c_{Sn(II)}$. At the same time, the amount of oxygen included in the coatings increases with the content of Co. It was supposed [16] that the source of oxygen can be $Co(OH)_2$ formed at the electrode surface.

As has been mentioned earlier, codeposition of Sn and Co begins within the region of the limiting current of the first metal. Each metal forms separate phases

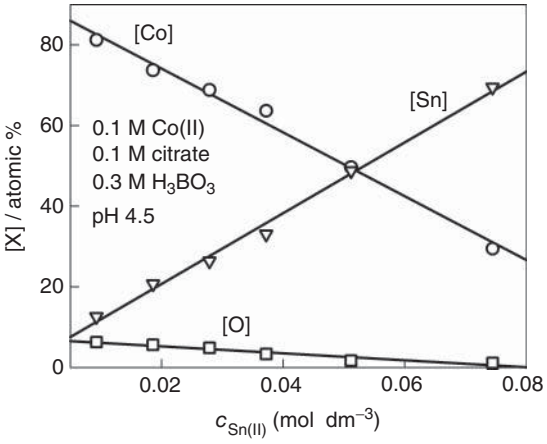

Figure 9.7 Variations of elemental composition in the surface of coatings deposited at 10 mA cm^{-2} from solutions containing different total concentration of Sn(II).

at initial stages of alloy crystallization, unevenly located in the coating. They can be observed visually as separate white (Sn) and deep gray (Co) zones. Evidently, Co forms a separate phase due to a considerable overvoltage of Co crystallization on foreign (Sn) substrate. With increase in the current density (when the potential becomes more negative), the amount of a deep gray (Co) phase increases as long as the compact coating containing about 80 mass% of Co is formed. This state corresponds to a fairly constant (about −0.9 V) potential although current densities can be different in solutions of different composition.

When cathodic polarization slightly increases and the alloy composition changes up to 76 mass% of Co, bright coatings are obtained. Quite a high rate of H_2 evolution can cause alkalization of the surface layer sufficient for $Co(OH)_2$ to form. This is corroborated by the data obtained by X-ray photoelectron spectroscopy [16] showing correlation between the amount of cobalt and

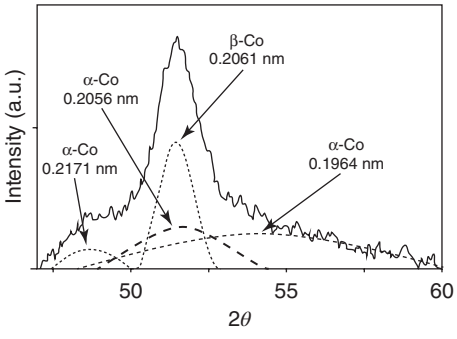

Figure 9.8 X-ray diffraction patterns of Sn–Co coatings containing 86 mass% of Co. The sample removed from the substrate.

oxygen in the surface of the coating (Figure 9.8). Oxygen binding energy was established to be equal to 531.2 eV; the same value can be attributed to both $Co(OH)_2$ and CoOOH. Etching of the electrode surface by Ar^+ shows that the amount of oxygen decreases with the thickness of the coating and tends to zero at the depth of 40 nm. Thus, the source of oxygen might be Co(II) hydroxides capable of forming gel-type aggregates, which, in turn, can cause the brightening effect.

Broad XRD peaks were observed within the scanned 2θ range. The maxima of the peaks correspond to the following d values: 0.2062, 0.1267, and 0.1079 nm, which may be attributed to the β-Co phase, as well as to that of α-Co. Figure 9.8 represents a fragment of XRD pattern of the Sn–Co coating containing 86 mass% of Co. This broad peak was analyzed using XRD peak separation program accounting for the Gaussian intensity distribution. As a result of the analysis, three broad peaks and one sharp peak were obtained. The maxima of the first three peaks correspond to the following d values: 0.2171, 0.2056, and 0.1964 nm. These peaks could be attributed to the α-Co phase with increased crystal lattice parameters caused by the replacement of some cobalt atoms having larger atomic radii. The sharp peak is attributable to the β-Co phase with increased crystal lattice. Thus, the Sn–Co coating containing 86 mass% of Co could be considered to be solid solution of tin in α-Co and β-Co. Both latter phases were found to be formed only in solutions of Co(II) containing some brighteners [19]. In contrast to the data reported in [11, 12], no evidence is available in XRD patterns for intermetallic Sn–Co phases such as γ'-Co_3Sn_2 or $CoSn_2$. The β-Sn phase is predominant in the coating containing 37 mass% of Co (Figure 9.9). There are some additional peaks: that of the Cu substrate and another that cannot be attributed to any known phase involving Co or Sn.

Sn–Co coatings containing from 15 to 86 mass% of Co can be obtained in solutions under discussion. The coating composition may also be adjusted by means of various surfactants, which exert a selective influence over the rate of partial processes.

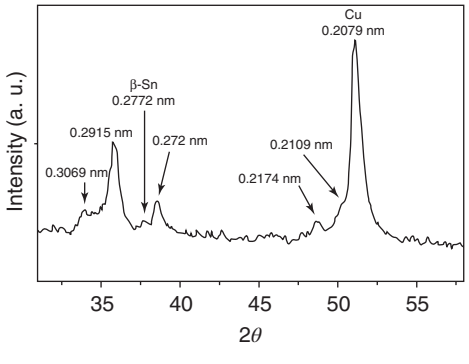

Figure 9.9 X-ray diffraction patterns of Sn–Co coatings containing 37 mass% of Co. Line of Cu comes from the substrate.

9.3
Deposition of Brass Coatings

Brass (Cu–Zn) coatings are widely used in industry because of their high corrosion resistance and attractive decorative properties. For a long time, commercial plating was based on toxic cyanide baths that have no comparable alternatives to the present. Therefore, brass electrodeposition, based on other eco-friendly Zn(II) and Cu(II) complexes, is of considerable interest. In this respect, different ligands, which can be used commercially without damage to the environment, have been tested. Mention should be made of noncyanide baths containing pyrophosphate [20–23], EDTA [24, 25], glycerol [26], and other polyalcohols [27, 28], as well as salts of organic acids such as citrate [29, 30], tartrate [31–33], or glucoheptonate [34, 35]. The last substance has also found its application in different processes including brass plating. It was found that the composition of the deposits obtained at pH 10 was almost constant over a wide current density range and this bath was recommended for commercial use. As glucoheptonate is very similar to gluconic acid, the latter substance has drawn our attention as promising ligand for brass plating [36, 37].

Distribution of the complexes and the ligand species can be obtained on the basis of material balance equations involving the respective stability constants. The composition of Cu(II) solutions containing gluconate and sulfate was analyzed earlier (Section 8.3.1, Figure 8.9); similar data for Zn(II) gluconate solutions are presented in Section 8.3.3. We used the same stability constants to obtain the distribution data in mixed Cu(II) and Zn(II) gluconate solutions (Figure 9.10). These data show that Zn(II) and Cu(II) sulfate complexes predominate in sufficiently acidic media. In weakly acidic solutions (pH > 5), gluconate anions L^- become predominant and this results in the increase in CuL^+ molar fraction.

Similar, but slightly weaker effect is also observed for less stable ZnL^+ complexes. In contrast to Cu(II) species, formation of OH-containing ZnLOH complexes becomes obvious at pH > 5. Simulations showed that the amounts of the remaining hydroxo-complexes are negligible, and they can be omitted from

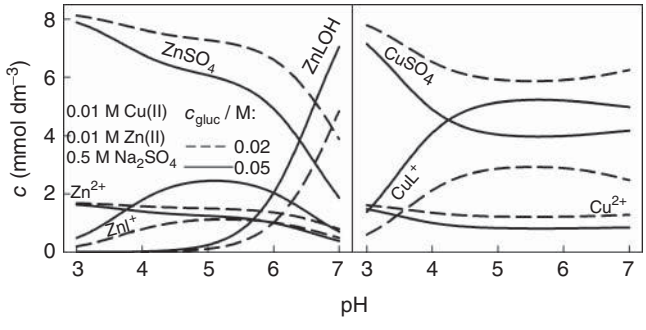

Figure 9.10 Distribution of complex species in 0.01 M Zn(II) + 0.01 M Cu(II) solutions containing 0.5 M Na_2SO_4 and gluconic acid with total concentration of 0.02 M (dashed lines) and 0.05 M (solid lines).

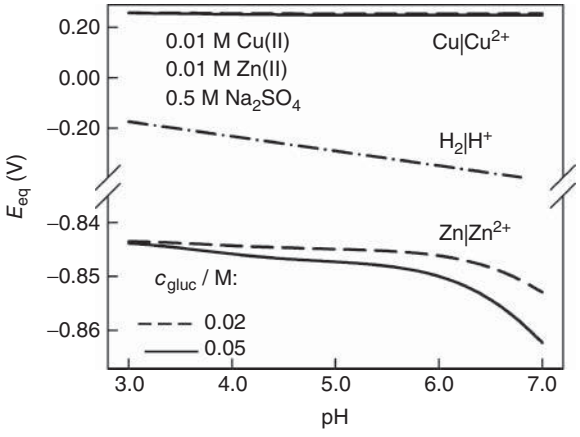

Figure 9.11 Equilibrium potentials of Cu|Cu^{2+} H_2|H^+ and of Zn|Zn^{2+} electrodes calculated from distribution data (Figure 9.10).

consideration. The distribution of the free ligand species is simpler and has no special features. Protonated species predominate at pH < 4, but their content falls in less acidic media giving place to the active forms of ligands. A similar regularity also applies to a lactone (Lac), the concentration of which remains ~20 times lower than that of LH.

As the complexation degree of system varies slightly over the wide pH range (3 < pH < 6), the equilibrium potentials of Cu|Cu^{2+} and Zn|Zn^{2+} electrodes actually stay at the same level (Figure 9.11). Positions of E_{eq} show that the Cu(II) reduction should be the first process occurring at the lowest cathodic polarizations. Further, the hydrogen evolution is thermodynamically permissible and the Zn(II) reduction is the last cathodic process possible at sufficiently negative potentials.

Kinetics of partial processes (Cu(II) and Zn(II) reduction) was discussed earlier. Hydrogen evolution is a side process undesirable in the brass electrodeposition. Its rate depends both on pH and ligand concentration, because gluconic acid is involved as a proton donor. Too intensive hydrogen evolution that is observed at pH < 4 results in unacceptably low current efficiencies. However, due to a high overvoltage, this process becomes tangible in metal-free solutions only at −0.65 V (Figure 9.12). Besides, its rate falls with solution pH. Therefore, in the studies of zinc and copper codeposition, we focused our attention on weakly acid media.

Favorable conditions for codeposition of two metals are usually achieved when their equilibrium potentials are close. However, this is not the case of Cu(II)-Zn(II) system, because the standard potentials of Zn|Zn^{2+} and Cu|Cu^{2+} electrodes are equal to −0.763 and 0.337 V, respectively, and are significantly different. However, a certain depolarization of Zn(II) reduction is expected that is consistent with the energetic effects of alloy formation. A shift of the equilibrium potential value can be obtained from the thermodynamic relationship (9.2). According to Ref. [38], ΔG averages −25 and −30 kJ mol^{-1} for brasses containing 20–30 at% of zinc. Then, Eq. (9.2) yields ΔE values in the range of 0.13–0.16 V. The result obtained

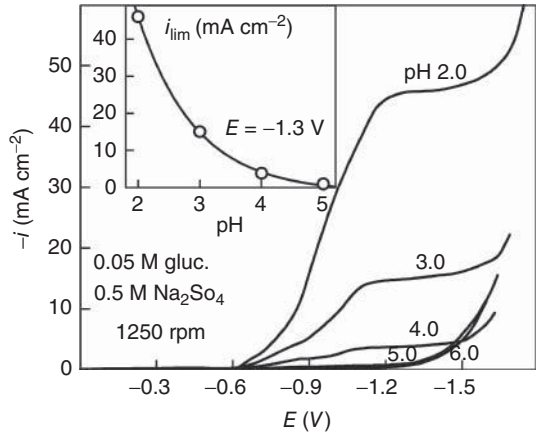

Figure 9.12 RDE voltammograms obtained for 0.05 M sodium gluconate solutions at pH indicated at the curves (Cu electrode, 1250 rpm). Limiting current densities (i_{lim}) versus pH are plotted in the inset.

shows that the certain depolarization is quite probable. However, the residual difference between equilibrium potentials (~0.8 V) cannot be compensated through the use of ligands, as stabilities of Zn(II) and Cu(II) complexes are rather similar. Therefore, the codeposition of zinc and copper is expected at sufficiently large overpotentials of Cu(II) reduction.

Net voltammograms obtained at $5 < pH < 7$ show a clear effect of the intensity of forced convection. This suggests that the diffusive mass transport is an important factor that controls the codeposition. Elemental analysis of coatings and measurements of the current efficiency were performed at constant potentials using RDE. The data obtained allowed us to split the net voltammograms into partial curves. It can be seen from Figure 9.13 that Cu(II) reduction is a single electrochemical process occurring at $-0.5 < E < 0$ V. If E is shifted to more negative values, the rate of Zn(II) reduction increases to a larger extent than copper codeposition. Therefore, the zinc content in the coatings increased with cathodic polarization. Such behavior is also observed at other gluconate concentrations (inset in Figure 9.13) over a wide region of potentials ($-1.05 < E < -0.5$ V).

Earlier (Section 8.3.1) we found that the rate of Cu(II) reduction falls radically with increasing pH. It is noteworthy that the same effect in mixed Cu(II) and Zn(II) gluconate solutions is observed (Figure 9.14). When pH increases, the rate of the net process falls over a wide region of potentials ranging up to −0.9 V. Such behavior is mainly conditioned by the suppression of Cu(II) reduction that takes place as pH increases. As the rate of hydrogen evolution also falls with pH, the limiting current of Zn(II) reduction becomes prominent at $E < -0.95$ V.

Comparison of voltammetric data obtained at the same RDE rotating velocities for Zn(II)-free and Zn(II)-containing Cu(II) solutions shows that in both cases, current densities are similar over a wide E region ranging up to −0.6 V. As pH increases, the rate of hydrogen evolution falls. Furthermore, the Cu(II) reduction

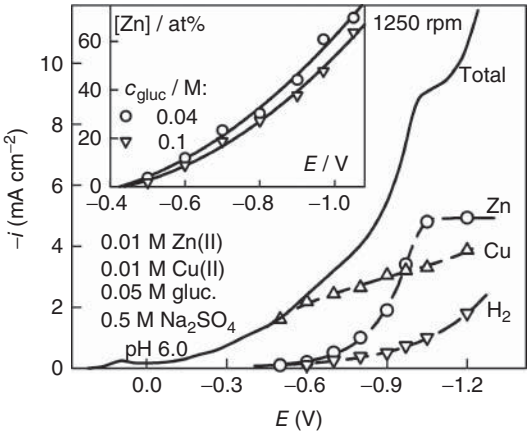

Figure 9.13 Net (solid line) and partial (symbols and dashed lines) voltammograms obtained for the solution of indicated composition. RDE: 1250 rpm. Zinc content in the coatings, obtained at other gluconate concentrations, is presented in the inset.

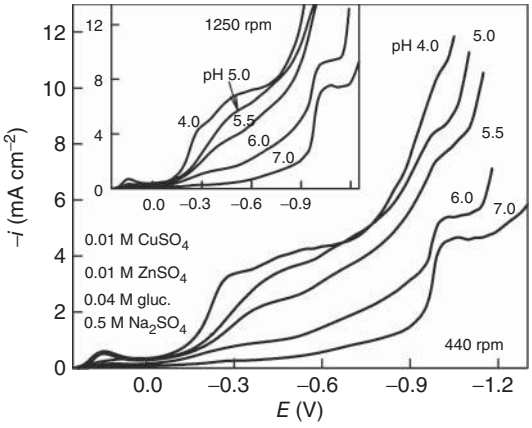

Figure 9.14 RDE voltammograms obtained for 0.05 M sodium gluconate solutions at pH indicated at the curves (Cu electrode, 1250 rpm). Limiting current densities (i_{lim}) versus pH are plotted in the inset.

is also suppressed in neutral media. Then, the Zn(II) reduction prevails at $E < -0.8$ V in mixed Cu(II) and Zn(II) solutions with well-defined limiting current located at $-1.15 < E < -0.95$ V (Figure 9.15).

When the currents of Cu(II) reduction and hydrogen evolution are eliminated from the net voltammograms, the residual plots are very similar to those obtained for Zn(II)–gluconate system (Figure 8.44) except for the UPD region. Similar effects have been observed in the case of Cu–Zn electrodeposition from glucoheptonate baths [34]. In contrast with Cu(II)-free solutions, the onset of Zn(II) reduction takes place at more positive potentials. The largest depolarization effect was observed at pH 6, when deposited zinc was detected even at −0.5 V.

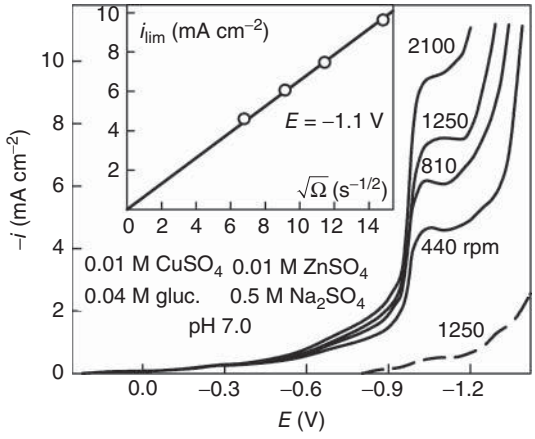

Figure 9.15 RDE voltammograms obtained for electrodes in mixed Cu(II) and Zn(II) gluconate solutions at pH 7.0 and different intensity of forced convection (solid lines). The dashed curve was obtained in the absence of Cu(II) and Zn(II). Limiting current densities in Levich coordinates are plotted in the inset.

For coatings obtained at pH 5, this effect was weaker and Zn(II) reduction began at about −0.72 V. The latter case is in agreement with the previous thermodynamic estimation.

The effect of gluconate varies with the electrode potential. When the cathodic polarization is sufficiently low ($E > -0.4$ V), a weak inhibition of Cu(II) reduction is observed with increasing c_{gluc} (Figure 9.16). Similar and stronger effects were also observed in the case of simple Cu(II) gluconate solutions at lower pH. For instance, gluconate gives rise to the substantial increase in cathodic polarization

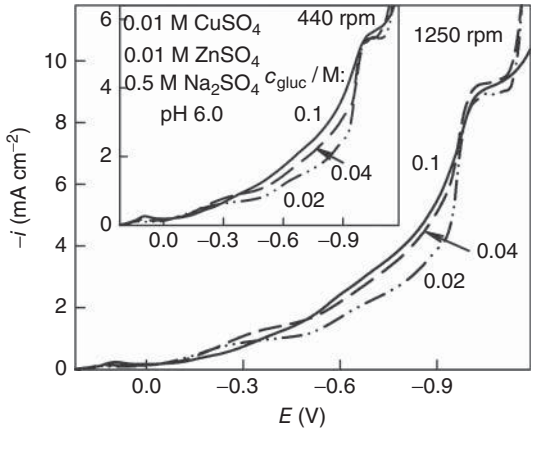

Figure 9.16 RDE voltammograms obtained at 440 (inset) and 1250 rpm for 0.01 M Zn(II) and Cu(II) solutions at different gluconate concentrations that are indicated at the respective curves.

at pH 3 over a similar potential region [39]. At pH 4, a shift in current peaks toward more negative E values is observed [40]. However, at more negative potentials ($-0.9 < E < -0.5$ V), gluconate shows an opposite effect and supports a certain augment in cathodic *i*. It should be noted that the coatings obtained in this potential range contain both zinc and copper. The effects observed can be associated with a competitive adsorption of gluconate and OH^- ions provided that the latter surfactant causes a stronger suppression of Zn and Cu codeposition. Similar effects were also observed in the Sn(II)–gluconate system where the reduction of Sn(II) was found to be accompanied by adsorption phenomena whose inhibitive character increased with solution pH [41, 42].

It can be concluded that the composition of Cu–Zn coatings should depend on both the solution composition and electrolysis parameters, and this is clearly seen from the EDS and XPS data. At 932.5 eV, Cu $2p_{3/2}$ XP spectra contain a peak that can be attributed to Cu^0 (metal state) and Cu_2O. In both cases, the binding energies (E_b) are identical and differ only by ~0.1 eV (see Ref. [43] and references therein). To distinguish between these cases, we made use of Auger $Cu(L_3M_{4,5}M_{4,5})$ spectra that showed two peaks of Cu and Cu_2O at 334.5 and 337 eV, respectively (Figure 9.17). The first binding energy is about 0.5 eV lower than that for pure copper. The change in this parameter can be treated as the E_b shift arising from the interaction between Cu and Zn in the brass lattice. Analogous variations were also observed in zinc spectra: with decreasing zinc content in the Cu–Zn alloy, the photoelectron and Auger peaks were shifted toward lower binding energies [43].

Likewise, both Zn and ZnO are indistinguishable in XP spectra, but their binding energies are well-separated in Auger spectra (Figure 9.18). Zinc in the form of ZnO prevails in the coatings deposited in the UPD region at −0.6 V. It has been

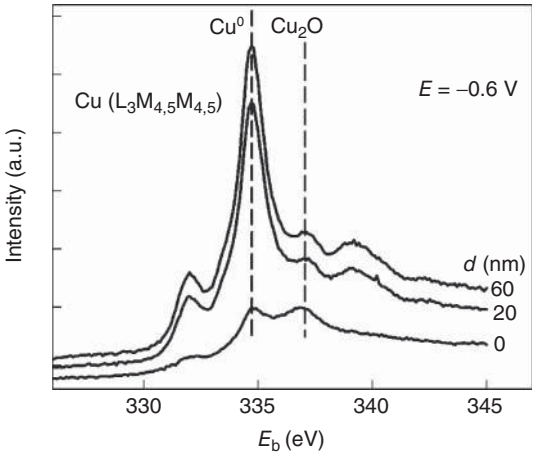

Figure 9.17 Auger spectra of Cu–Zn coatings deposited at −0.6 V in the solution containing 0.01 M Zn(II), 0.01 M Cu(II), and 0.5 M Na_2SO_4 at pH 6.0. The thickness (*d*) of surface layer deleted with Ar^+ beam is indicated at the respective curves.

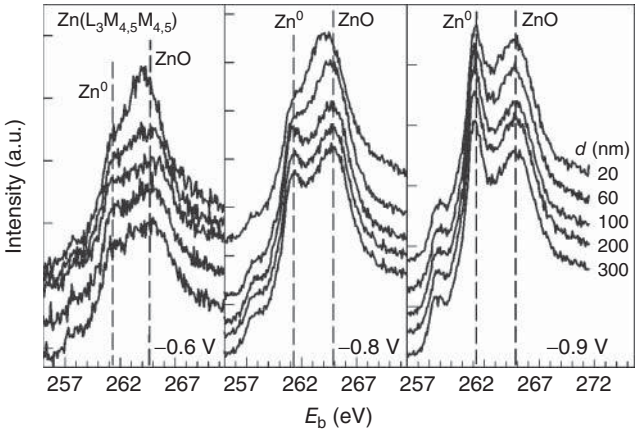

Figure 9.18 Auger spectra of Cu–Zn coatings deposited at the indicated potentials. The solution composition is the same as in Figure 9.17.

questioned in due time [26] whether or not Zn(II) can be fully reduced in non-cyanide solutions. Our experiments show that the metallic Zn^0 is clearly evident at −0.8 V and its amount increases with cathodic polarization. In the case of the solution under discussion, the estimated equilibrium potential of $Zn|Zn^{2+}$ electrode (E_{eq}) is about −0.86 V. According to the thermodynamic data that are discussed in Ref. [36], the underpotential deposition of zinc is possible at potentials that are by 0.13–0.16 V higher than E_{eq}. Then, the onset of zinc UPD is expected at −0.7 V. In relation to this, the reduced Zn^0 was really detected in the UPD region (Figure 9.18).

The Auger and XPS analysis combined with Ar^+ etching revealed the presence of Cu_2O in the surface layer. This oxide is absent in deeper layers, while ZnO persists throughout the coatings (Figure 9.19). On average, the coatings obtained at $-0.9 < E < -0.8$ V include ~3 at% of ZnO. A similar effect was observed in the case of Cu–Zn coatings electrodeposited in solution with D-mannitol [28]. XRD measurements evidenced the presence of ZnO in the whole volume of the coating. It was supposed that the origin of ZnO could be $Zn(OH)_2$ that accumulates at the electrode surface and incorporates into the coatings. Analogous phenomena are also possible in gluconate solutions. According to our estimations (Figure 8.45), the decomposition of ZnLOH complexes at the electrode surface may promote a significant local alkalization. For example, surface pH can be changed from 6 to 11, when cathodic current density increases. Then, $Zn(OH)_2$ can be easily formed and incorporated into porous deposits. This reasoning does not hold for Cu(II): very strong Cu(II)–gluconate complexes are formed in alkaline media [44] interfering with the hydroxide formation. Thus, the surface Cu_2O seems to arise from the interaction of the samples with air atmosphere.

Variations in the elemental composition of the coatings versus electrode potential (upper part of Figure 9.20, EDS data) are in satisfactory agreement with

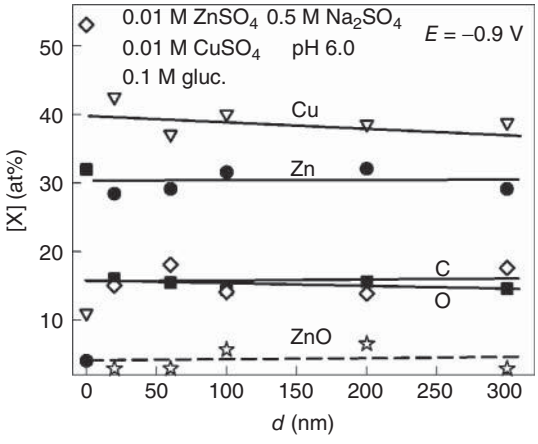

Figure 9.19 An example of distribution of elements at different depths (d) of Cu–Zn coatings deposited at −0.9 V in the solutions of indicated composition. The partial fraction of ZnO is shown by a dotted line.

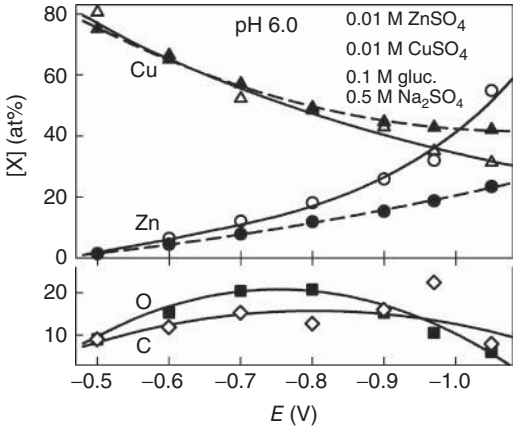

Figure 9.20 Upper part: distribution of copper and zinc in the coatings deposited at different potentials in sulfate-free (dotted lines) and sulfate-containing (solid lines) solutions. The content of carbon and oxygen is shown in the lower part. EDS data.

the respective XPS data. As the cathodic polarization increases, the rate of Zn(II) reduction increases as well. This observation is consistent with the disposition of partial voltammograms [36]. Effect of sulfate develops progressively with cathodic polarization. Diminution of Zn in the coatings, deposited in sulfate-free solutions, is accompanied by the respective increase in the content of oxygen (not shown).

It is remarkable that the deposits obtained under different conditions contain oxygen and carbon. XPS data show (Figure 9.19) that these side elements prevail on the surface of coatings, that is, at a depth $d \lesssim 20$ nm. However, they are also

Table 9.2 Binding energies detected in XP and Auger spectra.

XPS peak	Bond	E_b (eV)	Auger peak	Bond	E_b (eV)
Zn $2p_{3/2}$	Zn^0	1021.3–1021.7	Zn ($L_3M_{4,5}M_{4,5}$)	Zn^0	261.2–261.4
	ZnO	1022.1–1022.6	—	ZnO	264.0–265.4
Cu $2p_{3/2}$	Cu^0	932.3–932.5	Cu ($L_3M_{4,5}M_{4,5}$)	Cu^0	334.5–334.8
	Cu_2O	932.1–932.5	—	Cu_2O	336.8–337.1
	CuO	933.2–933.8	—	—	—
C 1s	C–C, C–H	284.3–285.1	—	—	—
	C–OH, C=O	285.4–286.6	—	—	—
	COO–	287.4–289.7	—	—	—
O 1s	O^{2-}	529.5–529.8	—	—	—
	C–OH, C=O	531.1–531.5	—	—	—
	H_2O_{ads}	532.0–533.0	—	—	—

present in deeper and more uniform layers, and this finding is supported by EDS data. It can be seen from the binding energies (Table 9.2) that the state of carbon in the coatings is very similar to that in gluconic acid.

In the case of sulfate-containing solutions (Figure 9.20, lower part), total amounts of impurities vary weakly with the potential and oxygen exceeds carbon over the E range where the formation of ZnO occurs. This regarding, it is possible to conclude that the ratio of the rest oxygen and carbon in the coatings is approximately equal to the [O]/[C] = 1.17 ratio in gluconic acid. This is in line with a concept suggested by us previously [36, 39] that the chemisorption of gluconate is accompanied by its partial destruction and the incorporation of ligand fragments into the deposits.

Required distribution of the elements in the coatings can also be adjusted by controlling the composition of the solution including gluconate concentration. An increase in c_{gluc} results in the relative suppression of Zn(II) reduction and in the respective enrichment of Cu–Zn deposits in copper. Besides, gluconate improves the qualitative characteristics of the deposits. When the molar gluconate concentration is four to five times higher than the total concentration of Zn(II) and Cu(II), compact brass coatings can be obtained over a wide potential region ($-0.97 < E - 0.6$ V) with the current efficiency ranging from 80 to 100%. The amount of Zn in the Cu-Zn phase varies from ~10 to 40%, as is in the brasses that are widely used in practice. In the case of solutions containing less (0.04 M) gluconate, this E range narrows ($-0.8 < E - 0.6$ V) and the trend has been toward greenish black powdery coatings. The granular Cu–Zn deposits are formed in this case (Figure 9.21, left side images). Their growth is characteristic of the solution with 0.04 M of gluconate (Figure 9.21, left side images). The cracking of the coatings was observed only at potentials less negative than −0.7 V. According to the scanning electron microscopy (SEM) images (Figure 9.21, right side), a higher concentration of gluconate in the solution (0.1 M) prevents the growth of granular deposits, especially at less negative potentials ($-0.9 < E < -0.6$ V). At −0.97 V,

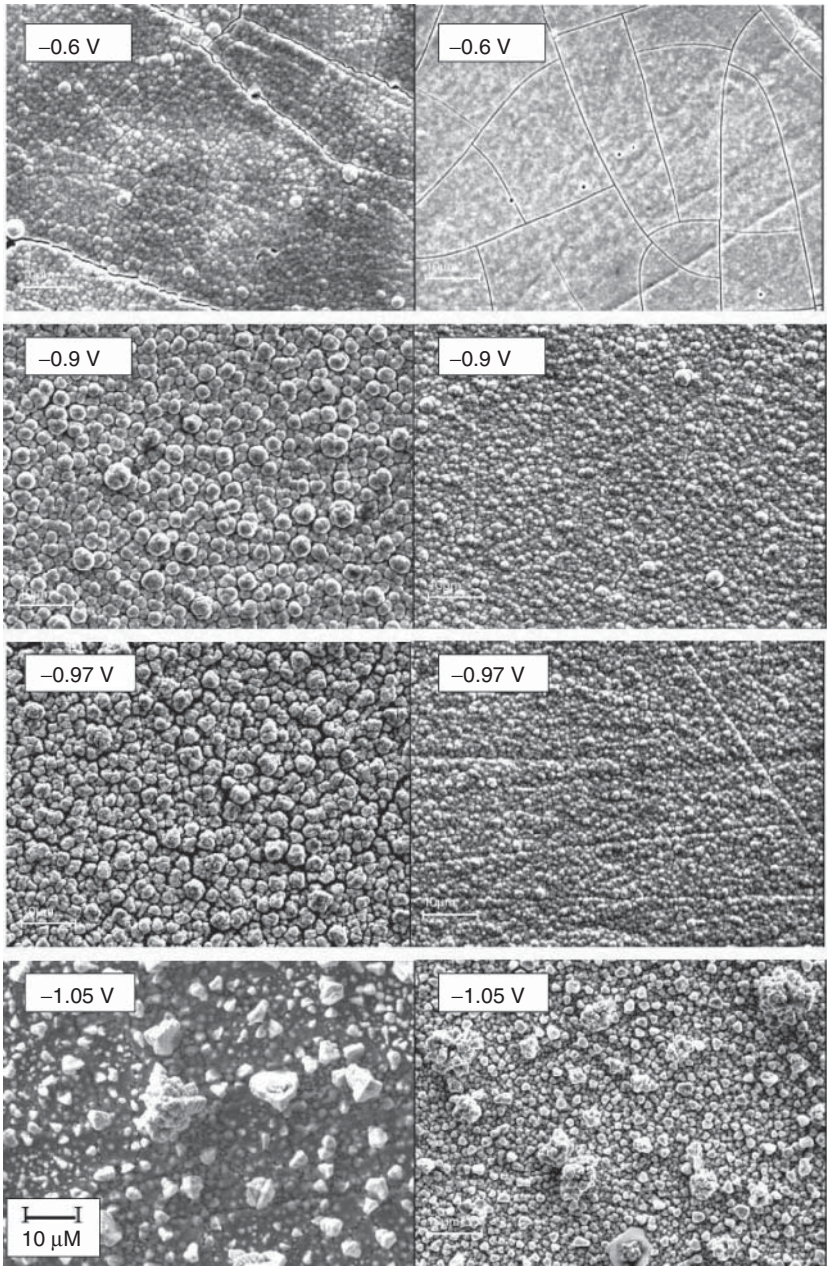

Figure 9.21 SEM images of Cu–Zn deposits obtained at the indicated potentials in the solution with 0.04 M (left side images) and 0.1 M (right side images) of gluconate.

dendritic deposits appeared. A higher quantity of Zn in the deposits obtained in the solutions with lower amount of gluconate as well as the morphology of the deposits indicate that gluconate hinders mostly the electrodeposition of zinc. The more pronounced granular growth could be responsible for the emergence of three Cu–Zn phases instead of two in the case of 0.1 M of gluconate.

The main Cu–Zn phases detected in various brass coatings are as follows:

- *α phase* is a solid solution of zinc in copper with copper crystal lattice *fcc*. The limiting solubility of zinc in copper is 39 wt%.
- *β phase* is an ordered solid solution based of the CuZn compound with an *scc* lattice.
- *γ phase* is Cu_5Zn_8 with a rhombohedral lattice.
- *ε phase* is $CuZn_3$ with a hexagonal closely packed lattice.
- *η phase* is a solid solution of copper in zinc with the crystal lattice of zinc (hexagonal structure).

The XRD patterns shown in Figure 9.22 testify that the Cu–Zn coatings electrodeposited at $-0.9 < E < -0.7$ V contain two phases: α-CuZn and pure Cu. The same phases were also detected in the coatings produced at lower c_{gluc} over the same potential range. In all cases, the α phase involves the saturated solid solution of Zn in copper containing 38.8 at% of Zn. At potentials less negative than the reversible potential of Zn reduction (−0.87 V), the Cu–Zn deposit is always comprised of α-CuZn and pure Cu. As can be seen from Figure 9.22, the amount of the latter phase decreases as the potential becomes more negative. Cu–Zn deposits formed at −0.97 V in the solution containing 0.04 M of gluconate include three phases: α, ε, and γ (Figure 9.23, lower pattern). Only α and ε phases were detected in the coatings deposited at the same potential in the solution with 0.1 M of gluconate. A reduced amount of Zn in the latter deposit could be the reason of the observed difference in the phase composition.

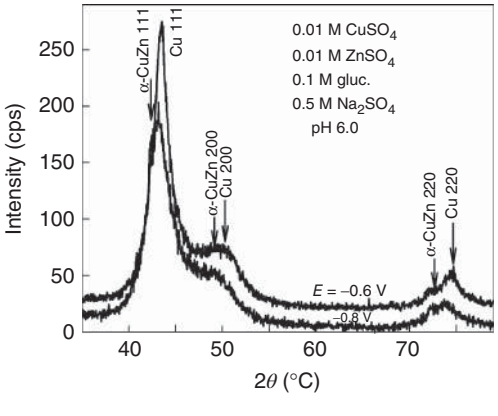

Figure 9.22 XRD patterns for CuZn coatings electrodeposited at different potentials in the electrolyte solution containing 0.1 M of gluconate.

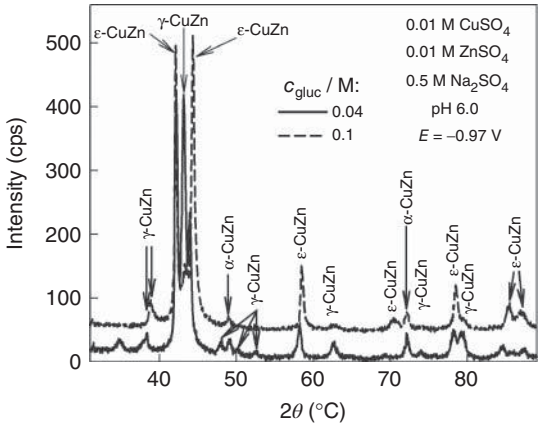

Figure 9.23 XRD patterns for Cu–Zn coatings electrodeposited at a potential of −0.97 V in the solutions with different amounts of gluconate.

9.4 Deposition of Bronze Coatings

Copper–tin alloys are among the most beneficial coatings that are used for various purposes. They show good solderability, malleability, and ductility and have good corrosion resistance. Besides, the coatings known as *yellow bronze* (containing 10–15 mass% of tin) confer excellent decorative properties to the substrate. To obtain the desired characteristics of bronze coatings, the control of Cu and Sn codeposition is of fundamental importance. For this purpose, different polyethers (operating as surfactants) in combination with some other organic compounds (brighteners, stabilizers, etc.) are widely employed in modern plating industry.

As we already mentioned, favorable conditions for codeposition of two metals are usually achieved when their equilibrium potentials are close. Standard potentials of the $Sn|Sn^{2+}$ and $Cu|Cu^{2+}$ electrodes are equal to −0.136 and 0.337 V, respectively, and Eq. (9.1) yields the ratio of $[Cu^{2+}]/[Sn^{2+}] = 10^{-16}$ that is too low to be profitably employed in a real system. At least we failed to find the ligand that could offer such high difference in complexation degree of Cu(II) and Sn(II). However, a certain depolarization of Sn(II) reduction determined by Eq. (9.2) is expected, which is consistent with the energetic effects of alloy formation. The so-called α-phase (supersaturated solid tin solution in copper) prevails in yellow bronze coatings, but the relevant thermodynamic data available in literature refer, as a rule, to high temperatures. With the aim of rough estimation of depolarization effect, ΔG values, given in [45] for 1000 K, were extrapolated to room temperature using the entropy of alloy formation [46] $\Delta S = 20\,\mathrm{J\,mol^{-1}\,K^{-1}}$. This procedure yields $\Delta G = 25\ \mathrm{kJ\,mol^{-1}}$ and $\Delta E = 0.13\,\mathrm{V}$. Similar use of thermodynamic data listed in Ref. [47] results in $\Delta E = 0.14\,\mathrm{V}$. Eventually, the data given in Ref. [48] for 25 °C allowed us to obtain the standard potential for the

electrode reaction:

$$3Sn^{2+} + 2Cu_3Sn + 6e = Cu_6Sn_5. \quad (9.9)$$

This quantity was found to be 0.18 V higher than that of $Sn|Sn^{2+}$electrode. The results obtained show that certain depolarization is quite probable. The rest difference between the equilibrium potentials (~0.3 V) might be compensated through the proper use of ligands that could produce strong Cu(II) complexes but display a sufficiently lower affinity to Sn^{2+} ions (stability constant of Cu(II) complexes should be higher by ~10 orders of magnitude). In our opinion, a real solution of this problem lies ahead. From the aforementioned details, it might be assumed that the kinetic control of electrochemical reduction is gaining in importance. The use of surfactants that selectively influence partial processes offers possibilities for effective control of metal codeposition.

Recently, much attention was focused on the role of polyethers in deposition processes [49–74]; however, for the most part, these investigations are concerned with single metals. Most concepts of copper electrodeposition that were elaborated at the end of the twentieth century (see reviews [62, 63]) have been acceptable up to now. Our investigations [75–88] dealt with ethylene glycol, its oligomers, and polyethylene glycols (PEGs) with the common formula $HO(-CH_2-CH_2-O)_m-H$. The number *m* covered the range from 1 to 900. Besides, polyethers laprol and sintanol that are used in industrial baths were studied. The former surfactant is a block-polymer of ethylene and propylene glycols with common formula X–O–X, in which the fragment X represents the chain $-[CH_2-CH(CH_3)-O]_{10}-[(C_2H_4-O)_{12}-CH_2-CH(CH_3)-O]_2-H$. Another surfactant $C_nH_{2n+1}-O-(C_2H_4-O-)_mH$ ($n = 10-12$, $m = 8-10$) is known as *sintanol DS-10* in Russia; Hoechst in Germany also produced similar substance, Pegepal C. Due to a comparatively long hydrocarbon radical C_nH_{2n+1}, this substance acts as an effective wetting agent and inhibitor for plating of tin and its alloys. The main purpose was to reveal the kinetic regularities of partial processes occurring in the Cu|Cu(II) and Sn|Sn(II) systems and to establish to what degree the observed regularities may be applied for copper and tin codeposition. Special attention was paid to the adsorption behavior of surfactants on Cu and Sn electrodes, emphasizing the role of their molecular mass (the length of hydrocarbon chain) in inhibition processes.

9.4.1
Surface Activity of Polyethers on Copper and Tin Substrates

Voltammetric and EIS data show that the adsorption ability of polyethers on copper and tin substrates is quite different. Voltammograms obtained for Cu(II) solutions that are carefully protected from chloride impurities contain well-defined plateaus of limiting current (Figure 9.24). Background currents are minor up to −0.4 V, where the hydrogen evolution becomes tangible. No pronounced effect of polyethers on the kinetics of Cu(II) reduction is observed. The results obtained are also in agreement with EIS data: the polyethers under investigation show a

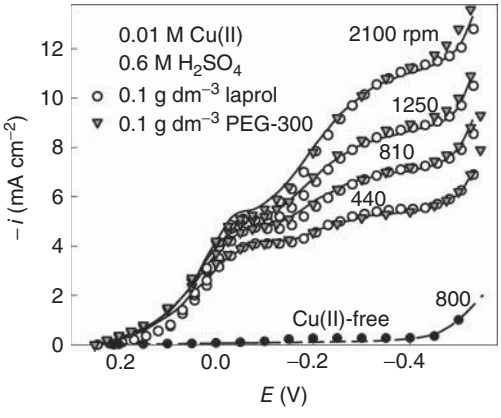

Figure 9.24 Cathodic voltammograms obtained for polyether-free Cu(II) solutions (lines) and in the presence of laprol (circles) or PEG-300 (triangles). Rotation velocity of RDE (revolutions per minute) is indicated at the respective curve. Voltammograms for Cu(II)-free 0.6 M H_2SO_4 solutions were obtained in the absence (line) and in the presence of laprol (circles).

minor effect on impedance spectra both in the Cu(II)-free and Cu(II)-containing solutions and the double layer capacitance (C_{dl}) remains actually on the same level, namely ~90 μF cm^{-2} at the open-circuit potential $E_{oc} = 0.25$ V [75]. Hence, polyethers show a rather weak adsorption in the absence of chloride ions. Moreover, the presence of Cu(II) in the solution is also required to initiate the inhibitive adsorption of such surfactants [58]. Then, the formation of multiple surface layers that represent a barrier to electron transfer becomes possible. It may be deduced that discrepancies in literature data [51, 53, 56, 58, 62, 63] concerning Cu(II) systems seem to arise from a poor control of the purity of solutions.

RDE voltammograms of Sn(II) reduction obtained for the surfactant-free solutions are nearly reversible. They contain the plateau of limiting current (i_d) that obeys Levich equation with the diffusion coefficient $D = 6.2 \times 10^{-6}$ cm^2 s^{-1}. In contrast to copper system, just small amounts of polyether exhibit a significant effect on the rate of Sn(II) reduction over a wide range of potentials (Figure 9.25). At the same time, the Sn|Sn(II) systems cease to obey the regularities of diffusive mass transport, when the concentration of surfactant is increased. The effect of the intensity of forced convection reduces progressively with the surfactant concentration (c) and becomes negligible at sufficiently low c (see inset in Figure 9.25). The results obtained show that the Sn(II) reduction acquires indications of adsorption-controlled regime.

The inhibition activity of surfactants can be also revealed from impedance data (Figure 9.26). Nyquist plots obtained for polyether-free solutions at open-circuit potentials are nothing else than lines that are observed over a nearly entire range of applied frequencies. In accordance with voltammetric data, Sn(II) reduction is mainly controlled by diffusive mass transport in this case. The addition

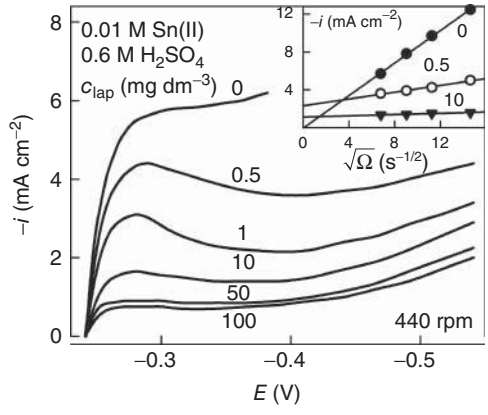

Figure 9.25 Cathodic voltammograms obtained at 440 rpm for 0.01 M Sn(II) solutions containing laprol, the concentration of which (mg dm^{-3}) is given at the respective curve. The effect of the intensity of forced convection at −0.38 V is presented in the inset in Levich coordinates.

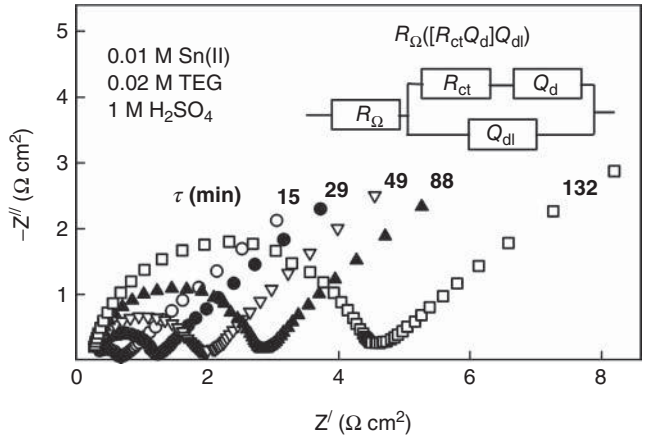

Figure 9.26 Equivalent circuit and Nyquist plots obtained at different exposure times τ of tin electrode in 0.01 M Sn(II) solutions containing 0.02 M of tetraethylene glycol (TEG). The open-circuit potential $E_{oc} = -0.25$ V is applied.

of polyether gives rise to a semicircle observed at simultaneous decrease in double-layer capacitance. The latter effect is observed for both Sn(II)-containing and Sn(II)-free solutions. For instance, C_{dl} decreases approximately six times when only 1 mg dm^{-3} of laprol is added into Sn(II)-free solutions and falls up to ~13 μF cm^{-2} at $c_{lap} = 0.1$ g dm^{-3} (open-circuit conditions, $E_{oc} = -0.26$ V) [88]. Somewhat higher C_{dl} values (~17 μF cm^{-2}) were obtained for laprol-containing solutions at $E_{oc} = -0.24$ V. The same order of C_{dl} magnitude remains at sufficiently low ($E > -0.29$ V) or high ($E < -0.4$ V) cathodic polarizations [76] (see

Figure 9.25). However, considerably stronger inhibition effects emerge at the potentials of negative slope of voltammograms ($-0.33 < E < -0.30$ V). In this case, C_{dl} falls to $7-9\,\mu F\,cm^{-2}$ and Z' acquires highly negative values ranging from -2.3 to $-4.5\,k\Omega\,cm^2$. Similar behavior is also typical of other polyethers [79, 85].

It should be noted that the semicircle part of Nyquist plots develops with the exposure time τ (Figure 9.26). Such plots are typical of the processes the rate of which is controlled by charge transfer and diffusive mass transport simultaneously. Impedance spectra obtained for Sn(II) solutions can be described with a frequency error less than 2% by means of equivalent circuit, the description code of which is $R_\Omega([R_{ct}Q_d]Q_{dl})$ (see Figure 9.26). Here, elements in series are given in square brackets and elements in parallel are enclosed in parentheses. The ohmic resistance of the solutions R_Ω was found to be actually independent of tetraethylene glycol (TEG) concentration and equal to $0.24 \pm 0.01\,\Omega\,cm^2$. Diffusion and double-layer impedances are presented by the constant phase elements (CPEs) Q_d and Q_{dl}, respectively. Time-independent parameters of Q_d were found to be as follows: $Y_0 = 0.37 \pm 0.02\,\Omega^{-1}\,cm^{-2}\,s^n$ with $n = 0.48 \pm 0.02$. The value of Warburg coefficient calculated for the 0.01 M Sn(II) solution with D given is equal to $0.384\,\Omega^{-1}\,cm^{-2}\,s^{0.5}$ and fairly coincides with the experimental value. The exponent n obtained for Q_{dl} varies between 0.88 and 0.91, this being indicative of a capacitive character of the double-layer impedance. According to the analysis performed, in contrast to R_Ω and Q_d, other elements (charge transfer resistance R_{ct} and double-layer impedance Q_{dl}) vary with time. Therefore, the exchange current density i_0, obtained from the well-known equation

$$i_0 = \frac{RT}{nFR_{ct}} \tag{9.10}$$

changes as well. The effective double-layer capacitance was calculated by the equation [89]:

$$C_{dl} = Y_0^{1/n}\left[\frac{1}{R_\Omega} + \frac{1}{R_{ct}}\right]^{(n-1)/n}. \tag{9.11}$$

The data in Figure 9.27 show an obvious correlation between the structure of the double layer and kinetics of Sn(II) reduction: both i_0 and C_{dl} vary in the same manner. The decrease in C_{dl} with time seems to arise from the progressive saturation of the interface with an adsorbed TEG, causing an increasing inhibition of tin reduction. This manifests itself in the respective lowering of the exchange current density. A more than 10-fold decrease in i_0 is observed after 2 h, as compared with the surfactant-free solution.

It should be noted that the adsorption of polyethers with a high molecular mass (laprol or sintanol) occurs significantly faster; a steady state can be attained in 5–10 min. The results obtained give grounds to suppose that the adsorption of surfactant is the main factor responsible for the inhibition of cathodic process. From this point of view, voltammetric data might be treated invoking a simple kinetic model. According to it, the active and passive sites with different current

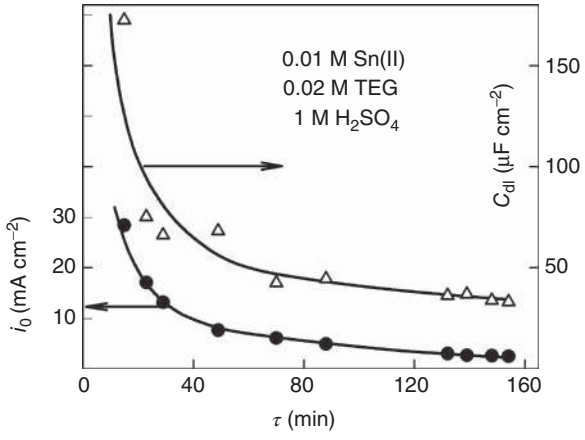

Figure 9.27 Variations of the exchange current density i_0 (ordinate to the left) and the effective double-layer capacitance C_{dl} (ordinate to the right). Sn electrode was kept for the time τ in the Sn(II) solution of indicated composition.

densities are formed on the electrode surface. Then, the surface coverage θ can be obtained from the relation

$$i = i_{\theta=0}(1-\theta) + i_{\theta=1}\theta, \tag{9.12}$$

where $i_{\theta=0}$ is the current density in the surfactant-free solution and $i_{\theta=1}$ concerns a fully saturated adsorption layer. The latter value can be obtained by linear extrapolation of values to $1/\sqrt{c} \rightarrow 0$. On the other hand, according to the model of two parallel capacitors [90], a quite identical equation (with C instead of i) is valid for double-layer capacitance. Thus, both voltammetric and impedance data may be used for determination of surface coverage. Appropriate experimental data were fitted to Frumkin isotherm

$$Bc = \frac{\theta}{1-\theta}\exp(-2a\theta), \tag{9.13}$$

where B is the adsorption constant and a is a parameter accounting for the interaction between adsorbed species (see Figure 9.28). In all cases, voltammetric data were obtained at ~−0.3 V; however, θ values, obtained for sintanol at the open-circuit potential (−0.242 V) from capacitance data, are very close. In all probability, adsorption parameters weakly depend on E in this region. It is interesting to note that the repulsive interaction between adsorbed molecules is specific to laprol and PEG-1000 ($a < 0$), whereas the attractive forces prevail in the adsorption layer formed by sintanol ($a > 0$). As mentioned earlier, the latter substance contains a comparatively long hydrocarbon chain. Note that positive a values are characteristic of similar aliphatic compounds [90]. Large variations in B quantities arise, for the most part, from different molecular masses of surfactants.

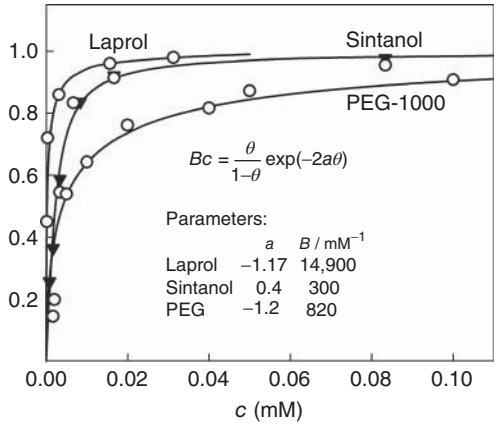

Figure 9.28 Adsorption isotherms obtained for tin electrode from impedance (triangles) and voltammetric (circles) data. Experimental data are fitted to Frumkin isotherm (solid lines) with the listed parameters.

9.4.2
Effect of Halides. Formation of Surface Complexes

Halides exert an essential influence on the adsorption of polyethers. It is particularly remarkable that this effect is quite different for copper and tin electrodes. Significant enhancement of adsorption resulting in the inhibition of Cu(II) reduction is observed in the Cu|Cu(II) system, whereas diminished polymer adsorption was found to occur in the case of tin electrode. This can be seen from the example shown in Figure 9.29. In the case of copper system, Nyquist plots take the shape of arcs centered below the abscissa axis. An addition of Cl^- ions gives rise to a decrease in impedance as compared to that obtained for halide-free solution (dashed lines in Figure 9.29). This result is in accordance with voltammetric data [75]: chloride diminishes the polarization of Cu(II) reduction. However, the rest halides (Br^- and I^-) increase the impedance over an entire range of the frequencies applied. An opposite effect can be seen in the case of tin system (lower part of Figure 9.29). Both enhancement and suppression effects intensify in the sequence: $Cl^- < Br^- < I^-$.

The EC N2 (see Figure 8.12) was used for analysis of experimental data. It has been found that i_{01} values, obtained for 0.01 M Cu(II) solution containing TEG and 30 μM Br^-, decrease with c_{TEG} from 40 to 10 μA cm^{-2}, whereas i_{02} remains on the same level equal to ~1 mA cm^{-2}. Inequality $i_{01} \ll i_{02}$ shows that the transfer of the first electron is the rate-determining step. Similar data have also shown that co-adsorption of halides and sintanol results in a more than 10-fold reduction in the double-layer capacitance. In the case of bromide-containing solutions [81], C_{dl} can decrease up to ~5 μF cm^{-2}.

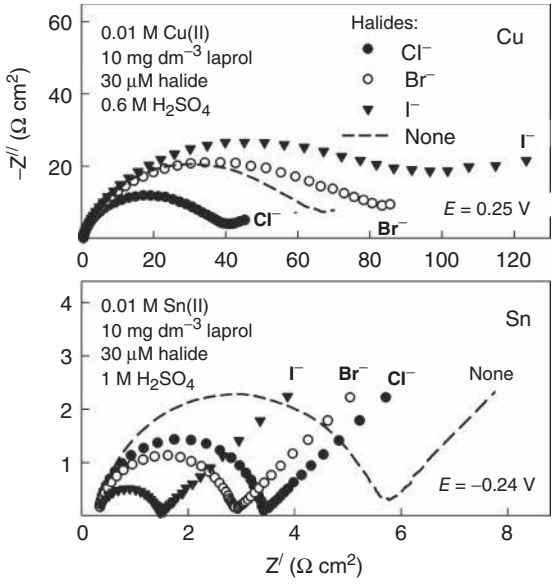

Figure 9.29 Comparison of Nyquist plots obtained for the copper (upper part) and tin (lower part) electrodes in 0.01 M Cu(II) or Sn(II) solutions containing laprol and 30 μM of different halides. Open-circuit conditions.

To obtain kinetic parameters, from voltammetric data, the rearranged kinetic relationship (5.22) was used:

$$i = 2i_{01}\left\{\exp\left(\frac{(2-\alpha_{c1})F}{RT}\eta\right) - \frac{[Cu^{2+}]_s}{[Cu^{2+}]_b}\exp\left(-\frac{\alpha_{c1}F}{RT}\eta\right)\right\} \tag{9.14}$$

which is valid at $i_{01} \ll i_{02}$. Expression for cathodic NTP is easily obtained from this equation using the relation (3.33):

$$\log\frac{|i|}{1-i/i_d} = \log 2i_{01} - \frac{\alpha_{c1}F}{2.303\,RT}\eta. \tag{9.15}$$

Voltammetric data, obtained for TEG-containing solutions, were transformed according to Eq. (9.15). Linear parts of NTP are observed over a certain range of potentials (Figure 9.30), where the normalized current density decreases with TEG concentration. It follows from NTP slopes that the cathodic charge transfer coefficient α_{c1} is equal to 0.50 ± 0.03 and 0.40 ± 0.02 for chloride- and bromide-containing solutions, respectively. The respective inhibiting action of TEG persists up to −0.03 and −0.1 V. Afterward, the process accelerates and i values approach those typical of surfactant-free solutions.

It is common knowledge that most organic compounds are adsorbed near the zero charge potential (E_{zc}), where the surface charge density is not too high. Different E_{zc} of copper electrode have been reported up to date. According to the results of the last investigations [91, 92] E_{zc} values, determined for the bare, specially

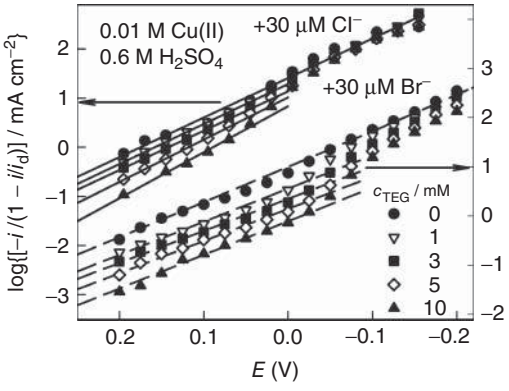

Figure 9.30 Normalized Tafel plots obtained for 0.01 M Cu(II) containing different amounts of tetraethylene glycol and 30 μM of chloride (upper part, ordinate to the left) or bromide (lower part, ordinate to the right).

renewed Cu surface, fall between −0.6 and −0.7 V. More positive values (close to 0 V), which were reported earlier by Yegorov and Novoselskij [93, 94], are now attributed to the presence of adsorbed oxygen on copper. It is highly probable that the most Cu electrodes, discussed herein, fall into the latter category. In this connection, some surface-enhanced Raman spectroscopy (SERS) experiments concerning the adsorption of anions are worthy of notice. According to Ref. [95], Cl^- ions are co-adsorbed with sulfate in 2M H_2SO_4 solutions at low overvoltages (at $-0.3 < E < 0$ V), while at high cathodic overvoltages, chloride is displaced by sulfate. Approximately the same range of specific (nonelectrostatic) Cl^- adsorption was established for Cu(II)-free perchlorate solutions [96]. SERS was also used to investigate copper electrode surfaces in the presence of Cl^- and PEG [58]. It was concluded that PEG can be adsorbed in two different forms. One predominates close to the open-circuit potentials (0.18 – 0.28 V) and may be a copper chloride complex with the PEG as a ligand. The other (simple neutral molecule) prevails at more negative potentials where chloride is desorbed. It is evident from Figure 9.30 that the region of TEG inhibitive adsorption clearly depends on the nature of halide. When Cl^- is replaced by Br^-, this region is shifted to more negative potentials by ~60 mV. It follows from C_{dl} measurements [94] that the E_{zc} of copper electrode are equal to 0.09, 0.025, −0.01, and −0.03 V in the presence of F^-, ClO_4^-, SO_4^{2-}, and Cl^- respectively; even a more negative value is plausible for bromide-containing solutions [93]. Keeping this in mind, it is safe to assume that desorption of halides is the main factor resulting in the destruction of the inhibitive adsorption layer. Then, the model [58, 73] might be accepted, according to which specifically adsorbed halides can act as species bridging the copper substrate with Cu(I) – polyether complexes, the formation of which is discussed elsewhere [62, 63] The possible structure of surface cluster is shown in Figure 9.31. Of course, this image needs special substantiation based on quantum-mechanics simulations.

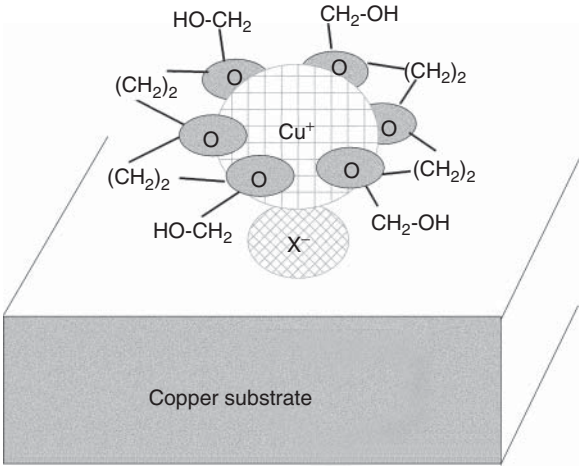

Figure 9.31 Image of surface cluster. Two TEG molecules form complex with Cu^+ ion that is attached to copper surface via specifically adsorbed halide X^-.

The aforementioned considerations seem to be hardly acceptable for tin, and the model of competitive adsorption is more suited in this case. If E_{zc} in the Sn|Sn(II) system is close to that established for perchlorate solutions [97] (−0.4 to −0.43 V), joint adsorption of both PEG and halide is possible over a wide potential region where Sn(II) reduction occurs (see Figure 9.25). Reasons for such different adsorption properties of Cu and Sn electrodes are not clear yet. Different hydrophilicity of copper and tin substrates might be among the factors responsible for the adsorption behavior of polyethers. According to [98], the hydrophilicity of metals should increase in the series: Sb, Bi < Pb, Tl, Hg < Sn, Cd < Ga < Zn < Ag < Au < Cu < Fe. This series is valid for polycrystalline surfaces of solid metals. It is obvious that the copper electrode is significantly more hydrophilic object as compared with tin. On the close-packed Cu[111] surface, the formation of cyclic water hexamers has been confirmed using low-temperature scanning tunneling microscopy and density functional theory calculations [99]. Due to a weaker adsorption of water on the tin surface, more favorable conditions are created for direct contact between PEG and metal, and the competitive adsorption of PEG and halides seems to occur. On the other hand, chloride-suppressed PEG adsorption was also observed [100] on the Pt electrode, and this effect increased with chloride concentration.

9.4.3
Effect of Length of the Hydrocarbon Chain

Among other factors that are responsible for PEG surface activity, the length of hydrocarbon chain seems to hold the lead. It has been established [101] that the binding strength between the adsorbed Cl^- and PEG is proportional to

the number of ether groups in PEG and the small PEG results in much more coverage defects than the large PEG. The effect of PEG molecular mass on its adsorption rate and the properties of adsorbates on platinum has been also considered [102].

Besides, PEG has been found to affect the kinetics of palladium deposition as well as both morphology and bulk properties of Pd deposits [103]: bulk defectiveness increased with the size of PEG molecules. Investigations of PEG role in electrodeposition of Zn–Cr alloys have shown [104] that large PEG molecules enhance Cr(III) reduction.

As mentioned earlier, the molecular mass of the surfactants under investigation varied in a wide range, beginning with ethylene glycol (EG) and its oligomers. In the case of copper electrode, a certain amount of halides was added in order to stimulate adsorption processes. It was established that experimental NTPs, obtained for EG-free solutions or in the presence of mono-, di-, and triethylene glycols, actually coincide and may be approximated by one line in a wide region of cathodic overvoltages. (Figure 9.32). Average exchange current density $i_{o1} = 0.13\,\mathrm{mA\,cm^{-2}}$ and $\alpha_{c1} = 0.4$ follow from these data. When TEG is added, the latter kinetic parameter remains approximately the same, but the exchange current density falls ~17 times. Uniform inhibitive effect of TEG is observed up to $\eta = -0.35$ V ($E = -0.1$ V) whereupon it becomes weaker due to the destruction of the adsorption layer. Kinetic parameters obtained from RDE voltammetric data are summarized in Table 9.3.

Hence, the inhibition properties of EG oligomers reveal themselves only in the presence of halides, if the number of ether oxygen atoms $m \geq 3$, that is, beginning with TEG. In this case, only the transfer of the first electron onto Cu^{2+} ions is affected. It should be noted that somewhat similar effects were found to occur on the Pt electrode [102]. According to this article, adsorption properties become distinct for PEGs with a molecular mass below 600. The main conclusion,

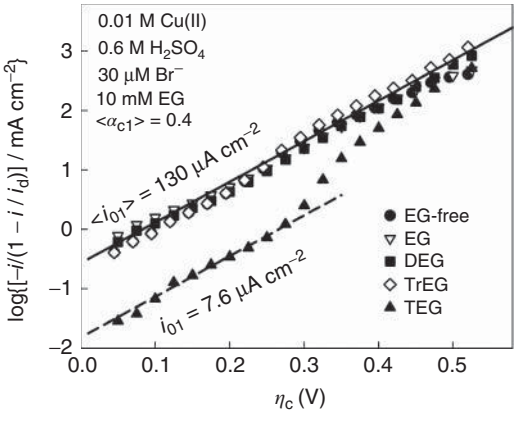

Figure 9.32 Cathodic RDE voltammograms transformed into NTP. 0.01 M Cu(II) solutions contain 10 mM of different EG oligomers as indicated.

Table 9.3 Effect of polyethylene glycols $HO-(CH_2-CH_2-O-)_mH$ on kinetic parameters of $Cu^{2+} + e \rightarrow Cu^{+}$ charge transfer process. 0.01 M Cu(II) solutions containing 30 μM Br^- and indicated quantities of PEG.

PEG	m	c_{PEG} (mg dm^{-3})	α_{c1}	i_{01} (μA cm^{-2})
TEG(PEG-200)	4	0	0.39	125
		200	0.39	37
		600	0.38	26
		1000	0.38	16
		2000	0.39	7.6
PEG-300	6–7	10	0.46	11
		100	0.46	3
		200	0.49	0.7
PEG-600	13	1	0.69	0.25
		2	0.59	1.2
		5	0.54	1.1
		10	0.54	0.7
		50	0.53	0.5
PEG-3000	68	0.1	0.51	21
		0.2	0.45	6.5
		0.3	0.51	0.2
		0.5	0.47	0.2

resulting from the above data, consists in the following: the inhibition degree of polyethers increases considerably with their molecular mass. To compare the exchange current densities, which fall drastically with the length of hydrocarbon chain, the molar concentration of each surfactant was multiplied by the number of unit chains ($-CH_2-CH_2-O-$) in it. In this way the "concentration of unit chains," c_{uc}, can be obtained. These data are presented in logarithmic coordinates in Figure 9.33. It can be seen that the inhibition activity of unit chain is different for each polyether and increases with the polymerization degree. Similar effects were also observed in the case of tin electrode. The inhibition activity of EG was evaluated from the impedance data. It was found that the shape of linear Nyquist plots does not actually change throughout 30 min in the presence of short EG oligomers (Figure 9.34). Close i_0 values (84 ± 4 mA cm^{-2}) were detected for these solutions. Only TEG showed an increased surface activity, giving rise to a small semicircle at high frequencies with $i_0 = 46$ mA cm^{-2}. This part of Nyquist plots becomes more pronounced at higher TEG concentrations. The inhibition activity of surfactants was estimated in a similar way: the i_0 values were normalized in respect to "1 mol of ethereal oxygen." According to the results obtained, the effect of molecules with 10–20 ethereal bonds is ~2000 times higher as compared with that of TEG. Thus, the length of hydrocarbon chain is also a prime factor responsible for the inhibition activity of polyethers on tin electrode.

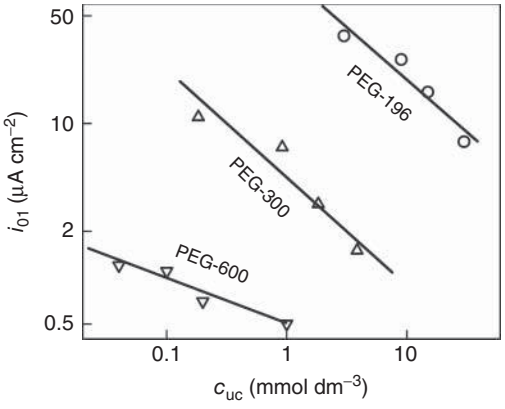

Figure 9.33 Variations of exchange current densities i_{01} obtained for 0.01 M Cu(II) solutions containing 30 μM Br^- and indicated PEGs. Their amount is transformed into "concentration of unit chains."

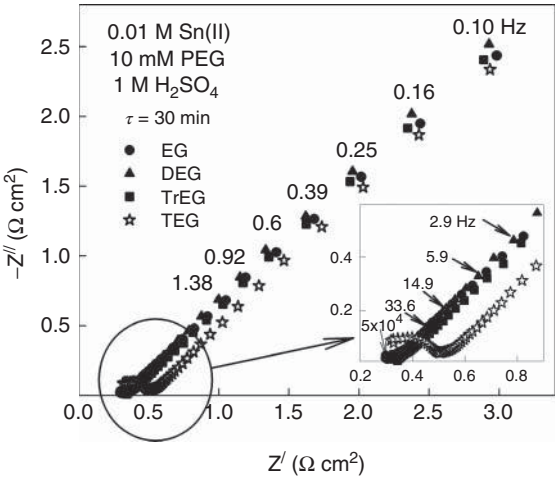

Figure 9.34 Nyquist plots obtained for tin electrode in 0.01 M Sn(II) solutions containing 0.01 M of different EG. High-frequency region is shown in the inset. Open-circuit potential $E_{oc} = -0.25$ V, exposure time $\tau = 30$ min.

9.4.4
Codeposition of Copper and Tin

Most of regularities that are typical of partial processes persist in the case of codeposition of Cu and Sn. Typical cathodic voltammograms are shown in Figure 9.35. Several regions corresponding to different electrochemical processes may be distinguished. Cu(II) reduction starts at its equilibrium potential equal to 0.24 V. It follows from Nernst equation that similar characteristic of $Sn|Sn^{2+}$ electrode is −0.24 V; therefore, the phase consisting of free tin should be stable at more

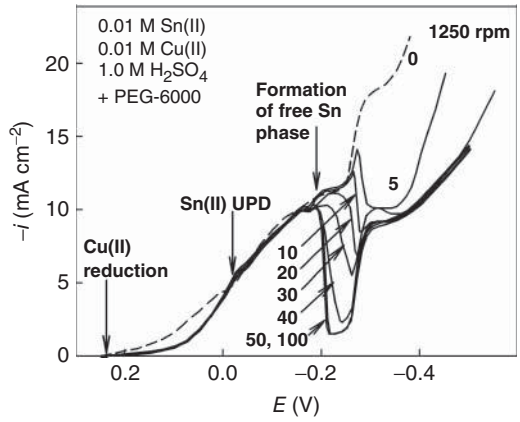

Figure 9.35 Effect of PEG-6000 on voltammograms of copper and tin codeposition. The concentrations of PEG (in mg dm^{-3}) are given at the respective curves. Cu-coated RDE, 1250 rpm.

negative potentials. Nevertheless, reduction of Sn(II) starts at ~0 V. Thus, codeposition of Cu and Sn starts with certain depolarization and with formation of specific Cu–Sn phases (see below).

To understand the peculiarities of voltammograms, some regularities regarding the partial processes of Cu(II) and Sn(II) reduction are expedient to invoke. As noted earlier, most polyethers do not show a noticeable inhibition activity on copper substrate in the absence of halides. Such behavior is also characteristic of other surfactants in mixed Cu(II) and Sn(II) solutions. However, when the $Sn|Sn^{2+}$ equilibrium potential is approached, the specific voltammetric minimum develops. The effect of surfactants becomes detectable at rather low concentrations (some mg dm^{-3}). Its depth depends both on their molecular mass and concentration and on the intensity of forced convection. This minimum deepens and the effect of forced convection weakens when the molecular mass of surfactant grows.

It was established that the formation of free tin phase followed by strong inhibitive adsorption is possible in this region. It is reasonable that this feature is absent in Sn(II)-free solutions. The minimum under discussion develops gradually on addition of small amounts of Sn(II), and its depth may be used as a measure of Sn(II) concentration in the presence of Sn(IV) [105]. Besides, anodic currents of Sn dissolution are observed in cyclic voltammograms at $E > -0.24$ V, when the reverse potential scan is applied (see below). An increase in current density arising at higher cathodic polarizations ($E < -0.4$ V) is concomitant with hydrogen evolution.

We have seen from the aforementioned details that halides show quite opposite effects on copper and tin electrodes. According to the impedance data [88], the adsorption properties of the yellow bronze appear much closer to those of copper if compared with tin. Halides in rather low (micromolar) concentrations have a perceptible effect on the codeposition process as well [78, 82]. Chlorides that

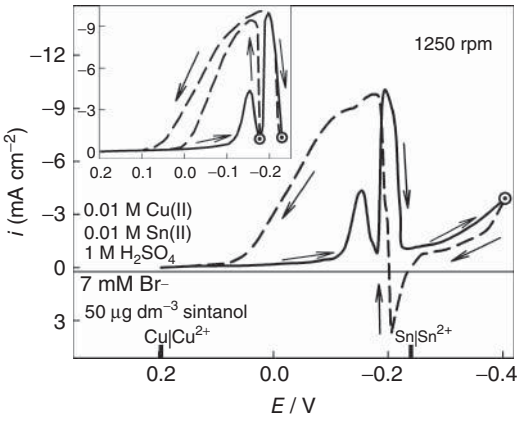

Figure 9.36 Cyclic voltammograms obtained for the solution of indicated composition. Direct and reverse scans are presented by solid and dashed lines, respectively. The onset of reverse scans is indicated by circles. The positions of equilibrium potentials of $Cu|Cu^{2+}$ and $Sn|Sn^{2+}$ electrodes are given on abscissa axis.

are often used in plating baths for improvement of anodic dissolution of copper increase to some extent the cathodic polarization and widen the current range of yellow bronze deposition. However, the tin content in the coatings increases in this case.

A drastically higher activity of bromide becomes evident at a concentration as low as 1–3 μM. By contrast, these ions narrow the range of yellow bronze deposition, lower the tin content in the coatings, and hinder the yellow bronze surface oxidation. The main feature of voltammetric behavior of bromides consists in the development of duplex current peak at $-0.1 < E < -0.2$ V (Figures 9.36 and 9.37). The height of both left (i_{p1}) and right (i_{p2}) peak decreases with bromide concentration, and this double structure vanishes at $[Br^-] > 30$ μM. Both current maxima clearly depend on the intensity of forced convection (Figure 9.37). Moreover, both i_{p1} and i_{p2} vary linearly with $\sqrt{\Omega}$ (Ω is an angular rotating velocity of RDE) and the approximating lines pass through the origin (see the inset in Figure 9.37). At relatively low bromide concentrations ($[Br^-] < 7$ μM), i_{p2} actually coincides with limiting current density of Cu(II) reduction ($i_{d,Cu}$) that is also given in the inset of Figure 9.37. Some difference between i_{p2} and $i_{d,Cu}$ is conditioned by partial current of Sn(II) reduction that starts at about −0.1 V in bromide-containing solutions. All these experimental data show that the partial process of Cu(II) reduction, which is commonly controlled by charge transfer and diffusion, encounters a strong inhibition in two regions. The first of them lies between i_{p1} and $i_{p2,}$ and the second region is located at $E < -0.24$ V.

It should be emphasized that the first inhibition region is well pronounced under forced convection conditions and is easily reproduced when the record of voltammograms is performed with tight control of rotating and scan parameters.

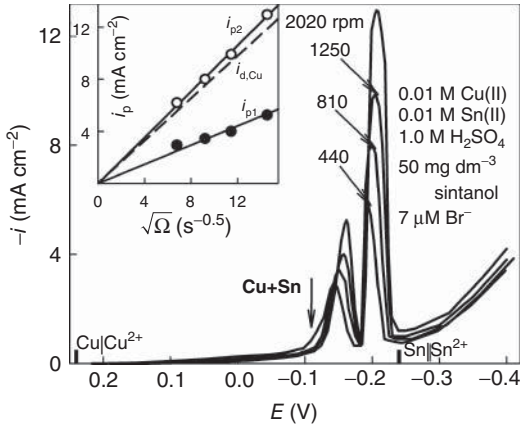

Figure 9.37 Effect of forced convection on voltammograms recorded using rotating disc electrode (RDE) at different reverses per minute (rpm). The positions of equilibrium potentials of $Cu|Cu^{2+}$ and $Sn|Sn^{2+}$ electrodes are given on abscissa axis. The inset demonstrates the Levich behavior of peak currents. The dashed line represents limiting currents obtained for Cu(II) reduction in Sn(II)-free solutions.

Attempts to interrupt the direct (cathodic) scan of the potential in the region of the first minimum and to fix it at −0.15 V causes rather fast (taking some seconds) rise of cathodic current from minimum value up to $i_{d,Cu}$. Such is not the case of the second characteristic minimum located at $E < -0.24$ V where the cathodic currents offer quite high stability.

Cyclic voltammograms obtained in the solutions under discussion acquire a peculiar shape. A fast rise of cathodic current and no further inhibition are observed if the reverse scan runs at potentials that are less negative than −0.24 V (Figure 9.36). When the potentials are carried back from farther cathodic polarizations, the anodic current originates at equilibrium potential of $Sn|Sn^{2+}$ electrode. This current is conditioned by dissolution of free tin phase that was formed theretofore. Further part of the reverse curve actually coincides with that obtained in halide-free solutions with direct scan (Figure 9.36). The height of i_{p1} reduces by ~40% during the second cyclic scan but further cycles produce the curves that are very close to each other. Similar voltammograms involving "reverse" anodic peaks have been also obtained in the presence of laprol [60]. If the nature of wide voltammetric minimum located at $E < E_{eq}^{Sn}$ is principally clear, the same cannot be said of the left minimum. The main handicap to the more exhaustive studies involves inaccessible control of instable surface states arising in this region. This complicated problem needs further special investigations, although some preliminary interpretation seems to be possible.

The effect of iodides is particularly powerful. The threshold iodide concentration is only 0.5 μM [78]. They inhibit copper electroplating so strongly that the yellow bronze deposition becomes unfeasible at rather low iodide concentrations exceeding 2–3 μM.

In our opinion, the main factor responsible for the aforementioned phenomena might consist in variations in surface activity of the coatings that, in turn, depend on their elemental and phase composition. The data for pure copper and tin substrates are considerably more extensive than these concerning Cu–Sn alloys. Impedance data [88] have shown that the adsorption ability of laprol on copper and yellow bronze is of the same order and differs radically from that on tin electrode.

It could be supposed that the first stages of Cu and Sn codeposition occurring at $E < E_{eq}^{Sn}$ involve the underpotential deposition of tin on foreign (copper) lattice. In other words, the formed layers of tin might be treated as intermediates that form further the integrated Cu–Sn lattice. While weakly bonded to copper, such formations could achieve certain properties that are somewhat similar to those of tin phase and thus cause the inhibition effects. Nevertheless, such surface structures seem to be unstable because a significant rise of current density approaching $i_{d,Cu}$ is observed at about −0.18 V (Figures 9.36 and 9.37). The state under discussion is not also reproduced when the reverse potential scans are applied. To obtain full clearness on the nature of the processes, quite a number of other factors should be too summed up, the regularities of adsorption being among them. It has been established [71, 79, 85] that the adsorption of similar surfactants on tin electrodes is controlled by both diffusion and electrosorption steps. Besides, the kinetics of such processes, as well as the inhibition degree of Sn(II) reduction, substantially depends on the electrode potential [55, 76]. Two kinds of inhibition activity of laprol have been observed [76] at different *E:* moderate at low cathodic polarization and very strong at −0.3 V with high (−2.3 to −4.5 kΩ cm^2) negative charge transfer resistance.

The role of halides that show quite opposite effects on copper and tin electrodes is also important and requires respective evaluation. It must be accepted that only bromides are particular ions capable of creating of two inhibition regions. Chlorides seem to be too weak and iodides seem to be too strong surfactants for such behavior.

It follows from the aforementioned discussion that polyethers play a peculiar role in codeposition of copper and tin. If halides are absent in the solution, surface complexes containing polyethers are not formed on copper and/or yellow bronze surface and the formation of bronze coatings is not accompanied by noticeable adsorption of surfactants. However, if a germ of pure tin phase is formed for some reason, its growth is immediately suppressed by significant inhibitive adsorption of polyether.

As mentioned earlier, UPD of tin results from the formation of specific copper-rich phases. Their composition depends on both the solution composition and electrolysis conditions. A specific feature of electrochemically deposited bronze coatings is the presence of various phases that are thermodynamically stable only at high temperatures. In addition, our investigations [83, 84, 87] demonstrated that Cu–Sn coatings obtained in the presence of some polyethers contain the intermediate *hcp* phase of α-CuSn. This phase is also a solid solution of tin in copper,

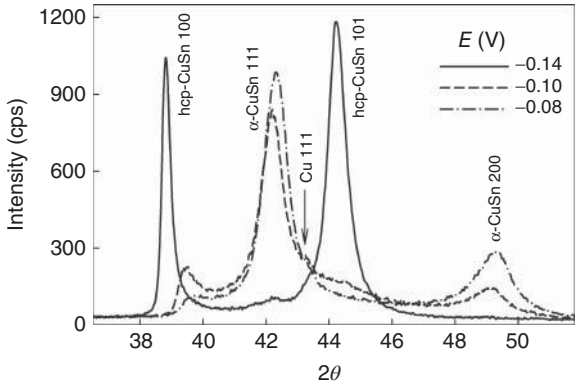

Figure 9.38 XRD patterns of Cu–Sn coatings deposited at indicated potentials in the solutions containing 0.01 M Cu(II), 0.01 M Sn(II), 1 M H_2SO_4, and 0.1 g dm^{-3} PEG-40000.

however, with a hexagonal structure [83]. When heated at 350 °C, this phase transforms into ζ-$Cu_{10}Sn_3$. This unusual phase has never been detected in the cast alloys. We associate its formation with the underpotential deposition of tin on copper at $E > -0.2$ V.

Representative XRD patterns of CuSn deposits obtained in the solution containing PEG-40000 are shown in Figure 9.38. It is evident that the phase composition strongly depends on potential: with an increase in negative potential, the quantity of the α-CuSn *fcc* phase (supersaturated solid solution of tin in copper) decreases while the quantity of *hcp* increases.

An example of phase composition is shown in Figure 9.39. The deposits obtained in the PEG-free solution present a mixture of pure copper, α-CuSn phase (supersaturated solid solution of tin in copper) and *hcp* phase. The content of pure Cu decreases with PEG molecular mass (except PEG-40000), but the α-CuSn phase prevails in all cases. The tendency was observed according to which the luster characteristics of coatings improve when the content of *hcp* phase decreases. For

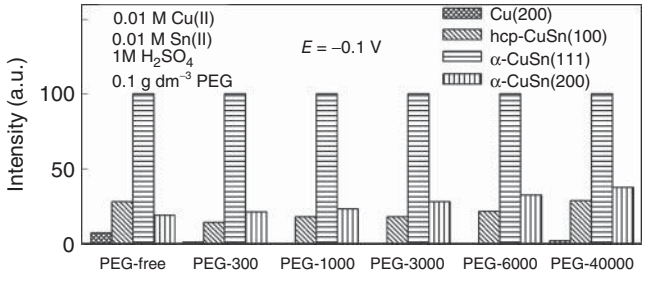

Figure 9.39 Phase composition of bronze coatings obtained at −0.1 V in the solutions containing different polyethylene glycols. XRD data are normalized with respect to XRD peak 111 of α-CuSn *fcc* phase.

instance, addition of a brightener (benzaldehyde) to sintanol-containing solutions reduces this phase by half.

9.4.5
Related Phenomena: Current Oscillations

Early studies of this system have shown [60] that periodic current oscillations appear in the region of deep voltammetric minimum (see Figure 9.35). These periodic phenomena can arise spontaneously and are more frequent in the case of more concentrated Cu(II) and Sn(II) solutions containing a sufficiently large amount of polyether. As an example, a solution of the following composition could be mentioned: 0.2 M Cu(II), 0.2 M Sn(II), 1 M H_2SO_4, and 2 g dm^{-3} laprol. A typical shape of current oscillations observed under potentiostatic conditions in such solution is shown in Figure 9.40 (inset). As seen from this figure, the amplitude and frequency of oscillations depend on the potential applied. Besides, there is an obvious correlation between parameters i_A and f that are the reverse of each other.

Oscillatory behavior of electrochemical systems is not uncommon. The most familiar in this respect are the systems containing surface-active substances. Most surfactants are capable of forming inhibiting adsorption layers, which are responsible for a significant decrease in the cathodic current in a certain range of potentials. For instance, the electroreduction of copper [106] or tin [107] in the presence of inhibitors is accompanied by oscillation phenomena.

The most vivid example of another group of electrochemical oscillators might be the Hg|In(III), SCN^- system involving potential-dependent catalysis by thiocyanate of In(III) reduction. This system was investigated rather extensively [108–112]. According to the mechanism proposed in [109], the formation of adsorbed $In(SCN)_2^+$ complexes is the rate-determining step followed by fast electroreduction of this species. As in the case of aforementioned systems, the

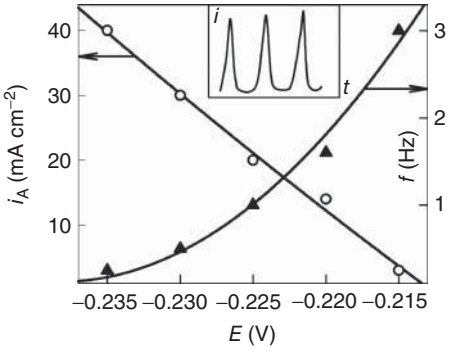

Figure 9.40 Dependencies of oscillation amplitude, i_A (ordinate to the left), and its frequency, f (ordinate to the right), on electrode potential, E. A typical shape of current oscillations is shown in the inset.

active and passive states are possible as well. The main difference lies in the fact that an overall electrochemical process proceeds much faster in the region of adsorption potentials.

As in the case of anodic processes, current oscillations occur in the potential region where there is a transition between the metal active and passive state and vice versa. The systems exhibiting oscillations are related to electrodissolution of iron and less to that of other metals such as cobalt, stainless steel, copper, and silver (see, e.g., [113–116] and references therein). In this case, the periodic process involves formation and dissolution of comparatively thick films of metal oxides, hydroxides, or other insoluble compounds.

Periodic phenomena including electrochemical oscillators have been the subject of a vast number of recent investigations. A comprehensive list of references regarding various aspects of oscillatory behavior and related phenomena seems to be too long to present here. However, it is fair to refer to earlier work on the relationship between impedance spectroscopy and stability by de Levie [110]. The usefulness of impedance diagrams in discussing the stability properties of electrochemical cells has been studied in detail by Epelboin and coworkers; the main results are reviewed in [117].

A considerable contribution to the development of theory of electrochemical oscillators has been made owing, mainly, to the investigations carried out by Koper *et al.* First of all, the research concerning the analysis of electrochemical instabilities [118] and the mathematical unification of a class of electrochemical oscillations and their design procedures [119] should be mentioned. An exhaustive quantitative description of oscillations involving the analysis of various types of bifurcations [120] requires detailed information on the kinetics and the mechanism of electrochemical processes. As it does not always happen that such data are available, the aforementioned problems often remain unclarified. Such a limitation has been obviated to a significant extent due to the idea regarding the usefulness of impedance spectroscopy data for predicting the stability features of electrochemical systems (see, e.g., [110, 117–119, 121]). For this purpose, a simplified equivalent circuit $R_s(Z_F C_{dl})$ for an electrochemical process may be presented [118] as a double-layer capacitance, C_{dl}, and faradaic impedance, Z_F, in parallel, with an resistance, R_s, in series. The latter usually comprises the ohmic cell resistance.

According to the generalization made in [111, 112], oscillations are possible, if:

- a negative faradaic impedance, $Z_F < 0$, exists;
- the condition of $R_s > |Z_F|$ is satisfied.

Several reasons may be responsible for the first inequality: potential-dependent adsorption of inhibitor or desorption of catalyst, electrostatic effect at low ionic strength. (e.g., a reduction of anions at negatively charged surface), or the case when the available electrode surface decreases with an increase in polarization (inhibition or passivation).

The electrode impedance cannot be measured when oscillations occur. Therefore, we investigated slightly modified solution (0.1 M Cu(II), 0.2 M Sn(II),

1 M H_2SO_4, and 5 g dm^{-3} laprol) that shows no oscillations when the cathodic voltammogram is recorded. Prior to the impedance measurements, a 5 min pre-electrolysis was conducted at a certain applied potential in the solution under investigation. Nyquist plots indicated by letters $a-c$ are given on Figure 9.41. Corresponding potentials, at which the impedance was measured, are indicated at the voltammogram (inset) by the same letters. Nyquist plots obtained at potentials corresponding to a positive slope of the voltammogram involve well-defined semicircles at sufficiently high frequencies. Their shape is similar to that presented in part c. In contrast, both real and imaginary negative impedances are observed in the region of negative slope (plots a and b). Two limits of impedance spectra should be considered. When a frequency $\omega = 2\pi f \to \infty$, a real component of the impedance approaches an ohmic resistance of the solution, R_Ω, that was found to be equal to 1.20 Ω. Another limit is obtained at $\omega \to 0$, then $Z'(0)$ should be equal to a polarization resistance, R_{pol}, following from the reciprocal slope of the steady-state voltammogram. It is obvious that R_{pol} depends on the kinetics of faradaic process (solution composition, E, etc.).

Let us return to the physical meaning of the resistance R_s. As mentioned earlier, when obtained from impedance data, this quantity presents the resistance of the solution, R_Ω, between the tip of Luggin capillary and the electrode. As the ohmic drop in the solution is not negligible and a fixed potential difference is applied across the electrode and series resistor, in the strict sense, the experimental conditions are not truly potentiostatic. This effect can be enhanced using an external resistance, R_{ext}, in series with the electrochemical cell. Then, the resistance $R_s = R_\Omega + R_{ext}$ can be varied through changes in the R_{ext} and the condition of $R_s > |Z_F|$ can be met in this way.

Nyquist plots obtained for the region of well-defined negative slope of the voltammogram intersect an abscissa axis at Z' of −1 to −7 Ω depending on the potential value. For example, $Z' \approx -3.5\,\Omega$ and corresponding frequency $f \approx 0.25$ Hz for the plot on Figure 9.41b obtained at $E = -0.19$ V. If the external resistance $R_{ext} = 3.5\,\Omega$ is inserted in series with an electrochemical cell and the voltage, V, corrected for ohmic drop (i.e., $V = -0.197$ V) is applied, the current oscillations are observed under such conditions. At the same time, the Nyquist plot should shift to the right so that it passes through the origin at the aforementioned characteristic frequency (about 0.25 Hz). Speaking in images, the "superconductivity" created for the certain frequency is favorable for the respective oscillations.

Effect of the external resistance can be seen from the data in Figure 9.42. They were obtained at $c_{Cu(II)} = 0.09$ M, where there was no evidence of oscillatory behavior of the system at $R_{ext} = 0$. The value of $R_{pol} = -4\,\Omega\,cm^2$ was found from the negative slope of voltammogram. The amplitude of oscillations increases with increasing external resistance under potentiodynamic conditions (sweep rate $\nu = 2$ mV s^{-1}). At the same time, the range of potentials, wherein oscillations occur, passes a minimum at $R_{ext} = 2.5\,\Omega$.

Some problems were experienced in the construction of the comprehensive stability diagram, owing to a very narrow range of oscillation potentials and

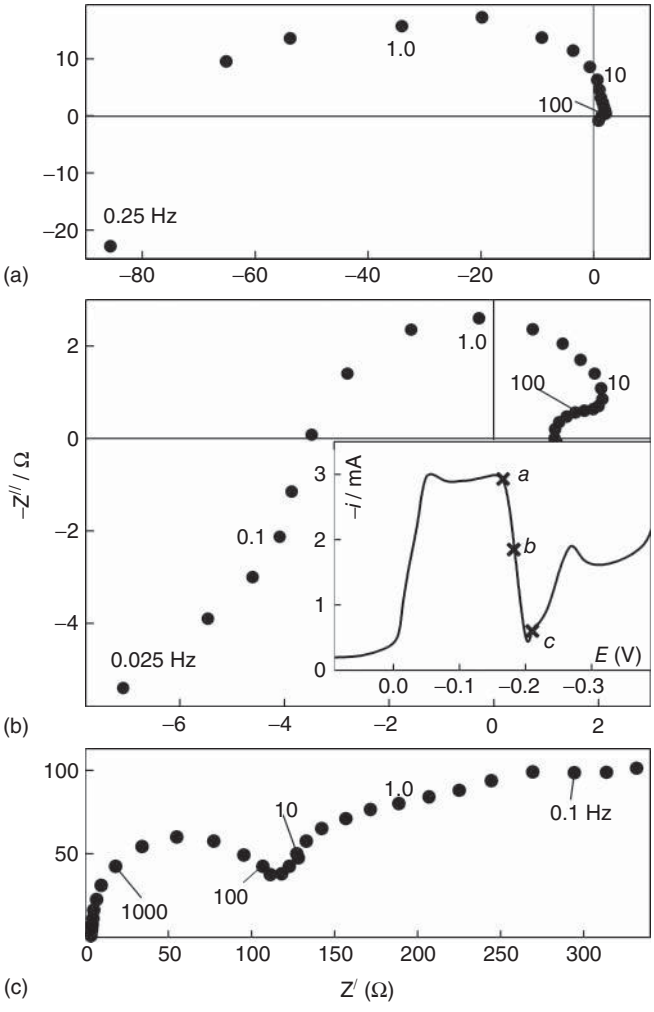

Figure 9.41 Nyquist plots obtained at different potentials for the solution containing 0.1 M Cu(II), 0.2 M Sn(II), 1 M H_2SO_4, and 5 g dm^{-3} laprol. A frequency in Hertz is given at some points. The data shown in parts *a*–*c* of the figure were obtained at potentials indicated by the respective symbols on the voltammogram (inset). Electrode surface ~0.3 cm^2.

the changes of system properties with electrolysis time. Therefore, only several plausible points were available from impedance measurements. Phase diagrams (Figure 9.43) seem to have the familiar fish-shape that is typical of Hopf bifurcation [118, 119, 121]. Oscillations were found inside the fish shown in Figure 9.43. More information on the oscillatory behavior of this system is available from our publications [122, 123].

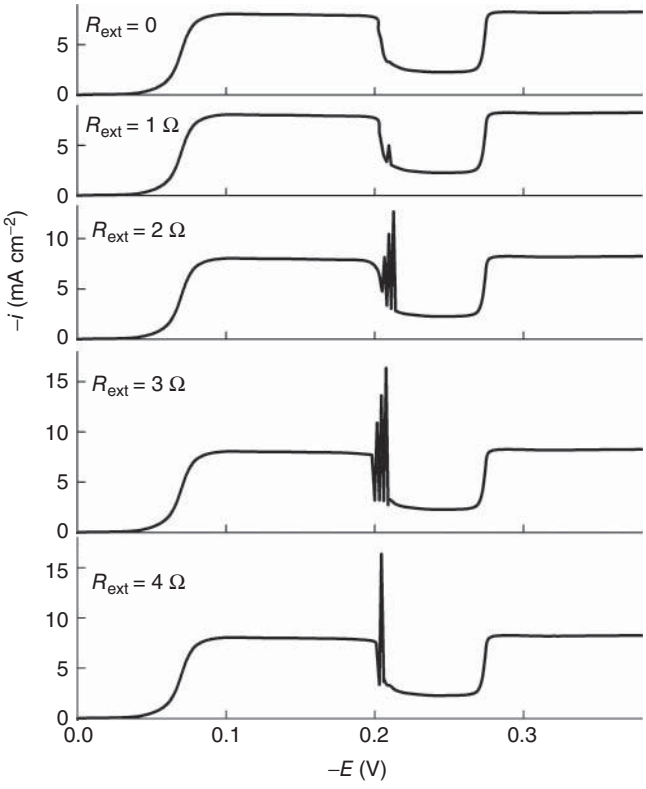

Figure 9.42 Influence of an external resistance (indicated at the curves) on the shape of voltammograms. $c_{Cu(II)} = 0.09$ M.

9.5
Codeposition of Cobalt and Molybdenum

Alloys of metals of the iron subgroup with molybdenum or tungsten are characterized by high hardness, wear, and corrosion resistance. It is worthy of note that most of these qualities are also preserved at rather high temperatures. Besides, Co–Mo systems feature weak magnetic properties that can be used in designing various devices intended for control of electric circuits. Finally, Ni–Mo alloys are characterized by high catalytic activity in hydrogen evolution and can serve as effective cathodes for electrochemical synthesis in an alkaline medium. All this allows considering the objects under discussion as materials promising for application in practical production.

The aforementioned systems are usually obtained by such conventional methods as fusion or condensation of required components on various supports. However, it is possible to use electrolysis of solutions or melts. Both these electrochemical methods have their advantages and disadvantages.

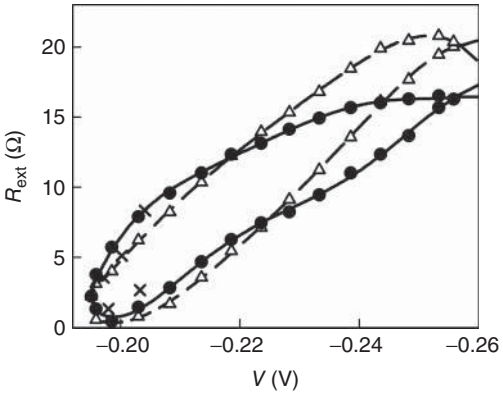

Figure 9.43 Linear stability diagrams. Experimental plots show the onset of oscillations observed by insertion of an external resistor, R_{ext}, at constant applied voltage, V. Duration of electrolysis equals about 10 min (dashed line) and 20 (solid line) min. Coordinates of points indicated by crosses were determined from the impedance data.

The main fault of electrolysis of aqueous solutions consists in the fact that it is not always possible to achieve full reduction of Mo(VI) or W(VI) compounds to the metallic state. Therefore, various intermediates are present in galvanic coatings: WO_2, MoO_2 [124–127], Mo_2O_3 [128], Mo_2O_5, Mo_3O_8 [129]. There are also reports on formation of nonstoichiometric compounds of the $Mo_3O_{8-x}(OH)_x$ type and also of mixed Mo(IV)–Mo(V) oxides [127, 129]. These products can undergo further reduction, while its mechanism remains unclear. Some authors imply that intermediate oxides are reduced at the participation of adsorbed atomic hydrogen or Ni^+ ions that also represent an intermediate of Ni(II) reduction [128]. In a number of processes occurring with participation of ligands, other mechanisms are also possible. According to [130–132], adsorbed MoO_2–$NiCit^-$ particles are formed in citrate solutions that further participate in the cathodic process. Similar mechanisms were suggested in other papers [124, 126, 127]. The interpretation of experimental data is often related to problems regarding assessment of the solution composition. It is characteristic that various chemical reactions resulting in the formation of a rather wide spectrum of diverse products occur already in solutions containing only Mo(VI) or W(VI). Addition of ligands or other substances to them leads to additional increase in the number of components. Therefore, data on the composition are as often as not incomplete and sometimes controversial. Identification of Mo(VI) complexes remains so far problematic. For example, citrate complexes of the $H_rMoO_4Cit^{(5-r)-}$ type were detected and attempts were made to estimate their stability [126]. Reliability of formation of one of them ($r = 3$) was confirmed using the method of Raman spectroscopy [133]. Later [134], other citrate complexes of Mo(VI) were also detected, such as $H_xMoO_7O_{24}^{(6-x)-}$, $NiMoO_{24}H_6^{4-}$, $H_x(MoO_4)_2Cit^{(7-x)-}$, and $H_xMoO_4Cit^{(5-x)-}$, their stability constants were not as yet determined. The most part of the data in the literature points to occurrence in the Co(II) and Mo(VI)

solutions of rather complicated chemical and electrochemical transitions, their mechanism requiring further investigation.

Some information on distribution of complexes and protonated ligand forms can be obtained on the basis of calculations using well-known material balance equations containing stability constants of the corresponding particles. For example, let us consider Co(II) and Mo(VI) solutions containing one of the most common ligands, citric acid. An argument in favor of such a choice is the fact that information on the types of citric complexes and their stability is more detailed, as compared to those of the other hydroxyacids. It is quite probable that conclusions following from the analysis performed may be extended to other systems containing similar ligands.

In the case of acidic or neutral media, citric acid can be presented by the symbol of LH_3 that points to the presence of three –COOH groups in the molecule of this ligand capable of generating hydrated protons. As follows from analysis of the literature [17, 18, 135], in the case of pH < 7, one may restrict oneself to consideration of the following reversible processes:

$$Co^{2+} + pL^{3-} + qH^{+} \rightleftarrows CoL_pH_q^{2+q-3p}, \tag{9.16}$$

$$MoO_4^{2-} + pL^{3-} + qH^{+} \rightleftarrows MoO_4L_pH_q^{-2+q-3p}, \tag{9.17}$$

$$L^{3-} + mH^{+} \rightleftarrows LH_m^{m-3}, \tag{9.18}$$

Constants of equilibria (9.16) and (9.17) are the overall stability constants (β_{pq}) of the corresponding complexes, while similar characteristics (β_m^H) of the processes represented by the common relationship (9.18) determine stability of the protonated ligands. The results of calculations carried out using the data of various sources from the literature [124, 132, 134] (Table 9.4) are presented in Figure 9.44. It is easy to see that addition of the ligand results in an increase in the complexation degree of both the metals, but this effect is better pronounced in the case of Co(II) complexation. As concentration of "free" Co^{2+} or MoO_4^{2-} ions is rather low, they are not reflected in Figure 9.44. However, these quantities were used to estimate the equilibrium potentials of the corresponding redox processes:

$$MoO_4^{2-} + 8H^{+} + 6e \rightleftarrows Mo + 4H_2O, \tag{9.19}$$

Table 9.4 Cumulative stability constants of Co(II) and Mo(VI) citrate complexes.

Complex	*pq*	log β_{pq}	Complex	*pq*	log β_{pq}	Ligand	*m*	log β_m^H
$CoL_pH_q^{2+q-3p}$	10	5.5	$MoO_4L_pH_q^{-2+q-3p}$	11	13.7	LH_m^{m-3}	1	5.6
	11	9.3		12	16.3		2	10
	12	11.25		—	—		3	13

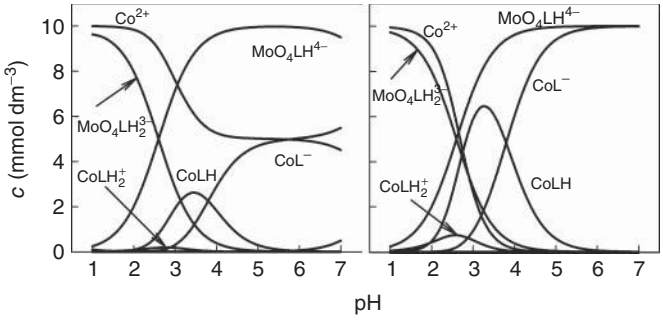

Figure 9.44 Distribution of complex particles in solutions containing 10 mM Co(II), 10 mM Mo(VI), and (left side) 15 mM or (right side) 40 mM citric acid.

$$Co^{2+} + 2e \rightleftarrows Co, \tag{9.20}$$

$$H_3O^+ + e \rightleftarrows \frac{1}{2}H_2 + H_2O. \tag{9.21}$$

The required values of standard potentials were substituted into the corresponding Nernst equations that took the following form at 25 °C:

$$E_{eq}^{Mo} = 0.154 - 0.0787pH + 0.0098\log\{MoO_4^{2-}\}, \tag{9.22}$$

$$E_{eq}^{Co} = -0.77 + 0.0295\log\{Co^{2+}\}, \tag{9.23}$$

$$E_{eq}^{H} = -0.059\,pH, \tag{9.24}$$

where braces correspond to the activity of the relevant particle. The data in equilibrium potentials presented in Figure 9.45 can serve as a basis for a number of important conclusions. The equilibrium potentials in acidic media form the series of $E_{eq}^{Mo} < E_{eq}^{Co} < E_{eq}^{H}$. This means that the first partial process in the case of the cathodic electrode polarization must be hydrogen evolution. An increase of polarization results in development of conditions for Co(II) reduction, while formation of metallic molybdenum becomes possible even at negative enough potentials. It will be noted that the results obtained characterize the possibility of occurrence of partial processes but contain no information on their kinetics. The rate of partial processes that largely depends on overpotential is the subject of a separate research.

The obtained potential diagrams allow selecting the optimum solution compositions. As potentials of the redox systems of Co|Co(II) and $H_2|H_3O^+$ draw together at an increase in pH, the most attractive media are weakly acidic ones. Herewith, an excess of ligand is undesirable, but its concentration must not be too low. Otherwise, low-soluble hydroxides may be formed in the solution bulk due to loss of the system stability. Similarly, the composition of the Co(II) and Mo(VI) containing malic or tartaric acid was considered. As we found no available data in

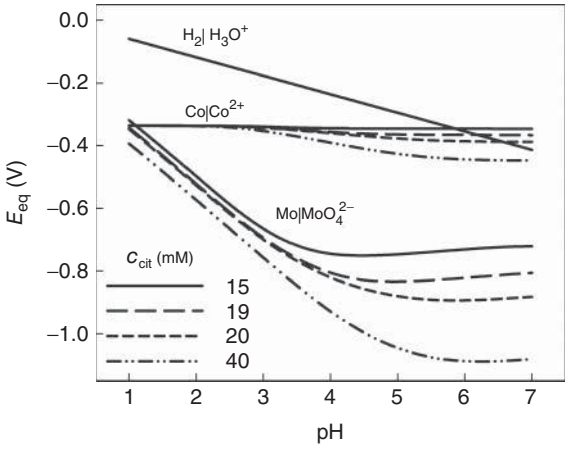

Figure 9.45 Dependencies of equilibrium potentials of partial processes on pH of solutions containing 10 mM Co(II), 10 mM Mo(VI) and different concentrations of citric acid (mM) as indicated.

the literature on the stability of malate and tartrate complexes, the equilibrium characteristics of these systems were evaluated only approximately. Nevertheless, the main conclusions on the sequence of equilibrium potentials remain similar to those in the case of citrate solutions.

In the case of cobalt and molybdenum codeposition from hydroxy acid-containing solutions, elucidation of the electrochemical behavior of ligands is one of the top-priority problems. Voltammetric data show that similar regularities are characteristic for most of the used ligands, including glycolic, malic, tartaric, and citric acids. In the first instance, one should point out that the character of polarization curves is independent of the nature of the cathode and the data obtained using a copper, gold, or platinum electrode practically coincide. As seen from typical examples presented in Figures 9.46 and 9.47, cathodic curves registered under a linear potential sweep feature a characteristic current maximum. Its position depends on the potential sweep rate and falls into the potential range from −0.75 to −0.85 V. The height of the current peak (i_p) increases in proportion to the value and the approximating lines pass through the origin of coordinates (insets in Figures 9.46 and 9.47). The obtained experimental data evidence that the cathodic process in the ligand solutions occurs irreversibly and is simultaneously controlled by diffusion mass transport and charge transfer process.

The cathodic process rate grows at an increase in the total ligand concentration and at a decrease in pH, that is, at an increase in the solution acidity. Analysis of the obtained data and the literature gives grounds to conclude that the main cathodic process in the hydroxyacid solutions is hydrogen evolution. Ligands also participate in this process playing the role of labile proton donors. Thus, owing to a shift in the chemical equilibriums resulting in additional dissociation of organic acids, the surface layer is constantly supplied with H_3O^+ ions. One may assume that the

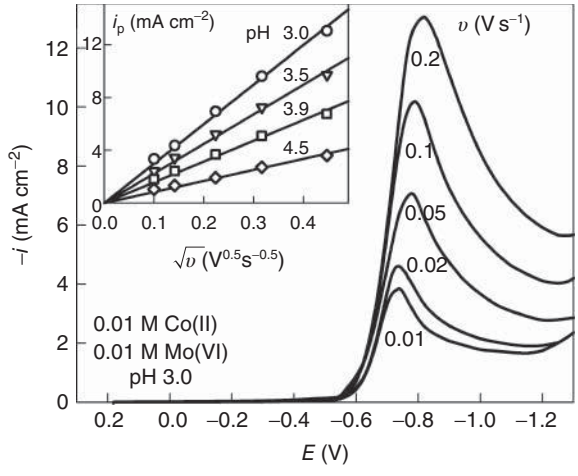

Figure 9.46 Cathodic voltammograms obtained in solutions containing 0.04 M tartaric acid and 0.3 M K_2SO_4 with pH 3.0 at different potential sweep rates (v) as indicated. Inset: dependence of peak current on $\sqrt{v}$ at different pH.

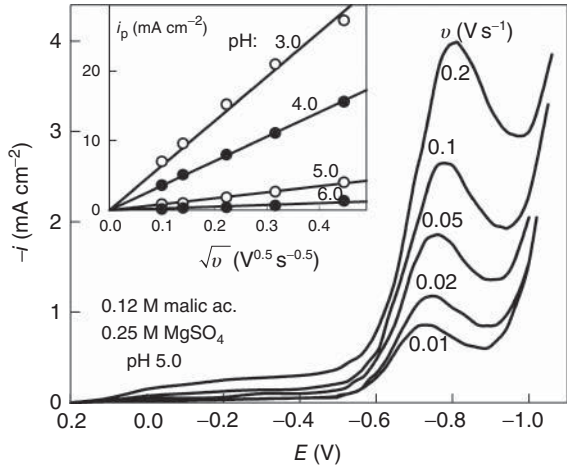

Figure 9.47 Cathodic voltammograms obtained in solutions containing 0.12 M malic acid and 0.25 M $MgSO_4$ with pH 5.0 at different potential sweep rates (v) as indicated. Inset: dependence of peak current on $\sqrt{v}$ at different pH.

intermediate of this partial process (atomic hydrogen) can assist reduction, at least partial, of molybdate.

Co(II) complexes are reduced at more negative potentials simultaneously with hydrogen evolution. Therefore, cathodic voltammograms obtained in Co(II) and malic acid solutions contain poorly defined plateau of limiting current density (i_{lim}) [136]. The rate of this partial process grows at an increase in cathodic polarization. Besides, i_{lim} decreases at an increase in the ligand concentration. If an

excess of ligand is absent in the Co(II) solution, i_{lim} obeys Levich equation at diffusion coefficient $D = 5.7 \times 10^{-6}$ cm^2 s^{-1}. This value is typical for most of similar complex systems. However, if the ligand concentration is increased, linearity of dependencies of i_{lim} on is retained, but the slopes of Levich plots are decreased [136]. Such regularities characteristic for the systems with lack of the ligand are also observed in the citrate Co(II) solutions. In this case, the "limiting currents" observed in the experimental voltammograms must be considered as prewaves and their height depends on the distribution of complexes in the solution bulk as described in Chapter 4. In the case of the system under consideration, i_{lim} is proportional to the difference of $(c_{Co(II)} - c_{lig})$, while the true limiting current density (i_d) depends only on the overall Co(II) concentration. This current is often screened by the hydrogen evolution process and is not detected in the experimental curves.

Hydrogen evolution also remains the main electrochemical process in the molybdate solutions. Voltammetric curves of molybdate solutions generally contain no limiting current regions and only monotonic current increase is observed at an increase in the cathodic polarization. However, a plateau of i_{lim} can be detected in the steady-state voltammograms of not very acidic (pH 5) solutions containing equimolar amounts of molybdate and the ligand. In this case, an interesting dependence of i_{lim} on the intensity of forced convection is observed. At $c_{lig}/c_{Mo(VI)} = 3$, a linear dependence of i_{lim} on $\sqrt{\Omega}$ is observed. However, when this ratio is decreased, i_{lim} ceases to depend on the electrode rotation rate. Voltammograms of such mixed solutions usually maintain the shape typical for the ligand solutions. These results agree with the assumption that hydrogen evolution assists Mo(VI) reduction. Mo(VI) reduction seems to occur with participation of an intermediate (atomic hydrogen), but not all molybdate is reduced to metallic state. Partial reduction of Mo(VI) is evidenced by characteristically colored intermediates, the formation of which can be visually observed on a gold electrode.

Hydrogen evolution causing the alkalization at the electrode surface may become a reason for formation of different insoluble compounds and passivation of electrode surface. Therefore, to increase the buffer capacity of the solution, an addition of boric acid is desired. Besides, Mg^{2+} ions can also hinder such effects by binding the excess of hydroxyl ions. The experiments showed that Mg(II) sulfate is not completely indifferent electrolyte and affects both kinetics of partial processes and composition of the obtained coatings. This effect depends largely on pH: Mg(II) assists Co(II) reduction at pH 6, but the opposite effect is observed at pH 4. Co–Mo coatings obtained in the absence of Mg(II) contain more molybdenum, but the content of nonmetallic impurities herewith is increased. In the solutions with a higher Mg(II) concentration, molybdenum inclusions are observed in the coatings, but their amount does not exceed 1%.

The results of studies performed with different hydroxyacids are basically similar. The current efficiency depends to some extent on the nature of ligand; For instance, it is higher in the solutions containing malic acid as compared with citrate solutions. The composition of Co–Mo coatings depends on the solution

composition and conditions of electrolysis. More oxygen is detected on the surface of samples than in the deeper layers of Co–Mo coatings. Its major part is contained in oxides, but a certain amount corresponds to the carboxyl group, which points to destructive adsorption of hydroxyacids. After about 3 nm of the surface layer is etched away by means of Ar^+ ions, the major part of oxygen is removed from the surface and the rest of the oxygen remains within Co(II) oxides and partially reduced molybdenum.

Conditions favorable for Co(II) reduction seem to be also beneficial to the reduction of Mo(VI) to Mo(0). One may assume that the contact with metallic cobalt phase is required for full molybdate reduction.

References

1. Brenner, A. (1963) *Electrodeposition of Alloys*, Academic Press, New York.
2. Müller, B.F. (1976) Zinn- und Zinnlergierungsüberzüge. *Jakob. Oberflächentech.*, **32**, 303–306.
3. Knodler, A.S. (1977) Legierungsabscheidung. *Jakob. Oberflächentech.*, **33**, 166–174.
4. Chapman, A.H., Hampshire, W.B., and Maykuth, D.J. (1983) Tin coatings: present and future. *Plat. Surf. Finish.*, **70** (12), 40–44.
5. Liebscher, A. (1997) Legierungsabscheidung. Entwicklung, Möglichkeit und Grenzen der Anwendung. *Galvanotechnik*, **88** (3), 754–762.
6. Cuthbertson, J. (1951) Recent developments in tin and tin – alloy plating. *J. Electrodep. Tech. Soc.*, **27**, 13–22.
7. Miyashita, H. and Kurikawa, S. (1970) Electrodeposition of tin-cobalt alloy. *J. Metal Finish. Soc. Jpn.*, **21** (2), 79–81.
8. Clark, M., Elbourne, R.C., and Mackau, C.A. (1972) Discussion of annual conference papers. An electrodeposited bright tin-cobalt intermetallic compound, CoSn. *Trans. IMF*, **50** (3), 180–182.
9. Davies, A.E. (1954) Progress in tin – nickel electroplating. *Trans. IMF*, **31**, 401–415.
10. Hemsley, J.D.C. and Roper, M.E. (1979) Tin-cobalt alloy plating from a sulphate electrolyte. *Trans. IMF*, **57** (2), 77–80.
11. Abd El Rehim, S.S., Refaey, S.A., Schwitzgebel, G., Taha, F., and Saleh, M.B. (1996) Electrodeposition of Sn-Co alloys from gluconate baths. *J. Appl. Electrochem.*, **26** (4), 413–418.
12. Jaen, J., Varsanyi, M.L., Kovacs, E., Czako-Nagy, I., Buzas, A., Vertes, A., and Kiss, L. (1984) Structural studies of electrodeposited tin—cobalt alloys. *Electrochim. Acta*, **29** (8), 1119–1122.
13. Tyutina, K., Lukyanova, L., and Selivanova, G. (1984) Electrodeposition of tin-cobalt alloy. *Zaschita Metallov*, **20** (3), 482–484.
14. Medvedev, G.I., Zhuravlev, V.I., Fursova, N.Y., and Gan'shina, I.P. (1998) Electrodeposition of tin-cobalt from sulphate electrolyte with organic additives. *Zh. Prikl. Khim.*, **71** (6), 937–940.
15. Survila, A., Mockus, Z., and Kanapeckaitė, S. (2000) Kinetics of Sn and Co codeposition in citrate solutions. *Electrochim. Acta*, **46** (4), 571–577.
16. Survila, A., Mockus, Z., Juškėnas, R., and Jasulaitienė, V. (2001) Electrodeposition of Sn and Co coatings from citrate solutions. *J. Appl. Electrochem.*, **31** (10), 1109–1116.
17. Survila, A. and Žukauskaitė, A. (1995) Codeposition of copper and tin by electrolysis of the solutions containing citrate complexes. *Elektrokhimiya*, **31** (11), 1254–1260.
18. Sillen, L.G. and Martel, A.E. (eds) (1964, 1971) *Stability Constants of Metal–Ion Complexes*, Special Publications No. 17 and 25, Chemical Society, London.
19. Kirilova, I., Ivanov, I., and Rashkov, S. (1996/97) Deposition of bright cobalt

coatings from sulphate – chloride electrolyte. *Bulg. Chem. Comm.*, **29** (2), 204–216.
20. Kostrova, G.F. and Obozinskaya, V.A. (1985) Determination of optimal conditions electrolytic deposition of decorative brass coating of pyrophosphate electrolyte. *Sov. Electrochem.*, **21**, 352–354.
21. Johannsen, K. (2001) Effect of temperature and bulk stirring on electroplating of brass from pyrophosphate electrolyte. *Plat. Surf. Finish.*, **88** (6), 104–108.
22. Beattie, S.D. and Dahn, J.R. (2003) Comparison of electrodeposited copper-zinc alloys prepared individually and combinatorially. *J. Electrochem. Soc.*, **150** (11), C802–C806.
23. Senna, L.F., Diaz, S.L., and Sathler, L. (2003) Electrodeposition of copper–zinc alloys in pyrophosphate-based electrolytes. *J. Appl. Electrochem.*, **33** (12), 1155–1161.
24. Povetkin, V.V., Zakharov, M.S., and Muslimov, R.R. (1999) Electrodeposition of copper-zinc alloy from trilonate electrolytes. *Russ. J. Appl. Chem.*, **72**, 1367–1369.
25. de Almeida, M.R.H., Barbano, E.P., de Carvalho, M.F., Carlos, I.A., Siqueira, J.L.P., and Barbosa, L.L. (2011) Electrodeposition of copper–zinc from an alkaline bath based on EDTA. *Surf. Coat. Technol.*, **206** (1), 95–102.
26. Vagramyan, T., Leach, J.S.L., and Moon, J.R. (1979) On the problems of electrodepositing brass from non-cyanide electrolytes. *Electrochim. Acta*, **24** (2), 231–236.
27. Carlos, I.A. and de Almeida, M.R.H. (2004) Study of the influence of the polyalcohol sorbitol on the electrodeposition of copper–zinc films from a non-cyanide bath. *J. Electroanal. Chem.*, **562** (2), 153–159.
28. Juškėnas, R., Karpavičienė, V., Pakštas, V., Selskis, A., and Kapočius, V. (2007) Electrochemical and XRD studies of Cu–Zn coatings electrodeposited in solution with D-mannitol. *J. Electroanal. Chem.*, **602** (2), 237–244.
29. Assaf, F.H., Abd El Rehim, S.S., Mohamed, A.S., and Zaky, A.M. (1995) Electroplating of brass from citrate-based alloy baths. *Indian J. Chem. Technol.*, **2** (3), 147–152.
30. Ferreira, F.B.A., Silva, F.I.G., Luna, A.S., Lago, D.C.B., and Senna, I.F. (2007) Response surface modeling and optimization to study the influence of deposition parameters on the electrodeposition of Cu–Zn alloys in citrate medium. *J. Appl. Electrochem.*, **37** (4), 473–481.
31. Aotani, K., Kaneko, I., Takahashi, S., and Oiwa, M. (1971) Bright copper-zinc alloy plating. *J. Met. Finish Soc. Jpn.*, **22**, 496–500.
32. Abd El Rehim, S.S. and El Ayashy, M.E. (1978) Effect of some plating variables on the electrodeposition of Cu-Zn alloys from alkaline tartrate baths. *J. Appl. Electrochem.*, **8** (1), 33–39.
33. de Filippo, D., Rossi, A., and Atzei, D. (1992) A tartrate-based alloy bath for brass-plated steel wire production. *J. Appl. Electrochem.*, **22** (1), 64–72.
34. Fujiwara, Y. and Enomoto, H. (1988) Electrodeposition of Cu–Zn alloys from glucoheptonate baths. *Surf. Coat. Technol.*, **35** (1), 101–112.
35. Fujiwara, Y. and Enomoto, H. (1988) Characterization of Cu–Zn deposits from glucoheptonate baths. *Surf. Coat. Technol.*, **35** (1), 103–124.
36. Survila, A., Mockus, Z., Kanapeckaitė, S., and Stalnionis, G. (2013) Kinetics of zinc and copper reduction in gluconate-sulfate solutions. *Electrochim. Acta*, **94**, 307–313.
37. Survila, A., Mockus, Z., Kanapeckaitė, S., Stalnionis, G., Juškėnas, R., and Jasulaitiene, V. (2013) Codeposition of zinc and copper in gluconate-sulfate solutions. *J. Electrochem. Soc.*, **160** (10), D428–D433.
38. Skirstymonskaya, B.I. (1964) Electrodeposition of alloys. *Russ. Chem. Rev.*, **33** (4), 220–233.
39. Survila, A., Mockus, Z., Kanapeckaitė, S., Pileckienė, J., and Stalnionis, G. (2011) Cathodic processes in copper(II) solutions containing gluconic acid. *Russ. J. Electrochem.*, **47** (2), 129–135.
40. Survila, A. and Kanapeckaitė, S. (2012) Kinetics of cathodic processes in Cu(II) gluconate solutions containing an excess

of sulphate. *Electrochim. Acta*, **78**, 359–364.
41. Survila, A., Mockus, Z., Kanapeckaitė, S., and Stalnionis, G. (2012) Kinetics of Sn(II) reduction in acid sulphate solutions containing gluconic acid. *J. Electroanal. Chem.*, **667**, 59–65.
42. Survila, A., Mockus, Z., Kanapeckaitė, S., Grigucevičienė, A., and Stalnionis, G. (2012) EIS characterization of Sn|Sn(II), gluconic acid system. *Electrochim. Acta*, **85**, 594–599.
43. Milošev, I. and Strehblow, H.-H. (2003) Electrochemical behavior of Cu-xZn alloys in borate buffer solution at pH 9.2. *J. Electrochem. Soc.*, **150** (11), B517–B524.
44. Pecsok, R.L. and Juvet, R.S. Jr., (1955) The gluconate complexes. I. Copper gluconate complexes in strongly basic media. *J. Am. Chem. Soc.*, **77** (1), 202–206.
45. Alcock, C.B. and Jacob, K.T. (1974) Solute-solute and solvent-solute interaction in α-solid solutions of Cu + Sn, Au + Sn and Cu + Au + Sn alloys. *Acta Metall.*, **22** (5), 539–544.
46. Saunders, N. and Mlodownik, A.P. (1990) The Cu-Sn system. *Bull. Alloy Phase Diagrams*, **11** (3), 278–287.
47. Martyak, N.M. and Seefeldt, R. (2004) Additive-effects during plating in acid tin methanesulfonate electrolytes. *Electrochim. Acta*, **49** (25), 4303–4311.
48. Tyurin, A.G. (2008) Thermodynamics of chemical and electrochemical stability of aluminum, silicon, and tin bronzes. *Prot. Met.*, **44** (3), 292–300.
49. Meibuhr, S., Yeager, E., Kozawa, A., and Hovorka, F. (1963) The electrochemistry of tin I. Effects of nonionic addition agents on electrodeposition from stannous sulfate solutions. *J. Electrchem. Soc.*, **110** (3), 190–202.
50. Gerenrot, Y.E., Dimarskaya, P.I., and Eichiss, A.P. (1967) The structure of the copper-tin galvanic coatings. *Zashchita Metallov*, **3** (34), 465–471.
51. Hill, M.R.H. and Rogers, G.T. (1978) Polyethylene glycol in copper electrodeposition onto a rotating disk electrode. *J. Electroanal. Chem.*, **86** (1), 179–188.
52. Glarum, S.H. and Marshall, J.H. (1983) An admittance study of the tin electrode. *J. Electrochem. Soc.*, **130** (5), 1088–1096.
53. Yokoi, M., Konishi, S., and Hayashi, T. (1983) Mechanism of the electrodeposition and dissolution of copper in an acid copper-sulfate bath. 5. Acceleration mechanism in the presence of Cl-ions. *Denki Kagaku*, **51** (6), 460–464.
54. Medvedev, G.I. and Tkachenko, N.A. (1984) Electrodeposition of copper-tin alloy of sulfuric acid electrolyte in the presence of DS-10 sintanol. *Zashchita Metallov*, **20** (3), 392–394.
55. Medvedev, G.I. and Trubnikova, N.A. (1984) The study of the kinetics of electrodeposition of tin from sulfate electrolyte in the presence of DS-10 sintanol. *Elektrokhimiya*, **20** (6), 846–849.
56. Reid, J.D. and David, A.P. (1987) Effects of polyethylene glycol on the electrochemical characteristics of copper cathodes in an acid copper medium. *Plat. Surf. Finish.*, **74** (1), 66–70.
57. Pearson, T. and Dennis, J.K. (1990) The effect of pulsed reverse current on the polarization behaviour of acid copper plating solutions containing organic additives. *J. Appl. Electrochem.*, **20** (2), 196–208.
58. Healy, J.P., Pletcher, D., and Goodenough, M. (1992) The chemistry of the additives in an acid copper electroplating bath: part I. Polyethylene glycol and chloride ion. *Electroanal. Chem.*, **338** (1), 155–165.
59. Kelly, J.J. and West, A.C. (1992) Copper deposition in the presence of polyethylene glycol I. Quarz crystal microbalance study. *J. Electrochem. Soc.*, **145** (10), 3472–3476.
60. Galdikienė, O. and Mockus, Z. (1994) Cathodic process in copper–tin deposition from sulphate solutions. *J. Appl. Electrochem.*, **24** (10), 1009–1012.
61. Franklin, T.C. (1994) Some mechanisms of the action of additives in electrodeposition. *Plat. Surf. Finish.*, **81** (4), 62–67.
62. Stoychev, D. and Tsvetanov, C. (1996) Behaviour of poly (ethylene glycol) during electro deposition of bright copper

coatings in sulfuric acid electrolytes. *J. Appl. Electrochem.*, **26** (7), 741–749.
63. Stoychev, D. and Tsvetanov, C. (1998) On the role of poly(ethylene glycol) in deposition of galvanic processes copper coatings. *Trans. IMF*, **76** (2), 73–79.
64. Noyanova, G.A., Kosmodamianskaya, L.V., and Tyutina, K.M. (1999) Electrodeposition of Cu-Sn alloy from sulphate electrolytes. *Zashchita Metallov*, **35** (6), 617–620.
65. Jovič, V.D. and Jovič, B.M. (2001) Copper electrodeposition from a copper acid baths in the presence of PEG and NaCl. *J. Serb. Chem. Soc.*, **66** (11-12), 935–952.
66. Medvedev, G.I. and Makrushin, N.A. (2002) The study of the kinetics of electrodeposition of tin from sulphate electrolyte with organic additives. *Zh. Prikl. Khim.*, **75** (8), 1260–1262.
67. Bonou, L., Eyraud, M., Denoyel, R., and Massiani, Y. (2002) Influence of additives on Cu electrodeposition mechanisms in acid solution: direct current study supported by non-electrochemical measurements. *Electrochim. Acta*, **47** (26), 4139–4148.
68. Wu, B.-H., Wan, C.-C., and Yang, Y.-Y. (2003) Void – free anisotropic deposition for IC interconnect with polyethylene glycol as the single additive based on uneven adsorption distribution. *J. Appl. Electrochem.*, **33** (9), 823–830.
69. Beatie, S.D. and Dahn, J.R. (2003) Single bath, pulsed electrodeposition of copper-tin alloy negative electrodes for lithium-ion batteries. *J. Electrochem. Soc.*, **150** (7), A894–A898.
70. Medvedev, G.I., Makrushin, N.A., and Ivanova, O.V. (2004) Copper-tin alloy electrodeposition from a sulfate electrolyte. *Zh. Prikl. Khim.*, **77** (7), 1120–1122.
71. Medvedev, G.I. and Makrushin, N.A. (2004) The electrodeposition of tin sulfate, in the presence of electrolyte synthanol, formaldehyde and allyl alcohol. *Zh. Prikl. Khim.*, **77** (11), 1799–1803.
72. Finke, A., Poizot, P., Guéry, C., and Tarascon, J.-M. (2005) Characterization and Li reactivity of electrodeposited copper-tin nanoalloys prepared under spontaneous current oscillations. *J. Electrochem. Soc.*, **152** (12), A2364–A2368.
73. Hebert, K.R., Adhikari, S., and Houser, J.E. (2005) Chemical mechanism of suppression of copper electrodeposition by poly (ethylene glycol). *J. Electrochem. Soc.*, **152** (5), C324–C329.
74. Dow, W.-P., Yen, M.-Y., Lin, W.-B., and Ho, S.-W. (2005) Influence of molecular weight of polyethylene glycol on microvia filling by copper electroplating. *J. Electrochem. Soc.*, **152** (11), C7690–C7775.
75. Survila, A., Mockus, Z., Kanapeckaitė, S., and Samulevičienė, M. (2002) Adsorption behaviour of laprol 2402 C on copper electrode. *Pol. J. Chem.*, **76** (7), 983–991.
76. Survila, A., Mockus, Z., and Kanapeckaitė, S. (2002) Adsorption behaviour of laprol 2402 C on a tin electrode. *Trans. IMF*, **80** (3), 85–87.
77. Survila, A., Mockus, Z., and Kanapeckaitė, S. (2003) Effect of halides on adsorption properties of polyether laprol 2402 C on copper and tin electrodes. *J. Electroanal. Chem.*, **552**, 97–103.
78. Survila, A., Mockus, Z., Kanapeckaitė, S., and Jasulaitienė, V. (2004) Co-deposition of copper and tin from acidic sulfate solutions containing polyether laprol 2402C: The effect of halides. *Russ. J. Electrochem.*, **40** (8), 855–859.
79. Survila, A., Mockus, Z., Kanapeckaitė, S., and Samulevičienė, M. (2005) Effect of sintanol DS-10 and halides on tin(II) reduction kinetics. *Electrochim. Acta*, **50** (14), 2879–2885.
80. Bražinskienė, D. and Survila, A. (2005) Effect of ethylene glycol and its oligomers on the copper (II) electroreduction kinetics in halide-containing acid sulfate solutions. *Russ. J. Electrochem.*, **41** (9), 979–984.
81. Survila, A., Mockus, Z., Kanapeckaitė, S., and Samulevičienė, M. (2006) Effect of sintanol DS10 and halides on copper(II) reduction kinetics. *Trans. IMF*, **84** (2), 94–98.
82. Mockus, Z., Kanapeckaitė, S., Jasulaitienė, V., and Survila, A. (2006) Electrodeposition of yellow bronze from

acidic sulfate baths containing polyether laprol and micromolar additives of halides. *Prot. Met.*, **42** (5), 485–490.

83. Juškėnas, R., Mockus, Z., Kanapeckaitė, S., Stalnionis, G., and Survila, A. (2006) XRD studies of the phase composition of the electrodeposited copper-rich Cu-Sn alloys. *Electrochim. Acta*, **52** (3), 928–935.

84. Survila, A., Mockus, Z., Kanapeckaitė, S., Jasulaitienė, V., and Juškėnas, R. (2007) Codeposition of copper and tin from acid sulphate solutions containing polyether sintanol DS-10 and micromolar amounts of halides. *Electrochim. Acta*, **52** (9), 3067–3074.

85. Survila, A. and Bražinskienė, D. (2007) Inhibition activity of ethyleneglycol and its oligomers on tin electrode. *J. Solid State Electrochem.*, **11** (1), 65–70.

86. Survila, A., Mockus, Z., Kanapeckaitė, S., Jasulaitienė, V., and Juškėnas, R. (2009) Codeposition of copper and tin from acid sulphate solutions containing polyether sintanol DS-10 and benzaldehyde. *J. Appl. Electrochem.*, **39** (10), 2021–2026.

87. Survila, A., Bražinskienė, D., Kanapeckaitė, S., Mockus, Z., and Jasulaitienė, V. (2010) Codeposition of copper and tin from acidic sulphate solutions containing polyethylene glycols. Effect of length of the hydrocarbon chain. *J. Solid State Electrochem.*, **14** (4), 507–514.

88. Survila, A., Mockus, Z., Kanapeckaitė, S., and Samulevičienė, M. (2001) EIS characterization of laprol 2402C adsorption on copper, tin and bronze electrodes. *Chemistry (Vilnius)*, **12** (3), 210–215.

89. Brug, G.J., van den Eeden, A.L.G., Sluyters-Rehbach, M., and Sluyters, J.H. (1984) The analysis of electrode impedances complicated by the presence of a constant phase element. *J. Electroanal. Chem.*, **176**, 275–295.

90. Damaskin, B.B., Petrii, O.A., and Batrakov, V.V. (1971) *Adsorption of Organic Compounds on Electrodes*, Plenum Press, New York.

91. Clark, G.J., Andersen, T.N., Valentine, R.S., and Eyring, H. (1974) A comparison of the immersion and open-circuit scrape methods for determining the potential of zero charge of metal electrodes. *J. Electrochem. Soc.*, **121** (5), 618–622.

92. Lukomska, A. and Sobkowski, J. (2004) Potential of zero charge of monocrystalline copper electrodes in perchlorate solutions. *J. Electroanal. Chem.*, **567** (1), 95–102.

93. Egorov, L.Y. and Novoselskii, I.M. (1971) Properties of the electric double layer copper electrode. *Elektrokhimiya*, **7** (7), 988–990.

94. Novoselskii, I.M., Konevskih, N.I., and Egorov, L.Y. (1972) Properties of the electrical double layer copper electrode IV. Differential capacitance of copper electrode in a solution of sodium perchlorate. *Elektrokhimiya*, **8** (10), 1480–1481.

95. Brown, G.M. and Hope, G.A. (1996) A SERS study of SO_4^{2-} and Cl^- ion adsorption at a copper electrode in-situ. *J. Electroanal. Chem.*, **405** (1), 211–216.

96. Niaura, G. and Malinauskas, A. (1993) Surface-enhanced Raman scattering from chloride on copper electrodes. *Chem. Phys. Lett.*, **207** (4), 455–460.

97. Andersen, T.N., Andersen, J.L., and Eyring, H. (1969) Nature of fresh metal surfaces in aqueous solutions. *J. Phys. Chem.*, **73** (11), 3562–3570.

98. Afanas'ev, B.N. and Akulova, Y.P. (2000) A correlation between the hydrophilicity of a metal and its surface tension. Calculation of the bond energy of water molecules adsorbed on an uncharged metal surface. *Prot. Met.*, **36** (1), 25–30.

99. Michaelides, A. and Morgenstern, K. (2007) Ice nanoclusters at hydrophobic metal surfaces. *Nat. Mater.*, **6** (8), 597–601.

100. Bahena, E., Mendez, P.F., Meas, Y., Ortega, R., Salgado, L., and Trejo, G. (2004) An EQCM study of polyethyleneglycol 8000 adsorption and its coadsorption with Cl^- ions on Pt in perchloric acid solutions. *Electrochim. Acta*, **49** (6), 989–997.

101. Dow, W.-P., Yen, M.-Y., Lin, W.-B., and Ho, S.-W. (2005) Influence of molecular weight of polyethylene glycol on

microvia filling by copper electroplating. *J. Electrochem. Soc.*, **152** (11), C769–C775.

102. Safonova, T.Y., Smirnova, N.V., and Petrii, O.A. (2006) Adsorption of polyethylene glycol on platinum electrode from acidic solutions. *Russ. J. Electrochem.*, **42** (9), 995–1000.

103. Safonova, T.Y., Khairullin, D.R., Tsirlina, G.A., Petrii, O.A., and Vasiliev, S.Y. (2005) Palladium—polyethylene glycol quasitemplate electroplates: the effect of polymer molecular weight. *Electrochim. Acta*, **50** (24), 4752–4762.

104. Akiyama, T., Kobayashi, S., Ki, J., Ohgai, T., and Fukushima, H. (2000) Role of polyethylene glycol in electrodeposition of zinc–chromium alloys. *J. Appl. Electrochem.*, **30** (7), 817–822.

105. Rozovskis, G., Mockus, Z., Pautienienė, V., and Survila, A. (2002) Electrochemical determination of Sn(IV)/Sn(II) ratio in tin sol formed in copper-tin sulphate solution containing laprol 2402C. *Electrochem. Commun.*, **4** (1), 76–79.

106. Jehring, H. and Kuerschner, U. (1977) Elektrochemische oszillationen bei der inhibierten kupferabscheidung an der quecksilberelektrode. *J. Electroanal. Chem.*, **75** (2), 799–808.

107. Clarke, M. and Bernie, J.A. (1967) Abnormal high throwing power and cathode passivity in acid tin plating baths. *Electrochim. Acta*, **12** (2), 205–212.

108. de Levie, R. and Husovsky, A.A. (1969) On the negative faradaic admittance in the region of the polarographic minimum of In (III) in aqueous NaSCN solution. *J. Electroanal. Chem.*, **22** (1), 29–48.

109. PospisŸil, L. and de Levie, R. (1970) Thiocyanate electrocatalysis of the reduction of In(III). *J. Electroanal. Chem.*, **25** (2), 245–255.

110. de Levie, R. (1970) On the electrochemical oscillator. *J. Electroanal. Chem.*, **25** (2), 257–273.

111. Koper, M.T.M. and Sluyters, J.H. (1991) Electrochemical oscillators: an experimental study of the indium/thiocyanate oscillator. *J. Electroanal. Chem.*, **303** (1), 65–72.

112. Koper, M.M.T. and Sluyters, J.H. (1991) Electrochemical oscillators: their description through a mathematical model. *J. Electroanal. Chem.*, **303** (1), 73–94.

113. Sazou, D. and Pagitsas, M. (1991) Polarization behaviour of a cobalt rotating disc electrode in sulphuric acid solutions in the absence and presence of chloride ions. *J. Electroanal. Chem.*, **304** (1), 171–185.

114. Wang, C., Chen, S., and Yu, X. (1994) The nature of the potentiostatic current oscillations at iron/sulfuric acid solution interfaces. *Electrochim. Acta*, **39** (4), 577–580.

115. Lou, W. and Ogura, K. (1995) Current oscillations observed on a stainless steel electrode in sulfuric acid solutions with and without chromic acid. *Electrochim. Acta*, **40** (6), 667–672.

116. Sazou, D. and Pagitsas, M. (1995) Experimental bifurcation analysis of the cobalt/phosphoric acid electrochemical oscillator. *Electrochim. Acta*, **40** (6), 755–766.

117. Epelboin, I., Gabrielli, C., Keddam, M., and Takenouti, H. (1984) in *Comprehensive Treatise of Electrochemistry*, vol. **4** (eds J.O.'M. Bockris, B.E. Conway, E. Yeager, and R.E. White), Plenum Press, New York, p. 151.

118. Koper, M.T.M. (1992) The theory of electrochemical instabilities. *Electrochim. Acta*, **37** (10), 1771–1778.

119. Koper, M.T.M. and Sluyters, J.H. (1993) On the mathematical unification of a class of electrochemical oscillators and their design procedures. *J. Electroanal. Chem.*, **352** (1), 51–64.

120. Koper, M.T.M. (1995) Some simple bifurcation sets of an extended Van der Pol model and their relation to chemical oscillators. *J. Chem. Phys.*, **102** (13), 5278–5287.

121. Koper, M.T.M. (1996) Stability study and categorization of electrochemical oscillators by impedance spectroscopy. *J. Electroanal. Chem.*, **409** (1), 175–182.

122. Survila, A., Mockus, Z., and Juškėnas, R. (1998) Current oscillations observed during codeposition of copper and tin from sulfate solutions containing

laprol 2402C. *Electrochim. Acta*, **43** (8), 909–917.

123. Survila, A. and Mockus, Z. (1999) Current oscillations and a negative impedance observed during the copper and tin codeposition from solutions involving laprol 2402C as a surface-active substance. *Electrochim. Acta*, **44** (11), 1707–1712.

124. Gomez, E., Pellicer, E., and Valles, E. (2003) Influence of the bath composition and the pH on the induced cobalt–molybdenum electrodeposition. *J. Electroanal. Chem.*, **556**, 137–145.

125. Sanches, L.S., Domingues, S.H., Marino, C.E.B., and Mascaro, L.H. (2004) Characterisation of electrochemically deposited Ni–Mo alloy coatings. *Electrochem. Commun.*, **6** (6), 543–548.

126. Gomez, E., Pellicer, E., and Valles, E. (2005) An approach to the first stages of cobalt–nickel–molybdenum electrodeposition in sulphate–citrate medium. *J. Electroanal. Chem.*, **580** (2), 222–230.

127. Gomez, E., Pellicer, E., and Valles, E. (2005) Developing plating baths for the production of cobalt–molybdenum films. *Surf. Coat. Technol.*, **197** (2), 238–246.

128. Obradovic, M.D., Stevanovic, R.M., and Despic, A.R. (2003) Electrochemical deposition of Ni–W alloys from ammonia–citrate electrolyte. *J. Electroanal. Chem.*, **552**, 185–196.

129. McEvoy, T.M. and Stevenson, K.J. (2003) Electrochemical quartz crystal microbalance study of the electrodeposition mechanism of molybdenum oxide thin films from peroxo-polymolybdate solution. *Anal. Chim. Acta*, **496** (1), 39–51.

130. Podlaha, E.J. and Landolt, D. (1996) Induced codeposition I. An experimental investigation of Ni-Mo alloys. *J. Electrochem. Soc.*, **143** (3), 885–892.

131. Podlaha, E.J. and Landolt, D. (1996) Induced codeposition II. A mathematical model describing the electrodeposition of Ni-Mo alloys. *J. Electrochem. Soc.*, **143** (3), 893–899.

132. Podlaha, E.J. and Landolt, D. (1997) Induced codeposition III. Molybdenum alloys with nickel, cobalt, and iron. *J. Electrochem. Soc.*, **144** (5), 1672–1680.

133. Murase, K., Ando, H., Matsubara, E., Hirato, T., and Awakura, Y. (2000) Determination of Mo (VI) species and composition in Ni-Mo alloy plating baths by Raman spectra factor analysis. *J. Electrochem. Soc.*, **147** (6), 2210–2217.

134. Gomez, E., Pellicer, E., and Valles, E. (2003) Detection and characterization of molybdenum oxides formed during the initial stages of cobalt–molybdenum electrodeposition. *J. Appl. Electrochem.*, **33** (3-4), 245–252.

135. Ishikawa, M. and Enomoto, H. (1989) Complexation of Ni (II) with citrate in nickel–citrate plating baths. *J. Surf. Finish. Soc. Jpn.*, **40**, 1266.

136. Survila, A., Kanapeckaitė, S., Valsiūnas, I., and Jasulaitienė, V. (2010) Partial processes during cobalt and molybdenum codeposition from solutions containing hydroxy acids. *Russ. J. Electrochem.*, **46** (10), 1167–1174.

10
Spontaneous Formation of Photosensitive Cuprous Oxide Layers

When considering the second kind electrodes in Section 2.3, copper covered by Cu_2O was referred to as a *prominent example*. Cuprous oxide layers developed in electrochemical systems are interesting from various points of view. In the first place, such layers are known to form during copper corrosion. Research in this field are very important and large in number (see, e.g., Ref. [1–12] and references therein). Extensive investigations of photoelectrochemical phenomena in these systems provide further insights into the corrosion mechanism and may be useful in improving copper corrosion resistance. However, these problems are not the main objective of the present review.

We should like to focus our attention on the systems containing ligands that are capable of forming various Cu(II) complexes. Spontaneous formation of copper oxides in such systems belongs to processes that often attend the electroreduction of Cu(II) [13–24] and may affect not only the kinetics, but also the mechanism of the charge transfer reaction. The most pronounced conditions for its development arise in systems containing Cu(II) complexes, which are stable in a wide pH region. Again, oxide layers developed in electrochemical systems containing ligands are interesting in themselves, because their properties may be essentially different from those known for single crystals or polycrystalline compact forms. The latter are known as *substances* exhibiting *p*-type semiconductor properties and, therefore, sensitive to optical perturbation.

Prospects for practical implementation of semiconducting Cu_2O layers have also been the object of considerable attention. Very interesting idea is to use cuprous oxide as a material for the conversion of solar energy into electrical or chemical energy. In spite of the fact that there were some doubts [25] regarding the expediency of using Cu_2O with *p*-type conduction for this purpose, recent advances hold promise in this area. Hara *et al.* considered [26] that the illuminated particles or specially fabricated films of cuprous oxide can serve as an effective catalyst for decomposition of water. Illuminated Cu_2O particles showed high efficiency while working as photocathode in a photovoltaic cell [4].

The data available in the literature show that various conditions of oxide formation were used: anodic oxidation of copper, exposure of Cu electrode in contact with solution under open-circuit conditions, calcination of Cu in the open atmosphere, and so on. Surface oxides developed during anodic polarization of

Electrochemistry of Metal Complexes: Applications from Electroplating to Oxide Layer Formation, First Edition.
Arvydas Survila.

the Cu electrode or under conditions of its corrosion show the most complex composition. They may consist of Cu_2O, or Cu_2O and CuO (the so-called duplex layer [6]), and their behavior corresponds to the *p*-type conductivity. At the same time, a number of authors [1, 2, 5, 27] who have investigated Cu_2O films on copper substrates have observed an *n*-type conductivity. The same point of view is, actually, shared in [2] but the electron conductivity of the oxide layer is associated with the CuO admixture that either has *p*-type conductivity or imparts such conductivity to the cuprous oxide at the expense of the stoichiometric excess of oxygen. In accordance with [2], the interface could be imagined in the form of alternating layers: Cu|*n*-Cu_2O|*p*-Cu_2O|*n*-CuO|*p*-CuO| electrolyte. Deviations from stoichiometry are supposed to be present in the layers of *n*-Cu_2O and *p*-CuO.

Oxide layers formed in electrochemical systems involving Cu(II) complexes possess less complex compositions. As an example, we refer to the XPS data obtained for layers developed in Cu(II)–glycolic acid solutions [28]. A single peak was found in the Cu $2p_{3/2}$ spectrum (binding energy of 932 ± 0.1 eV) that was attributed to Cu_2O. At the same time, no peaks typical of CuO or $Cu(OH)_2$ were present. Thus, it should be stated that the main component of such oxide layers is Cu_2O. Besides, some data were indicative of the adsorption of OH^- or water, as well as of deviations from the stoichiometry in the oxide layer [8, 12, 29]. The largest amount of oxygen was found on the surface of all the samples, this being the result of oxidation in the atmosphere. This surface layer is very thin (1–2 nm) and is easily removed by sputtering.

At present, there is no doubt that the (photo)electrochemical properties of oxide layers depend strongly on the conditions under which they are built up. Hence, the possibility exists to obtain Cu_2O-containing formations with characteristics that are not typical of monocrystals or polycrystalline compacts. The nature of the ligands, as well as the composition of the ligand-containing solutions, is of great importance here.

10.1 Two Mechanisms of Cu_2O Formation

As mentioned earlier, oxides can be formed on copper electrodes in various ways, and two main mechanisms are worthy of consideration. One of these is simply copper corrosion, which often occurs in Cu(II)-free naturally aerated solutions. Intermediate Cu^+ ions derived from copper oxidation are able to react with OH^- anions yielding unstable CuOH that, in turn, decomposes into cuprous oxide and water

$$2Cu + 2OH^- - 4e \rightarrow Cu_2O + H_2O. \tag{10.1}$$

Released electrons are usually consumed in the reduction of dissolved oxygen. The rate of such a conjugated process depends on different factors, such as the oxygen concentration, the acidity of the medium, the copper surface state, and so on. Corrosion intensity can be also suppressed by inhibitors.

Another mechanism is involved in the Cu(II)-containing solutions where Cu^+ ions are generated due to the interaction between Cu^{2+} and the metallic phase of the copper electrode

$$Cu + Cu^{2+} \rightleftarrows 2Cu^{+}. \tag{10.2}$$

The latter process attains equilibrium, if the Cu^+ concentration does not exceed some critical (maximum) value specified by the relation [30]

$$\log [Cu^{+}]_{max} = -0.84 - pH. \tag{10.3}$$

Otherwise, an excess of Cu^+ ions will react with OH^- yielding Cu_2O. The net reaction of this process may be written as

$$Cu + Cu^{2+} + 2OH^{-} \rightarrow Cu_2O + 2H_2O. \tag{10.4}$$

The condition (10.1) can be rearranged introducing the equilibrium constant of the process (10.2). Then,

$$\log [Cu^{2+}]_{max} = 4.54 - 2pH. \tag{10.5}$$

Eqs. (10.3) and (10.5) refer to the main relationships that determine the conditions for formation of stabile Cu_2O.

In the presence of substances that are capable of forming of Cu(II) complexes, the $[Cu^{2+}]$ value would depend on the nature and concentration of ligands. In the case of ligand-free Cu(II) systems, Cu_2O is stable in the relatively narrow pH range that is obvious from Pourbaix diagrams. pH range becomes considerably wider in the presence of ligands, because they stabilize the system and prevent the precipitation of $Cu(OH)_2$. However, Pourbaix diagrams are of limited use in this case, because complexation effects are neglected. Therefore, an individual analysis of the distinct system is required. One of possible approaches is described in Section 2.3.

10.2 Composition of Oxide Layers

Oxide layers formed in various electrochemical systems possess rather similar compositions. As an example, we refer to the XPS data obtained for layers developed in Cu(II)–glycolic acid solutions. A single peak was found in the Cu $2p_{3/2}$ spectrum at a binding energy of 932.2 ± 0.1 eV. The closest reference energies are 932.4 ± 0.1 eV for Cu and 932.2 ± 0.2 eV for Cu_2O. It must be said that no peaks typical of CuO (933.6 ± 0.2 eV) or $Cu(OH)_2$ (934.9 ± 0.2 eV) were present. In accordance with these data, an O 1s binding energy of 530.0 ± 0.2 eV and a Cu L3M45M45 kinetic energy of 916.7 ± 0.1 eV were detected for all the samples (reference energies for Cu_2O are 530.4 ± 0.2 and 916.6 ± 0.4 eV, respectively). Another parameter found from the Auger spectra, 918.7 ± 0.2 eV, coincides with that (918.8 ± 0.2 eV) established for pure copper [15]. Thus, it should be stated that the main component of the oxide layers is Cu_2O. It is necessary to

discuss the peaks observed in the O 1s spectra at higher binding energies of 531 – 532 eV. Their presence might be conditioned by the adsorption of $O\tilde{H}$ or water, as well as by deviations from the stoichiometry in the oxide layer. The latter phenomenon seems to be responsible for the AES energies of 917.1 ± 0.1 eV that are intermediate between values given for Cu_2O (916.6 eV) and CuO (917.9 eV). Similar conclusions on the composition of oxide layers follow also from the data obtained for the corrosion system.

The largest amount of oxygen was found on the surface of all the samples; this being the result of oxidation in the atmosphere. This surface layer is very thin (1 – 2 nm) and is easily removed by sputtering. The subsequent distribution of oxygen depends on the thickness of the oxide layer. As will be seen next, oxide layers may be destroyed to a large extent when the appropriate negative polarization is applied.

10.3 Kinetics of Cu_2O Formation

It is evident that the Cu^{2+} concentration is one of the main factors that control the rate (w) of Cu_2O formation. Immediate data of this process can be obtained from electrochemical quartz crystal microgravimetry (EQCM) measurements, because the variations of oscillation frequency with time can serve as a measure of the rate of formation of solid phase (see Eq. (8.20)). It follows from typical examples given in Figure 10.1 that two kinds of $\Delta f - t$ dependencies are usually observed. The linear plots obtained for the β-alanine and ethylenediamine systems are indicative of a constant w over a wide range of exposure times. Taking

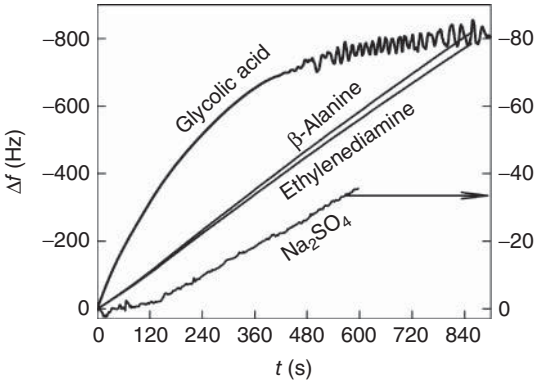

Figure 10.1 Frequency variations of quartz crystal oscillations recorded in 0.01 M Cu(II) solutions containing 0.04 M glycolic acid (pH 5.9), 0.04 M β-alanine (pH 5.6) or 0.005 M ethylenediamine (pH 5.3), and 0.3 M K_2SO_4 as a supporting electrolyte. Open-circuit potentials E_{oc} are equal to 0.20, 0.24, and 0.25 V, respectively. Data obtained for corrosion system (0.5 M Na_2SO_4, pH 5.6) are shown at right ordinate.

into account the stoichiometry of reaction (10.4), we found that w is equal to 0.14 and 0.15 nmol cm^{-2} s^{-1} for ethylenediamine and β-alanine solutions, respectively. Similar plots and similar w value were also obtained for glycolic acid solution at pH 4.9. However, the rate of oxide formation increases with solution pH and, at pH 5.9, the EQCM plot acquires a different shape. That is, this curve obeys a kinetic equation that is typical of first-order reactions

$$-\Delta f = a(1 - e^{-kt}). \tag{10.6}$$

The initial value $w = 0.5$ nmol cm^{-2} s^{-1} gradually decreases approaching the region, where oscillations arise.

It could be interesting to compare the aforementioned kinetic characteristics with similar parameters characterizing the corrosion system. Variations of oscillation frequency in naturally aerated 0.5 M Na_2SO_4 solutions (pH 5.6) are approximately 10-fold lower. Besides, a certain increase in f is observed initially, this being indicative of the active anodic dissolution of copper with no oxide formation. Nevertheless, the saturation of the surface layer with Cu^+ ions seems to take a rather short time and then the oxide formation attains a constant rate equal to ~0.05 nmol cm^{-2} s^{-1}. It should be noted that this value was obtained by considering the stoichiometry of process (10.1), which differs from that given by reaction (10.4).

Quite interesting results were obtained for Cu(II) solutions containing maleic acid. This ligand differs from the substances considered earlier in that it produces complexes with both Cu^{2+} and Cu^+ ions. Moreover, it is particularly remarkable that the Cu(I) complexes are significantly more stable than the respective Cu(II) compounds. Addition of maleic acid gives rise to the intensification of Cu^+ generation due to the shift of the equilibrium (10.2) to the right. Simulations based on the material balance equations show that deep chemical changes are possible in the system with 90% transformation of Cu(II) into Cu(I). The EQCM data (Figure 10.2) are in line with these points. Two types of EQCM plots may be distinguished. The first group concerns pH ≤ 5 and is characterized by a positive slope of the curves that clearly demonstrates the loss of electrode mass throughout the entire experiment. Though estimated critical pH for Cu_2O formation is 3.6, increase in the electrode mass is observed only at pH > 5 where the plots acquire a negative slope in some time. This suggests that the process (10.4), resulting in the increase in electrode mass, becomes possible. Rates of both processes are approximately of the same order (0.4–0.8 nmol cm^{-2} s^{-1}). It is remarkable that the initial rate of copper corrosion grows with solution pH despite the fact that the concentration of Cu^{2+} ions decreases in this case due to the rise in the complexation degree. Consequently, the activity of copper surface should be considered as the main factor that controls the kinetics of heterogeneous process (10.1). On the other hand, Cu_2O formation also accelerates with pH.

More data regarding kinetics of Cu_2O formation can be obtained from voltammetric experiments. In this connection, some electrochemical properties of oxide layers should be previously considered.

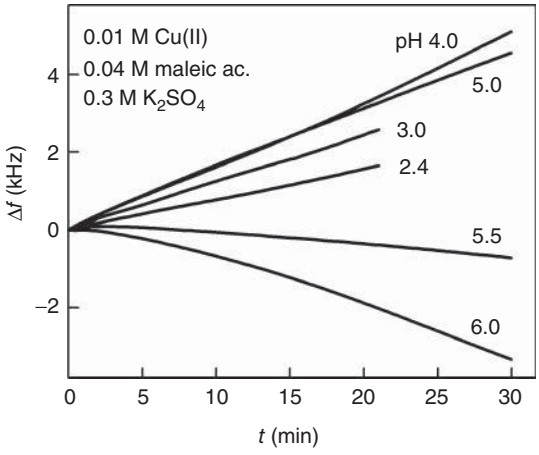

Figure 10.2 Frequency variations of quartz crystal oscillations recorded in 0.01 M Cu(II) solutions containing 0.04 M maleic acid and 0.3 M K_2SO_4 at different pH as indicated. Open-circuit conditions, $E_{oc} = 0.23$ V.

10.4 Electrochemical Reduction of Oxide Layers

Oxide layers formed on the electrode surface can be identified by (photo) electrochemical or spectrophotometric methods. In voltammetry, an electrochemical activity of Cu_2O can be also employed. The following process occurs at sufficiently high cathodic polarizations:

$$Cu_2O + 2H^+ + 2e \rightarrow Cu + H_2O \tag{10.7}$$

manifesting itself in the presence of characteristic voltammetric peaks. A typical plot obtained after 20-min exposure of Cu electrode to the Cu(II) ethylenediamine solution is presented in Figure 10.3 by line. Very similar curves are also obtained for Cu(II) solutions containing β-alanine and some other ligands. As the cathodic polarization increases, the rate of Cu(II) reduction also grows to reach the plateau of limiting current density at $-0.5 < E < -0.2$ V. Further, at $E = -0.75$ V, a sharp current peak arises. This peak disappears at the reverse potential sweep (toward more positive values). Besides, this peak is also absent on the curve recorded repeatedly after the first cycle.

Consideration of transformed EQCM data (symbols in Figure 10.3) helps to clarify the nature of current peaks. The results obtained by the two different methods (Figure 10.3) are very close in the region of the first current maximum ($-0.35 < E < 0.2$ V), which should be attributed to the copper electrodeposition. However, later on, they differ and the EQCM transform yields a minimum in the region of the characteristic voltammetric peak at −0.71 V. It must be said that the EQCM voltammogram in the latter region presents a certain linear combination of the rates of two processes. The first of these is the reduction $Cu^{2+} + 2e \rightarrow Cu$ resulting in an increase in the electrode mass ($\Delta m = 63.45$ g

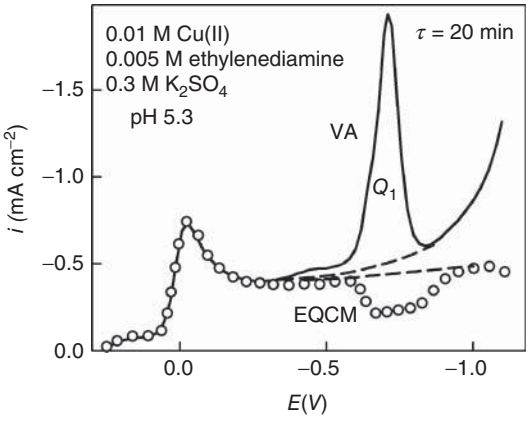

Figure 10.3 Comparison of voltammetric (line) and EQCM (circles) data obtained for a Cu(II)–ethylenediamine solution of composition as indicated with $v = 5\,\text{mV}\,\text{s}^{-1}$. The Cu electrode was exposed to the solution under open-circuit conditions for 20 min.

when 2 mol of electrons are transferred). The second process is given by reaction (10.7) and, on the contrary, gives rise to the opposite mass changes: ($\Delta m = -16\,\text{g}$ under the same conditions). It follows from the aforementioned fact that the charge Q_1 calculated by the integration of the voltammogram in the current peak region should be $63.45/16 \approx 4$ times higher than Q_2 defined in a similar region of the transformed EQCM data (Figure 10.3, the areas between the respective solid and adjacent dotted curves). Indeed, the Q_1 and Q_2 values obtained (~42 and ~10 mC cm^{-2}, respectively) satisfy this condition fairly well. It can also be seen that the reduction process begins at $E = -0.35$ V, though the current peak is substantially shifted to higher negative overvoltages.

To investigate the behavior of the current peak in more detail, the potential sweep technique was used under natural convection conditions. The coordinates of the current peak were found to agree with the model describing electroreduction of the adsorbed layer (e.g., see Ref. [31]). Such a model is inapplicable when Cu_2O layer is treated as a phase with a constant activity. However, the analysis of the experimental data shows that the amount of Cu_2O accounts for several tens of monolayers and the properties of cuprous oxide are more typical of adsorbed polylayers than of the Cu_2O phase. According to this model, the potential of the current peak E_p does not depend on the potential sweep rate v for a reversible process and varies linearly with log v in the case of the irreversible process. This is supported by the experimental data (Figure 10.4) when oxide layers are not too thick (exposure times are equal to 5 and 10 min). For somewhat thicker layers ($\tau = 20$ min), a deviation from the theory is observed. The slopes of the lines in Figure 10.4 are equal to ~1.1 ($\tau = 5$ min) and ~1.16 ($\tau = 10$ min). A comparison of these values with the theoretical value ($-2.3RT/\alpha n_\alpha F$ [31]) yields $\alpha = 0.5$ at $n_\alpha = 2$

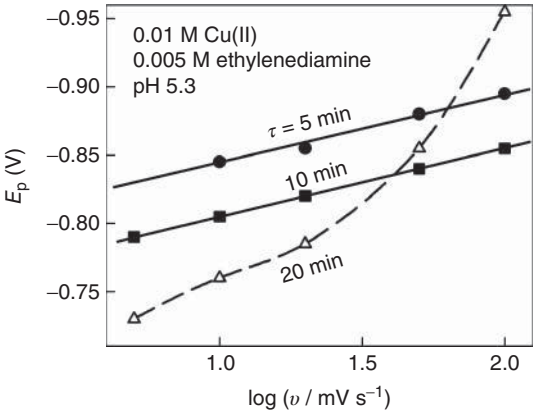

Figure 10.4 Variations of E_p with $\log v$ at the various exposure times τ indicated on the curves.

(reduction of a Cu_2O particle requires two electrons to be transferred). The following relationship is also valid for the model under discussion:

$$i_p = -\frac{\alpha n^2 F^2 v \Gamma}{2.718RT}. \tag{10.8}$$

Actually, the experimental i_p that was read from the level of the current plateau varies linearly with v (Figure 10.5). Equation (10.8) allows us to estimate the charge $Q = nF\Gamma$ employed for Cu_2O reduction. Then, the rate of oxide formation can be expressed as follows:

$$w = \frac{1}{2F}\frac{dQ}{dt}. \tag{10.9}$$

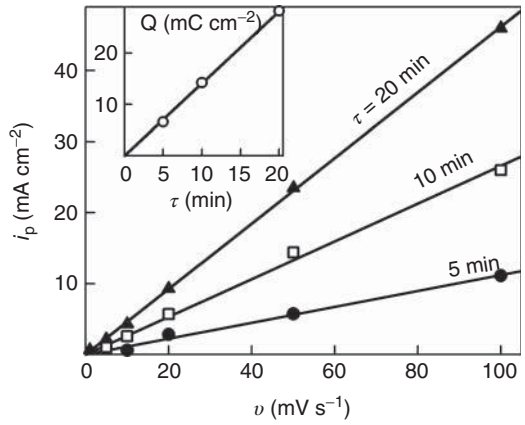

Figure 10.5 Variations of peak current with potential scan rate at the various exposure times τ indicated at the curves. The charge Q employed for Cu_2O reduction is given in the inset.

It follows from the data given in the inset of Figure 10.5 that the Cu_2O formation rate is equal to 0.12 nmol s^{-1} cm^{-2} provided that the total amount of Cu_2O formed is reduced in the region of the current peak. A similar value (0.14 nmol s^{-1} cm^{-2}) follows from the data obtained by the EQCM technique under open-circuit conditions (Figure 10.1).

Very similar data were obtained for Cu_2O layers formed in the system Cu|Cu(II), gluconic acid [28]. When the Cu electrode was exposed to the Cu(II) solution for less than 5 min, no current peak was observed. However, at longer exposure times, the critical Cu^+ concentration was accumulated and the formation of Cu_2O became possible. Considering the absence of current peaks on the reverse voltammograms, it was concluded that Cu_2O is fully reduced during the direct potential scan. The charge Q following from the integration of current peak was used to estimate the rate of Cu_2O formation according Eq. (10.9). Again, actually the same value ($w = 0.125$ nmol s^{-1} cm^{-2}) was obtained.

Hence, Cu_2O reduction is an irreversible process that proceeds according to the regularities typical of the adsorbed layers. The height of voltammetric peak, which varies linearly with the potential scan rate, is suitable for the estimation of quantity of the oxide layers formed. It is very important to establish the nature of this peak, because similar current maxima could appear in the solutions where Cu_2O cannot be stable thermodynamically. For instance, a characteristic peak is observed in the glycolic acid system at sufficiently low pH in the region of potentials typical of Cu_2O reduction. However, this maximum possesses different properties: its height varies linearly with $\sqrt{v}$, is conditioned by the acidity of the solutions, and is actually independent of the presence of Cu(II) or exposure time. Such current peaks are caused by hydrogen evolution and are considered next.

Voltammetric data were used when investigating temperature effects in the ligand-deficient Cu|Cu(II), ethylenediamine system [23]. Analysis of the data obtained with different ligands shows [22] that the formation of oxide layers becomes more intensive when the complexation degree of the solutions decays and, consequently, the Cu^{2+} concentration increases. This gives grounds to consider the process (10.2) as the main rate determining step. Then, the rate of oxide formation should follow the equation:

$$w = k_0[Cu^{2+}] \exp\left(\frac{-\Delta E_a}{RT}\right), \tag{10.10}$$

where k_0 is the formal rate constant and ΔE_a is the activation energy. Simulations involving temperature-dependent stability constants produced interesting results. Though the stability of complexes becomes weaker with temperature, this effect is compensated to a great extent by a respective decrease in the stability of protonated ligands. The latter effect results in additional release of L species, which are capable of forming coordination bonds with Cu^{2+} ions. All these competitive interactions result in what might be qualified as a peculiarity of the solution: the effect of temperature on complexation degree is found to be quite weak and, specifically, $[Cu^{2+}]$ may be treated as a temperature-independent quantity. Then, the exponential term in Eq. (10.10) gives the effect of temperature in an explicit

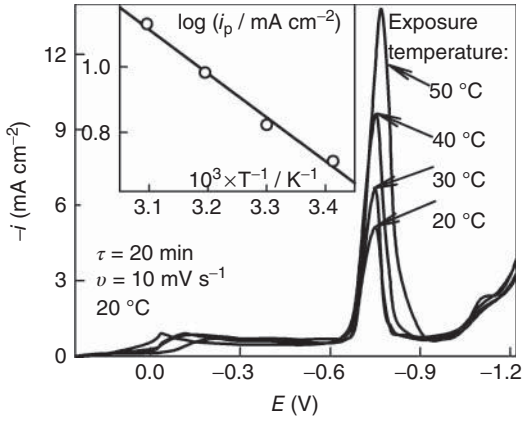

Figure 10.6 Voltammograms recorded at 20 °C in solutions containing 0.01 M Cu(II), 0.005 M ethylenediamine, and 0.3 M K_2SO_4 (pH 5.3). Prior to experiments, copper electrodes were exposed to the same solution at temperatures indicated at the curves.

form and

$$\frac{\mathrm{d}\ln w}{\mathrm{d}(1/T)} = \frac{-\Delta E_a}{R}. \tag{10.11}$$

As the peak current may serve as a measure for the Cu_2O formation rate, the term w in this relationship may be replaced by i_p.

$Cu|Cu_2O$ electrodes were formed for 20 min in the solution under discussion at different temperatures. Then, each specimen was immersed into the same solution and all voltammograms were recorded at the same (20 °C) temperature (Figure 10.6). As seen in this figure, a plateau of limiting current remains at the same level, whereas i_p increases gradually with the exposure temperature, and no significant shift in peak position occurs. Bearing in mind that the temperature dependence of $[Cu^{2+}]$ is very weak, it is possible to obtain linear $\log i_p - 1/T$ plots at constant τ and v (inset). The i_p values were read from the level of current plateau observed at $-0.6 < E < -0.2$ V. An analysis of the slope of approximating line performed on the basis of Eq. (10.10) with the condition that $i_p \sim w$ yields $\Delta E_a = 30\ \mathrm{kJ\ mol^{-1}}$.

In the case of a heterogeneous reaction, its rate may be defined as $w = A^{-1}\partial\Gamma/\partial t$, where A is a surface area and Γ is a surface concentration (adsorption) of the solid product (Cu_2O) formed. With established Γ and ΔE_a values and simulated concentration of Cu^{2+} ions, Eq. (10.10) yields $k_0 = 0.17\ \mathrm{s^{-1}}$. The obtained result shows that Cu_2O formation is not very fast. It follows from the analysis of its kinetics that approximately two monolayers could be formed over 1 min, provided that Cu_2O is uniformly distributed on the electrode surface. However, as we shall see next, it does not always happen.

10.5 Photoelectrochemical Properties of Oxide Layers

Topics to be discussed next relate to photoelectrochemistry that deals with a wide range of problems concerning the electrochemical current arising from the light perturbation. Fundamentals of this important field of electrochemical science can be found in special literature. Here we did not pursue goals to perform exhaustive investigations of photoelectrochemical phenomena and, for the most part, we restrict ourselves by common presentation of our observations.

Often, oxide layers on metals are semiconductors that are characterized by a large number of closely spaced, low-energy, mainly filled orbitals or energy levels (the valence band) and a large number of closely spaced, higher-energy, mainly vacant orbitals or energy levels (the conduction band). Energy regions of allowed states are separated by a forbidden region. In the ideal case of semiconductors with no surface states, no electrons or holes exist in this region. The energy gap between the highest level in the valence band and the lowest level in the conduction band is called the *bandgap*.

When a metal is intimately brought into contact with a semiconductor, the so-called Schottky barrier is formed. The potential distribution across this barrier is of specific character. The main region over which the potential changes is within the semiconductor itself, often extending over many nanometers. The important point is that as the bias on the semiconductor is altered, the change in potential is also entirely accommodated within this depletion.

The presence of depletion or space-charge layer has important consequences. If light of energy exceeding the bandgap is incident on the semiconductor, then the electron–hole pairs are created. They do not undergo recombination because the electric field within the space-charge region promotes the separation of the electrons and the holes. The electrons move to the electrolyte interface for a *p*-type material, while the holes move to it for an *n*-type material. There the holes can be captured by an acceptor state in solution, driving an electrochemical reaction. At the same time, the electron can pass round an external circuit to the counter electrode and take part in the electrochemical reaction. Two cases are possible. A second different electrochemical couple may be involved resulting in true photoelectrochemical process, such as the photo-splitting of water. Alternatively, the same redox couple in solution may recapture the electron. Then, electronic work is done in the external circuit but there is no net chemical change. Thus, *p*-type semiconductor electrodes function as photocathodes. Relevant processes can be considered in the case of *n*-type semiconductor electrodes that function as photoanodes.

We have already mentioned that the photoelectrochemical properties of oxide layers depend strongly on the conditions under which they are formed. When Cu_2O develops in systems containing Cu(II) complexes, the main factors responsible of the type of conductivity are the nature of ligand and the pH of solution. Single crystals or polycrystalline compact forms of Cu_2O are known to be *p*-type semiconductors with a band gap of 2.1 eV. However, common *p*-type

conductivity is rather rare for oxides formed in ligand-containing solutions; such cuprous oxide develops in the solutions containing ethylenediamine [19] that can act as reductant. More often, *n*-Cu_2O species are formed, as in weakly acid solutions containing such ligands as amino [11, 16, 17] or hydroxy acids [22, 24]. It was found [22] that the type of conductivity can alter during the development of oxide layer. Then, the transition from *p*- (thin initial layers) to *n*-type conductivity (thicker layers) is observed. Thin *p*-Cu_2O layers are formed in alkaline solutions containing tartaric or malic acids [22]. Eventually, it should be mentioned that the sign of photoresponse can vary with the wavelength of the perturbing light [32].

Both oxides respond to light perturbation over a wide range of visible spectrum. For instance, *n*-Cu_2O generates a negative photopotential under open-circuit conditions, or positive photocurrent as the external bias voltage is applied. This effect is very sensitive to the presence of oxides and may be used, initially, for their detection. The development of the photoresponse is shown in Figure 10.7. The onset of the negative photopotential is detectable after just 20–30 s when only one monolayer of Cu_2O is formed.

A band gap of 2.1 eV is consistent with the threshold wavelength (λ_{max}) equal to ~590 nm. Experiments performed with monochromatic illumination make it possible to establish this quantity for *n*-Cu_2O (Figure 10.8). In accordance with the type of conductivity, the light perturbation of Cu electrode under open-circuit conditions results in the generation of a negative photopotential. Its pulses obviously depend on the quantum energy and decrease with the wavelength. The photoresponse disappears at ~590 nm that is consistent with the λ_{max} given earlier.

Similar behavior shows *n*-Cu_2O formed in Cu(II) solutions containing glycolic acid [33]. Though the level of photoresponse depends on the light intensity, the onset of photoeffects under discussion takes place at quantum energy of ~2.1–2.3 eV (Figures 10.9 and 10.10). So, a band gap of *n*-Cu_2O is characterized by the value close to that of *p*-Cu_2O.

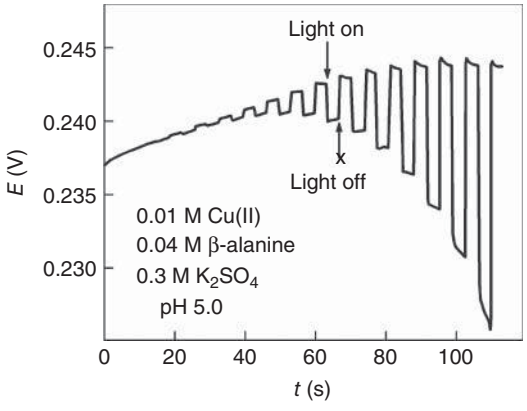

Figure 10.7 Onset of the photopotential under open-circuit conditions in a β-alanine solution of composition as indicated.

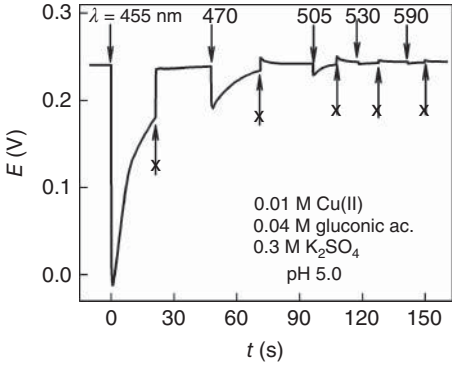

Figure 10.8 Photopotential generated with light pulses of different wavelengths. Respective arrows indicate the start and the end of light perturbation. The initial exposure time $\tau = 10$ min.

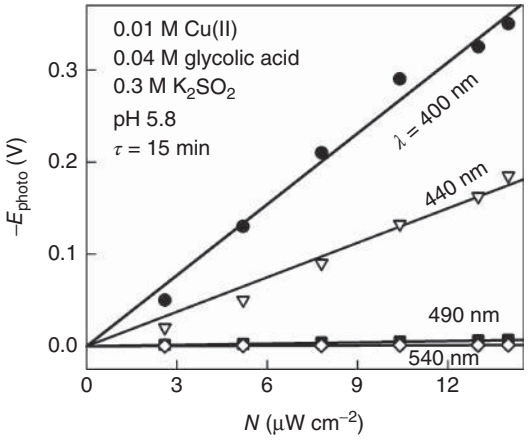

Figure 10.9 Dependencies of photopotential on quantum energy at different power densities and wavelengths of monochromatic light. Open-circuit conditions.

The photoresponse manifests itself under cathodic polarization conditions as well. The level of photocurrent carries information on the thickness of oxide layers until it is less than the depth of penetration of the disturbing light. Photocurrents are observed at potentials ranging up to the voltammetric peak where oxide layer reduces. Generally, a single reduction peak occurs; however, more complicated cases are also possible. Among these is the glycolic acid system with well-defined response to optical perturbation (Figure 10.10). The most intensive photocurrents are observed on the direct scan of the voltammogram up to the first reduction peak. A major part of Cu_2O is reduced in this region, but a certain quantity of the oxide remains on the electrode. This residual Cu_2O is able to produce a weaker but quite detectable photoresponse. The latter disappears on further scanning of the electrode potential, this being indicative of the complete destruction of the oxide

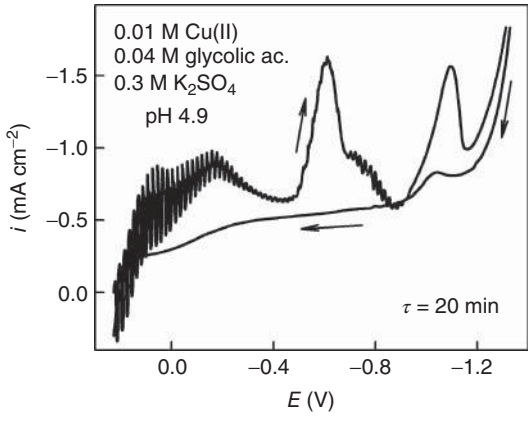

Figure 10.10 Cyclic voltammogram recorded under chopped illumination conditions. Polychromatic irradiation, the initial exposure time $\tau = 20$ min.

layer. When the reverse scan is applied, the system exhibits no response to optical perturbation. In accordance with *n*-type conductivity, anodic photocurrents are observed at $E > 0.05$ V. The highest response is generated near the open-circuit potential. When oxide layers are formed sufficiently long (60 min), the anodic pulses can range up to 20 mA cm^{-2}. It is conceivable that this is the most intense response of Cu_2O layers formed in electrochemical systems to the present day.

As the cathodic polarization is increased, the photocurrent weakens, disappears, hereupon the opposite in sign current emerges again (Figure 10.11). The explanation of photocurrent inversion is given in [1], according to which the inversion potential of semiconducting oxide films on copper coincides with the flat-band potential. Its position depends on different factors including the quantum energy and power density of the perturbing light, the solution pH, the

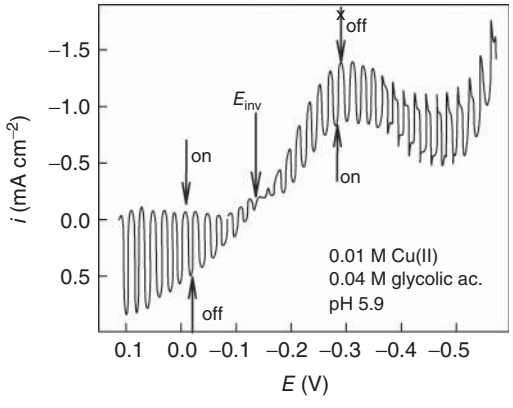

Figure 10.11 Inversion of photocurrent. The initial exposure time $\tau = 1$ h.

thickness of oxide layers, and so on. More information on this effect can be found in Refs. [16, 20, 22, 24, 33].

10.6 Photoelectrochemical Stability of Oxide Layers

We have discussed earlier that Cu_2O layers can be destroyed when a sufficiently negative potential is applied and Cu_2O reduction process takes place. However, the layers that are electrochemically stable under open-circuit conditions undergo a breakdown when exposed to light. Conditions for photodestruction can be disclosed from a comparison of energy levels in the semiconductor and in the solution. A requisite for this purpose diagram is presented in Figure 10.12. The data related to semiconductor properties of Cu_2O (band gap, position of band edges) were taken from Gerischer [34]. To calculate energy levels of decomposition processes as well as other redox reactions involving solution components, concentrations of corresponding components were calculated making use of stability constants of Cu(II)–β-alanine complexes and analogous characteristics of protonated ligands. Besides, it was established that formation of solid CuO phase is hardly probable in weakly acid solutions due to complex formation effects.

We should like to draw the reader's attention that the data in Figure 10.12 are given in the so-called "absolute" or "vacuum" scale, which is commonly used in the electrochemistry of semiconductors. The potential on the absolute scale is the electrical work required to bring a unit positive test charge into the conducting phase of the electrode from a point in vacuum just outside the system. It is known

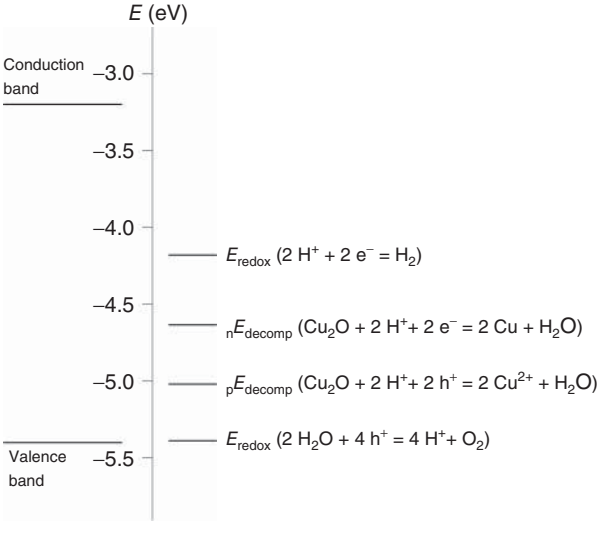

Figure 10.12 Energy correlation between band edges and the Fermi levels of electrode reactions in aqueous solution of 0.01 M Cu(II) and 0.04 M β-alanine at pH 5.5.

that the absolute electrode potential cannot be calculated in the framework of thermodynamics without introducing certain model assumptions. This value can be obtained from Volta potential difference and surface potential values of a metal and a solution. For the surface potential of water, various models provided result in about 0.1 V; then the absolute potential of the standard hydrogen electrode (SHE) was estimated to be 4.5 ± 0.1 V (with this value, the standard potentials of other couples and reference electrodes can be expressed on the absolute scale). The respective Fermi energy on SHE (electrochemical potential of electrons, in eV) is the same quantity but opposite in sign, that is, −4.5 eV [31].

As the Fermi levels for both cathodic and anodic decomposition are located inside the band gap, Cu_2O seems to be unstable cathodically as well as anodically [34]. Photodestruction processes are as follows:

- the cathodic process involving electrons

$$Cu_2O + 2H^+ + 2e^- \rightarrow 2Cu + H_2O \tag{10.12}$$

- the anodic process involving holes

$$Cu_2O + 2H^+ + 2h^+ \rightarrow 2Cu^{2+} + H_2O. \tag{10.13}$$

Conclusions following from the energy diagram are supported by experimental results. Characteristic photoresponse to optical perturbation is shown in Figure 10.13 together with the *in situ* EQCM data. Initially there is an abrupt decrease in the open-circuit electrode potential. After passing through a sharp minimum, a steady-state E_{oc} of the illuminated electrode is slowly attained. Negative photopotentials are indicative of the presence of *n*-Cu_2O. According to [35], initial E changes are directed toward the flat-band potential.

Contrary to the dark conditions, the resonance frequency of quartz crystal, coated with Cu|Cu_2O layer, continuously increases after a light perturbation is

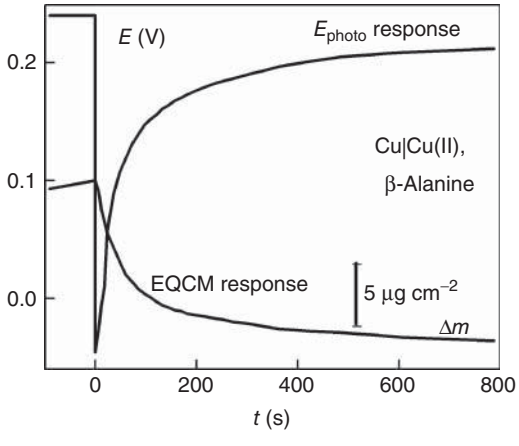

Figure 10.13 Typical photo (ordinate to the left) and EQCM responses observed in the β-alanine system. Laser illumination ($\lambda = 488$ nm, $N = 0.1$ W cm^{-2}) was applied at $t > 0$.

applied. Note, this pronounced effect could not be caused by quartz heating. The temperature coefficient of the AT-cut quartz crystal used in investigations was close to zero. Besides, special experiments with the temperature-sensitive microprobes showed very weak heating effects (an increase in the electrode temperature did not exceed 0.5 °C). Therefore, it could be concluded that the frequency changes were caused by the respective losses in mass that arise from the breakdown of surface oxide.

It follows from (10.12) or (10.13) that the photoelectrochemical disintegration of Cu_2O suggests consumption of H^+ ions at the electrode surface. This process should be accompanied by a comparatively slow, diffusional mass transport in the solution. The sharp potential drop after the illumination is switched on creates the conditions that are similar to those for the potential step method. It can be showed that the quantities presented at $t > 0$ in Figure 10.13 vary linearly with $1/\sqrt{t}$ that is characteristic of diffusion-controlled processes.

Similar mass effects are also observed under cathodic polarization conditions. When repeatedly excited with light pulses, the changes in time of both electrode potential and mass are similar to those shown in Figure 10.13. At low ΔE, pulses of anodic photocurrent are observed. With the ΔE increase, the photocurrent pulses decrease and, at certain inversion potential, vanish completely. Then, with the further ΔE increase, pulses change their sign, that is, become cathodic. This phenomenon was already considered (see Figure 10.11). However, in contrast to the changes of photocurrent, the sign of the mass changes is the same over the entire polarization range applied. That is, in any case the electrode mass decreases if the light is switched on and increases if it is switched off. Thus, the illumination gives rise to the decomposition of the surface layer, similarly as it does under open-circuit conditions.

It can be seen from the reactions (10.12) and (10.13) that the oxygen released from cuprous oxide should react with hydronium ions increasing the surface pH. This effect can be confirmed experimentally by probing with pH-sensitive microelectrodes. One of them, $Sb|Sb_2O_3$ microprobe, was used in the following experiments. This antimony microelectrode (AME) is reversible with respect to H^+ ions and its equilibrium potential is determined unambiguously by the solution pH (see Section 3.4.1). The design of the equipment permitted the position of the AME tip to be controlled with an accuracy of 10 μm. The distance of closest approach of the AME to the electrode surface, Δx, was arbitrarily taken as zero.

A typical result is shown in Figure 10.14: the pH increases with light perturbation and returns to the initial value when the light is switched off. The latter quantity is ~0.5 lower than bulk pH, because the formation of Cu_2O starts again in the dark giving rise to the surface pH decrease. The pH variations are exhibited most powerfully at the very surface of the electrode and become weaker when the distance from the surface is increased.

Thus, the results of investigations show that oxide layers formed in the β-alanine system are not stable at the illumination conditions. However, it is hardly possible to state that this conclusion could be extended to all electrochemical systems where the formation of cuprous oxide layers is possible. As

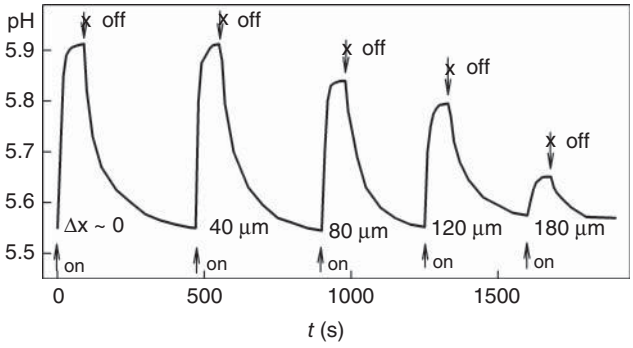

Figure 10.14 Variations of surface pH under chopped illumination conditions in the β-alanine system at different distances Δx between the Cu surface and an $Sb|Sb_2O_3$ microelectrode. $c_{Cu(II)} = 0.01$ M, $c_L = 0.04$ M, bulk pH 5.6.

their (photo)electrochemical properties depend strongly on the conditions under which they are built up, more stable oxide layers are also expected. In this connection, electrochemically deposited Cu_2O layers, which showed enhanced resistance to cathodic photocorrosion [4], are noteworthy.

10.7 Influence of Oxide Layers on Kinetics of Cu(II) Reduction

Electrode processes involving Cu(II) complexes consist of different chemical and charge transfer steps (Chapters 8 and 9) that present the certain difficulties relating the quantitative analysis of the reduction kinetics. The problems become even more complicated when surface oxides are formed. Due to their electrochemical activity over the certain potential range, a separation of the total current into respective partial ones is required.

At sufficiently low cathodic polarizations, oxide layers usually show a low electrochemical activity and their influence can be reduced to the formation of the certain barrier for charge transfer. This effect becomes weaker, when oxides are unevenly distributed on the electrode surface occupying some sites. SEM micrographs of freshly prepared copper coating (part A) and of that exposed for 30 min in the gluconate-containing Cu(II) solution (part B) are shown in Figure 10.15. A polycrystalline layer with well-exhibited crystallographic edges and faces forms during preparation of working electrode. Copper crystallites as large as 1–4 μm cover a great part of the surface. No oxygen was detected on such coatings. Surface oxides are formed at pH 5 and the amount of surface oxygen increases with exposure time. As this takes place, the tendency of segregation of Cu_2O is observed. A typical result of such process can be seen from Figure 10.15b. Cu_2O crystallites, ~50–140 nm in size, are distributed nonuniformly and seem to cover some steps, kink, and other sites that are most liable to anodic dissolution. Bare copper is visible between Cu_2O crystallites. However, impedance spectra obtained for both electrodes do not differ significantly and the Nyquist plots are similar in

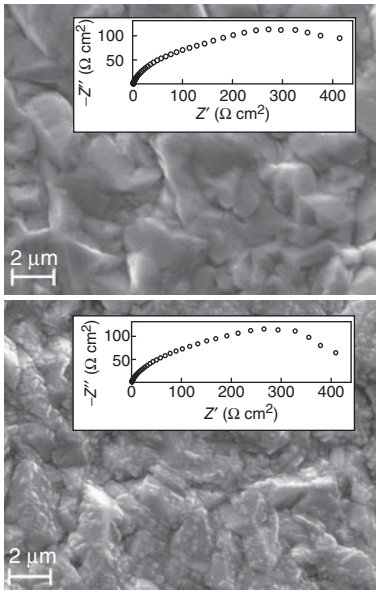

Figure 10.15 Morphology of freshly prepared copper coating (a) and of that exposed for 30 min in the solution containing 0.01 M Cu(II), 0.04 M gluconate, 0.3 M K_2SO_4 at pH 5 (b). Respective Nyquist plots obtained at the open-circuit potentials are shown in the insets.

shape. Thus, it is evident that the electrochemical properties of electrode surface do not change drastically when the compact semiconducting layer is not formed.

The situation reverses when thicker and more uniform distributed oxide layers develop. Besides, the differences in types of conductivity are also embodied most conspicuously in impedance data. As a case in point, two sets of Nyquist plots are shown in Figure 10.16. Arcs with centers below the abscissa are typical of *p*-Cu_2O (part a), whereas loops indicative of inductive character of the impedance are inherent for *n*-Cu_2O (part b). An interpretation of the data obtained is somewhat simpler in the case of *p*-Cu2O. The fact that the two arcs can be separated at sufficiently long exposure times gives grounds to propose the equivalent circuit $R_\Omega(R_{ox}Q_{ox})([R_1W_1]\ [R_2W_2]Q_{dl})$ (shown in Figure 10.17). Two subcircuits are in series. One of these, $([R_1W_1]\ [R_2W_2]Q_{dl})$, represents the Cu(II) reduction proceeding by two one-electron steps and contains the respective charge transfer resistances and Warburg impedances. The subcircuit $(R_{ox}Q_{ox})$ seems to be attributable to the oxide layer. The experimental impedance spectra can be fitted to this circuit with rather high accuracy (Figure 10.17). Similar results may be also obtained in the case of *n*-Cu_2O using a more complicated equivalent circuit $R_\Omega(R_1Q_1[C_1(R_2C_2[R_3L])])$ [36]. However, the physical sense of some its elements, such as the inductance L or negative resistance R_2, is not clear yet and needs further analysis.

We have already noted (Section 10.3) that the rate of Cu_2O formation depends primarily on the Cu^{2+} concentration and, consequently, on the complexation degree of the system that increases in the series of ligands: β-alanine, α-alanine, and glycine. On the contrary, the extent of Cu_2O formation decreases with ligand nature in the order indicated and photoresponse in the glycine-containing Cu(II)

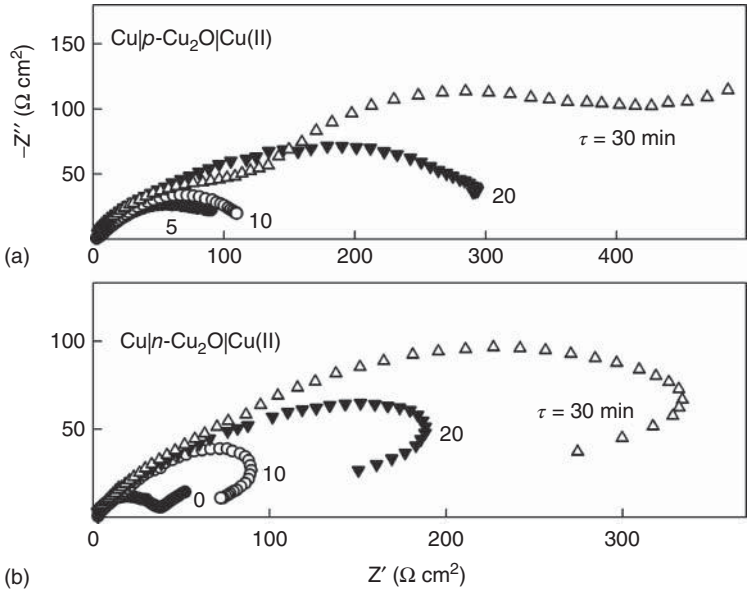

Figure 10.16 Nyquist plots recorded in 0.01 M Cu(II) solution at pH 4.9.Before measurements, the copper electrodes were exposed for the times indicated in the solutions containing: (a) 0.01 M Cu(II), 0.005 M ethylenediamine (pH 5.3) and (b) 0.01 M Cu(II), 0.04 M β-alanine (pH 6.1). 0.3 M K_2SO_4 was present in all the cases.

solutions becomes rather weak. Critical pH value for Cu_2O formation in the solutions containing 0.01 M Cu(II) and 0.04 M glycine is about 4. Therefore, certain oxidation of copper surface is probable in slightly acid and alkaline media. The shape of cathodic voltammograms depends on solution pH. At pH 5, prewaves characteristic of ligand-deficient systems are observed (see Figure 4.5). To establish kinetic parameters of Cu(II) reduction, experimental voltammograms were transformed to normalized Tafel plots (NTPs) provided that CuL^+ species is electrically active. An example of NTP obtained at pH 5 is shown in Figure 5.2. Kinetic parameters obtained from this NTP were used for simulation of entire voltammograms and a good agreement between experimental and simulated data was observed (Figure 5.2). It was also concluded that the transfer of the second electron is the rate-determining step [14].

When pH is 8.3, voltammograms exhibit two increases (Figure 10.18), the first of them being placed at $E > -0.14$ V and the second one at $E < -0.2$ V. When the rotation speed of rotating disc electrode (RDE) is high enough, these two regions are separated by the area of a sharp fall in current density. It is particularly remarkable that in the first increase, the NTP coincides actually with the one for pH 5 yielding the same kinetic parameters (a standard rate constant and a cathodic charge transfer coefficient). However, other kinetic parameters attributable to the transfer of the first electron follow from the NTP obtained for the second increase. Hence,

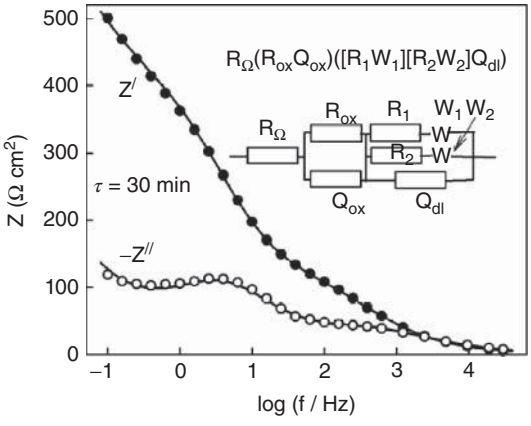

Figure 10.17 Experimental impedance spectrum taken from Figure 10.16a at $\tau = 30$ min (symbols) and that simulated for given equivalent circuit (lines) at the following values of its parameters: $R_\Omega = 0.26\,\Omega\,cm^2$, $R_{ox} = 122\,\Omega\,cm^2$, $Y_{ox} = 5.3 \times 10^{-5}\,\Omega^{-1}\,cm^{-2}\,s^{0.628}$, $R_1 = 307\,\Omega\,cm^2$, $Y_{W1} = 8.34 \times 10^{-3}\,\Omega^{-1}cm^{-2}\,s^{0.5}$, $R_2 = 10\,\Omega\,cm^2$, $Y_{W2} = 1.42 \times 10^{-4}\,\Omega^{-1}\,cm^{-2}\,s^{0.5}$, and $Y_{Qdl} = 2.25 \times 10^{-4}\,\Omega^{-1}\,cm^{-2}\,s^{0.776}$.

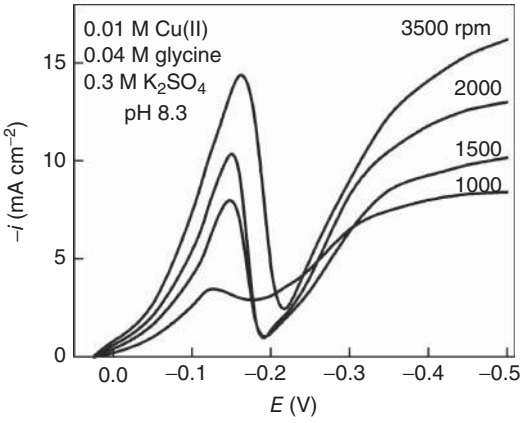

Figure 10.18 Experimental voltammograms for pH 8.3 recorded at different rotation velocities as indicated.

experimental voltammogram at pH 8.3 can be described with two different sets of kinetic parameters (Figure 10.19).

To reveal the reasons for such specific voltammetric behavior, it is necessary to analyze the influence of cathodic polarization on Cu_2O stability. Kinetic relations (5.19) and (5.20) derived for stepwise charge transfer mechanism can be used for this purpose, taking into account that monoligand complexes of Cu(II) and Cu(I) (CuL^+ and CuL, respectively) are electrically active. With this provision, also using the expressions for stability constants for the electrically active complex (EAC), it

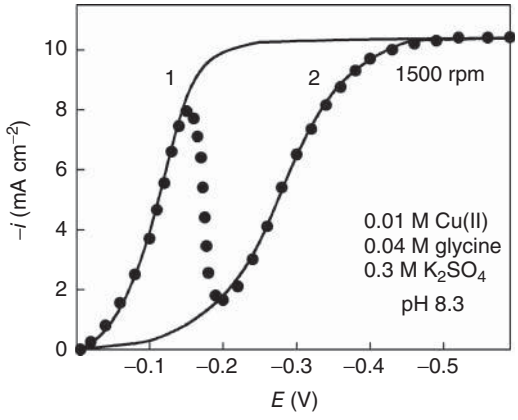

Figure 10.19 Comparison between experimental (symbols) and theoretical (solid lines 1 and 2) voltammograms simulated with two different sets of kinetic parameters.

may be shown that:

$$\frac{[Cu^+]_s}{[Cu^+]_b} = \frac{i_{01}\frac{[Cu^{2+}]_s}{[Cu^{2+}]_b}\exp\left(-\frac{\alpha_{c1}F}{RT}\eta\right) + i_{02}\exp\left(\frac{\alpha_{a2}F}{RT}\eta\right)}{i_{01}\exp\left(\frac{\alpha_{a1}F}{RT}\eta\right) + i_{02}\exp\left(-\frac{\alpha_{c2}F}{RT}\eta\right)}. \tag{10.14}$$

Two limiting cases follow from this relationship. If the second electron transfer is a reversible one ($i_{02} \to \infty$), it may be obtained for sufficiently large cathodic overvoltages such that:

$$\frac{[Cu^+]_s}{[Cu^+]} = \exp\left(\frac{F}{RT}\eta\right). \tag{10.15}$$

Hence, while increasing cathodic polarization, $[Cu^+]$ decreases by the exponential law. On the contrary, when the process rate is determined by the second electron transfer step and the transfer of the first electron is reversible ($i_{01} \to \infty$), Eq. (10.14) rearranges into:

$$\frac{[Cu^+]_s}{[Cu^+]} = \frac{[Cu^{2+}]_s}{[Cu^{2+}]}\exp\left(-\frac{F}{RT}\eta\right). \tag{10.16}$$

In this case, while increasing the cathodic polarization, the change of $[Cu^+]_s$ is determined by two multipliers, the first of which decreases and the second one increases.

It is seen from the given relationships that the character of the $[Cu^+]_s$ dependence on η requires analysis in every real case using values of the kinetic parameters of both steps of the process. Such analysis has been performed [16] using the aforementioned relationships, material balance equations, and results of pH evaluation at the electrode surface. The potential of Cu_2O destruction estimated by Eq. (10.1) was found to be equal to about −0.13 V. At pH 8.3, this value coincides with the position of current maximum, but at pH 5, it falls in the region where the

voltammogram comes out on the limiting current plateau. Therefore, the peculiar maximum observed at pH 8.3 has not been detected at pH 5.

The results obtained show that the transfer of the second electron is the rate-determining step, when Cu(II) reduction takes place in the presence of thin oxide layers. This is in line with the potentiometric data [37], according to which the process $Cu(II) + e \rightleftarrows Cu(I)$ with high exchange current density is able to control the E_{oc} value of $Cu|Cu_2O$, Cu(II) electrode. A break-up of oxide gives rise to the change of mechanism. Then, the transfer of the first electron becomes the rate-determining step that is typical of most Cu(II) reduction processes.

On substitution of α-alanine for glycine, the complexation degree becomes ~3.5 times lower and the respective increase in photosensitive is observed. Nevertheless, changes in the electrochemical properties of α-alanine system are moderate.

The β-alanine system is outstanding in this respect. Its complexation degree is lower by 2–3 orders of magnitude and the level of photoresponse is by 3–4 orders higher as compared with glycine system. Tens of Cu_2O monolayers developed in this system exert a pronounced inhibitive effect on Cu(II) reduction [15], reducing significantly the exchange current density. Attempts to construct NTP with different EAC have failed even in the potential region where Cu_2O reduction is absent. A real progress in this field lies ahead.

References

1. Wilhelm, S.M., Tanizawa, Y., Liu, C.-Y., and Hackerman, N. (1982) A photo-electrochemical investigation of semiconducting oxide films on copper. *Corros. Sci.*, **22** (8), 791–805.
2. Pointu, B., Braizaz, M., Poncet, P., and Rousseau, J. (1981) Photoeffects on the Cu/H_3PO_4 interface: part I. Experimental data. *J. Electroanal. Chem.*, **122**, 111–131.
3. Pointu, B., Braizaz, M., Poncet, P., and Rousseau, J. (1983) Photoeffects on the Cu/H_3PO_4 interface: part II. Band model of the interface in darkness. *J. Electroanal. Chem.*, **151** (1), 65–77.
4. De Jongh, P.E., Vanmaekelbergh, D., and Kelly, J.J. (2000) Photoelectrochemistry of electrodeposited Cu2 O. *J. Electrochem. Soc.*, **147** (2), 486–489.
5. Di Quarto, F., Piazza, S., and Sunseri, C. (1985) Photoelectrochemical study of the corrosion product layers on copper in weakly acidic solutions. *Electrochim. Acta*, **30** (3), 315–324.
6. Collisi, U. and Strehblow, H.-H. (1986) A photoelectrochemical study of passive copper in alkaline solutions. *J. Electroanal. Chem.*, **210** (2), 213–227.
7. Collisi, U. and Strehblow, H.-H. (1990) The formation of Cu_2O layers on Cu and their electrochemical and photoelectrochemical properties. *J. Electroanal. Chem.*, **284** (2), 385–401.
8. Millet, B., Fiaud, C., Hinnen, C., and Sutter, E.M.M. (1995) A correlation between electrochemical behaviour, composition and semiconducting properties of naturally grown oxide films on copper. *Corros. Sci.*, **37** (12), 1903–1918.
9. Feng, Y., Siow, K.-S., Teo, W.-K., Tan, K.-L., and Hseih, A.-K. (1997) Corrosion mechanisms and products of copper in aqueous solutions at various pH values. *Corrosion*, **53** (5), 389–398.
10. Babić, R., Metikoš-Huković, M., and Lončar, M. (1999) Impedance and photoelectrochemical study of surface layers on Cu and Cu–10Ni in acetate solution containing benzotriazole. *Electrochim. Acta*, **44** (14), 2413–2421.
11. Zerbino, J.O. (1999) Ellipsometric and photocurrent characterization of oxide

films formed on copper in borax solution with and without benzotriazol. *Electrochim. Acta*, **45** (4), 819–825.

12. Kalinauskas, P., Valsiūnas, I., Survila, A., and Jasulaitienė, V. (2001) Photosensitive oxide layers developed on copper electrode in 0.5 M Na_2SO_4 solution. *Mater. Sci.*, **7** (3), 137–142.
13. Survila, A., Kalinauskas, P., and Uksienė, V. (1991) Transform of optical signal into electrical one in the Cu/Cu(II), β-alanine system. *Chemija*, **1** (180), 154–163.
14. Survila, A. and Uksienė, V. (1992) The electroreduction kinetics of Cu(II)-glycine complexes in aqueous solution. *Electrochim. Acta*, **37** (4), 745–749.
15. Survila, A. and Uksienė, V. (1993) Influence of phase layers on the kinetics of electrodeposition of copper from solutions containing glycine, α- or β-alanine. *Sov. Electrochem.*, **29** (2), 202–205.
16. Survila, A., Kalinauskas, P., and Uksienė, V. (1993) Photoelectrochemical phenomena at the interface Cu/Cu(II), glycine, α- or β- alanine. *Electrochim. Acta*, **38** (18), 2733–2740.
17. Survila, A., Kalinauskas, P., Ivaškevič, E., and Kutner, W. (1997) Simultaneous photoelectro chemistry and piezoelectric microgravimetry, with the use of electrochemical quartz crystal microbalance, of surface layers formed at the Cu/Cu(II), β-alanine interface. *Electrochim. Acta*, **42** (19), 2935–2941.
18. Survila, A., Kalinauskas, P., and Uksienė, V. (1998) Variations of pH at the Cu/Cu(II), β-alanine interface under dark and illumination conditions. *Chemija*, **1**, 51–54.
19. Survila, A., Survilienė, A., and Stalnionis, G. (1999) EQCM study of electroreduction of copper(II)-ethylenediamine complexes. *Chemija*, **10** (3), 203–208.
20. Survila, A., Kalinauskas, P., and Valsiūnas, I. (1999) Photoelectrochemical phenomena at Cu/Cu(II), ethylenediamine interface. *Chemija*, **10** (4), 275–280.
21. Survila, A., Kanapeckaite, S., and Survilienė, A. (2001) Cathodic processes in ligand-deficient Cu|Cu(II), ethylenediamine system. *J. Electroanal. Chem.*, **501** (1-2), 151–159.
22. Survila, A., Kalinauskas, P., and Valsiūnas, I. (2002) Effect of ligands on formation of photosensitive oxide layers on copper electrode. *Russ. J. Electrochem.*, **38** (10), 1068–1073.
23. Survilienė, A. and Survila, A. (2002) Effect of temperature on oxide formation in ligand-deficient Cu|Cu(II), ethylenediamine system. *Russ. J. Electrochem.*, **38** (11), 1216–1219.
24. Būdienė, J., Kalinauskas, P., and Survila, A. (2004) Photoresponse from oxide layers developed on copper electrode in Cu(II) solutions containing glycolic acid. *Chemija*, **15** (1), 7–11.
25. Rajeshwar, K., Singh, P., and DuBow, J. (1978) Energy conversion in photoelectrochemical systems—a review. *Electrochim. Acta*, **23** (11), 1117–1144.
26. Hara, M., Kondo, T., Komoda, M., Ikeda, S., Shinohara, K., Tanaka, A., Kondo, J., and Domen, K. (1998) Cu_2O as a photocatalyst for overall water splitting under visible light irradiation. *Chem. Commun.*, **3**, 357–358.
27. Bertocci, U. (1978) Photopotentials on copper and copper alloy electrodes. *J. Electrochem. Soc.*, **125** (10), 1598–1602.
28. Survila, A., Pileckienė, J., Kanapeckaitė, S., and Kalinauskas, P. (2012) Formation of cuprous oxide layers in Cu(II) solutions containing gluconic acid. *J. Solid State Electrochem.*, **16** (2), 521–527.
29. Niaura, G. (2000) Surface-enhanced Raman spectroscopic observation of two kinds of adsorbed OH^- ions at copper electrode. *Electrochim. Acta*, **45** (21), 3507–3519.
30. Pourbaix, M. (1966) *Atlas of Electrochemical Equilibria in Aqueous Solutions, Part 2*, Pergamon, London, p. 386.
31. Bard, A.J. and Faulkner, R.L. (2001) *Electrochemical Methods. Fundamentals and Applications*, John Wiley & Sons, Ltd, New York.
32. Valeev, A.S. (1981) Photo electrochemical method for studying the processes of anodic dissolution of metals. *Elektrokhimiya*, **17** (12), 1830–1836.
33. Būdienė, J., Kalinauskas, P., and Survila, A. (2006) Photoelectrochemical properties of oxide layers developed on copper

electrode in Cu(II) solutions containing glycolic acid and small amounts of chloride. *Chemija*, **17** (2-3), 8–11.

34. Gerischer, H. (1977) On the stability of semiconductor electrodes against photodecomposition. *J. Electroanal. Chem.*, **82** (1), 133–143.

35. Perone, S.P., Richardson, J.H., Deutcher, S.B., Rosenthal, J., and Ziemer, J.N. (1980) Laser induced photoelectrochemistry: time-resolved coulostatic-flash studies of photooxidation at n-TiO_2. *J. Electrochem. Soc.*, **127** (12), 2580–2588.

36. Survila, A., Survilienė, A., Kanapeckaitė, S., Būdienė, J., Kalinauskas, P., Stalnionis, G., and Sudavičius, A. (2005) Oxide layers developed on copper electrodes in Cu(II) solutions containing ligands. *J. Electroanal. Chem.*, **582** (1-2), 221–229.

37. Survila, A.A. and Uksienė, V.A. (1989) Potentials of unpolarized copper electrodes in solutions of glycine, α-alanine, and β-alanine complexes of Cu(II). *Sov. Electrochem.*, **25** (7), 856–860.

11
Hydrogen Evaluation Involving Ligands as Proton Donors

Hydrogen evolution often attends the electrodeposition of metals. This side reaction should be taken into account when this main process is studied. Most often, the onset of the hydrogen evolution is followed by a progressive rise of the voltammogram. However, when the plating solutions contain such ligands as aforementioned hydroxy acids, these substances can generate hydrated protons (H_3O^+ ions) establishing the conditions for the chemical step + electrochemical step (CE) mechanism. Then, hydronium ions are formed additionally in a chemical reaction that precedes the electron transfer step.

To describe this mechanism quantitatively, an approach considered in Chapter 3 can be applied. For definiteness, let us consider a system containing a weak acid LH_2. The main reversible processes occurring in such a system can be depicted as follows:

$$LH^- + H^+ \rightleftarrows LH_2, \tag{11.1}$$

$$L^{2-} + H^+ \rightleftarrows LH^-, \tag{11.2}$$

$$H^+ + OH^- \rightleftarrows H_2O. \tag{11.3}$$

Further, a set of differential equations, containing the respective kinetic terms, should be written for each component, except the water that is present in a large excess. Linear combinations of these equations (for details see Section 3.3) produce the following equations that contain no kinetic terms:

$$\frac{\partial c_{ac}}{\partial t} = D\frac{\partial^2 c_{ac}}{\partial x^2}, \tag{11.4}$$

$$\frac{\partial c_H}{\partial t} = D\frac{\partial^2 c_H}{\partial x^2}, \tag{11.5}$$

where the total (analytical) concentration of acid

$$c_{ac} = [LH_2] + [LH^-] + [L^{2-}] \tag{11.6}$$

and the total concentration of proton donors and acceptors

$$c_H = 2[LH_2] + [LH^-] + [H^+] - [OH^-]. \tag{11.7}$$

Electrochemistry of Metal Complexes: Applications from Electroplating to Oxide Layer Formation, First Edition.
Arvydas Survila.

More extensive analysis shows that similar equations are obtained in the case of systems containing any number of proton donors.

The second remark concerns the total concentrations that are defined by Eqs. (11.6) and (11.7). Whereas c_{ac} has a clear physical meaning, the second one, c_H, looks as made-up quantity. Moreover, c_H can turn negative at sufficiently high pH, but then the hydrogen evaluation involving hydronium ions becomes unfeasible. Notice that a similar approach, constructed in such way and involving c_H values, was used earlier for the analysis of electrochemical processes occurring in the systems containing metal complexes and protonated ligands.

The certain gradient of c_H developed in the diffusion layer is determined by the relationship following from the first Fick's law:

$$i = -nFD\frac{\partial c_H}{\partial x}\bigg|_{x=0}, \tag{11.8}$$

where $n = 1$ is the charge number of the electrode reaction.

Forasmuch an acid by itself is assumed as electrically inactive substance, $\partial c_{ac}/\partial x$ should be taken as zero at the electrode surface; then, c_{ac} is constant over the entire range of diffusion layer. Solution of the differential Eq. (11.5) in combination with common initial conditions and boundary condition (11.8) yields the analog of Eq. (3.10):

$$\Delta c_H(t) = -\frac{1}{nF\sqrt{\pi D}}\int_0^t \frac{i(t-u)}{\sqrt{u}}\Psi(u)\mathrm{d}u, \tag{11.9}$$

where $\Delta c_H(t)$ is the difference between the bulk and surface concentrations of proton donors and u is an auxiliary variable having dimension of time.

The next problem lies in the determination of interrelations between the concentrations of individual species. With this aim, the results of analysis performed in Section 3.4.2 could be applied to the present problem. They show that the image of ideally labile system seems to be acceptable, when the rate constants for LH_2 or LH^- dissociation are sufficiently high. The lower limit of k_{-1} could be estimated at $10\,s^{-1}$ (steady-state conditions); for linear potential sweep conditions, this limit is supposed to be one to two orders higher. According to the data obtained with hydrodynamic modified rotating disc electrode (RDE) [1], the k_{-1} values for formic, acetic, and propionic acids are 4.83×10^5, 3.46×10^6, and $2.88\times10^6\,s^{-1}$, respectively, but polarographic measurements produce one order lower quantities [2]. Anyway, these acids and similar acids could be treated as sufficiently labile.

Voltammetric experiments were carried out with solutions containing different organic acids and an excess of supporting electrolyte (sodium or potassium sulfate). The presence of the latter substance made it possible to minimize the effect of migration on the mass transport processes. The acids under study are listed in Table 11.1; their symbols LH or LH_2 render a number of mobile protons (H^+ ions) that can be released in acidic water solutions. Due to a sufficiently high difference between the standard potentials of $Cu|Cu^{2+}$ and $H_2|H^+$ electrodes, partial processes of Cu(II) reduction and hydrogen evolution are well-separated,

Table 11.1 Selected stability constants of organic acids.

Substance	Formula	Symbol	Stability constant	
			$\log \beta_1$	$\log \beta_2$
Glycolic acid	$HO–CH_2–COOH$	LH	3.63	—
Malic acid	$HOOC–CH_2–(CH–OH)–COOH$	LH_2	4.24	7.24
Tartaric acid	$HOOC–(CH–OH)_2–COOH$	LH_2	4.26	7.4
Gluconic acid	$HO–CH_2–(CH–OH)_4–COOH$	LH	3.7	—

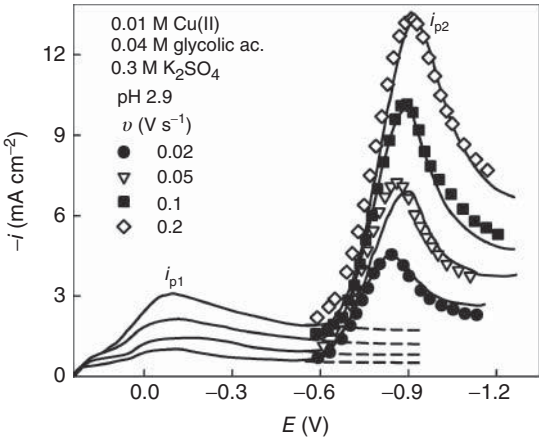

Figure 11.1 Comparison of voltammetric data obtained at different potential sweep rates *v* for Cu(II)-containing (solid lines) and Cu(II)-free (symbols) solutions. The limiting currents of Cu(II) reduction (dotted lines) served as base lines for the latter data.

unless very stable Cu(II) complexes are formed. This can be seen from a typical example shown in Figure 11.1. Experimental voltammograms contain two well-defined maxima that are indicative of two different cathodic processes.

The first current peak (i_{p1}) observed at a relatively low cathodic polarization ($E_{p1} \approx -0.1$ V) results from Cu(II) reduction. A further increase in cathodic polarization gives rise to the second process with a distinctive current peak (i_{p2}) observed at $E_{p2} \approx -0.9$ V. Generally, this maximum can be conditioned by different reasons, such as Cu_2O reduction or hydrogen evolution. In the first case, the peak current depends on the exposure time and electrode surface is photosensitive. Besides, electrochemical quartz crystal microgravimetry (EQCM) data allow us to distinguish between these cases (cf. Figures 8.11 and 10.3): no extra changes in copper electrode mass are observed in this region when the hydrogen evolution occurs. Moreover, similar current peaks are also observed in Cu(II)-free solutions. The voltammograms obtained in the latter case and brought to the level of partial Cu(II) reduction current (dotted lines in Figure 11.1) coincide sufficiently well with the data recorded in the presence of

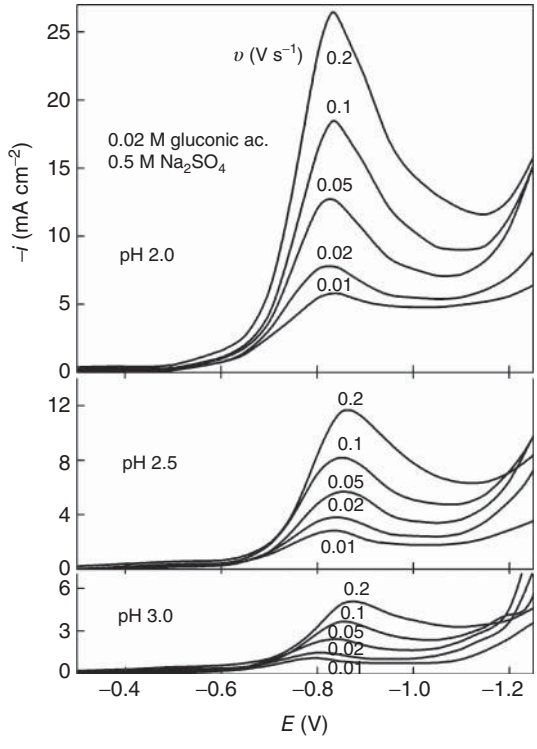

Figure 11.2 Voltammograms obtained for 0.02 M gluconic acid solutions containing 0.5 M Na_2SO_4 at different pH. Potential sweep rates are indicated at the respective curves.

Cu(II). This effect, as well as large difference between E_{p1} and E_{p2}, gives grounds to suppose that the two partial processes may be analyzed independently.

Solution pH should be mentioned in the first place as a factor that determines the rate of hydrogen evolution. This can be clearly seen from the typical data shown in Figure 11.2. As expected, current density significantly falls with increase in solution pH, that is, when the concentration of hydronium ions decreases. However, when pH is kept constant, the rate of the process increases with the total concentration of acid. This effect will be analyzed next in more detail. Finally, the supporting electrolyte plays a part in these processes: the height of the second current peak decreases gradually when sulfate is replaced by perchlorate (Figure 11.3). This implies that not only LH^- or LH_2 but also HSO_4^- should be attached to proton donors.

Most of the experimental data obtained are typical of every acid under investigation. Peak currents (that further are simply symbolized as i_p) increase with the potential sweep rate ν and linear dependencies between i_p and $\sqrt{\nu}$ are observed (Figures 11.4 and 11.5). Slopes of these lines, S, increase, when the acidity of solutions grows (pH falls) and the acid concentration is increased. The observed phenomena are consistent with the aforestated assumptions concerning the

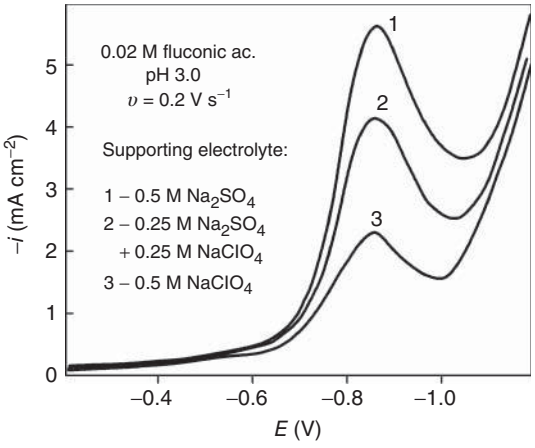

Figure 11.3 Comparison of voltammetric data obtained at $v = 0.2\,\mathrm{V\,s^{-1}}$ for 0.02 M gluconic acid solutions containing different supporting electrolytes as indicated.

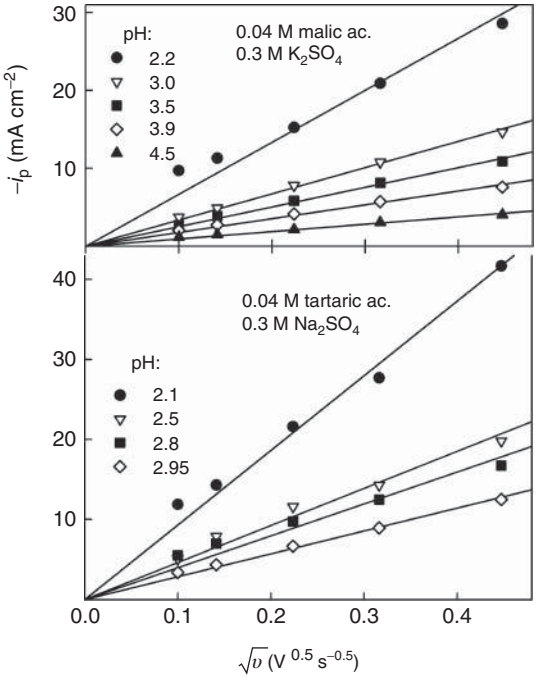

Figure 11.4 Peak current densities versus $\sqrt{v}$ obtained at different pH for 0.04 M malic and tartaric acid solutions.

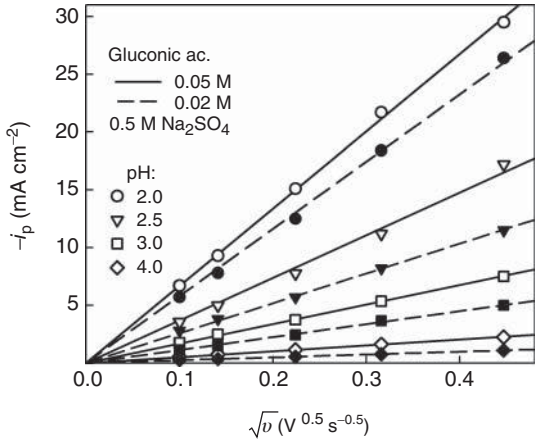

Figure 11.5 Peak current densities versus $\sqrt{v}$ obtained at different pH for 0.02 M (dashed lines) and 0.05 M (solid lines) gluconic acid solutions.

mechanism of electrode reactions. As the position of current peaks depends on v (Figures 11.1 and 11.2 and the data given below), the cathodic process should be considered as irreversible. Then, the simplified kinetic equation is valid for sufficiently high overvoltages:

$$\log i_{\text{norm}} = \log i_0 - \frac{\alpha n F}{2.303RT}\eta, \tag{11.10}$$

where normalized current density is defined by the relationship

$$i_{\text{norm}} = \frac{|i|}{[\text{H}^+]_s/[\text{H}^+]_b}, \tag{11.11}$$

Procedures of data treatment were as follows. Firstly, the special integration of experimental voltammograms, transformed into $i-t$ functions, is performed with Eq. (11.9) and Δc_{H} quantities, as E functions, are obtained. The second step consists in determination of distribution of proton donors at the electrode surface under cathodic polarization conditions. For this purpose, material balance equations are used. When increasing cathodic overvoltage, surface c_{H} decreases from the bulk value (initial state) to zero (limiting current region). It must be emphasized that the surface concentration of the electrically active substance (hydronium ions) **does not fall to zero**, in contrast to common redox processes. In the absence of proton donors, a neutral medium is created at the electrode surface ($[\text{H}^+]_s = [\text{OH}^-]_s$), otherwise an alkalization occurs(see Eq. (11.7) at $c_{\text{H}} = 0$).

Notice that the same data can be presented as E functions, because the interrelation between surface c_{H} and E is easily obtained. This makes it possible to assign the value of $[\text{H}^+]_s$ at any potential of voltammograms and to transform them into normalized Tafel plots (NTPs). Some results of the procedures performed are shown in Figure 11.6. The data obtained at different v are very close and can be approximated by one average NTP. The kinetic parameters of charge transfer

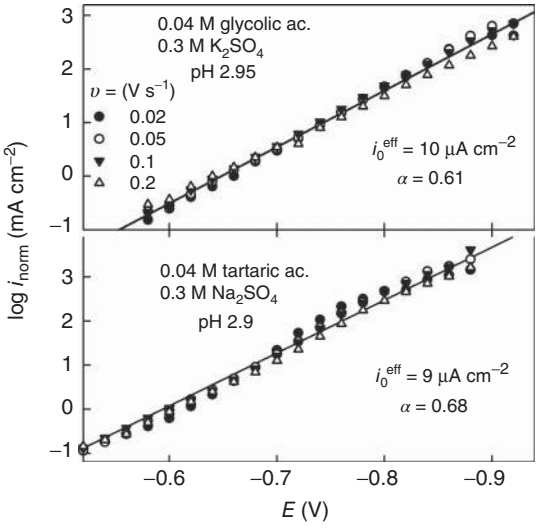

Figure 11.6 Normalized Tafel plots obtained at different potential sweep rates for 0.04 M glycolic (upper part) and tartaric (lower part) acid solutions. Indicated kinetic parameters are calculated from general regression lines.

Table 11.2 Equilibrium characteristics acid solutions and kinetic parameters of hydrogen evolution.

Acid	c_{ac} (mM)	c_{slf} (M)	pH	c_H (mM)	10^6 D (cm^2 s^{-1})	α	i_0^{eff} (μA cm^{-2})	S (mA cm^2 V^{-05} $s^{0.5}$)	
								Simulation	Experiment
Glycolic	40	0.3	2.95	43.3	6.8	0.61	10	26.9	26.7
Malic	40	0.3	3.0	76.2	3.1	0.64	8	32.7	33.6
Tartaric	40	0.3	2.9	85.0	2.1	0.64	9	30.1	30.7
Gluconic	20	0.5	3.0	39.5	1.5	0.60	8	11.4	11.2

process obtained by Eq. (11.10) are shown in Figure 11.6 and listed in Table 11.2. Though the equilibrium potential of $H^+|H_2$ electrode is uncertain in H_2-free solutions, the exchange current density, named "effective," was determined by extrapolation of NTP to the theoretical quantity defined by the relationship:

$$E_{eq} = -\frac{2.303RT}{F}pH. \tag{11.12}$$

Low i_0^{eff} values are responsible for a high overvoltage of hydrogen evolution: current densities are low over a wide initial range of potentials. The rise of voltammograms is observed at rather negative potentials ranging up to ~−0.6 V.

It was of interest to make use of the relationships (5.30) and (5.31) describing the coordinates of current peaks. In so doing, the concentration term in Eq. (5.30) was replaced by c_H. The slopes $S \equiv \partial i_p/\partial\sqrt{\nu}$ were analyzed with values of α, D, and c_H

taken from the foregoing analysis. According to the results obtained, experimentally determined slopes are in line with the quantities that follow from Eq. (5.30) (Table 11.2).

Rather low diffusion coefficients obtained for malic, tartaric, and gluconic acid engage attention. As comparatively large acid molecules take place in the diffusion processes in this case, their moderate diffusion coefficients could reduce the values of the effective D (see Eqs. (3.30) and (3.31)). Alternatively, the effect of insufficient lability of these acids that was not taken into account must not be ruled out. Nevertheless, it can be seen from these data that the kinetic parameters of the charge transfer step, obtained for different acids, are quite similar. Then, according to Eq. (5.30), the linear interrelation between S and c_H should be governed only by the equilibrium and mass transport parameters. In this regard, all experimental data, obtained for different acid solutions at various c_{ac} and pH, were generalized and collected in Figure 11.7. It can be seen that a satisfactory approximation can be performed by single general regression line. The results obtained show that the processes of hydrogen evolution, proceeding in the systems under consideration, offer very similar features and the same theoretical model is acceptable for their description.

It is of interest to view the data concerning the position of current maxima in the scale of potentials. The presented model supposes a linear dependence between E_p and $\log \nu$, the slope of which is determined by the Eq. (5.31). This regularity is consistent with the most experimental data obtained for moderately acid Cu(II)-free solutions. For instance, the average slope of lines, presented in the lower part of Figure 11.8, is about 50 mV/decade; then, the value $\alpha \approx 0.6$ that follows from Eq. (5.31) is in agreement with experimental data listed in Table 11.2. However, E_p ceases to depend on ν in more acidic (pH 2.0) 0.02 M gluconic acid solutions; this being indicative of the reversible character of the charge transfer process. When

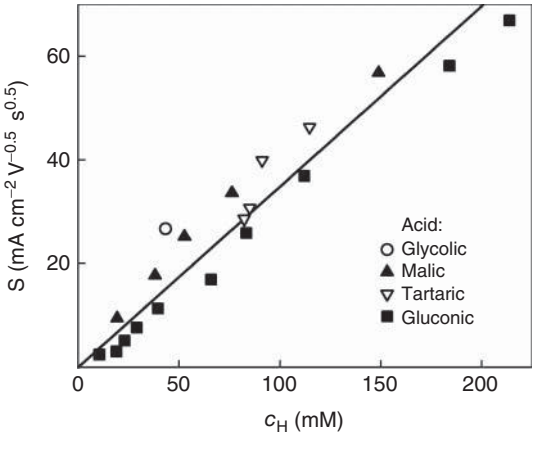

Figure 11.7 Experimental slopes $S \equiv \partial i_{p2}/\partial\sqrt{\nu}$ versus total concentration of proton donors. Summation of the data obtained for different solutions at $2.5 < \text{pH} < 4.0$.

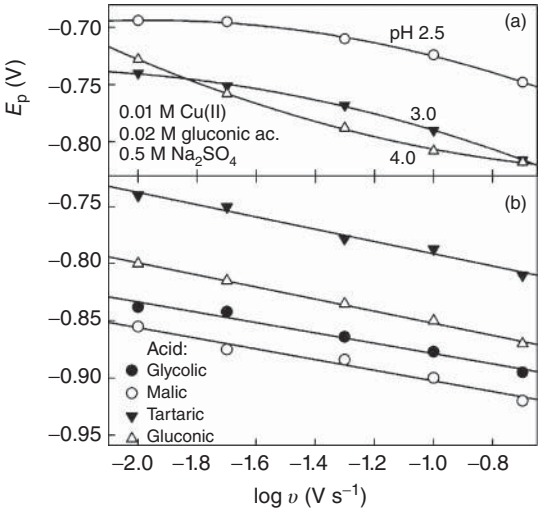

Figure 11.8 Dependencies of peak potentials on potential sweep rate presented in semilogarithmic coordinates. The data are obtained for 0.02 M gluconic acid solutions containing Cu(II) (part a) and for Cu(II)-free solutions (part b) the composition of which is given in the Table 11.2.

pH of such solutions was increased, a tendency for a certain increase in $\partial E_p/\partial \log \nu$ magnitudes was observed, but this was not the case of more concentrated (0.05 M) solutions.

Nonlinear E_p dependencies on $\log \nu$ are observed in the case of Cu(II)-containing solutions (Figure 11.8a). It is necessary to point out that the situation at the electrode surface is not exactly the same as that in identical Cu(II)-free solutions containing the same c_{ac} and pH. As was stated earlier, hydrogen evolution starts in the region of limiting current, where the surface concentration of Cu(II) approaches zero but c_{ac} and c_H remain unchanged. However, a certain amount of anions is released from reduced Cu(II)–hydroxy acid complexes that results in the shift of chemical equilibria and in the relevant increase in surface pH. Again, a simultaneous deposition of copper can also modify the properties electrode surface.

Kinetic parameters listed in Table 11.2 have been determined using not only experimental but also literature data. It is common knowledge that stability constants expressed in concentration terms depend on the ionic strength of solutions and on the nature of supporting electrolyte. Unfortunately, data given in different handbooks concern, as a rule, perchlorate or nitrate media and certain problems arise on fitting such data for sulfate media. Therefore, the reliability of the parameters established here depends also on the sureness of the data selected from literature. Nevertheless, it can be stated that the kinetic parameters of hydrogen evolution, occurring on the same copper substrate, are very similar in the case

of all the systems under investigation. Organic acids seem to be of minor importance for the charge transfer process and act in general as sufficiently labile proton donors.

References

1. Kanzaki, Y., Tokuda, K., and Bruckenstein, S. (2014) Dissociation rates of weak acids using sinusoidal hydrodynamic modulated rotating disk electrode employing Koutecky-Levich equation. *J. Electrochem. Soc.*, **161** (12), H770–H779.
2. Delahay, P. and Vielstich, W. (1955) Kinetics of the dissociation of weak acids and bases – Application of polarography and voltammetry at constant current. *J. Am. Chem. Soc.*, **77** (19), 4955–4958.

Concluding Remarks

The data presented in this book, as well as analysis of other published data, allow us to make some generalizations concerning the equilibrium and kinetic properties of systems containing labile metal complexes, comparing them with the properties of ligand-free systems. The term "ligand," as already noted, should be understood in the narrow sense of the word. Solutions of simple salts, of course, also contain complex ions, the inner coordination sphere of which is saturated by solvent molecules, when their concentration is at least 1 order of magnitude higher than that of metal ions. Such systems are similar to these with a large excess of ligand that actually contain only single complex species. When the metal concentration is changed, the complexation degree of this system varies to the certain extent, but the number of inner-sphere ligands in the coordination compound remains the same. This fact complicates the study of changes in the Electrically active complex EAC structure, such as a partial desolvation preceding the charge transfer.

However, our prime interest here is with systems, the ligand concentration in which is several orders of magnitude lower as compared with the solvent. Moreover, ligand-deficient solutions, which are not uncommon in plating industry, are of special interest. In such cases, a large number of complex species and protonated ligands can occur. On changing concentrations of metal and ligand or pH, the system composition can vary over a wide range, exhibiting unexpected behavior. For instance, the increase in M^{n+} concentration with dilution of solutions is possible.

The distribution of complex and ligand species in the solution is important initial information required for a comprehensive investigation of the electrochemical process. Firstly, this information is necessary for determination of the equilibrium potential, from which the fundamental kinetic parameter, the overvoltage, is reckoned. Unlike ligand-free solutions, for which the equilibrium potential varies linearly with log c_M, a more complex function is observed: sharp E_{eq} jumps occur at the equivalent ratio of c_L/c_M, the E_{eq} increase with the dilution of the solution is possible, and so on. The special features of complex systems also include the possibility of a profound change in the solution composition when the equilibration process involves formation of intermediates that are capable of complex formation.

Electrochemistry of Metal Complexes: Applications from Electroplating to Oxide Layer Formation, First Edition.
Arvydas Survila.

On the other hand, bulk concentrations are required for estimation of the respective surface concentrations that are the terms of kinetic equations. To obtain the data for the solution layer adjacent to the electrode surface, mass transport of chemically interacting species should be considered. Quantitative formulation of this problem is based on differential equations representing Fick's second law and supplemented with the respective kinetic terms. It turns out that some linear combinations of these equations make it possible to eliminate kinetic terms. So produced common diffusion equations involve total concentrations of metal, ligand and proton donors (c_M, c_L, and c_H, respectively) as functions of time and space coordinates. It follows from the relationships obtained that the total metal concentration varies in the same manner as the concentration of free metal ions in the absence of ligand. Simultaneously, the total ligand concentration remains constant within the whole region of the diffusion layer. This proposition also remains valid for proton donors and acceptors.

Next, similar data for individual components of the system are to be found. One approach that has been often used in electrochemical investigations assumes that concentrations of components are close to the equilibrium ones when the system is sufficiently labile. Then expressions for the respective stability constants together with material balance equations are sufficient to obtain the required data. Though this approach sets unacceptable constraints on the EAC composition, it can be used as a satisfactory approximation when the rate constants of chemical steps exceed some critical values. Otherwise, the mass transfer problem should be solved without any simplifications accounting for the kinetics of chemical steps.

The above mass-transport regularities reveal certain peculiarities of the electrochemical processes in labile systems. These effects are responsible for sharp changes in the complexation degree at the electrode surface and are possible in two cases.

One of them relates to the cathodic processes in ligand-deficient[1)] systems. When the cathodic current density is increased, the surface c_M value falls with no change in c_L. Then, the transition from the ligand-deficient state to the state with the ligand excess is possible at certain current density. Another case concerns anodic processes at the excess of ligand. An increase in anodic current density involves the respective increase in the surface c_M that, in turn, results in the occurrence of the lack of ligand at the electrode surface. Similar transitions are well known in the potentiometric titration and are accompanied by sharp changes in the electrode potential. The latter manifest itself in various voltammetric characteristics of electrode processes. The additional current plateau (prewave) appears on cathodic voltammograms, and the anodic "limiting current" becomes observable due to this transition. Respective analogs emerge when various transient techniques are applied: two transition times appear in chronopotentiometry or two current peaks can be observed in LPS voltammetry.

1) Here, the active form of ligand capable of forming coordination bounds is meant. Some protonated ligand species does not possess this capability.

According to the concepts of thermodynamics, equilibrium characteristics of the reversible electrochemical process depend on the initial and final states and do not depend on the mechanism of equilibration. Therefore, any version of Nernst equation applied to the charge transfer process involving any metal complex should yield the same equilibrium potential. This means that there is no thermodynamic limitation on the composition of the electrically active complex, and any metal-containing species may be treated as a possible EAC.

In reality, not all types of complexes exhibit electrochemical activity. The charge transfer often proceeds by the inner-sphere mechanism involving a removal of some ligands from the inner coordination sphere. This promotes adsorption and a decline in the potential barrier of electron transfer. For this reason, the predominating species in the solution complex with saturated inner coordination sphere does not need to be electrically active. The cases are known when the total current is supplied by a single EAC, and certain chemical step precedes its formation. Sometimes, the EAC can differ substantially from the predominating species, as it takes place in the Zn(II)–cyanide system where the $Zn(OH)_2$ species were supposed to be electrically active. Since kinetic factors and the activation energy first of all are responsible for the electrochemical activity of complexes, special methods should be applied for establishing the EAC composition. They are mostly based on the analysis of reaction order with respect to ligand.

When a single EAC predominates in the system, the determination of kinetic parameters should present few problems, and a quantitative description of electrochemical kinetics becomes comparatively simple. This book contains a number of examples when simulated and experimental data coincide well. Among these are prewave-containing voltammograms that are typical of ligand-deficient systems. In addition, theoretically predicted anomalous high slopes of voltammetric characteristics were observed experimentally for reduction of Sn(II)–citrate complexes.

Most of scientific principles of individual metal plating are appropriate for metal codeposition processes. The same mass-transport model is acceptable for alloy electrodeposition, considering that the partial current densities are identified. In addition, certain regularities established for individual processes are usually inherent in codeposition. At the same time, some specific problems arise. One of them involves the necessity to bring together the equilibrium potentials of metals as close as possible. This can be realized by a proper selection of ligands. Besides, codeposition can be optimized bringing into play kinetic factors that enable to increase selectively the cathodic polarization of more noble metal. It is best to realize such opportunity in the ligand-deficient solutions. Certain depolarization of the reduction of less noble metal is consistent with the energetic effects of alloy formation. Sometimes, this effect is referred to as the underpotential deposition (UPD).

Electrochemical codeposition often results in formation of different microstructures and phases. Moreover, electrodeposited binary alloys may or may not be the same in phase structure as those formed by simple melting. In addition, electrodeposited phases are not always in the thermodynamic equilibrium and can

show specific surface properties. We should like to pay attention on the remarkable function of some surfactants in bronze coating. Most polyethers show quite different adsorption behavior on copper and tin electrodes. In contrast to tin, these surfactants adsorb on copper only in the presence of halides when the specific surface complexes are formed. Copper-rich bronze coatings show similar adsorption behavior. When halides are absent and surface complexes are not formed, the bronze electrodeposition is not accompanied by noticeable adsorption of surfactants. However, if a germ of pure tin phase is formed for some reason, its growth is immediately suppressed by significant inhibitive adsorption of polyether. Control over formation of copper surface complexes makes it possible to keep in check the codeposition of copper and tin.

Electrochemistry of metal complexes is rich in events. Changes arising from electrolysis are often accompanied by other interesting processes, and a spontaneous formation of photosensitive oxide layers is among them. Cuprous oxide layers developed in electrochemical systems are interesting from various points of view. In the first place, such layers are known to form during copper corrosion. Extensive investigations in this field provide further insights into corrosion mechanism and may be useful in improving copper corrosion resistance. Again, oxide layers developed in electrochemical systems containing ligands are interesting in themselves, because their properties may be essentially different from those known for single crystals or polycrystalline compact forms. The latter are known as substances exhibiting p-type semiconductor properties, but Cu_2O formed in electrochemical systems often show n-type conductivity. Very interesting idea is to use cuprous oxide as a material for the conversion of solar energy into electrical or chemical energy.

It was found that the Cu^{2+} concentration is one of the main factors that control the rate of Cu_2O formation under open-circuit conditions. In turn, this quantity depends on the complexation degree of the ligand-containing Cu(II) solutions; therefore, the (photo)electrochemical properties of oxide layers depend strongly on the conditions under which they are built up. The nature of the ligands, as well as the composition of the ligand-containing solutions, is of great importance here.

Common p-type conductivity is rather rare for oxides formed in ligand-containing solutions; such cuprous oxide developed in the solutions containing ethylenediamine, which can act as a reductant. More often *n*-Cu_2O species are formed, as in weakly acid solutions containing such ligands as amino or hydroxy acids. It was found that the type of conductivity can alter during the development of oxide layer. Then the transition from p-type (thin initial layers) to n-type conductivity (thicker layers) is observed.

Two types of the oxide response to the light perturbation are commonly investigated: the onset and development of the photopotential under open-circuit conditions, and the emergence of photocurrent when the electrode potential is controlled. The experiments carried out at different quantum energies showed that the band gap for electrochemically formed oxide layers is close to that established for compact Cu_2O crystals and does not depend on the type of conductivity.

Analysis of the energy correlation between band edges and the Fermi levels of electrode reactions in aqueous solution showed that the Fermi levels for both cathodic and anodic decompositions of Cu_2O are located inside the band gap. This is indicative of cathodic and anodic instabilities. The photodecomposition of oxide layers was confirmed by EQCM data.

Oxide layers can be reduced electrochemically that manifests itself as a well-defined current peak on the cathodic voltammogram. Since the amount of Cu_2O accounts for several tens of monolayers, the properties of cuprous oxide are more typical of adsorbed polylayers than of the Cu_2O phase: the peak height varies linearly with the potential sweep rate and is proportional to the amount of Cu_2O formed.

What is more, oxide layers exhibit a certain effect on Cu(II) reduction as well. When they are sufficiently thin (Cu(II)–glycine system), two regions on voltammogram with different kinetics and mechanism can be distinguished. The transfer of the second electron was found to be the rate-determining step, when Cu(II) reduction takes place at oxidized surface. A break-up of oxide at certain potential gives rise to the change of mechanism. Then, the transfer of the first electron becomes the rate-determining step that is typical of the most Cu(II) reduction processes. The effect of thicker layers is less clear. Tens of Cu_2O monolayers exert a pronounced inhibitive effect on Cu(II) reduction, reducing significantly the exchange current density.

Hydrogen evolution often attends the electrodeposition of metals. This side reaction should be taken into account when this main process is studied. Most often the onset of the hydrogen evolution is followed by a progressive rise of the voltammogram. However, when plaiting solutions contain protonated ligands, these substances can generate hydrated protons (H_3O^+ ions) establishing the conditions for the CE mechanism. In this case, voltammograms take a shape that is characteristic of other electrochemical processes including the reduction of metal complexes. Thus, LPS voltammograms display current peaks the height of which depends on potential sweep rate. If the total concentration of proton donors and acceptors is positive ($c_H > 0$), the limiting current proportional to c_H can be observed on the steady-state voltammograms when $c_H \to 0$. These findings provide a prerequisite to exert control over hydrogen evolution.

It is reasonable that all problems of electrochemistry of metal complexes could not receive a comprehensive survey in this book. For instance, an interesting area – spectroelectrochemistry of complexes – was not enclosed into review; all concerned are referred to the extensive literature on this subject. We suppose that topical issues considered above may extend to other systems as well. Then general conclusions drawn here might be used in investigations dealing with electrochemical processes at the surface of metallic implants or with mass transport through membranes occurring, for example, in biomimetic systems. There is no doubt that this field of electrochemistry and its continual progress will have a substantial impact on the future of humanity.

Index

Electrochemistry of Metal Complexes: Applications from Electroplating to Oxide Layer Formation, First Edition. Arvydas Survila.

WILEY END USER LICENSE AGREEMENT

Go to www.wiley.com/go/eula to access Wiley’s ebook EULA.